Chitosan/PEO blend films crosslinked by genipin as potential membranes for controlled drug release and protein separation

Chitosan/PEO Blend Films Crosslinked by Genipin as Potential Membranes for Controlled Drug Release and Protein Separation

by

Jie Jin

A doctoral thesis submitted in partial fulfilment of the requirements for the award of

Doctor of Philosophy of Loughborough University

Supervisors: Dr. M Song

Professor D. J. Hourston

Institute of Polymer Technology and Materials Engineering

Loughborough University

October 2004

ABSTRACT

This study was conducted in order to develop novel chitosan/poly(ethylene oxide)(PEO) blend films crosslinked by genipin as potential membranes for potential medical applications, such as controlled drug carriers and separation of proteins from eleutherococcus senticosus (ES).

Genipin, a naturally occurring and non-toxic crosslinking reagent, was used to form chitosan and chitosan/PEO blend networks. Genipin is found in traditional Chinese medicine and extracted from Gardenia fruit. Importantly, it overcomes the problem of physiological toxicity inherent in the use of common synthetic chemicals as crosslinking agents.

The miscibility and morphology of chitosan /PEO blends were examined by means of differential scanning calorimetry (DSC), Fourier transform infrared spectroscopy (FT-IR) and small angle X-ray scattering (SAXS). The experimental results indicate that the chitosan/PEO blends are miscible over the whole composition range. A phenomenon was observed for chitosan/LPEO (lower molecular weight PEO) blends: when the composition of chitosan was less than 60% by weight, the melting points increased as the composition of chitosan was increased. It is believed that there are strong molecular interactions between chitosan molecules and the molecules in the crystalline phase of LPEO in the chitosan/LPEO blends.

FT-IR and UV spectra analysis of the crosslinking reaction of chitosan revealed that the hydroxyl groups (3400 cm^{-1}) and the amide groups (1645 cm^{-1}) in chitosan participated actively in the reaction. SAXS results showed that a heterogeneous structure exists in the chitosan/HPEO (or /LPEO) blend networks. Crosslinking by genipin restricts crystallisation and leads to smaller crystals.

The mechanical properties, the stability in water, the swelling behaviour and surface properties of the films were also investigated. Improvements in the mechanical properties and the stability were achieved when the blends were crosslinked by genipin. The swelling characteristics of the crosslinked chitosan and chitosan/PEO blend films exhibit sensitivity to the environmental pH and

temperature. The polar functionalities in PEO and genipin help to improve the wetting capability of the films.

In order to get a better insight into the effect of solution pH on film formation of chitosan solution, which has an influence on mechanical properties of chitosan films, conformation of chitosan macromolecules in solutions were studied. The results of static laser light scattering showed that chitosan has an extended chain conformation in low pH solutions and a tendency to aggregate in high pH solutions. In the dilute chitosan solution, a coil to globule transition of the single chain occurred. In low pH solutions, a homogenous gel network was obtained due to intermolecular chain association during gelation, resulting in better mechanical properties of chitosan films.

In order to understand the effect of crosslinking temperature on mechanical properties of chitosan films, the temperature dependence of crosslinking reaction were studied. The results from FT-IR and UV spectra analysis showed that at a lower crosslinking temperature, a homogeneous crosslinking reaction occurred and this resulted in better elongation at break of the chitosan films. At higher temperatures, heterogeneous crosslink density in the films formed.

For the purpose of potential medical applications, the controlled release of vitamin B_{12} and ES was investigated. The drug release rate was controlled by the mesh size of the membrane, which can be adjusted by a number of factors, such as crosslink density, the presence of PEO in the membrane, external pH, and the degree of deacetylation of chitosan. The potential study of protein separation from ES using the chitosan membranes was performed. The crosslinked chitosan membrane has the ability to separate proteins from ES.

Acknowledgements

It gives me great pleasure to express my sincere gratitude to my supervisors, Dr. M. Song and Professor D. J. Hourston, for their supervision through the course of this research work. I have benefited immensely from their considerable help, encouragement and inspiration throughout this time.

I would like to thank the EPSRC for its financial support, which has made this research possible.

I am also very grateful to the Bioproducts Company (Taiwan) for providing crosslinking reagent of genipin and the Institute of Chinese Medicine (China) for providing a Chinese medicine of eleutherococcus senticosus (ES).

I was fortunate to receive the help of Dr. G. Li of the Changchun Institute of the Academy of Science (China) for small angle X-ray scattering experiments and the assistance of Professor He of the Science and Technology University (China) for static laser light scattering experiments. I deeply appreciate all that they have done for me.

I would also like to express my appreciation to all the staff and research students in IPTME for their help and support.

Last, but not least, I wish to thank my son, Stephen, for his aid during my study, and in particular for his efforts in checking this manuscript.

TABLE OF CONTENT

Chapter 3 Experimental

LIST OF FIGURES

CHAPTER 1

Introduction and Aims

1.1 Background on Biomaterials

Polymeric biomaterial science is a modern and interdisciplinary field with great prospects [1]. It primarily involves the medical use of biocompatible polymers in applications such as sutures, heart valves, hip and knee joints, intraocular and contact lenses, dental implants, various drug delivery systems and tissue regeneration [2-5]. Since the 1980s, it has shown remarkable development [3-5]. In recent years, in particular, polymeric biomaterials have become more attractive and of increasing interest. These smart materials have resulted in the development of advanced technologies of controlled drug and targeting delivery and the new concept of tissue engineering [5].

For a material to be a biomaterial, the minimum requirements are biocompatibility, biodegradability and non-toxicity [6]. These properties are essential for biomaterials as they are always in direct contact with living cells that are very vulnerable to, and could be readily killed by, physical and chemical stimuli. Clearly, not only the polymer, but also its possible degradation products, any residual monomer and all additives should be free of harmful effects. These requirements have not always been met.

Chitosan, a natural biomaterial, has recently attracted much attention from scientists in different parts of the world [4,5]. It has been re-evaluated and found to be a useful resource as a functional material that more than satisfies the above criteria [7,8,9]. The characteristics of chitosan make it suitable for use in various biomedical applications, such as artificial skin, tissue regeneration and drug delivery systems [1-3,10]. For such applications, especially in tissue regeneration, chitosan must be mechanically satisfactory as well as meeting the minimum requirements for a functional biomaterial. In terms of mechanical performance, for example in structured materials in hip reconstruction and replacement, the biomaterial's strength and other physical properties are critically important and the most difficult to satisfy.

For these reasons, the application of chitosan as a biomedical material has been limited to a few specific areas [4,5].

To achieve optimum effectiveness in biomedical applications, it is often desirable to crosslink biological molecules. The presence of free amino groups in chitosan enables it to be crosslinked. Conventional [11,12,13] crosslinking methods have involved reaction with dialdehydes, such as glutaraldehyde, digycidyl ethers or epoxides, whose chemically synthesized nature and non-exemption from the cause of physiological toxicity [14] pose problems. Recently, it was found that genipin is a biological material and it is suitable as a naturally occurring crosslinking agent with crosslinkable functional groups, such as amino groups or the like [15]. It incorporates easily into biomaterials and is free of harmful effects [15]. It is, therefore, a possible solution to the above problem.

1.2 Aims of the Project

This project intends to develop novel chitosan/PEO blend films, which are crosslinked by naturally occurring genipin, for medical applications. Its main aspects are as follows.

Preparation of novel chitosan/PEO blend films crosslinked by genipin

Chitosan (CS) and chitosan/poly(ethylene oxide) (PEO) blend films crosslinked by genipin will be prepared. Two different molecular weight samples of PEO, one 20,000g/mol and the other 600g/mol, will be used. PEO is chosen as the second component because it is a flexible polymer and it would greatly change the mechanical properties of the blends. PEO is also a biologically inert material [16], and therefore, suitable for biomedical applications. Thus, the blends are designed to produce mechanically resilient, chemically inert and stable films. In order to obtain the most suitable chitosan/PEO blend films for controlled drug release systems, the chitosans with different degrees of deacetylation will be used to produce the novel films.

Studies on morphology and physical properties

To obtain optimum novel films, the study of morphology and physical properties of the films will be carried out. These will include molecular interactions between chitosan and PEO, miscibility of chitosan/PEO blends, phase behaviour of crosslinked chitosan/PEO blends, mechanical and surface properties, and swelling behaviour and stability of these chitosan/PEO films. A number of techniques will be employed, such as Fourier transform infrared spectroscopy (FT-IR), differential scanning calorimetry (DSC), small angle x-ray scattering (SAXS), tensile test and contact angle measurement.

Studies on conformation of chitosan macromolecules in aqueous solution

Chitosan is an acidic soluble polymer. Solution pH may influence its solution properties and this may also affect the mechanical properties of the chitosan film. In order to understand better these properties, the conformation of chitosan macromolecules in aqueous solutions will be investigated by means of static laser light scattering (SLLS). Muti-chain aggregation behaviour and single chain coil-to-globule transition (collapse) of chitosan macromolecules in the solution will be investigated.

Studies on temperature-dependence of the crosslinking reaction

In order to understand the effect of crosslinking on the mechanical properties, the temperature-dependence of the crosslinking reaction of chitosan with genipin will be studied by means of Fourier transform infrared spectroscopy (FT-IR) and ultraviolet/visible spectrometry (UV). From this study, the details of the crosslinking process will be observed and the effect of crosslinking temperature on mechanical properties of chitosan films will be understood.

Medical applications: controlled drug release and protein separation

For medical applications we propose to develop such biofilms as potential functional membranes for controlled drug delivery systems. Vitamin B_{12} and eleutherococcus senticosus (ES), which is an herbal Chinese medicine, will be chosen as the two drug models for the controlled-release studies. The drug release behaviours from a carrier

under both conditions of fixed and moving boundaries will be performed and their release mechanism will be investigated.

We also propose to develop these biofilms as potential membranes for separating protein from ES. ES is a powerful tonic herbal medicine that has been widely used in a number of countries in the world to treat heart disease, diabetes and blood circulatory problems [17]. However, because of its high protein content, ES can only be taken in tablet form, and therefore, its use is limited. We aim to use these membranes to widen its use by separating off the un-wanted protein.

CHAPTER 2

Literature Review

2.1 Polymeric Biomaterials

A biomaterial is defined as a material that is capable of establishing an interaction with the surrounding biological environment without stimulating an adverse response by the host [18,19].

There are three sources of polymeric biomaterials [20-23].

1. Natural polymers, mainly polysaccharides and some proteins, such as cellulose, starch, chitin/**chitosan**, hyaluronan, gelatin and collagen etc. These polymers are biocompatible and primarily attacked and degraded by enzymes.
2. Synthetic polymers, particularly aliphatic polyesters such as poly(glycolic acid) (PGA), polylactic acid (PLA) and poly(ε-caprolactone) etc. The main mechanism of degradation is the hydrolysis of the backbone chains.
3. Modifications of natural or synthetic polymers such as graft and block copolymers, polymer blends and networks etc.

For polymeric biomaterials to be in contact with blood, tissue and organs in the human body without any toxic effects or provoking a reaction from the body's immune system, they must have excellent biocompatibility [1-5, 24]. Interactions occur between a biomaterial and the living tissue when the foreign material comes in contact with the living body. As a result, the biomaterial may undergo detectable alteration in surface and bulk structure, giving rise to hydrolysis, deterioration, and fatigue [1,20-23]. The living body, on the other hand, responds to the foreign material by invoking an immune reaction. Hence, a material is said to be biocompatible, or more specifically, interfacially biocompatible when such adverse biological responses do not occur, or occur at much reduced rates [1,5]. Biocompatible polymers must often also be biodegradable, and non-harmful products should be generated as a result of their biodegradation. In the human body, biomaterials can erode and degrade step by step due to the ubiquitous distribution of water or enzymes, and the degradation products do not introduce any disturbance in the body. Eventually, by diffusion,

oxidation and metabolic processes, the final products are naturally occurring, such as water and carbon dioxide, which are excreted by the kidneys and lungs.

Functional groups of a polymeric material are usually responsible for its biocompatibility and/or biodegradability and may impart to it either therapeutic or toxic characteristics. For example, carboxylic groups induce the therapeutic activity of many drugs [4]. Cell and protein binding reactions and growth may be strongly affected by functional groups of an implanted polymer. Encapsulation of an implant is triggered by adsorption of various proteins on its surface and adhesion of cells from the adjacent tissue. The nature of such a biofilm may be strongly influenced by the surface properties of the polymeric material. Cell and protein binding reactions and growth of the attached cells can be effectively manipulated by appropriate functionalization of the surface of such implants [1, 2, 4].

As indicated above, an implanted polymeric material may be considered to be 'biocompatible', if its insertion into the body does not provoke an adverse reaction. A thrombus is quickly formed when most polymers come into contact with blood cells. Materials with non-thrombogenic blood-compatible surface must, therefore, be used in contact with the blood stream. Truly biocompatible polymers used for medical purposes should be able to recognize and cooperate in harmony with bio-assemblies and living cells without any non-specific interactions [1-5,20-24]. To achieve these goals, appropriate functional groups should be incorporated into surfaces, which would resist non-specific adsorption of proteins [25].

Biodegradable polymers (also called bioerodible or bioresorbable polymers) may be of synthetic or natural origin. Non-toxic alcohols, acids and other low molecular products, easily eliminated by the body, are formed as a result of hydrolysis *in vivo* for such biocompatible polymers. High molecular weight polymers with hydrolytically unstable crosslinks may be bioerodible as a result of the breakdown of their crosslinked chains. Finally, water-insoluble polymers may be converted into water-soluble ones as a result of ionisation, proteination, or hydrolysis of side chains. Such conversions do not significantly affect molecular weight, but may be responsible for bioerosion in typical applications. Progress in the field of tissue engineering depends on the development of novel biocompatible, fully bioresorbable polymers

and the introduction of processing techniques, which will enable reproducible three-dimensional architectures on the macro- and nanometre scales [1,3,5].

Chitosan has more than satisfied the above criteria [7,8]. Chitosan has not only been extensively used in biotechnology, health care, food and beverages, chitosan has also been found to be a promising base material for numerous blending, grafting and coating bio-applications [20-23] to improve and achieve the desired properties. Because chitosan has favourable biological properties, such as biodegradability and biocompatibility, it has attracted a lot of attention in the life science and it emerges as an important biomedical material of the future [3].

2.2 Chitosan as a Biomaterial

2.2.1 Introduction of chitosan

2.2.1.1 Definition and chemical structure of chitosan

Chitosan is a naturally occurring polysaccharide. It is also the principal component of chitin, which is one of the most naturally abundant biopolymers, being second only to cellulose and is found in the cell walls of fungi such as mushrooms, yeasts, and the hard outer shells of insects and crustaceans, like crabs, shrimp and krill [26-29]. Chitosan is produced by alkaline deacetylation of chitin. The structures of chitin and chitosan are depicted in Figure 2.2.1. The backbone consists of β-1,4-linked glucosamine with a high degree of N-acetylation, a structure very like that of cellulose, except that the acetyl amino group replaces the hydroxyl group on the C-2 position. Thus, chitosan is poly(N-acetyl-2-amino-2-deoxy-D-glucopyranose). The N-acetyl-2-amino-2-deoxy-D-glucopyranose (or Glu-NH_2) units are linked by (1→ 4) β-glycosidic bonds [30,31].

The difference between chitin and chitosan is essentially related to the possibility of solubilizing the polymer in dilute acidic media. Thus, when the structure can be dissolved in this kind of solvent, it corresponds to chitosan, in the reverse case, to chitin. Therefore, the degree of acetylation (DA), which is related to the balance

between acetylated and deacetylated residues, is essential to define these two terms. When chitin is deacetylated in heterogeneous conditions, the solubility in water is only achieved for DA generally below 30% [32]. Nevertheless, on reacetylating chitosan in homogeneous conditions, it is possible to observe a solubilization up to a DA close to 60% [32,33]. As a consequence, the frontier between chitin and chitosan can be located at a DA of 60%. As we shall see, DA is also an interesting adaptable parameter whose simple modification allows us to provide this series of copolymers with a very great variety of properties. In numerous circumstances, this opportunity gives the advantage of avoiding some difficult and expensive chemical modification.

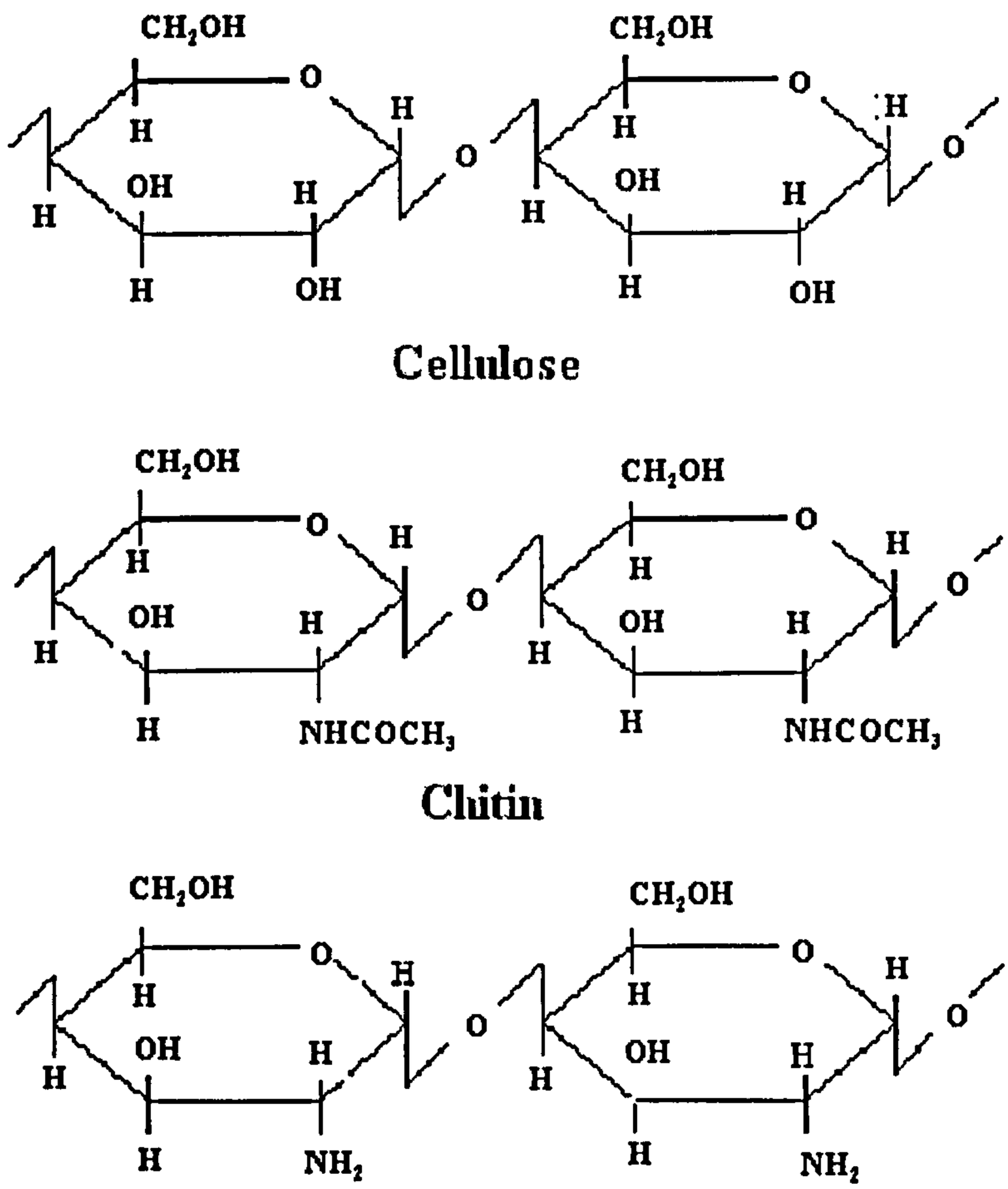

Figure 2.2.1 Chemical structures for cellulose, chitin and chitosan.

2.2.1.2 Production of chitosan

Chitin is produced essentially from the cuticles of crustaceans, especially from crab and shrimp shells. Another interesting source is presented by the endoskeletons of cephalopods. Chitin is closely associated with proteins, inorganic materials, which is mainly $CaCO_3$, and pigments and lipids. Various procedures have been adopted to remove these impurities [30].

Chitosan is synthesized from chitin by removing and refining the acetyl groups through a process called deacetylation [30]. The method is relatively simple and consists of two successive extractions. The first is demineralisation related to the presence of a more or less significant amount of calcium carbonate in the shell. This step is performed by means of mineral acids including HCl, HNO_3, CH_3COOH and HCOOH [30]. It must be performed with care, particularly for medical applications for which the mineral part must be eliminated, but also because polysaccharides are well known to be easily hydrolysed in acidic media. Demineralization with acid may be carried out at temperatures from 0 to 100°C. Table 2.2.1 shows the variation in the HCl concentrations and lengths of time of the treatments used. The second step is deproteinization, which consists of placing the material in alkaline media of sufficient concentration associated with moderate heating [29]. Also, the complete deproteinization is very important in the case of medical uses. A wide range of agents for the deproteinization includes NaOH, Na_2CO_3, KOH, K_2CO_3 etc. NaOH is the preferred agent. Table 2.2.2 shows the treatments for a wide variation in temperature and duration.

Chitosan is obtained from the *N*-deacetylation of chitin and all the methods are derived from the description given in two patents [34,35]. The extent of deacetylation is governed by the alkali concentration, the temperature and the time of reaction. The higher the concentration of alkali the lower the temperature and/or the shorter the time required. The treatment with 50 wt% NaOH at 100°C for 1 hour gave a product having 82% degree of deacetylation [30]. Extending the reaction time to 48 hours enabled almost 100% deacetylation to be achieved [30]. For the exoskeleton of crustaceans containing colouring matter, principally, carotenoids, this matter can be

destroyed by bleaching by using $KMnO_4$, NaOCl, SO_2, and $NaHSO_3$ [30]. The process for the production of chitosan can be described by Figure 2.2.2.

Table 2.2.1 Conditions for demineralisation of chitin-containing waste materials [30]

Material source	HCl Concentration (M)	Temperature (^{0}C)	Time (hour)
Shrimp	0.275	20	16
Shrimp	0.5	Not stated	Not Stated
Crab	0.65	20	24
Crab	1.0	20	12
Crab	1.0	20	1
Crab	2.0	20	48
Prawn	1.57	20-22°C	1-3

Table 2.2.2 Conditions for deproteinisation of chitin-containing waste materials [30]

Material source	NaOH Concentration (M)	Temperature (^{0}C)	Time (hour)
Shrimp	0.25	65	16
Prawn	0.125	100	0.5
Prawn	1.25	100	24
Crab	0.5	65	2
Crab	1.0	80	3
Crab	1.25	100	0.5
Crab	2.5	20	72

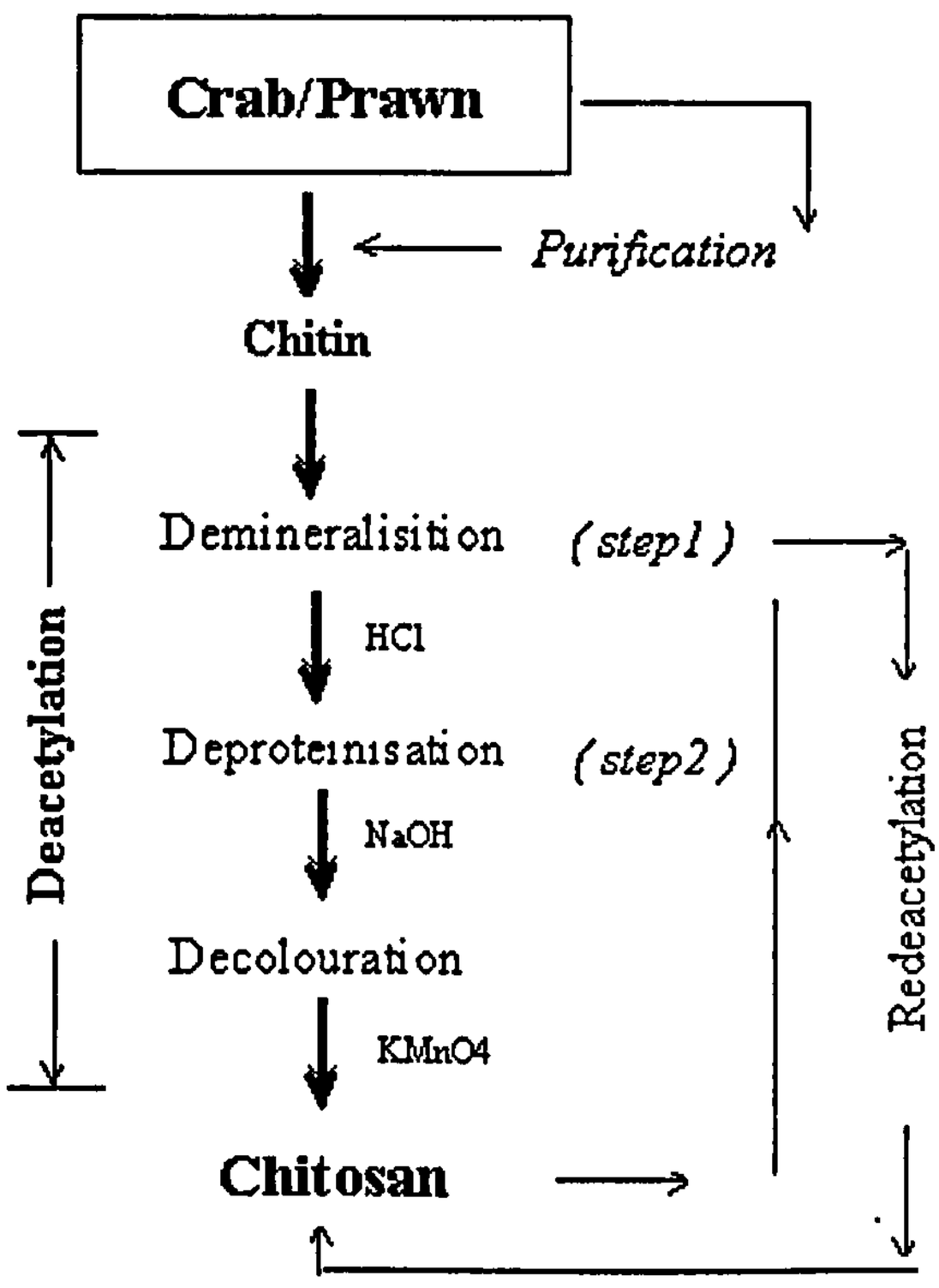

Figure 2.2.2 Chitosan production flow chart

For mild conditions, these methods allow us to reach in one step DA close to 10-15%. If repeated once, the deacetylation can be within 90-95%. Although each step operated in relatively drastic conditions contributes to an important deacetylation, the chain length becomes relatively low at the end of the treatment [30]. In order to avoid this problem, the use of sodium thiophenolate has been proposed, allowing both the catalysis of the reaction and the protection of the polymer chains from degradation. This method allows us also to considerably decrease the amount of sodium hydroxyde used [36].

Deacetylation of chitin yields chitosan, which is relatively reactive and can be produced in numerous forms, such as powder, paste, film, fibre, and others [37,38]. The degree of deacetylation (DD) usually ranges from 70% to 95% depending on the methods used [39]. The DD determines the content of free amino groups in chitosan

and is, therefore, one of the important chemical characteristics. The extent of deacetylation also depends on the applications. For instance, pharmaceutical grade chitosan would require 90 to 95% deacetylation, while the food grade requires between 75 and 80% [40]. The biomedical grade/purified chitosan is prepared by repeating the deacetylation process.

2.2.2 Physicalchemical properties of chitosan

Solubility of chitosan

Solutions of chitosan corresponds to the most important physical state for this polymer, either from a fundamental point of view or for the very great number of applications obtained from this physical form. The solution behaviour of chitosan is informative of the properties of this polymer. Indeed, it reflects the role of the structural parameters and the molecular weight distribution, based on the interactions with the solvent and on the molecular and supramolecular organisation [30]. The various interactions in which this polymer can be involved can be understood from solution behaviours.

As seen from the chemical structure schematised in Figure 2.2.1, chitosan is highly functionalized. When the glucosamine residues are in the free amine form, these structures are strongly involved in the formation of three-dimensional networks by hydrogen bonding [30] and hydrophobic and van de Waals interactions [30]. So, the solubility of chitosan depends on parameters such as the degree of deacetylation, the molecular weight and various environmental parameters[30].

At neutral or basic pH, chitosan contains free amino groups and is insoluble in water, while at acid pH, chitosan is soluble in water due to protonation of the amino functions. The solubility depends on the degree of deacetylation and pH [31,36]. Chitosans with a low degree of deacetylation (≤40%) are soluble up to a pH of 9, whereas highly deacetylated chitosans (≥85%) are soluble only up to a pH of 6.5. The addition of salts to the solution interferes with the solubility of chitosans. The higher the ionic strength, the lower the solubility as charge neutralisation occurs by increasing concentration of the counterion. Increasing degree of deacetylation increases the viscosity [30]. This can be explained by the fact that high and low

deacetylated chitosans have different conformations. Chitosan has an extended conformation with a more flexible chain when it is highly deacetylated because of the charge repulsion in the molecule. However, the chitosan molecule has a rod-like shape or a coiled shape at a low degree of deacetylation due to the low charge density in polymer chain [41,42]. The viscosity of chitosan solution is also affected by factors such as concentration and temperature. As the concentration increases and temperature decreases, the viscosity increases [43].

For thermodynamic reasons, the solubility of a neutral polymer is known to decrease with increase in molecular weight [44]. In the case of chitosan, two factors play an additional role, the possibility of inter-chain associations by hydrogen bonding and the polyelectrolyte character.

The solubility of chitosan can also be constrained by use of acids, which can interact with chitosan in a particular way. The most typical behaviour is that of sulphate ions, which interact with chitosan [30,43].

Chitosan has specific solution properties. The following lists the key solution behaviour of the two amine forms of chitosan [30,43].

Free amine ($-NH_2$):

- Soluble in acid solutions
- Insoluble at pHs >6.5
- Insoluble in H_2SO_4
- Insoluble in most organic solvents

Cationic amine ($-NH_3+$):

- Soluble at pHs<6.5
- Forms viscous solutions
- Solution shear thinning
- Forms gels with polyanions

The origin and the quality of the materials and processes can also play an important role in the solubility of chitosan. Although the chemical structure of chitosan is independent of the source, the DA value and molecular weight are related to the source and the quality of the treatment.

Chitosan gel

Chitosan can exist in a gel state. This gel is always formed in the presence of water. The formation of a physical gel needs to be at a concentration sufficiently high to favour the chain entanglement necessary for the formation of a continuous gel. This critical concentration is well-known as C^* and is easily deduced from the inverse of intrinsic viscosity [43]. The formation of a gel can only be achieved when chitosan is initially in the form of a salt of a weak acid such as acetic acid. By contract, if chitosan is in the form of a hydrochloride, gel formation is not observed. The gel formation is related to the balance between attractive and repulsive interactions along the polymer chains and the ability to favour the formation of junction points by means of ordered domains. This balance can be influenced in different ways. It is obviously dependent on the molecular mobility of polymer chains in the media and on the degree of deacetylation [30,43]. In some circumstances, the gels are thermoreversible 30,43]. They can also be fully regenerated in the form of pure chitosan gels after a complete exchange of the components of the initial media of their formation [30,43].

The mechanical properties of chitosan gels are very interesting because of their numerous possible applications. As for all gels, they obviously depend on the density of reticulation, the polymer concentration in the gel, and the molecular weight. The limitation comes from the fact that the best gels are necessarily obtained from the highest molecular weights, the highest DA, and the highest polymer concentrations. The consequence is that it is difficult to prepare chitosan gels containing more than 2 % polymer because of high viscosities and the kinetics of gelation [43]. These gels are completely exchangeable in pure water with no major alteration of their properties and have significant potential of medical applications [43]. These gels are formed mainly due to the conjugation of hydrogen bounding and hydrophobic interactions. From a physical point of view, in addition to their good mechanical properties, in relation to a high polymer concentration, they necessarily have a high porosity. The

consequence is that these gels can be used to interact with a great variety of molecules [43].

Crystallinity and morphology

Chitosan is a semi-crystalline polymer and as such, most of its properties in the solid state depend essentially on the percentage of the crystalline part and sometimes on the crystalline form [30,43]. The degree of crystallinity is a function of the degree of deacetylation. The crystallinity, as measured by X-ray diffraction at the different degrees of deacetylation, is shown in Figure 2.2.3 [45]. During the deacetylation up to a degree of deacetylation of 71%, the crystallinity decreased slightly and then more rapidly, so that by 89% deacetylation the crystallinity peaks had almost disappeared and the sample was completely amorphous.

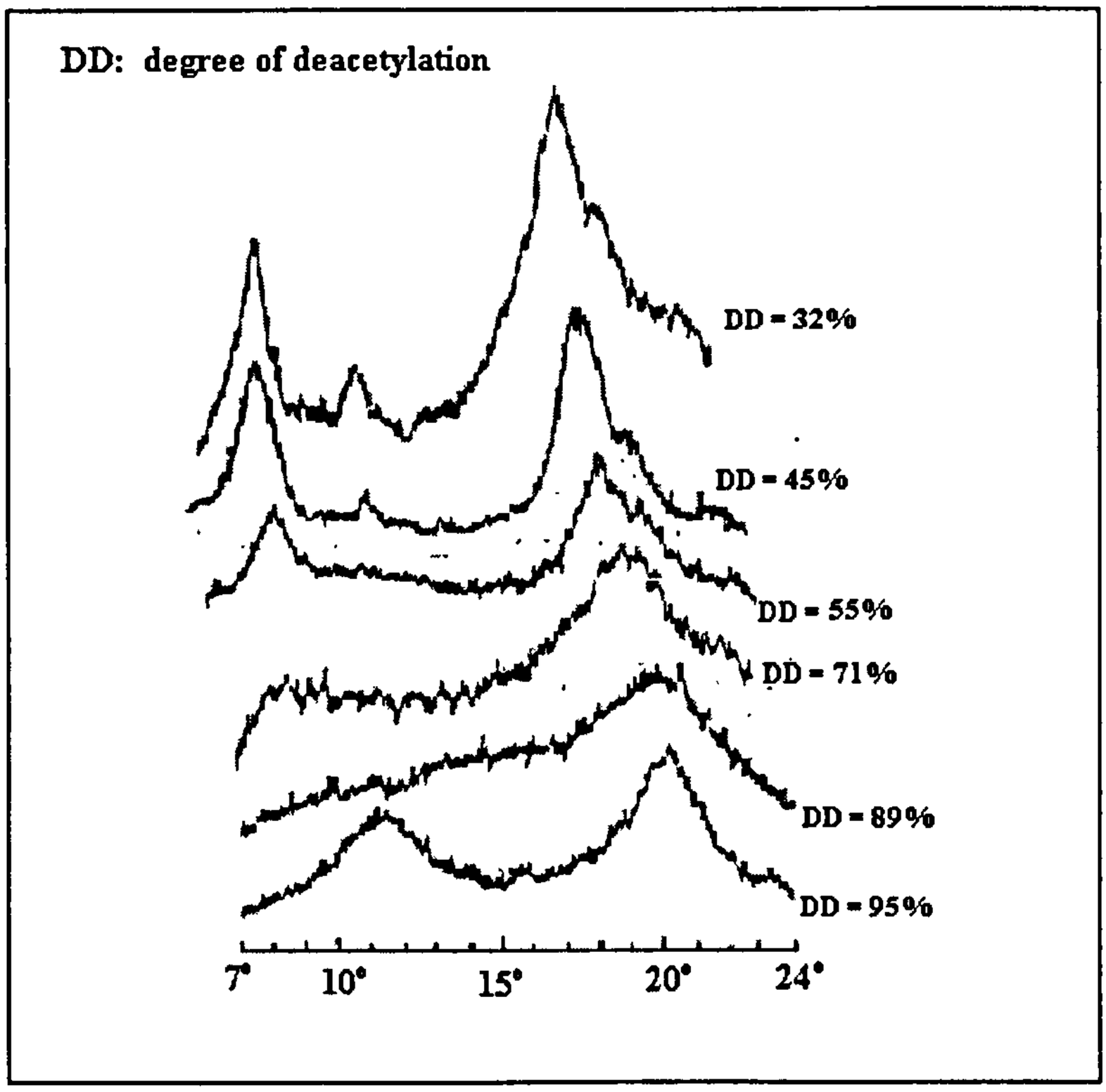

Figure 2.2.3 X-ray diagrams of chitosan with different degrees of deacetylation [44].

By 95% deacetylation, the material was again crystalline, but the peak position had moved as seen in Figure 2.2.3. 0 and 95% deacetylated chitosan give maximum crystallinity, while intermediate degrees of deacetylation give the lowest crystallinity [46]. The crystalline structure of chitosan means that it is stable and insoluble in aqueous solutions above pH 7, but fully soluble in dilute acids such as acetic and formic acids [30,43].

A number of changes in the infrared spectrum of chitin during deacetylation have been attributed to changes in the degree of crystallinity [47]. In the 2600-3800 cm^{-1} region, as the extent of deacetylation increases from 91% to 99%, three distinct, sharp peaks appear at 3455, 3365 and 3313 cm^{-1} as shown in Figure 2.2.4. These bands were described [47] as 'crystallisation-sensitive' bands.

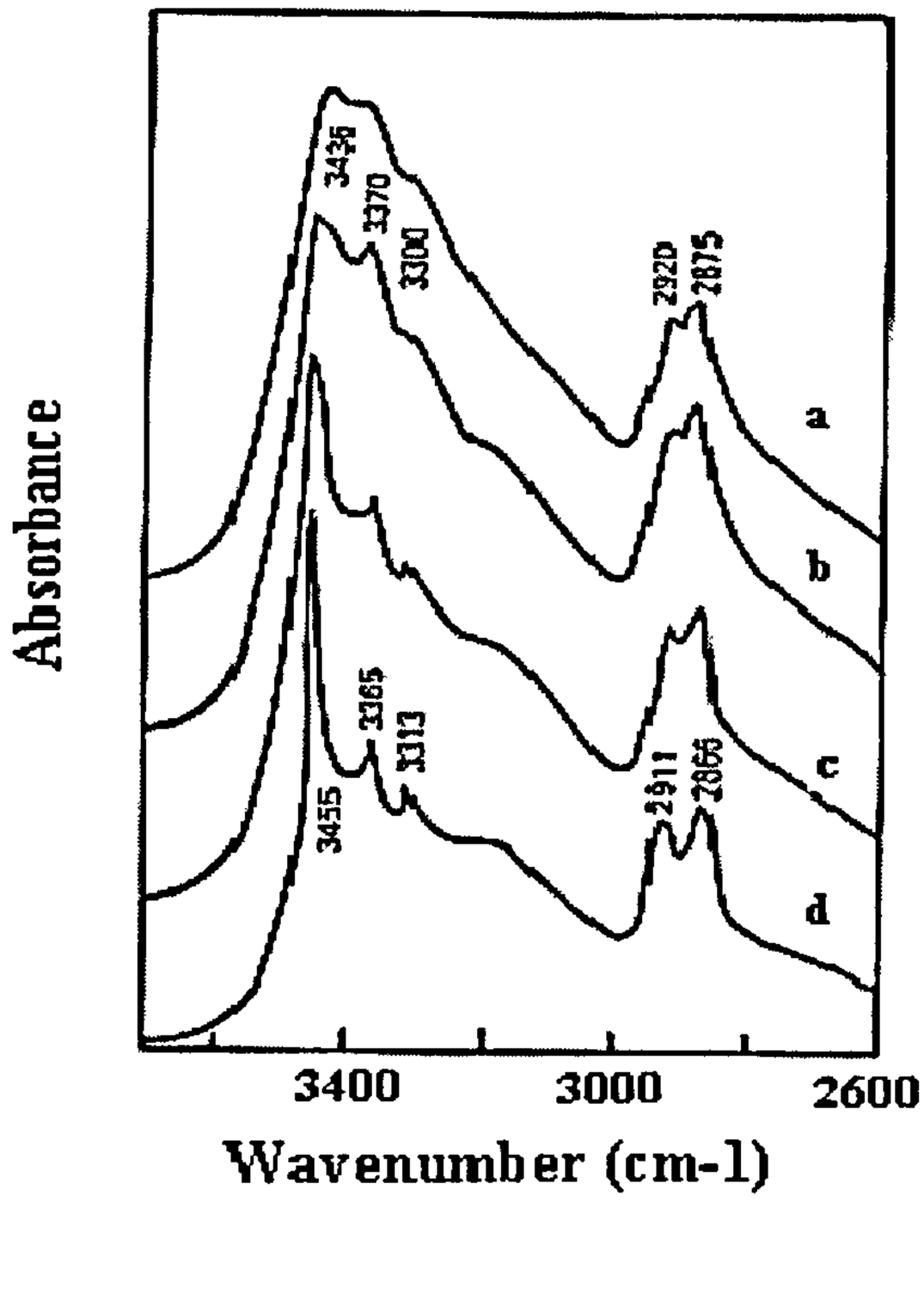

Figure 2.2.4 IR spectra of chitosan with different degrees of deacetylation [39]: (a) 88%, (b) 91%, (c) 96%, (d) 99%.

The solid state of chitosan can vary from a morphologyical point of view. Its properties in this state depend on the origin of the material and on the method of processing [30,43]. Moreover, they depend on whether chitosan is used as received from the manufacturer or whether it has been regenerated after solubilization. In former case, the material has the memory of the crystalline organisation and in the later case the solubilization destroys this organisation.

Hydrogen Bonding and Electrostatic Interactions

Alcohol, amine, amide, and ether functions present in the structure of chitosan can be involved in the formation of hydrogen bonds either with various substrates or by means of inter- and/or intra-molecular bonding [30,43]. The most important substrate in the formation of this kind of interaction is water. It participates in the formation of the hydrogen bonds responsible for the solubility of chitosan in water. Nevertheless, the competition between inter- and intra-molecular bonding is always present. This competition is regulated by the balance between attractive and repulsive interactions. Here, the degree of ionisation and the degree of deacetylation can play important roles. In the solid state, the hydrogen bonding is responsible for the ordered structures in the crystalline domains and for the inter-chain interactions which reinforce the stability of these domains.

The polyelectrolyte character of chitosan was clearly illustrated by Kurita *et al.* [47]. At acid pH, chitosan is a linear polyelectrolyte and has a high charge density. The chitosan molecules show strong positive charges that attract negatively-charged molecules and ionically bind them [30,49-51]. They also form gels with polycations at low pH and have antacid anti-ulcer activities [29,49-51]. The charge density allows chitosan to form insoluble ionic complexes or complex coacervates with a wide variety of water-soluble anionic polymers. The adsorption capacity for metal ions depends on the amine group concentration of the chitosan. It is not the total concentration, but the concentration of accessible amine groups that is important, since these are the ones available for complex formation. Because the chitosan charge density is pH dependent, transfer of these ionic complexes to physiological pH can result in the dissociation of a portion of the immobilised polyanion. This property can be used as a technique for drug delivery [4,5].

The chemical structure of chitosan is able to give rise to all the known interactions of chemistry. The nature of these interactions depends particularly on two parameters, the degree of deacetylation and the degree of ionisation of the ionised functions.

It can be seen from Figure 2.21 that chitosan has a reactive amino group at C_2 and a hydroxyl group at the C_6 positions, which can be modified chemically for various applications [52]. The important chemical reactions of chitosan were reviewed by Muzzaraelli in the late 1970s [53]. The more recent developments in the chemical modifications of chitosan, along with the resulting properties, were reviewed by Kurita [31].

Hydrophobic and van der Waals interactions

Hydrophobic and van der Waals interactions are often used to interpret results especially in the case of amphiphilic polymers such as biopolymers. If we consider the structure of chitosan, the –CH, $-CH_2$, $-CH_3$ and $-NH_2$, groups are hydrophobic. The conformation of chitosan in solution is relatively stressed and stiffness increases with DA. As a consequence, the deprotonation of amino groups and the increase of DA, temperature and dielectric constant influence not only the hydrogen bonding, but also this kind of interaction. When the temperature of chitosan increases, the solubility of chitosan decreases as a result of the disruption of hydrogen bonding with water and the increase in the hydrophobic and van der Waals interactions [30,43].

2.2.3 Biological properties

Biodegradability

Chitosan is completely absent in mammals. The first interesting biological property of chitosan is its ability to be biodegradable and bioresorbable. Chitosan-degrading enzymes were first identified by Monahghan *et al.* [54]. Studies with *Penicillium islandicum* indicates that the enzyme shows high specificity towards hydrolysis of the glycosidic link between C(1) of an N-acetyl-D-glucosamine residue and C(4) of a D-glucoisamine residue. The degradation process depends on the form of chitosan. Microcrystalline chitosan is more susceptible to enzymatic decomposition in comparison to standard chitosan [30]. The degradation process carried out in the

enzymatic media was also estimated according to the amount and type of liberated oligoaminosaccharides [30].

In vivo, chitosan is degraded by enzymatic hydrolysis. The primary agent is lysozyme, which appears to target acetylated residues [55]. However, there is some evidence that some proteolytic enzymes show low levels of activity with chitosan. The degradation products are chitosan oligosaccharides of variable length. The degradation kinetics appears [56] to be inversely related to the degree of crystallinity, which was controlled mainly by the degree of deacetylation. Highly deacetylated forms (e.g.>85%) exhibit the lowest degradation rates and may last several months in vivo, whereas samples with lower levels of deacetylation degrade more rapidly [56].

Biocompatibility

Chitosan lacks irritant or allergic effects and is biocompatible with both healthy and infected human skin [57]. The biocompatibility of chitosan has been studied. The first important results were obtained from experiments on dogs [58]. It was shown that in the case of a graft of aorta covered with chitosan, there was a good integration of the synthetic material owing to a local haemostasis on the surface of the material created by the chitosan coating. The direct injections of chitosan in blood have also been studied. In an experiment on rabbits, intravenous injection of chitosan oligomers was made at a dosage 4.5mg/kg body weight. No abnormal physiological symptoms were noticed after treatment for 11 days [59]. Some studies were performed in vitro on the role of the addition of chitosan solutions to cell suspensions. In the case of fibroblasts, it was observed that the presence of chitosan at low concentration inhibited the proliferation of the cells, but did not act as a cell killer [60].

2.3 Modification of Chitosan

2.3.1 Poly(ethylene oxide)

Since the 1960s, a range of synthetic biodegradable polymers has been developed, including poly(L-lactic acid) (PLA), polyglycolide (PGA) and poly(lactide-co-

glycolide) (PLG). Of recent interest is poly(ethylene oxide) (PEO). As shown below, PEO is a polyether type of the water-soluble synthetic polymer.

$$-[CH_2CH_2O]_n-$$

When the molecular weight is less than 10,000 Daltons, the polymer is called poly(ethylene glycol) (PEG). Polymers with a higher molecular weight are known as poly(ethylene oxide) [16]. Compared other polyethers, such as poly(propylene oxide), PEO is highly water soluble [60]. Kjellander and Florin [62] explained the higher water solubility of PEO in terms of a good structural fit between water molecules and the polymer, resulting in hydrogen bonding between the ether oxygen of PEO and water molecules.

With PEO, aqueous solubility decreases with increasing temperature. The decreased solubility at elevated temperatures is due to a decrease in hydrogen bonding and corresponding increase in hydrophobic interactions between polymer chains [63]. Bjorling *et al.* [64] reported that PEO adapts to a gauche conformation in polar solvents such as water and a trans-conformation in non-polar medium. The gauche conformation would be more suitable for hydrogen bonding.

At the solid-liquid interface, PEO anchored through terminal ends will interact with water molecules and extend into the bulk aqueous medium [65]. Surface-bound PEO molecules are very effective in preventing adsorption of other macromolecules by the steric repulsion mechanism [66].

PEO-rich surfaces have been prepared by physical adsorption of PEO [67]. Only high molecular weight PEO (M_w > 100,000) can be effectively adsorbed on hydrophobic surfaces [67]. PEO is relatively inert toward biological species, whether it exists in free homogeneous solution, is absorbed onto a substrate, is grafted onto polymer surfaces or formed into networks [68-70].

PEO is widely used to stablize aqueous colloids and dispersions, commonly by means of physical adsorption followed by steric repulsion of the modified particles [70,71]. The low molecular weight PEG is normally chosen as a pre-polymer in the synthesis

of polyurethanes, epoxies, and other polymers. PEG is widely used in the chemical, biochemical and biotechnological industries to make a variety of non-ionic surfactants [71].

PEO is both hydrophilic and hydrophobic, due to its solubility in both aqueous and non-polar solvents. In solutions, it tends to be highly dynamic, and yet it can readily pack and form crystalline solids. Despite its dynamics and mobility, it can complex and aggregate and develop specific helical and near-helical conformations [16]. More importantly, it can interact and complex with a variety of ionic and hydrogen bonding structures. PEO, as a molecule alone and as part of other molecules, is generally non-toxic and considered safe for a wide variety of food, cosmetic and biomedical applications [1-3]. It is a water soluble and biocompatible polymer, which are notable advantages of this material.

PEO has often been used as a biomaterial due to its well-documented biocompatibility [72]. It is also noted for its low protein binding affinity [71]. This is especially critical in medical applications where protein adsorption on surfaces tends to alter its properties. This was evident in the study carried out by Alcantar *et al.* where poly(ethylene glycol) (PEG)-covered surfaces showed efficacy in protein rejection when brought in contact with albumin in solution [73]. Nelson *et al.* [74] tested the affinity of albumin on PEO-treated surfaces and concluded that improved biocompatibility was achieved when the high albumin affinity drug, warfarin, was tethered to the surfaces by PEO.

Being a neutral and highly hydrophilic polymer, PEO tends to minimize electrostatic and hydrophobic interactions, respectively [75,76]. The high mobile and dynamic PEO chains create a strong repulsive interaction between proteins.

2.3.2 Chitosan and Poly(ethylene oxide) (PEO) Blends

Chitosan is an amino polysaccharide and is thus anticipated to have high potential as a specialty polymeric material. However, these potential benefits are scarcely utilized because of the problems associated with solubility, multifunctionality and reactivity. To develop advanced functions leading to utilization, much attention has been paid to

the modification of chitosan. Several chitosan modifications have been carried out up to now based generally on two types of processes: physicalchemical and chemical [77-82].

A chemical modification of chitosan based on a substitution of its amino - and/ or hydroxyl- groups has changed the behaviour of this polymer [77-82]. A physicalchemical modification of chitosan, concerned with suitable changes of molecular as well as super-molecular structure of the polymer, enables the creation of valuable forms of this natural high molecular weight compound with new, original properties and behaviour [77-82].

There have been some reports dealing with polyblends of chitosan with other natural or synthetic polymers [83-85]. For example, chitosan/poly(vinyl alcohol) blend film was found to have good dyeability, a chitosan/poly(vinyl alcohol) blend membrane was used in the pervaporation of ethanol and water [82,83], and chitosan/nylon-4 blends were found to have good mechanical properties and retain the excellent chelating ability of chitosan [85].

Recently, chitosan and poly(ethylene oxide) (PEO) blends have been reported for the preparation of membranes for haemodialysis [86] and semi-IPNs for pH-sensitive drug delivery [87].

Investigations by several researchers demonstrated favourable intermolecular interactions between chitosan and PEO [88,89]. Jiang and Han [88] studied the inter- and intra-molecular interactions between chitosan and PEG by means of a viscosity method. Experimental results were fitted into a revised calculation of the thermodynmic interaction to obtain the thermodynamic parameter, χ, where a negative value of χ indicates an attractive intermolecular interaction between chitosan and PEG.

Mucha *et al.*[89] further attested the miscibility of chitosan/PEO blends in the amorphous phase by the negative value of the Flory-Huggins interaction parameter. Their infra-red (IR) results proved that the intermolecular interaction between

chitosan and PEO molecules was by hydrogen bonding between the hydroxyl groups of chitosan and the ether oxygens of PEO, and that the amide groups do not participate in the molecular interaction between chitosan and PEO.

Wang *et al.* [90] further studied the miscibility of blends of PEO with two chitosans, which have the mole fraction of N-acetyl-D-glucosamine (F_A) values of 0.25 and 0.02, respectively. The results indicated that both commercial chitosan (0.25) and chitosan (0.02) are partially miscible with PEO due to the specific interactions between chitosan and PEO molecules. These interactions arise from the formation of intermolecular hydrogen bonds between chitosan and PEO. The specific interactions in chitosan (0.25)/ PEO blends are greater than in chitosan (0.02)/PEO blends, and maximum interaction was observed at 50% PEO content for the former and at 25% PEO content for the latter. This is because the PEO component is better dispersed in the continuous chitosan (0.25) phase than in the chitosan (0.02) phase due to the more amorphous structure of chitosan (0.25) compared with chitosan (0.02) [90].

The mechanical properties of chitosan/PEO blend films were examined by Alexeev *et al.* [91] and it was observed that the chitosan/PEO blends containing 16.7weight % of PEO had a 6 times improvement in the relative elongation at break and the tensile strength doubled. It was shown that at 16.7 weight % of PEO, the film structure is likely to be less heterogeneous, therefore, giving rise to the improved mechanical characteristics.

Recently, Khoo *et al.* [92] have investigated chitosan blends with hydrophilic polymers including poly(vinyl alcohol) (PVA), poly(ethylene oxide) (PEO) and poly(vinyl pyrrolidone) (PVP) as candidates for oral gingival delivery systems. The results from DSC, DMTA, FT-IR spectroscopy and tensile testing indicated that the chitosan/PEO and chitosan/PVP blends showed evidence of miscibility in all blend ratios studied, while the chitosan/PVA blend only showed evidence of interaction for the (50:50) and (80:20) blends, but not for the (20:80) blend. The study also indicated that chitosan blends were superior in other properties compared to chitosan alone. These included improved comfort and reduced irritation, ease of processing, improved flexibility, and enhanced dissolution. Blends of chitosan with different hydrophilic

polymers are thus promising candidates for formulation in oral mucosal delivery systems.

The porous structure chitosan/PEG blend membrane has been prepared by a selective dissolution method for the purpose of biomedical applications such controlled drug delivery [93]. The results indicated that the pore structure induced by this method is controlled by the compatibility of chitosan and PEG and by the multiphase structure.

2.4. Applications of Chitosan

Chitosan, being a deacetylated chitin, is a natural, biodegradable, water-insoluble biopolymer. Due to its better solubility in organic acids, chitosan is much more useful than chitin. Specific properties of chitosan specially connected with its biodegradability and bioactivity result in this polymer being a perfect raw material for several different applications such as in medicine, pharmacy, agriculture, food processing and cosmetics. The most observed and spectacular development of chitosan utilization in the above-mentioned areas started in the last few years [94,95], especially in the medical world. Table 2.4.1 highlights some of its applications.

2.4.1. General applications

Waste Water Treatments

The presence of a high amino content in chitosan makes it a powerful chelating agent [96] compared with other materials like activated sewage sludge, poly(p-amino-styrene) or bark. Harmful metal ions such copper, mercury, lead and uranium are readily removed from waste water. Hirano *at al.* [97] found that 40-74% of the available uranium could be recovered from river and lakewater and 3% from seawater. The extremely low recovery rate from seawater might have been caused by the presence of large quantities of other metal ions. Recent studies reported that the chelating ability of chitosan could be improved by homogenous hydrolysis [98-100] and complexation with polymers such as glucan [101].

Table 2.4.1 Applications of Chitosan

		References
Medical	Controlled release of drugs Artificial blood vessels Artificial skin/skin burns Wound healing ointments and dressings Contact lens/eye bandages Blood chlolesterol control Transportation of cells Dentistry Surgical sutures	1, 3, 4, 18, 118,132, 111, 112, 113, 114,115,116, 133,134,135,18 8
Food	Antichlolesterol and fat-binding Preservatives Food stabilizer Flavor and tastes Nutritional additives	1, 3, 4,
Waste and water treatment	Removal of metal ions Sewage effuents Drinking water Pools and spas	97,98, 99,100
Agriculture	Seed coating Hydroponic/fertilizer Controlled agrochemical release Nematocides and insecticides	103,104, 105
Cosmetics and toiletries	Hair treatment Moisturizers Face, hand and body creams Make up powder Nail polish Toothpaste Foam enhancing	106,107,108, 109
Pulp and paper	Surface treatment Photographic paper Carbonless copy paper	1,3,29,178
Product separation and recovery (bioapplications)	Immobilization of enzymes/cells Membrane separations Permeability control Reverse osmosis	1,4,5

No single decolourisation method is likely to be the optimum for all waste water streams [102]. Chitosan has an extremely high affinity for many classes of dyes, including disperse, direct, reactive, acid, vat, sulphur and naphthol dyes [30]. Chitosan is versatile in sorbing metals and surfactants, as well as derivatization to attract basic dyes and other moieties (e.g., proteins from food processing plants).

Waste water pH may be an important factor in the sorption of certain dyes onto chitosan because, at low pH, the free amino groups of chitosan are protonated, causing them to attract anionic dyes.

Agriculture

Chitosan has been used successfully to reduce environmental damage caused by agrochemicals, such as fertilizers, herbicides, and pesticides. Reports showed that coating fertilizer pellets with films of *N*-acetyl or *N*-propionyl chitosan warrant a controlled-release effect, where the herbicide was trapped in the chitosan gels and was released over an extended period of time. The release time was greatly increased as compared to the uncoated control beads [103].

Chitosan is also useful in improving soil properties and preparing hydroponic fertilizer. It was found that the *N*-methylenechitsan gel bed greatly reduced the rate of water evaporation. Not only that, when *N*-methylenechitosan was mixed with sand and clay, young seedlings in this mixture survived longer when watering stopped, than seeds in a sand bed [104].

An increase in crop yield was noted when chitosan was applied in a seed coating application. Beneficial effects such as inhibition of fungal pathogens in the vicinity of the seeds and enhancement of plant-resistant responses against disease were observed [105]. Being naturally occurring and biodegradable, pollution problems are greatly reduced and chitosan would easily find its way in potential agriculture applications.

Cosmetics

Another application of chitosan can be found in the cosmetic industries [106]. For example, chitosan has the ability to remove left-over starch contained in shampoos. Its use also has the effect of conferring shine and strength to hair due to interactions

between the polysaccharide and hair proteins. Other uses in cosmetics include moisturizers, hair and skin fixatives, hair conditioners, nail polishes, cleaners and bath lotions [107-109].

Food and nutrition

Animal nutritional studies have shown that the utilisation of whey may be improved if the diet contains small amounts of chitosan. This improvement is attributed to the change in the intestinal microflora brought about by the chitosan supplement [110].

Opthalmology

Chitosan possesses all the necessary characteristics for making contact lenses, including optical clarity, mechanical stability, gas permeability, wettability, sufficient optical correction and immunological compatibility [111]. Among these properties, gas permeability is the most important since oxygen must be transported from the tear fluid to the eye surface, whereas carbon dioxide needs to diffuse back from the eye surface to the fluid. These properties, coupled with the anti-microbial and wound healing benefits make chitosan suitable for the development of ocular bandage lenses [111].

Artificial skin

Chitosan has been employed for making artificial skin [116]. Several investigations were carried out and reported [117-119]. A design for long-term chronic use was proposed by Yannas *et al.*, whose focus was on a non-antigenic membrane, which serves as a biodegradable template for synthesis of neodermal tissue [120]. Chitin and chitosan can be made into fibres and have been found to be useful as absorbable sutures and in accelerating the healing of wounds by up to 75% [121-123]. Chitin sutures resist attack in bile, urine and pancreatic juice, which are problem areas with other absorbable sutures [123].

A chitosan-gelatin complex has been developed for surgical dressing by Sparkes and Murray [124], where the stiffness of the resulting dressing can be reduced by incorporating a certain amount of plasticiser such as glycerol and sorbitol into the mixture. It was claimed that, contrary to conventional biological dressings, this experimental dressing displayed excellent adhesion to sub-cutaneous fat. Another

development stemmed from polyelectrolyte complexes of chitosan with sulfonated chitosan, where Kim and Min [125] proposed that the oligomers of degraded chitosan by tissue enzymes accelerated wound healing. This material was found to be effective in regenerating the skin tissue in the area of the wound. Kifune *et al.* [126] developed a new wound dressing, Beschitin W, which contains a non-woven fabric and has been proven to be beneficial in clinical practice.

Mi *et al.* [127] designed a novel asymmetric chitosan membrane whereby a macroporous sponge-like sub-layer supported the skin surface top-layer. This membrane showed controlled evaporation water loss and excellent oxygen permeability. It also promoted drainage of wound extrudate with minimum exogenous microorganism penetration due to the dense skin layer and the inherent anti-microbial property of chitosan. The asymmetric membrane acted as a haemostatic agent and histological examination confirmed an increased epithelialization rate and a well-organized deposition of collagen in the dermis.

Biagini *et al.* [128] developed a N-carboxybutyl chitosan dressing for plastic surgery donor sites. This dressing could promote ordered tissue regeneration compared to control donor sites. Better histoarchitectural order, better vascularization and the absence of inflammatory cells were observed at the dermal level, while fewer aspects of proliferation of the malpighian layer were reported at the epidermal level.

A non-adherent wound dressing with sustained anti-microbial capability has been formulated and investigated by Loke *et al.* [129]. This double layer dressing comprises a carboxymethyl-chitin hydrogel upper layer capable of imbibing 4 times its own weight of water and is semi-porous to water vapour. The lower layer is a chitosan acetate foam incorporated with the anti-microbial agent chlorhexidine gluconate. *In vitro* drug release study showed that at the optimal loading concentration of 1% (w/v) chlorhexidine gluconate, the chitosan acetate foam was able to release up to 92% of its total chlorhexidine gluconate content at 37°C. It was reported that when placed on open wounds, this dressing serves the dual function of controlling fluid and heat loss from the wound and acting as a prophylaxis against wound sepsis [129].

Although great strides have been taken to improve the quality of care of burn victims and patients with diabetic ulcers, the current materials are not able to induce healing in close to 100% of the cases. Even in successful applications, the cosmetic results are not always favourable. Significant efforts in the development of a new class of materials for skin regeneration are needed [3].

2.4.2 Drug-delivery systems

Drugs are very important for health care and life. In recent years, the studies on anti-cancer drugs, anti-AIDS drugs [4,40], gene therapies and anti-sense drugs has been very active and brought great happiness to mankind. However, most drugs, including those mentioned above, are far from ideal for simple administration, e.g. by swallowing or injection. [4,5,40,130]. They may have very poor solubility or rapid metabolism and instability or unfavourable biodistribution or very high toxicities [131].

Controlled drug delivery technology represents one of the most rapidly advancing areas of science. Such delivery systems offer numerous advantages compared to conventional dosage forms including improved efficacy, reduced toxicity and improved patient compliance.

The science and technology in this field have advanced significantly since 1980s. Some drug delivery systems have been invented and developed, mainly including diffusion or biodegradation control systems, water penetration control systems, self-regulated controlled systems and external regulated control systems etc. [132-135].

All controlled release systems aim to improve the effectiveness of drug therapy. The different forms that improvement can take can be summarised by two types of control over drug release, temporal and distribution control.

In temporal control, drug delivery systems aims to deliver the drug over extended duration or at a specific time during treatment. Controlled release over an extended duration is highly beneficial for drugs that are rapidly metabolised and eliminated

from the body after administration and it ensures that the maximum possible benefit is derived from the drug. In distribution control, drug delivery systems aim to target the release of the drug to the precise site of activity within the body. A diverse range of mechanisms has been developed to achieve both temporal and distribution controlled release of drugs using polymers. This diversity is a necessary consequence of different drugs imposing various restrictions on the type of delivery system employed.

The drug is released by diffusion or biodegradation and enters the body systematically. Controlled-release dosage forms enhance the safety, efficacy and reliability of drug therapy [40]. They regulate the drug release rate and reduce the frequency of drug administration to encourage patients to comply with dosage instructions [5,40,136]. This is a very important aspect of health care. As a material for drug carrier use, polymers, especially chitosan, are playing an increasingly important role for the above control system formulations due to their enormously useful properties, such as degradability, non-toxicity and biocompatibility [7,8]. The degraded products of chitosan do not introduce any disturbance in the body. Hence, it can be a suitable matrix, available in different forms, for sustained release of various drug formulations. Various drugs may be incorporated into a chitosan matrix in a variety of forms for controlled-release therapies [136-143].

Chitosan direct compression tablets triggered the sustained release of prednisolone [144,145], a water-insoluble drug. The release rate was controlled by changing the relative amounts and degree of deacetylation of chitosan and sodium carboxymethycellulose. Interaction of the drug diclofenac with the chitosan amino groups is a possible reason for the sustained release [146].

Recently, chitosan has gained importance as a disintegration agent due to its strong ability to absorb water. It has been observed that chitosan contained in tablets at levels below 70% acts as a disintegration agent [147,148]. Neau *et al.* [149] studied the sustained-release characteristics of ethylcellulose tablets containing theopyylline as the model drug. Several equations were tested to characterize release mechanisms with respect to the release data. The investigations revealed that, at high drug loading, the drug was released by a diffusion mechanism with a rate that increased with increasing aqueous solubility. At low drug loadings, polymer relaxation also

became a component of the release mechanism. However, its contribution to drug release was less pronounced as drug solubility decreased, becoming negligible in the case of theophyline [147,148].

Micro-spheres are one of the most useful and most widely studied drug delivery systems for the release of therapeutic agents. Chitosan micro-sphere degradation can be controlled by various cross-linking agents for specific applications. The release of mitoxantrone from glutaraldehyde cross-linked chitosan micro-spheres has been studied [150]. The histological analysis showed that the micro-spheres were tolerated by the living tissue [151]. The controlled release of bovine albumin and interleukin-2 from alginate-chitosan micro-spheres has also been investigated. The sustained release of proteins from micro-spheres was for a greater duration than that from other micro-sphere formulations [152].

Thacharodi and Rao [153-155] reported permeation-controlled trans-dermal drug delivery systems using chitosan membranes. The drug release was significantly reduced when crosslinked chitosan membranes were used to regulate drug release in the devices. It was observed that the drug release rate depends on the crosslink density within the membranes. Highly cross-linked chitosan membranes released only approximately 35% of the drug compared with 70% from weakly cross-linked membranes [153-155].

Interfacial formation of a chitosan polyelectrolyte complex film on the surface of theophylline granules containing sodium tripolyphosphate has been investigated by Kawashima *et al.* [156]. This film coating on the granules significantly reduced release rate, which followed zero-order kinetics. Its thickness and hardness also affected the drug release rate [156].

Since chitosan is non-toxic and can be administered orally, it has mainly been studied as an oral delivery system in the form of tablets or micro-spheres. Its mucoadhesive and permeation enhancement properties have been used for trans-dermal and sustained gastrointestinal drug delivery. Its biodegradability and tissue compatibility make it a suitable component for implantable delivery devices. Despite the outstanding scientific progress being made in terms of the application of chitosan in

drug delivery systems, chitosan-based drug delivery products have not yet been launched on the market. With a wide range of potential applications in medicine and pharmaceutics, there is tremendous scope for future research on chitosan and its derivatives [40].

2.4.3 Separation membranes

Recent developments in the design of artificial kidney systems have made possible repetitive haemodialysis and the treatment of patients with kidney insufficiently. Haemodialysis is a method by which specific substances such as urea, uric acid, creatinin, among others, are separated from the blood in the course of so-called dialysis. During dialysis, the blood is led from blood vessel through an artificial kidney in which it flows along a semi-permeable membrane. An appropriately-composed rinsing liquid is located on the other side of the membrane into which the toxic substances travel through the semi-permeable membrane. The cleaned blood is then led back to the body. If such a treatment is not administered the blood becomes so strongly enriched with these harmful substances that sooner or later death occurs [4].

At present, commercially available dialysers are equipped with membranes made either of natural or synthetic hydrophilic and hydrophobic polymers. Previously, most membranes employed for haemodialysis were of a cellulosic basis, namely membranes of regenerated cellulose. Although advances have been made in the design of haemodialysis instruments, the problem of blood-membrane interactions remains a major obstacle in haemodialysis treatment [157]. Surface-induced thrombosis and serum complement activation are the most serious clinical consequences of blood-membrane interactions. Thrombus formation on biomaterial surfaces is initiated by plasma protein adsorption, followed by the adhesion and activation of platelets [158]. On haemodialysis membranes, heparin is infused frequently to minimize surface-induced thrombosis. Anti-coagulation with heparin is associated with several side-effects, including the high risk of haemorrhage [159]. Complement activation by the alternative pathway results in a transient disease in leucocyte count observed within 30 minutes of hemodialysis treatment [160]. There has been on effort to improve the blood compatibility of hemodilysis membranes

[161-163]. In addition to surface modification of existing membranes, it is necessary to identify other materials with improved permeability as well as blood compatibility properties.

Chitosan, which has excellent film-forming properties and good mechanical strength suitable for haemodialysis [164], has the potential to be used as an artificial kidney membrane [36], When in contact with blood, chitosan, unfortunately, promotes plasma protein adsorption, platelet adhesion and thrombosis [165,166]. In order to improve the blood compatibility of chitosan membranes, without compromising the permeability properties, extensive research efforts [167-175] are being directed towards developing new or modified materials

Several studies of chitosan/poly(vinyl alcohol) (PVA) blend membranes have been reported [167-172]. According to Miya et al. [167], chitosan formed clear homogenous blends with PVA, and the tensile strength of the blend was greater than the component value. These membranes showed good permeability.

Kim *et al.* [171] studied a chitosan/PVA blend membranes cross-linked with varying amounts of glutaraldehyde. The permeability was found to be pH dependent. The effect of cross-linking and blending of chitosan with PVA on the permeability of vitamin B-12 were also studied. The partition coefficients were nearly constant [172]. Albumin-blended chitosan membranes had superior permeability properties for smaller molecules compared to the standard cellulose membranes, and these membranes showed maximum reduction in platelet adhesion in comparison to other membranes as reported by some workers [173]. Chitosan membranes modified with thiol groups were investigated for the permeability of KCl and sucrose by glycol [174]. The study showed that permeation control can be achieved by varying the amount of crosslinking agent. Hirano *et al.* [175] prepared a series of membranes from chitosan and its derivatives and membranes showed improved dialysis properties.

Recently, chitosan/PEO blend membranes for haemodialysis were investigated by Amiji [86]. The results indicate improvements in the permeability and blood compatibility. The equilibrium hydration increased from 44% for chitosan to 62.5%

for chitosan/PEO blend membranes when the molecular weight of PEO was 10,000 or higher. Electron spectroscopy for chemical analysis (ESCA) suggested an increase in PEO on the membrane surface with increasing molecular weight in the blend. The permeability coefficient of urea and other solutes through chitosan/PEO blend membranes were much higher compared to those in chitosan membranes or in commercially available Cuprophan® membranes. The high permeability was either due to the porosity or an increased hydrophilicity of the membranes. Platelet adhesion and activation were significantly reduced on chitosan/PEO blend membranes. However, chitosan/PEO blend membranes did not prevent serum complement activation. The degree of complement was similar to that of Cuprophan® membranes. The permeability is limit to size of molecule [86]. It, therefore, appears that there is a need to develop better haemodialysis membranes to improve flow data such as permeability, greater selectivity and higher dialysis rate, and further improve platelet adhesion and activation to meet the highly demands of haemodialysis membrane applications [136].

2.5 Genipin as a Naturally Crosslinker for Chitosan

2.5.1 Introduction

The crosslinking of chitosan extends its medical applications into area such as, implants, wound dressings, blood substitutes and drug carriers by improving otherwise poor mechanical properties. For example, biological tissues have been used in manufacturing heart valve prostheses, small-diameter vascular grafts and biological patches [176-178.]. These biological tissues have to be fixed with a crosslinking agent and subsequently sterilized before they can be implanted in humans [179]. The fixation of biological tissue is to reduce antigenicity and immunogenicity and prevent enzymatic degradation [4]. Up to now, various crosslinking agents have been used in fixing biological tissues. These crosslinking agents are mostly synthetic chemicals such as formaldehyde [4], glutaraldehyde [4], dialdehyde and epoxy compounds [180]. However, these chemicals are all highly (or relatively highly) cytotoxic, which may impair the biocompatibility of biological tissues [4,7,8]. Glutaraldehyde is known [181] to have allergenic properties, giving rise to occupational dermatitis.

Like other synthetic chemical reagents, it is highly cytotoxic [181,182], and for gluteraldehyde, cytotoxicity occurred at concentrations greater than 10-25ppm. In tissue cultures, cytotoxicity needs to be as low as 3ppm [15]. There is, therefore, increasing demand for a crosslinking agent that is able to form suitable biocompatible products without adding any cytotoxicity problems. Genipin is a naturally occurring crosslinking agent, which seems to display promising characteristics.

2.5.2 Preparation and properties of genipin

Genipin can be obtained from an iridoid glycoside and geniposide, which are the primary active components, abundantly present in gardenia fruit (Gardenia jasmindides Ellis) as seen in Figure 2.5.1.

Figure 2.5.1 A photograph of the fruit of Gardenia jasmindides Ellis

The iridoid glycoside gardenia and geniposide are mainly gardenoside, chlorogenic acid and ursolic acid. The methods of isolating iridoid glycoside and geniposide from Gardenia jasmindides Ellis have been described by Endo and Taguchi [183]. In a water-ethanol commercial extract of the fruits, iridoid glycoside and geniposide made up 70% of the extract [184]

Genipin can be prepared from the latter by oxidation followed by reduction and hydrolysis, or by enzymatic hydrolysis [184]. Alternatively, racemic genipin may be prepared synthetically [185]. A variety of pharmacological activities of genipin has been reported; choleric action, inhibition of gastric acid secretion, and so on [186]. The chemical structure of genipin is shown in Figure 2.5.2.

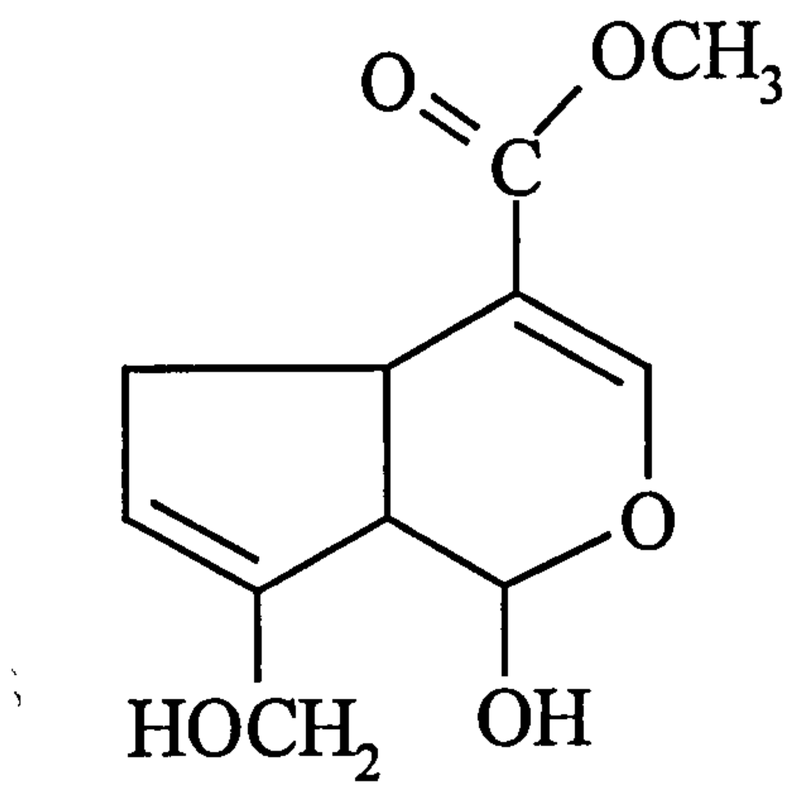

Figure 2.5.2 Chemical structure of genipin.

Reaction of genipin with glycine, alanine, histidine, lysine and glutamate in aqueous buffer solution converted the colourless starting materials to blue pigments. The dark blue pigments were obtained by its spontaneous reaction with amino acids or protein [28]. These dark blue pigments have been used in the fabrication of food dyes. Effect of pH on the formation of blue pigments was studied using a UV-vis spectrophotometer [187]. The optimum pH for the formation of the blue pigment was 7.0. The rate of the formation of blue pigment was a constant from genipin with amino acids at various temperatures. The resulting blue pigments are more stable in alkaline (pH 9.0) than in natural (pH 7.0) and acidic solutions (pH 5.0) [188].

Sung and co-workers [188-191] have undertaken studies to investigate the cytotoxicity, stability, feasibility and biocompatibility of genipin for biological tissue fixation. The results of a series of studies carried out on porcine pericardia crosslinked with genipin indicate that this agent can form stable crosslinked products [189]. In the feasibility study, it was found that genipin-fixed tissue has a resistance to enzymatic degradation comparable to the glutaraldehyde-fixed tissue. The biocompatibility of the genipin-fixed tissue was studied in a growing rat model subcutaneously [190]. It was found that the inflammatory reaction of the genipin-fixed tissue was significantly less than its glutaraldehyde- and epoxy-fixed counterparts. Genipin-fixed tissue has minimal calcium content, since calcification may lead to stiffening around an implant and eventual degradation and re-sorption into the surrounding tissue [190, 191]. In addition, genipin-fixed tissue also displayed compatible strength and resistance against *in vivo* degradation to its glutaraldehyde-fixed counterpart [188,192]. Also, it was found that tissue fixation in glutaraldehyde, epoxy compound, and genipin produced distinct crosslinking structures [193]. The differences in crosslinking structure affected the crosslinking characteristics and mechanical properties of the fixed tissues. It was observed that the genipin-fixed tissue had the greatest ultimate tensile strength and toughness among all the fixed tissues [193]. Furthermore, it was found that gelatine-derived bioadhesives display higher biocompatibility and less cytotoxicity when crosslinked with genipin than with other agents, such as formaldehyde, glutaraldehyde and epoxy compounds. For example, genipin was 10,000 times less cytotoxic than glutaraldehyde and shows a higher stability for 6-month storage periods [194, 195]. The aforementioned results demonstrated that genipin is a promising crosslinking agent for biological tissue fixation.

Genipin is, therefore, much less toxic than glutaraldehyde and many others commonly used synthetic cross-linking agents. As described in a World Patent [15], it was found that genipin is a biological material as a naturally occurring cross-linking agent with cross-linkable functional group, such as amino group or the like. Genipin was shown to be an effective crosslinking agent for treatment of biological materials intended for *in vivo* biomedical applications, such as prostheses and other implants, wound dressings and substitutes [15]. These attractive properties of genipin and the presence

of free amino groups in chitosan, which enable it to be crosslinked, prompt us to develop novel chitosan-based polymeric networks for medical uses.

2.6 Conclusions

In this chapter, an overview of the properties of chitosan has been given. It confirms quite well the interest in the use of such a polyscaccharide for numerous applications in the life sciences. The physical and chemical properties of chitosan, such as inter- and intra-molecular hydrogen bonding and cationic charge in acidic medium, make it useful in the development of conventional and novel pharmaceutical products. In particular, a number of investigations have shown that chitosan networks can act as a carrier for specific drug delivery systems. However, the present limitations upon using chitosan concern the cytotoxicity of the currently available crosslinking agents. Genipin is a novel naturally occurring agent and it can be used solve present problems.

CHAPTER 3
Experimental

In order to show the validity of this research, the details of the materials, the methods of sample preparation and the characterisation techniques used are described in this chapter.

3.1 Materials and Characterisation

3.1.1 Materials

Chitin was purchased from Fluka, UK. Its chemical structure was shown in Figure 2.2.1. Chitosan (CS) was produced from the chitin by deacetylation. The molecular weight of chitosan was measured by means of gel permeation chromatography (GPC). The degree of deacetylation of the chitosan was determined by Fourier transform infrared (FT-IR) specroscopy. Chitosan with three different degrees of deacetylation was employed in this study. The characteristics of the molecular weight and the degree of deacetylation of these chitosans are listed in Table 3.1.1

Poly(ethylene oxide) with a molecular weight, M_n, of 20,000g/mole (HPEO) was obtained from BDH Laboratory Supplies. Poly(ethylene glycol) powder with viscosity average molecular weight of 600g/mole (LPEO) was obtained from the Aldrich Chemicals, UK.

Genipin was obtained from Challenge Bioproducts Co., Taiwan. The structure of genipin was shown in Section 2.5 (Figure 2.5.1) and Figure 3.1.1 is its FT-IR spectrum.

Vitamin B_{12} (cyanocobalamin, approximately 98%) was bought from Fluka Chemical Co, UK. Hen egg white lysozyme (3xcrystallized and lyophillized) was obtained from Sigma. Eleutherococcus sentisocus (ES) was kindly provided by the Institute of Chinese Medicine, China.

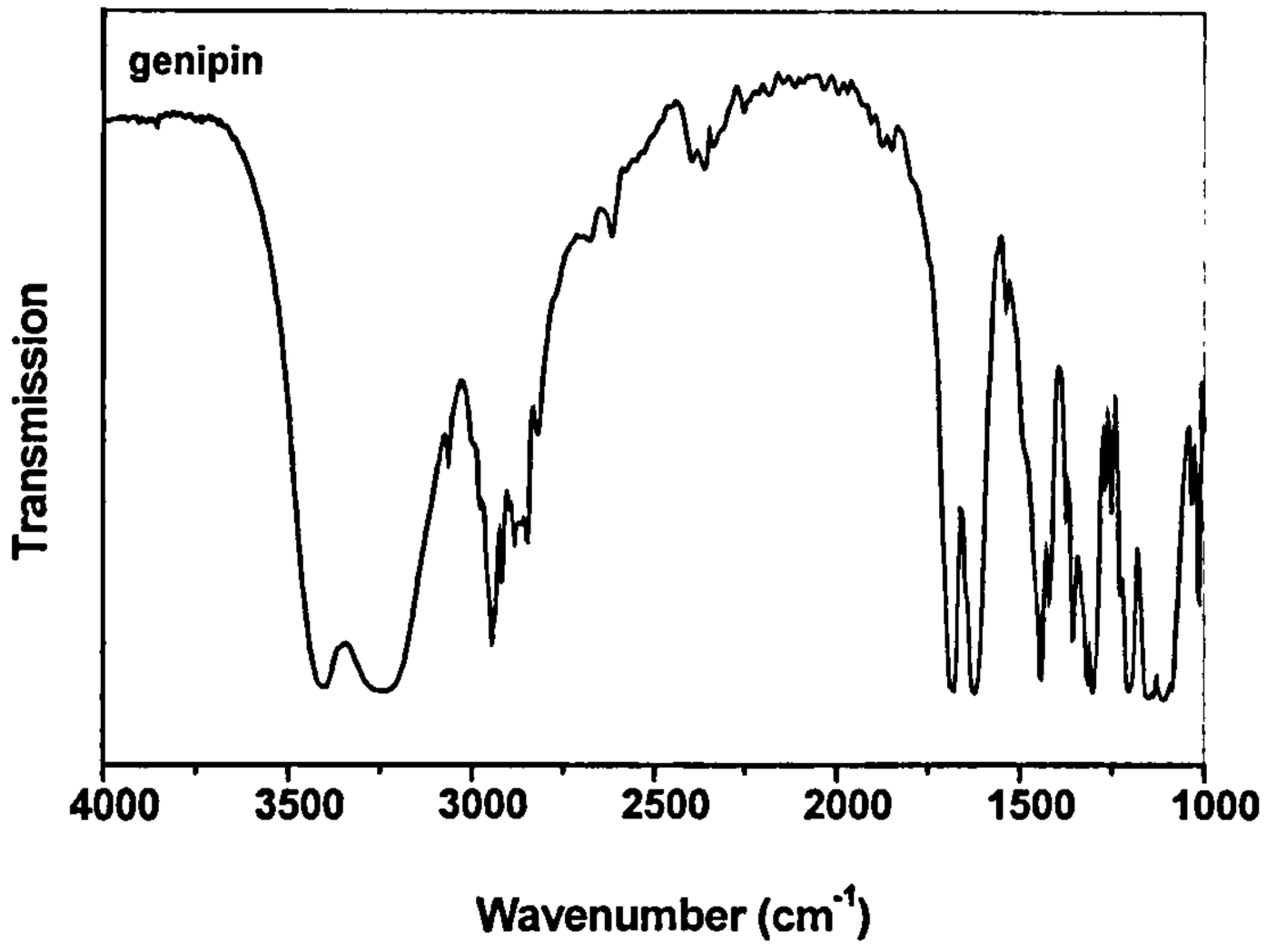

Figure 3.1.1 FT-IR spectrum of genipin

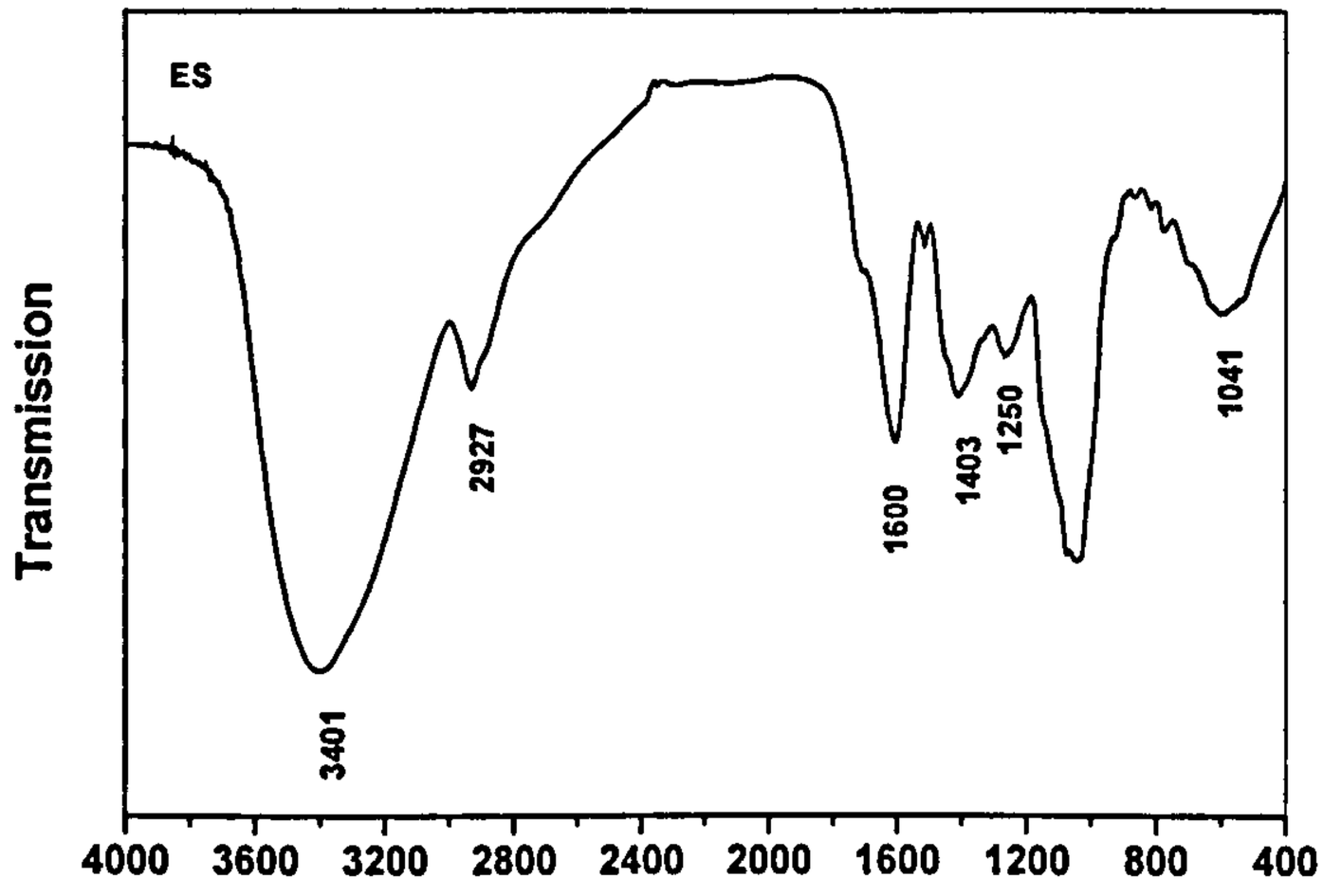

Figure 3.1.2 FT-IR spectrum of ES

Acetic acid and phosphate saline (PBS) were obtained from Aldrich Chemicals, UK. All chemicals were used without further purification, except for eleutherococcus sentisocus. The water used was deionised.

The purification of ES was carried out in the following manner. 5g of dried ES powders were dissolved in water, or water/ethanol mixture. The solution was stirred for 24h at room temperature and then filtered through filter paper. The filtrate was dried at about 35°C. The samples obtained then were kept in a cool chamber at below –35°C. Figure 3.1.2 is the FT-IR spectrum of ES.

3.1.2 Preparation of chitosan samples with different degrees of deacetylation (DD)

Chitosan is the deacetylated product of chitin, which was obtained by an alkali treatment. Dried chitin was put into 47% (wt) NaOH solution in a flask. The deacetylation reactions proceeded at 62°C for 2 hours under a nitrogen atmosphere. Then the products were washed in water at about 80°C to neutrality. To obtain chitosan with a high degree of deacetylation the alkali treatment was repeated.

Effective deacetylation was attained according to Mima's method [196]. Because of the inhomogeneity of the reaction, further deacetylation was prevented when the degree of deacetylation exceeded 90%. In order to obtain a higher degree of deacetylation of chitosan, i.e. up to 95%, threadlike chitosan with a degree of deacetylation of 87% was prepared by pouring the aqueous solution containing1.5%~2% chitosan and 2% acetic acid in a small stream into a large amount of 1N NaOH solution. The threadlike chitosan was subjected to alkali treatment, but continuous alkali treatment was completed at 90°C instead of 60°C. By a series of alkali treatments, the chitosan product was easily obtained with an acetylation degree of up to 95%. The whole process of the alkali/washing treatment is schematically shown below.

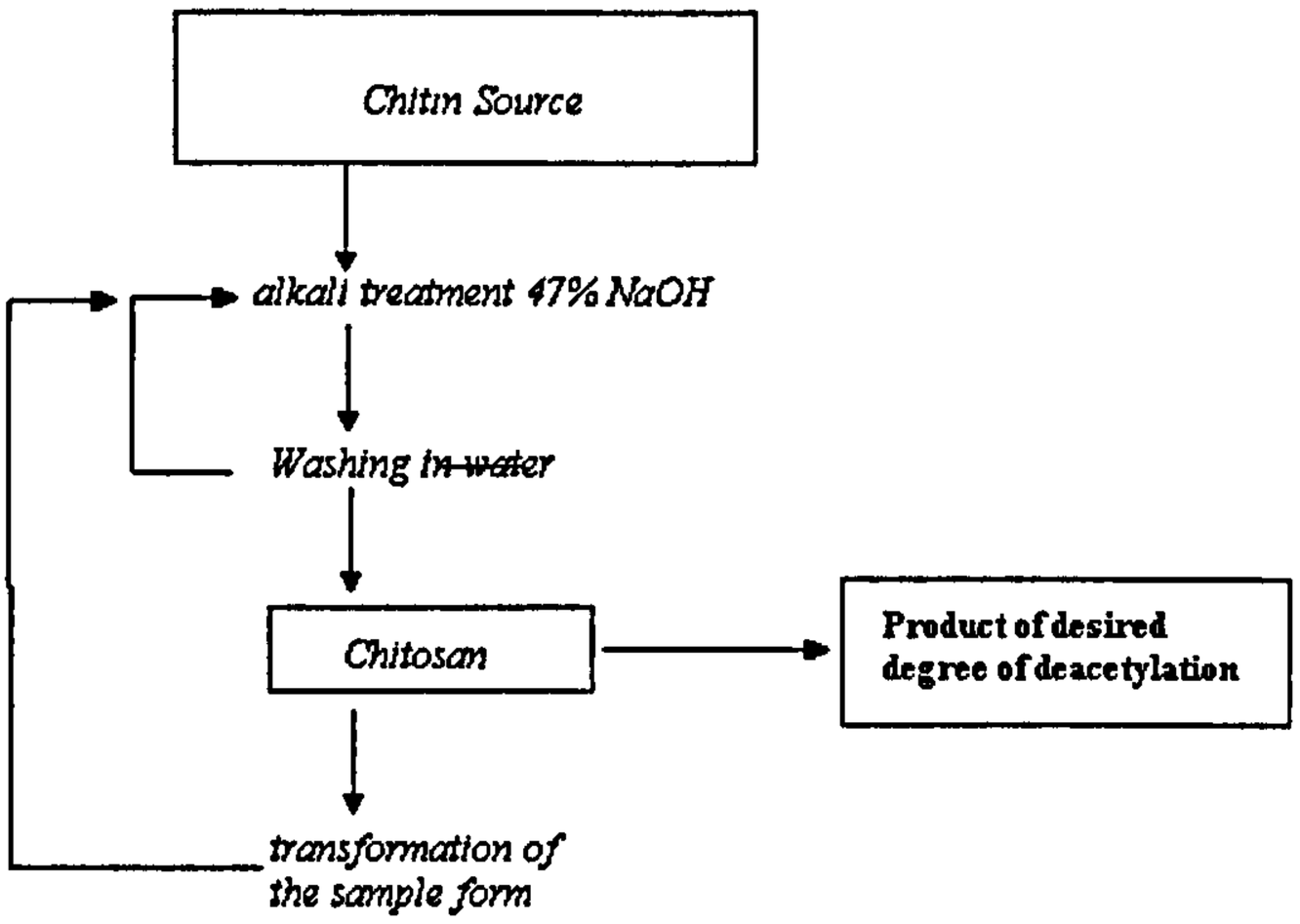

Figure 3.1.3 The schematic process of the alkali/washing treatment

Table 3.1.1 Characteristics of chitosan samples after deacetylation

Chitosan	Number of Steps	Temp (°C)	Reaction time(h)	DD (%)	M_w	M_w/M_n
Chitosan-1	2	62	4	72	3.0×10^4	3.3
Chitosan-2	4	62	8	85	3.3×10^4	5.5
Chitosan-3	5	62; 90	10	95	4.4×10^4	4.1

Figure 3.1.4 gives the infrared spectra of chitin and chitosan samples with different degrees of deacetylation.

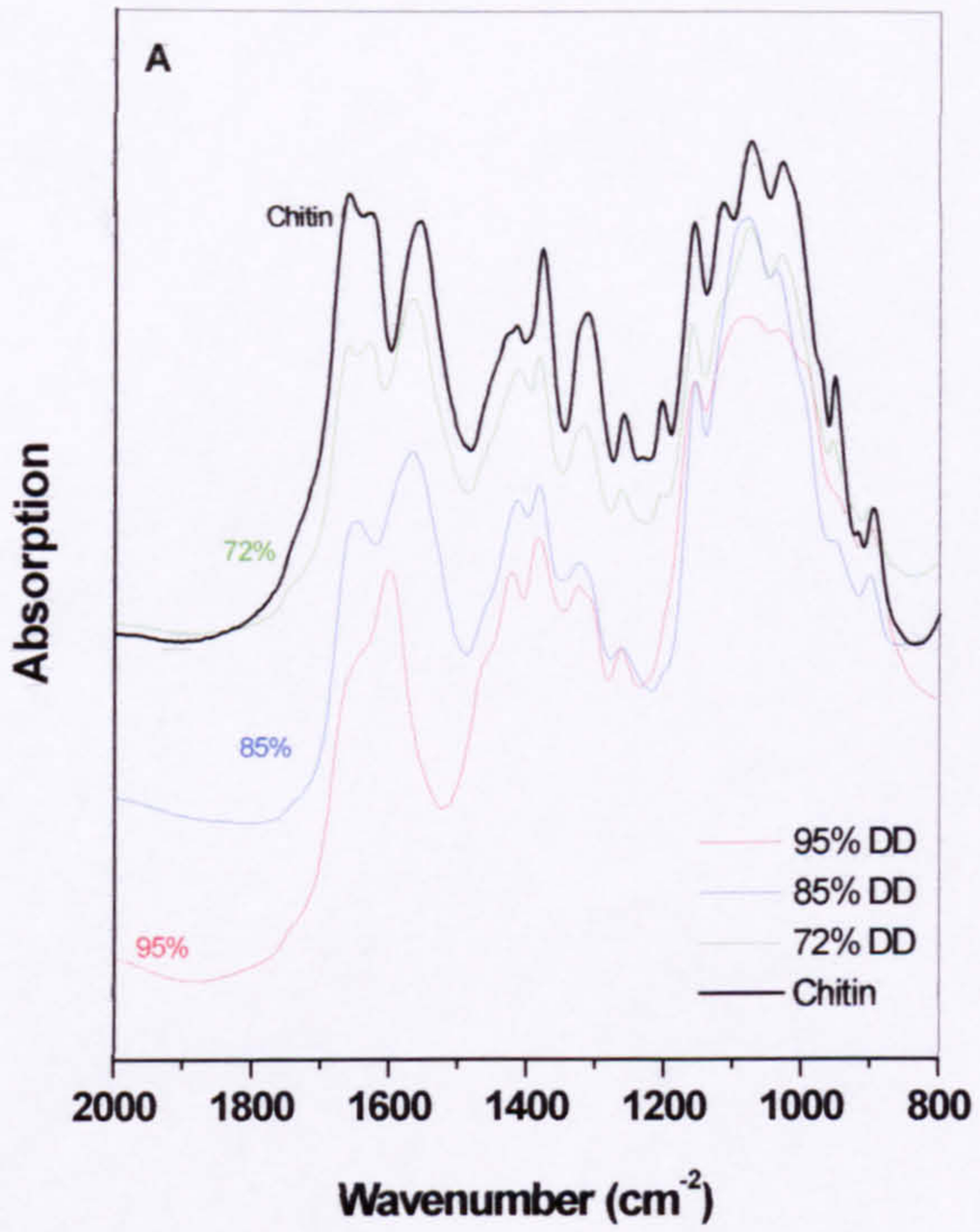

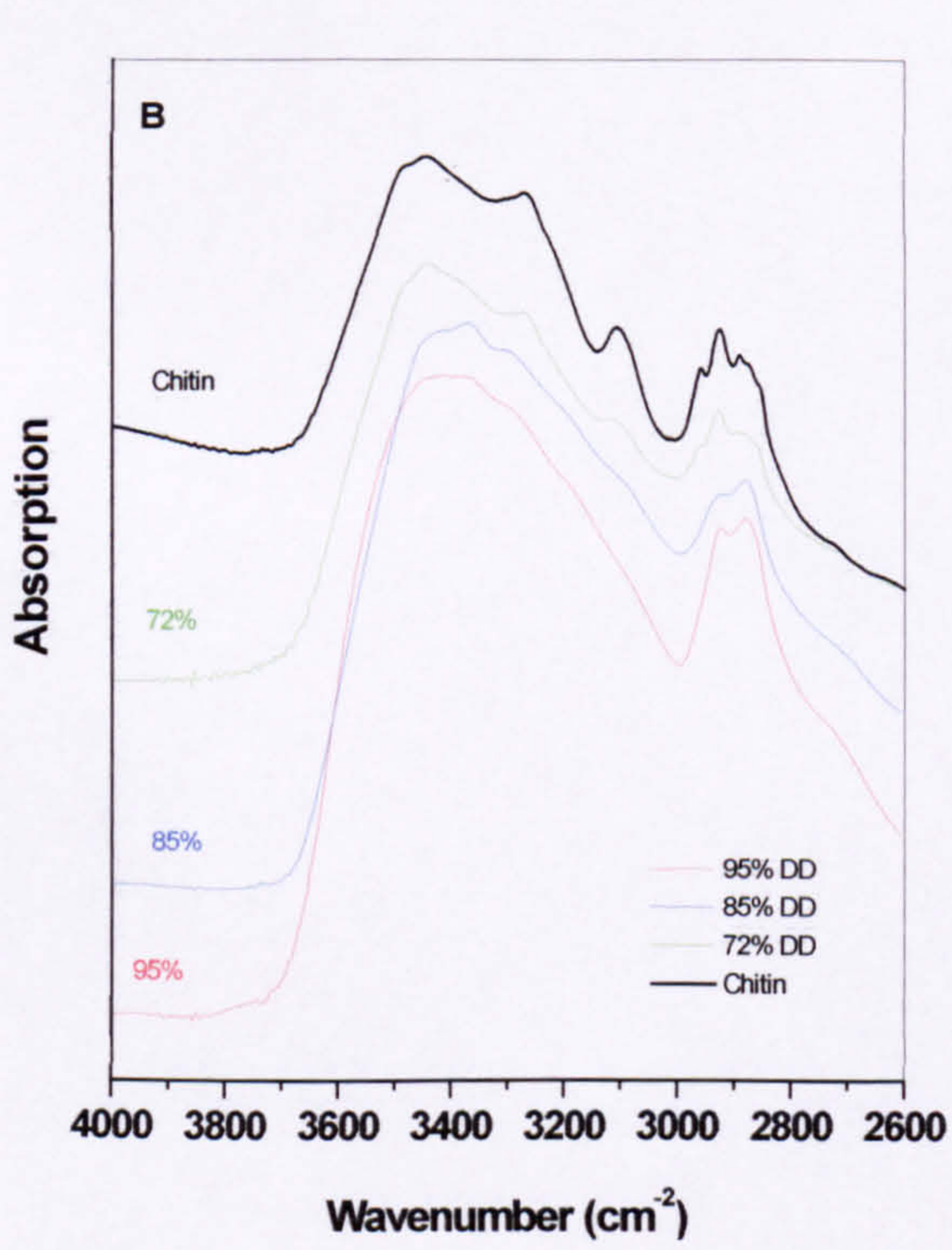

Figure 3.1.4 FT-IR spectra of chitosan for different degrees of deacetylation: (A) in the 2000-800 cm^{-1} region, (B) in the 4000-2600 cm^{-1}cm region.

As seen from Figure 3.1.4 part (A), the spectrum of chitin has a clear amide I band at 1655 cm^{-1}, which decreased as the degree of deacetylation increased. The spectrum of chitosan with a degree of deacetylation of 85% has only a slight upward swelling at this frequency. In the spectrum of chitosan with a degree of deacetylation of 95%, almost no trace of the amide band could be detected, which is evidence of high deacetylation.

In the 1655 cm^{-1} to 1560 cm^{-1} region, there were considerable changes as the extent of N-acetylation changed. These changes are attributed to the amino content in chitosan, as reported [197]. This characteristic can be used in the analysis of the degree of deacetylation of chitosan.

Figure 3.1.4 (B) shows the FT-IR spectra in the 2600-4000 cm^{-1} region. A broad 3468 cm^{-1} band with small shoulders at 3276cm^{-1} and 3100cm^{-1} was observed when the degree of deacetylation was 72%, then gradually disappeared with increasing of deacetylation. These changes mean that the degree of crystalinity decreases with increasing the degree of deacetylation of chitosan [47].

3.1.3 Determination of the degree of deacetylation of chitosan by FT-IR

The degree of deacetylation and the free amine group content are, of course, inversely related and the former may be obtained directly by determining the amide group concentration, or indirectly by determining the amine group concentration. There are a number of analytical tools [30, 198-201] to determine the degree of deacetylation including IR spectroscopy, pyrolysis-gas chromatography, gel permeation chromatography, UV spectroscopy, ^{1}H NMR spectroscopy, various titration schemes, and acid hydrolysis.

Infrared spectroscopy (IR) has been used frequently to determine the degree of deacetylation of chitosan. It is one of the most widely used techniques for chitosan analysis. The methods described in the literature [198-201] to determine the degree of deacetylation from IR spectra, which employed different probe (PB) and reference (RB) bands (the intensities of respective bands change, but not with the degree of deacetylation and baselines (BL)).

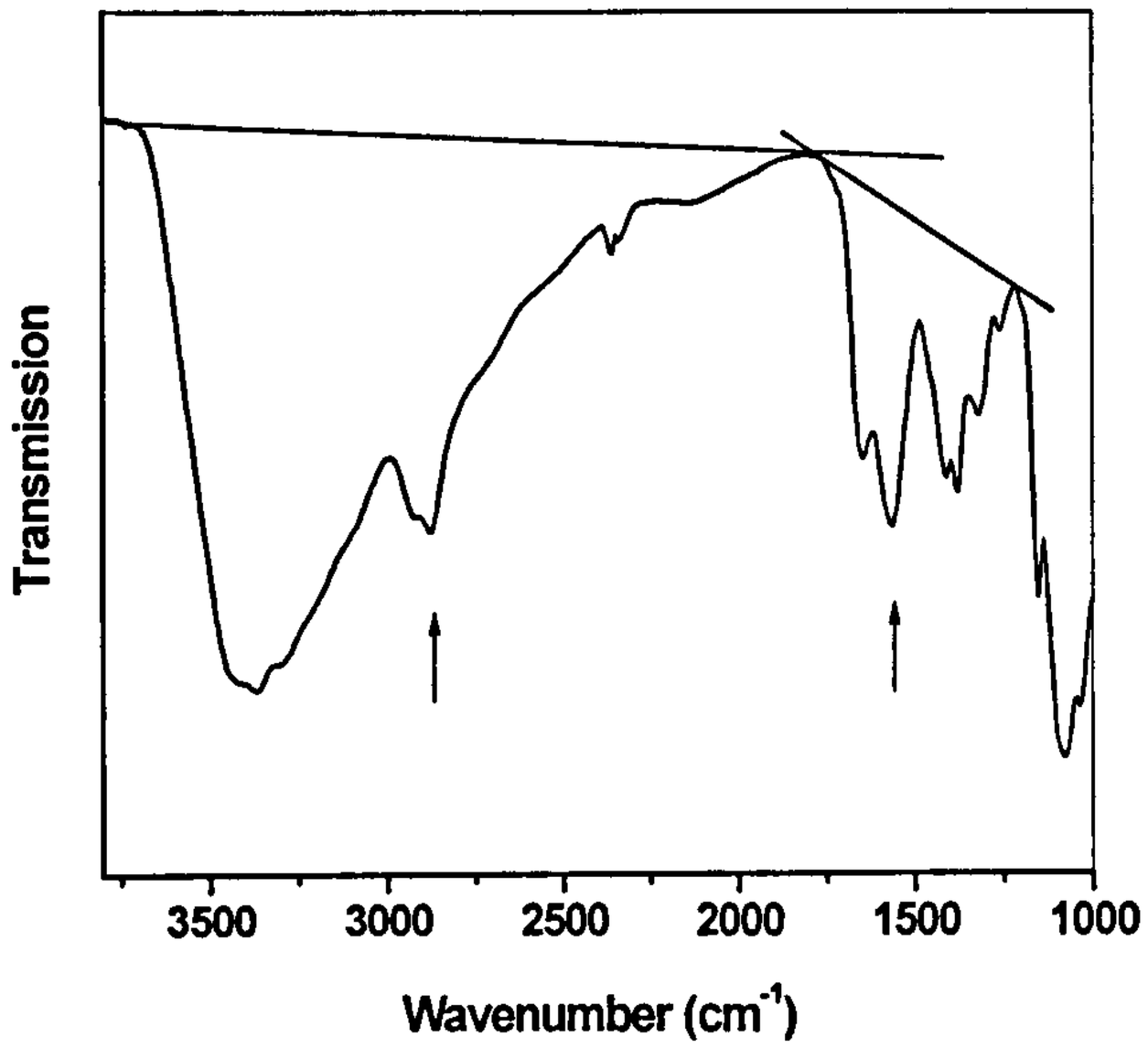

Figure 3.1.5 FT-IR spectrum of chitosan, and the baselines for determination of the peak absorbance.

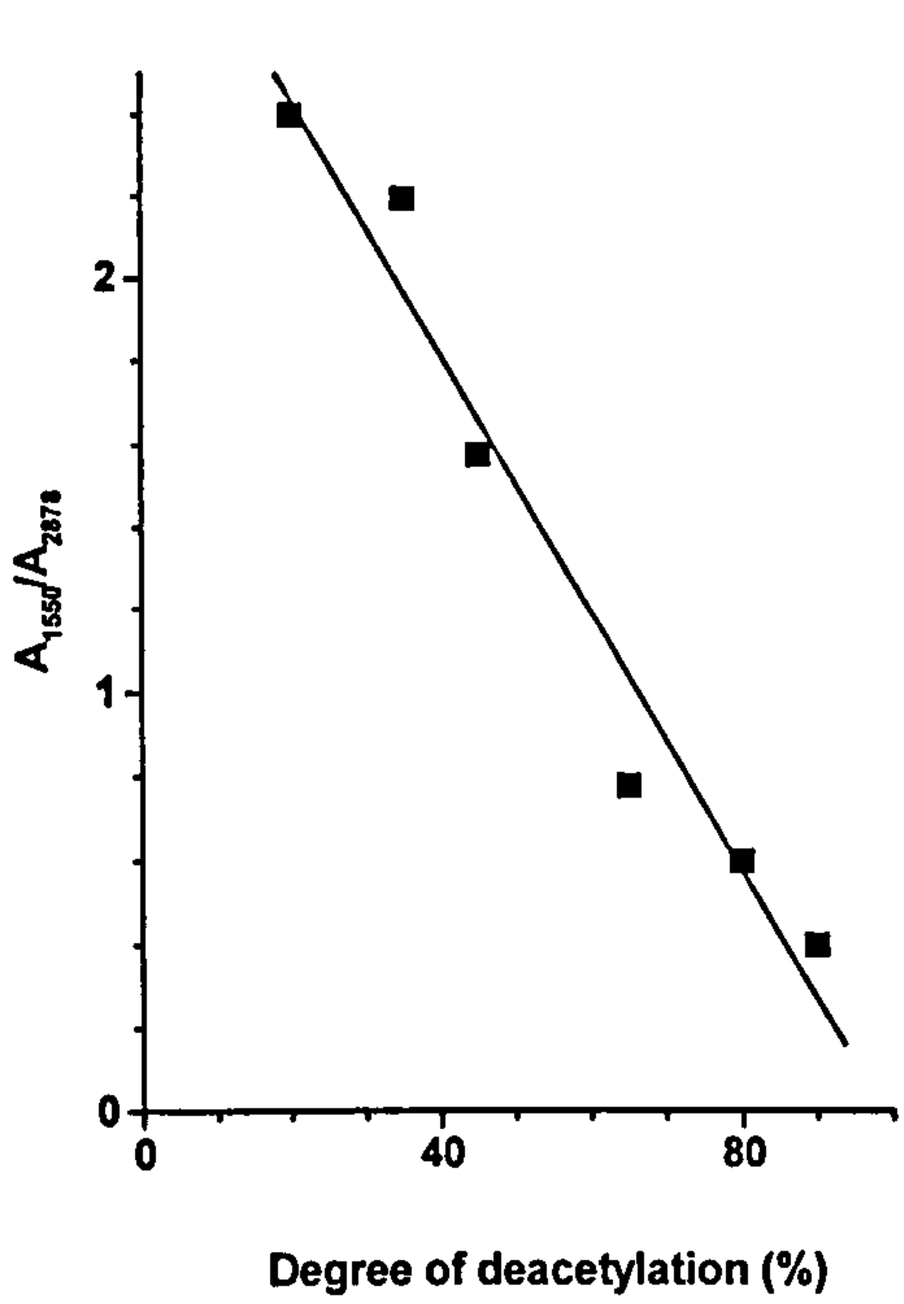

Figure 3.1.6 Standard calibration line obtained by IR spectroscopy using A_{1550}/A_{2878} [201].

The degree of deacetylation is calculated from the ratio of the absorbance (A) of the two bands, A_{PB}/A_{RB}, either directly, using a formula [199, 200], or using calibration lines [198-201].

The preparation of samples of chitosan for FT-IR measurements and the equipment used in the analysis are described in Section 3.3.3 and the spectrum is shown in Figure 3.1.5.

Figure 3.1.6 is the standard calibration line obtained by IR spectroscopy [201] using A_{1550}/A_{2878}. The degree of deacetylation of chitosan samples used in this research was found to be 72%, 85% and 95%, respectively.

3.1.4 Determination of molecular weight of chitosan by gel permeation chromatography (GPC)

The molecular weight of chitosan was determined by means of GPC. Sample solutions were prepared by adding 10mL of 0.5M sodium nitrate as solvent to 10 mg of sample and using 0.01M sodium dihydrogen phosphate to adjust to pH 2.0. Then the mixture was left for four hours to dissolve. The solution was then warmed at 70°C for ten minutes. After cooling, the solutions were filtered through a 0.45µm PVDF membrane prior to the chromatography. A column of Plgel 2 x mixed-OH of 30cm length was used. A flow-rate of 1.0ml/min and temperature of 30°C were used.

The GPC system used was calibrated with poly(ethylene oxide)/poly(ethylene glycol) calibrants. The data were acquired and processed using a Viscotek Triesc 3.0 software. The output for this polymer is shown in Figure 3.1.7 for the 95% DD sample..

GPC yields values of number and weight average molecular weight relative to the calibration standards used. The results for the three chitosans are listed in Table 3.1.1.

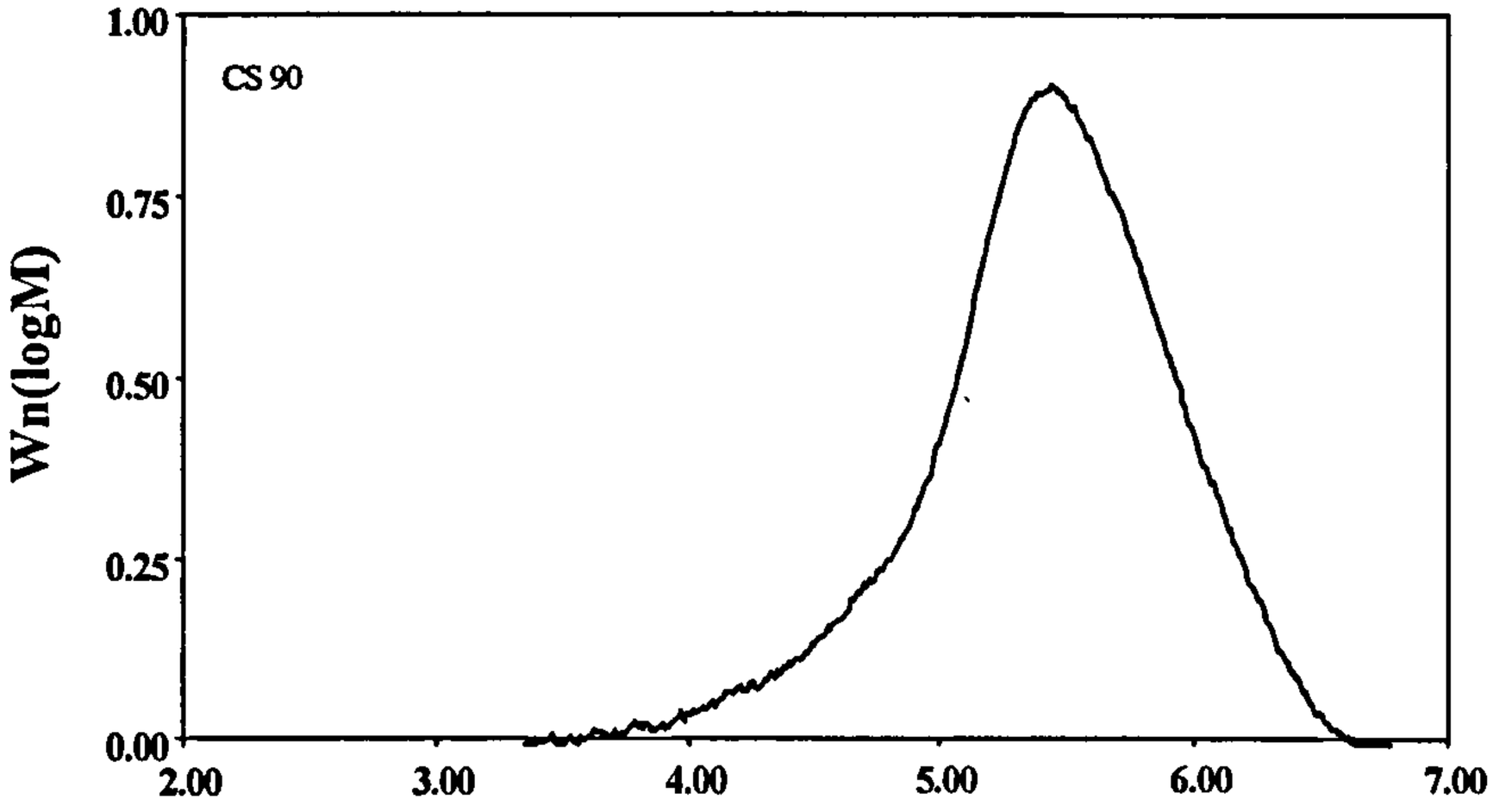

Figure 3.1.7 GPC chromatogram of chitosan (DD: 95%)

3.2 Sample Preparations

3.2.1 Chitosan/PEO blends

Chitosan was dissolved in 1.0wt% aqueous acetic acid. The concentration and pH of the prepared chitosan was 1.5wt% and 5.0, respectively. Chitosan was dissolved at room temperature overnight. Then the chitosan solution was filtered through filter paper to remove any un-dissolved gel. The clear lightly yellow chitosan solution was then mixed with 5% aqueous solution of HPEO or LPEO at 90:10, 80:20, 70: 30 etc at room temperature. The chitosan and PEO mixed solutions at different weight percentage ratios were stirred overnight at room temperature. The degassed and well-mixed solutions were then cast onto a glass plate, evaporated in an oven at 40^0C to remove the solvent and dried to constant weight. The thickness of dried films ranged from 0.3mm – 0.6mm.

For further mechanical property studies, the films were also prepared at the solution pHs of 2.5, 3.0, and 4.0, respectively.

3.2.2 Crosslinked chitosan/PEO blend films

0.5wt of genipin (genipin/chitosan = 0.5%) was dissolved in 2ml water and then added to the chitosan solution or the chitosan/HPEO (or /LPEO) mixed solution. The solution was stirred for 30 minutes at room temperature. After two hours, the solution started to turn light blue and became increasingly viscous (see Figure 3.2.1). The solution was then cast onto glass plates and dried to constant weight at 40°C. The crosslinked chitosan and chitosan/HPEO (or LPEO) blends become dark blue after 1 day (see Figure 3.2.2). The thickness of the dried films was measured to be 0.3 ~0.6mm.

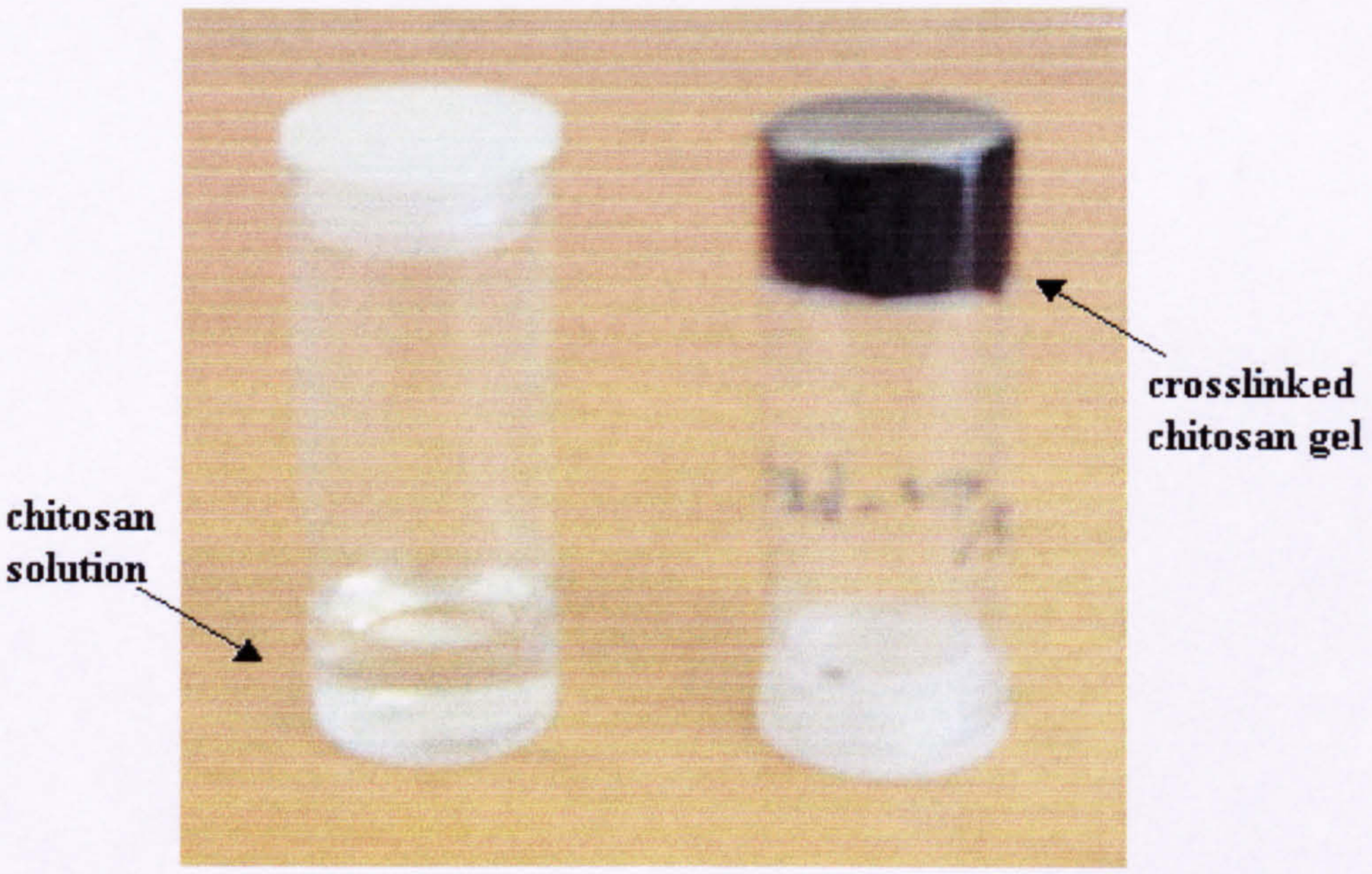

Figure 3.2.1 A photograph of a chitosan solution and a crosslinked chitosan gel

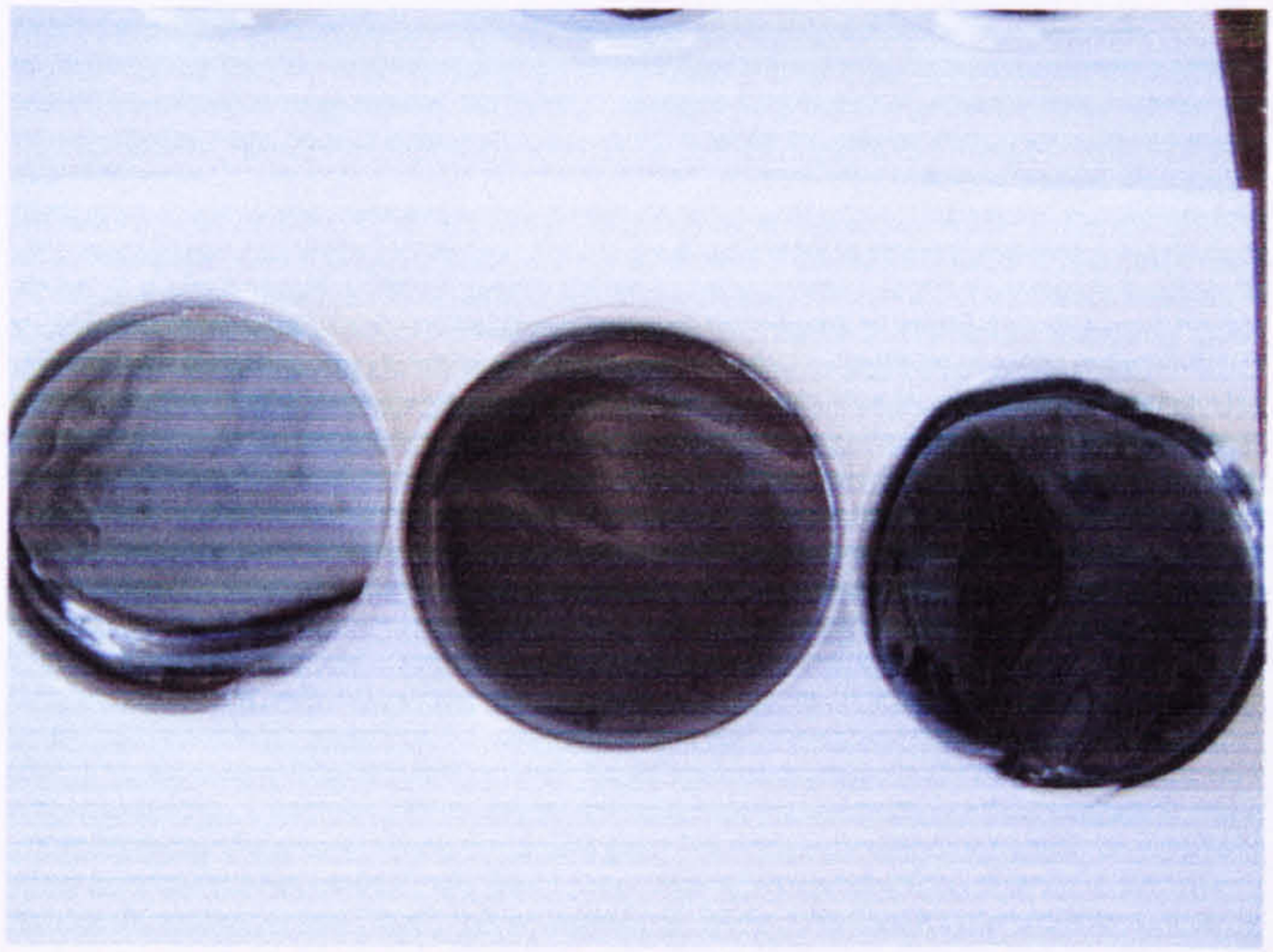

Figure 3.2.2 A photograph of crosslinked chitosan films

For further mechanical property studies, the films were also produced at 25°C and 60°C, respectively. For other studies such as those of swelling behaviour, controlled drug release and protein separation, films with different genipin contents were produced.

Table 3.2.1 Symbols for the CS/PEO blend series

System	CS Content (wt %)	PEO Content (wt %)
CS	100	0
CS/PEO 10	90	10
CS/PEO 20	80	20
CS/PEO 30	70	30
CS/PEO 40	60	40
CS/PEO 50	50	50
CS/PEO 60	40	60
CS/PEO 70	30	70
CS/PEO 80	20	80
CS/PEO90	10	90

Table 3.2.2 Symbols for the CS/PEO network series

System	Genipin content	CS Content (wt %)	PEO Content (wt %)
CSR/PEO 10	0.5 %	90	10
CSR/PEO 20	0.5 %	80	20
CSR/PEO 30	0.5 %	70	30
CSR/PEO 40	0.5 %	60	40
CSR/PEO 50	0.5 %	50	50
CSR/PEO 60	0.5 %	40	60
CSR/PEO 70	0.5 %	30	70
CSR/PEO 80	0.5 %	20	80
CSR/PEO 90	0.5 %	10	90
CSR	0.5 %	100	0

The abbreviation symbols used in the study for the CS/PEO blends and networks are shown in Tables 3.2.1 and 3.2.2.

3.2.3 Determination of crosslinking density in chitosan films

The crosslink density is defined as

$$\rho_c = \frac{1}{M_c} \qquad [3.2\text{-}1]$$

The crosslink density of chitosan was determined by swelling measurements. The Flory-Rehner equation was used to calculate M_c, the number average molecular weight between crosslinks [202]. The equation is:

$$-\left[\ln(1-u_r)+u_r+\chi u_r^2\right]=\rho V_0 M_c^{-1} u_r^{1/3} \qquad [3.22]$$

where χ is the chitosan-water interaction parameter (0.5917) [202], ρ is the density of chitosan (1.25g/cm^3), V_0 is the molar volume of water (18cm^3/mol), and u_r is the volume fraction of chitosan in the swollen state. u_r was obtained through the swelling

experiment and on the basis of W_d x1.003/[W_d x 1.003 + (W_s - W_d) x 1.25], where W_s and W_d are weights of the specimen in the dry and swollen states, respectively. The crosslink density and related parameters are listed in Table 3.2.3. The abbreviation symbols used in the study of the crosslinked chitosan samples with different crosslink densities are shown in Table 3.2.4.

The crosslink densities of chitosan films, which were formed under different conditions, such as different solution pHs and crosslinking temperatures, were calculated and shown in Table 3.2.5. The experimental data suggest that with the same amount of genipin, the crosslinking density was not affected by either the pH of the chitosan solutions or the crosslinking temperature.

Table 3.2.3 Crosslink density and related parameters

Genipin content (wt.%)	**W_d (g)**	**W_s (g)**	***H***	**u_r**	**Crosslink density (%)**
01	0.0477	0.170	0.720	0.238	0.26
0.3	0.0503	0.1519	0.669	0.284	2.23
0.5	0.0715	0.1954	0.634	0.316	4.65
0.8	0.1017	0.2493	0.592	0.356	9.22
1	0.0895	0.2034	0.560	0.386	14.35

H: the volume fraction of water in the films

Table 3.2.4 Abbreviation symbols used in the study of crosslinked chitosan samples

System	**Genipin content (%)**	**Crosslink density (%)**
0.1CSR	0.1	0.26
0.3CSR	0.3	2.23
0.5CSR	0.5	4.65
0.8CSR	0.8	9.22
1CSR	1	14.35

Table 3.2.5 Crosslink density for different crosslinking conditions

Genipin content (%)	pH of chitosan solution	Film-formation Temperature (^{0}C)	Water content H	Crosslink density (%)
0.5%	2.5	40	0.633	4.65
	3.0		0.615	4.41
	4.0		0.634	4.64
	5.0		0.620	4.49
	4.0	25	0.633	4.65
		60	0.616	4.47

3.2.4 Preparation of samples for studying the crosslinking process for FT-IR spectra measurement

Genipin was added into 0.5% chitosan solutions and dissolved under stirring at reaction temperature. At different reaction times, the crosslinked chitosan hydrogel was then dialysed against double-distilled water. After dialysis, a blue colour elastic gel was obtained. This crosslinked chitosan hydrogel was ground to powder and mixed with KBr, and then finally pressed into a disk.

3.2.5 Preparation of samples for studying the crosslinking process for UV spectra analysis

Genipin was dissolved in deionized water to prepare 50ppm of genipin solution. An aqueous chitosan solution was diluted and then added into the genipin solution at equimorlar ratio, and homogeneously mixed. The samples were analysed by UV spectrophotometers and monitored at time intervals to examine the variation of UV absorption between 190nm to 340nm.

3.2.6 Preparation of samples for static laser light scattering measurements

Chitosan solutions with different pHs were prepared with concentrations of 1×10^{-6} and 10^{-4} g/ml. All the solutions used for laser light scattering were clarified using a 0.5 μm Millipore filter to remove dust particles.

3.2.7 Preparation of drug carriers for drug release study

In order to study loaded drug release from a carrier, sorption and desorption experiments were employed.

The membranes, which had previously been kept in equilibrium with water, were immersed in the drug solution for 2 weeks until they attained equilibrium. The volume of samples was measured using a picometer with resolution of 10μm. The concentration of ES solution was determined by a UV spectrometer at 200nm. The concentration of ES absorbed by the membrane, C, was calculated by measuring the concentration of ES in the aqueous solution prior to (C_0) and after (C_∞) the sorption experiments, using the expression

$$C = \frac{(C_0 - C_\infty)V}{V_p} \qquad [3.2\text{-}3]$$

V and V_p are the volumes of the aqueous solution and membrane sample, respectively.

3.3 Instrumentation and Methods

3.3.1 Small angle X-ray scattering (SAXS)

The SAXS technique has been extensively used for the investigation of the morphology of polymer blends [204]. In this section, the principles of SAXS [204, 205] are reviewed and important points regarding the practical measurements are made.

Using Figure 3.3.1 parts (a) and (b), the principles of SAXS can be explained as

follows. If the sample has electron density inhomogeneities with colloidal size (1-100nm) and the incident beam, K_0, is applied to the sample, the corresponding scattered beam, K, can be observed as shown in Figure 3.3.1(a). In this case, the scattering angle to the incident beam is given as 2θ. There are other cases where the angle is defined as θ. However, in this study, the scattering angle is expressed as 2θ. The scattering intensity, $I(q)$, is expressed as a function of the scattering angle 2θ. The variable q can be expressed in terms of magnitude,

$$|q| = \frac{4\pi}{\lambda}\sin\theta \qquad [3.3.1\text{-}1]$$

or in vector terms,

$$\vec{q} = \frac{2\pi}{\lambda}\left(\vec{i} - \vec{i}_0\right) \qquad [3.3.1\text{-}2]$$

where $\vec{i}$ and $\vec{i}_0$ are the unit vectors of the scattering vector and the incident beam, respectively.

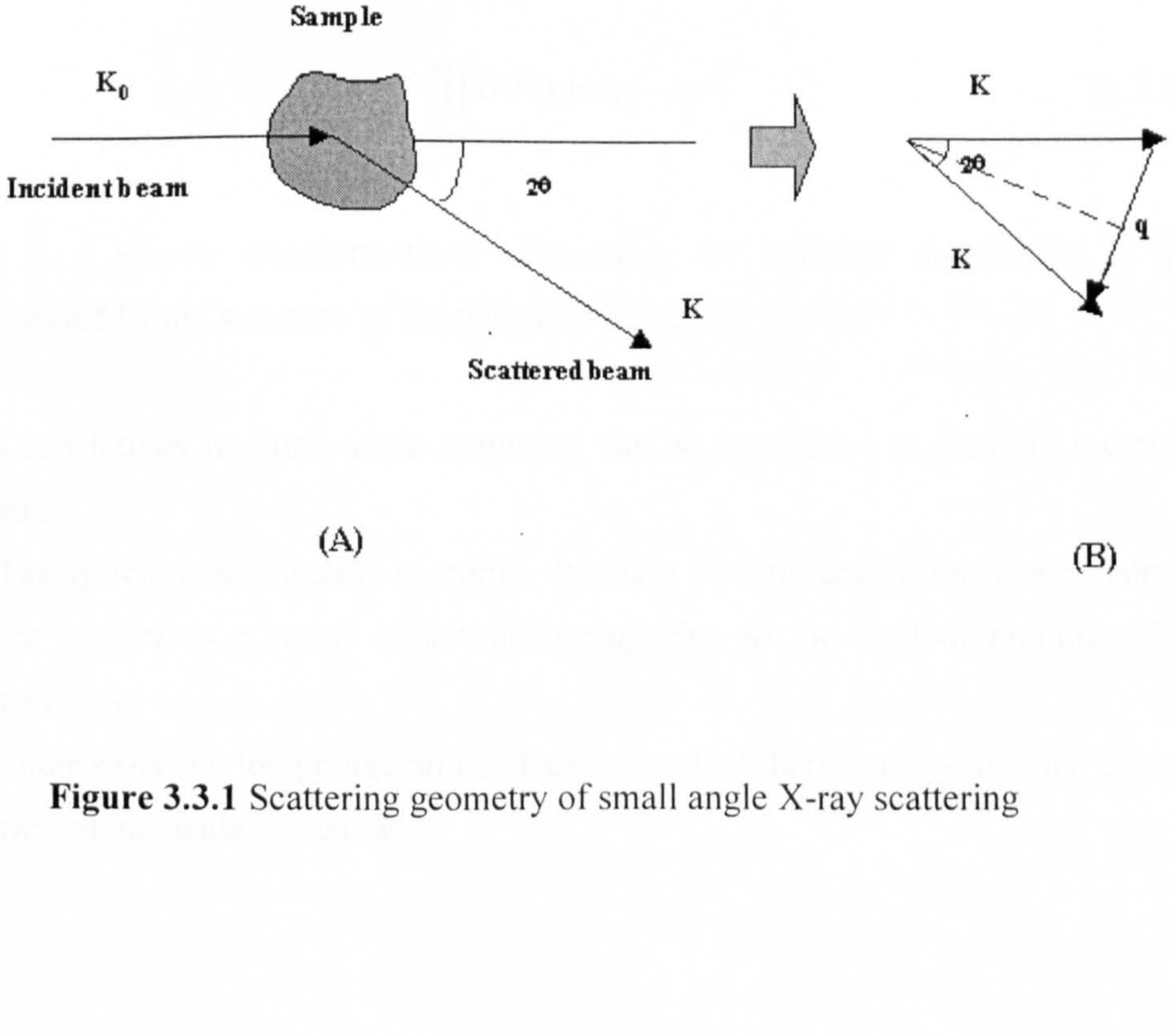

Figure 3.3.1 Scattering geometry of small angle X-ray scattering

The general scattering formula is given by the following equation.

$$I(q) = FF^* = \iiint_{V1} \iiint_{V2} dV_1 dV_2 \rho(r_1)\rho(r_2)\exp(-iq(r_1 - r_2)) \qquad [3.3.1\text{-}3]$$

where dV_1 and dV_2 represent a volume element at position r_1 and r_2, respectively. ρ_1 and ρ_2 are defined as the number of electrons per unit volume at position r_1 and r_2, respectively. $(r_1\text{-}r_2)$ means the relative distance for every pair of points. To calculate Equation 3.3.1-3, an auto-correlation function, $F(r)$, is defined by

$$F(r) = \iiint_V dV_1 \rho(r_1)\rho(r_2) \qquad [3.3.1\text{-}4]$$

where $r=(r_1\text{-}r_2)$.

Thus, the density of these points, which have the relative distance r, can be given by F(r). Furthermore, the second integration can be carried out using the auto-correlation function.

$$I(q) = \iiint_V dVF(r)\exp(-iqr) \qquad [3.3.1\text{-}5]$$

This is a Fourier transformation. Therefore, the intensity distribution in q is determined by the structure of the object, as expressed by $F(r)$.

Two restrictions in small angle scattering can be introduced to simplify the above equation.

(a) The system is statistically isotropic. It makes no difference if this is a property of the system as a result of a time-average due to the random motions of the particles.

(b) There exists no long range order. This means that there is no correlation between two points widely separated.

From the above restriction (a), the complex exponential in Equation 3.3.1-5 can be replaced by the fundamental formula of Debye [205].

$$\langle \exp(-iqr) \rangle = \frac{\sin qr}{qr} \qquad [3.3.1\text{-}6]$$

$$I(q) = \int 4\pi r^2 dr F(r) \frac{\sin qr}{qr} \qquad [3.3.1\text{-}7]$$

According to restriction (b), at large distances the electron densities become independent, and can be replaced with a mean value $<\rho>$. The auto-correlation function must also tend towards a constant value $V<\rho>^2$. For the mean value $<\rho>$, the following correlation function can be applied.

$$\langle \rho \rangle^2 = V\gamma(r) \qquad [3.3.1\text{-}8]$$

The correlation function allows one to transform the scattering data back into a real space distribution. The scattered intensity is then given by the following equation.

$$I(q) = V \int_0^\infty 4\pi r^2 dr \gamma(r) \sin(qr)/(qr) \qquad [3.3.1\text{-}9]$$

This is the most general formula for the diffraction of systems obeying the above restrictions (a) and (b). $\gamma(r)$ is found by the inverse transform correlation function.

$$V\gamma(r) = \frac{1}{2\pi^2} \int_0^\infty q^2 dq I(q) \sin(qr)/(qr) \qquad [3.3.1\text{-}10]$$

For practical measurements, the data treatment is very important. In the case of SAXS, the following data treatments should be considered.

(a) Raw data correlation

(b) Background subtraction

(c) Desmearing

First of all, the treatment of the raw SAXS data usually starts with a correction for the empty cell scattering, which is subtracted from the sample intensity. The second treatment is for the thermal motions of molecules in the sample. Because there exist density variations caused by not only the presence of different phases, but also by thermal motions of molecules in the sample, the resulting density variation gives rise to a background intensity. When a constant background level over a sufficiently large 2θ region is known, this level can simply be subtracted from the total observed intensity. The third treatment is for the smearing effect caused by slit collimation [206]. Applying this treatment can yield the pinhole pattern from the smeared pattern by taking into account the weighting function, which normally multiplies the intensity observed by using the slit geometry.

Spatially averaged morphological characteristics of the chitosan films were investigated by SAXS. These investigations were performed using a Kratky Compact Small Angle system at Changchun Institute of Applied Chemistry using a stationary-anode copper-target X-ray tube ($\lambda = 0.154$ nm) at room temperature. The fine-focus X-ray generator was operated at 45kV and 40mA. The measured intensity was desmeared and corrected for background scattering and photoelectric absorption [205] for all the samples.

3.3.2 Static Laser Light Scattering (SLLS)

SLLS is a classic and absolute analytical method, which measures the time-average fluctuations of the scattered light produced by molecules or macromolecules [206]. The intensity of the scattered light is analysed by photon correlation spectroscopy. The scattered intensity can be related to the structure of a polymer and it has been widely used to characterise synthetic and natural macromolecules [206].

When a monochromatic, coherent beam of light is incident on a dilute solution of macromolecules or a suspension of colloid particles and where the solvent refractive index is different from that of the solute (macromolecules or colloidal particles), the incident light is scattered by each illuminated macromolecule or colloidal particle in

all directions. The scattered light waves from different macromolecules or particles can be described in terms of two fundamental quantities: the momentum transfer (h**K**) and the energy transfer (h$\nabla\omega$) obeying the following conservation equations

$$h\mathbf{K} = h(\mathbf{k}_j - \mathbf{k}_s) \qquad [3.3.2\text{-}1]$$

$$h\nabla\omega = h(\omega_j - \omega_s) \qquad [3.3.2\text{-}2]$$

$h = 2\pi/h$ with h being Planck's constant; $\mathbf{k}_j$, $\mathbf{k}_s$ and ω_j, ω_s are, respectively, incident and scattered vectors and angular frequencies. A typical light scattering geometry is shown in Figure 3.3.2.

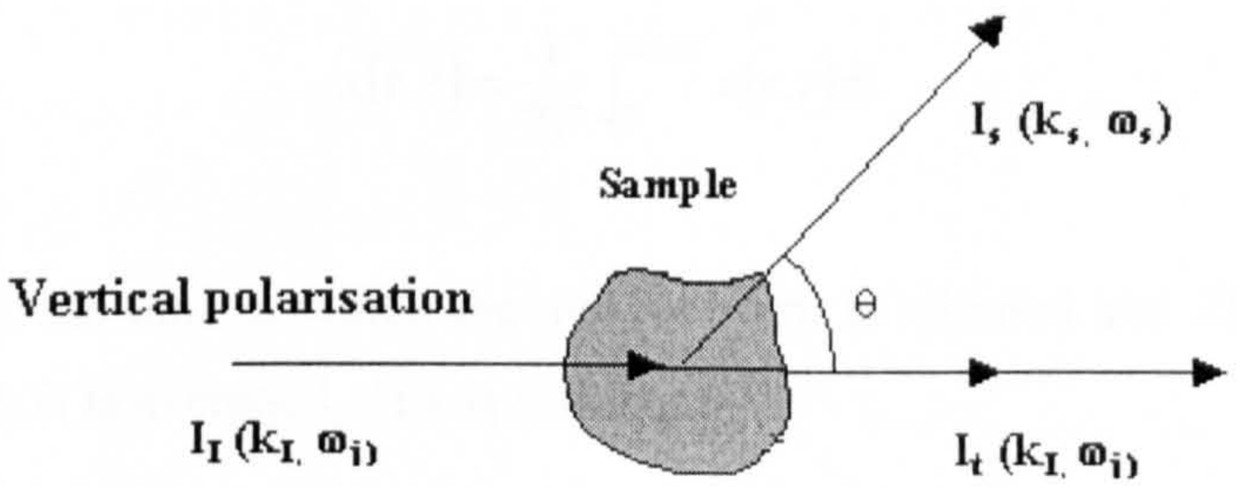

Figure 3.3.2 Scattering geometry of light scattering

I_I, I_s and I_t are, respectively, the incident, the scattered, and the transmitted intensities; θ is the scattering angle; and $K_I = 2\pi/\lambda_I$, $K_s = 2\pi/\lambda_s$ with $\lambda_j \equiv (\lambda_0/n) \cong \lambda_s$, λ_0 being the wavelength, and n the refractive index of the scattering medium. K[=($4\pi/$, λ sin ($\theta/2$)] is the magnitude of the momentum transfer vector. For visualisation of the geometry in Equation 3.3.2-1, we set the incident beam polarisation to be perpendicular to the plane of the paper and the scattering plane is defined by I_I and I_s.

The scattered light from a well-defined incident beam has a distribution of wave vectors and at each wave vector, $\mathbf{k_s}$, there can be a distribution of frequencies depending on the dynamics in the scattering medium. As the energy transfers in terms of frequency change ($\Delta\omega$) depend on the scattering dynamics, the scattered intensity fluctuates as a function of time.

The transfer of momentum ($\hbar\mathbf{K}$) corresponds to probing the structures of the system with a spatial resolution $R \sim \mathbf{K}^{-1}$. Measurements of the time-averaged scattered intensity $\langle I(\mathbf{K})\rangle$ can be related to the structural studies.

The time dependence of the correlation (or probability) function becomes important in a problem involving random signals and noise. The measured bulk property of x at equilibrium is a time-average value

$$\overline{x(r,t)} = \frac{1}{2T}\int_0^{0+2T} x(r,t)dt \qquad [3.3.2\text{-}3]$$

where t_0 is the time at which the measurement is initiated and $2T$ is the time period over which it is averaged. If x is stationary,

$$\langle x\rangle = \lim_{T\to\infty}\frac{1}{2T}\int_{-T}^{T} x(r,t)dt \qquad [3.3.2\text{-}4]$$

where $\langle x\rangle$ is the time average of x and is independent of t_0. The integration can be from $-T$ to T or to $2T$. We define the time correlation function of x(t) as

$$R_x(\tau) = \langle x(t)x(t+\tau)\rangle = \lim_{T\to\infty}\frac{1}{2T}\int_{-T}^{T} x(t)x(t+\tau)dt \qquad [3.3.2\text{-}5]$$

where τ is the delay time. $x(t)x(t+\tau) \equiv x(t_i)x(t_j)$ with $\tau = t_j - t_i$.

The integral indicates a time average over all starting times t inside the periodgram of length $2T$. Furthermore, we have taken the random process to be stationary, so that the joint probability distribution of x_1 and x_2 depends only on the time difference and

not the particular value of t_I and t_j. The limit exists provided that the average " power" in x(t), $R_x(0)$ ($\equiv \langle x^2(t) \rangle$, is finite.

$$\langle x(t+\tau)x(t)\rangle = \langle x(\tau)x(0)\rangle \qquad [3.3.2\text{-}6]$$

For time-invariant random processes, the correlation function is independent of t. Then

$$\tau \to 0 \qquad \langle x(t+\tau)x(t)\rangle \to \langle |x(t)|^2 \rangle \qquad [3.3.2\text{-}7]$$

$$\tau \to \infty \qquad \langle x(t+\tau)x(t)\rangle \to \langle x(\tau)\rangle\langle x(0)\rangle = \langle x\rangle \qquad [3.3.2\text{-}8]$$

The auto-correlation function of a non-periodic property x decays from its initial value $< x(t)^2 >$ as $\tau \to 0$ and becomes $< x(t)^2 >$ as $\tau \to \infty$. Figure 3.3.2 shows a schematic plot of the correlation function $\langle x(0)x(\tau)\rangle$.

The correlation function and power spectral density, S_x, was connected through Fourier transforms. The x_{2T} can be decomposed rigorously into its Fourier components.

$$x_{2T}(t) = \int_{-\infty}^{\infty} \hat{x}(\omega)\exp(-i\omega t)d\omega \qquad [3.3.2\text{-}9]$$

and

$$\hat{x}_{2T}(\omega) = \frac{1}{2\pi}\int_{-\infty}^{\infty} x_{2T}(t)\exp(i\omega t)dt \qquad [3.3.2\text{-}10]$$

For complex x we have

$$\langle x(t+\tau)x^*(t)\rangle = \int_{-\infty}^{\infty} d\omega \left(2\pi \lim_{T \to \infty} \frac{\hat{x}_{2T}(\omega)}{2T} \right) \exp(-i\omega\tau) \qquad [3.3.2\text{-}11]$$

which gives

$$\left\langle x(t+\tau)x^*(t)\right\rangle = \int_{-\infty}^{\infty} S_x(\omega)\exp(-i\omega\omega)d\omega \qquad [3.3.2\text{-}12]$$

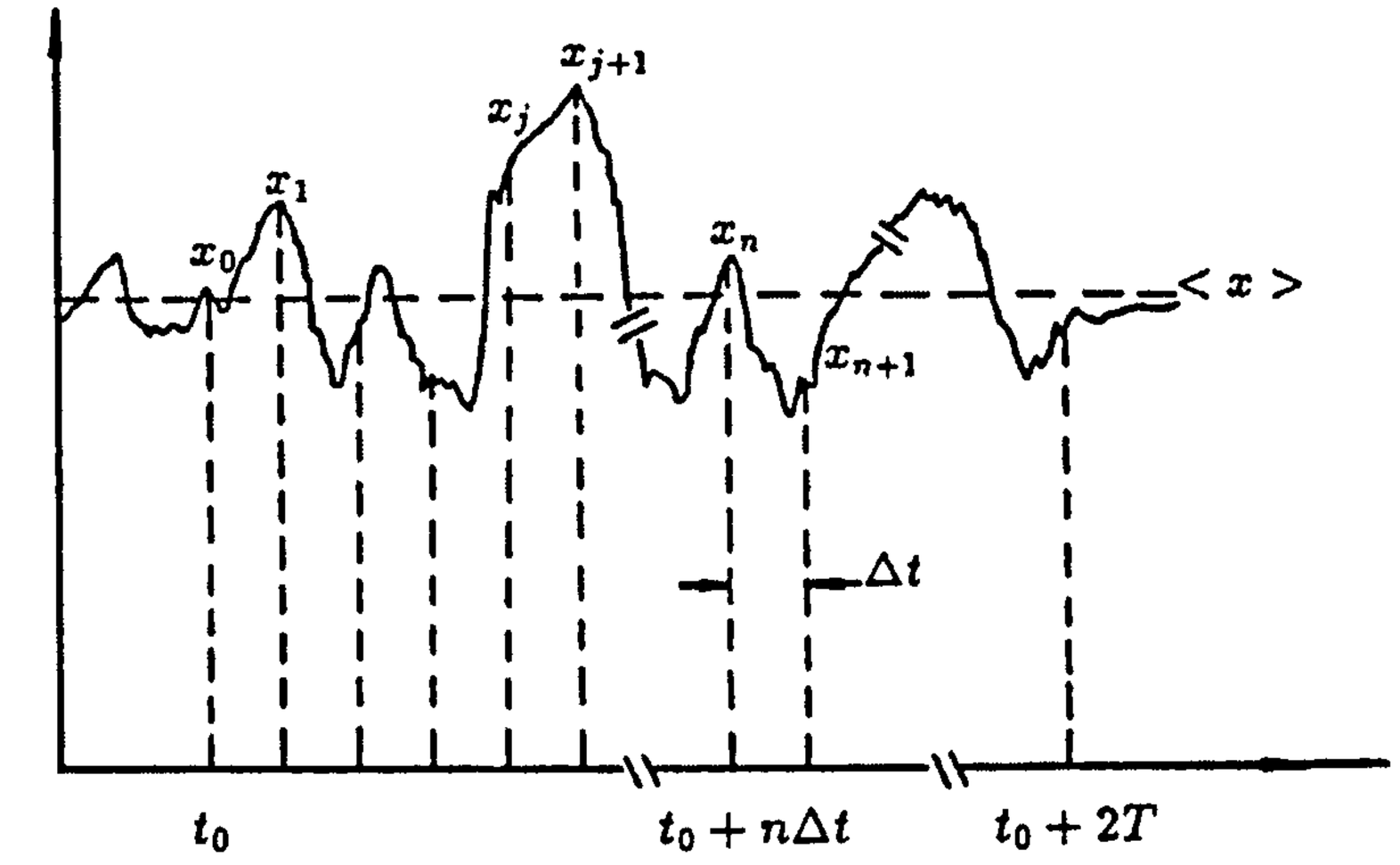

Figure 3.3.3 Schematic plot of the correlation function $< x(0)\, x(\tau)>$[206].

The correlation function is an inverse Fourier transform of the power spectral density $S_x(\omega)$ and the power spectra density is the time Fourier transform of the correlation function.

$$S_x(\omega) = \frac{1}{2\pi}\int_{-\infty}^{\infty}\left\langle x(t+\tau)x^*(t)\right\rangle \exp(i\omega\omega)d\tau \qquad [3.3.2\text{-}13]$$

A commercial laser light scattering spectrometer (ALV/SP-150) equipped with ALV-5000 digital time correlator was used with a solid-state laser (ADLAS DRY425II, output power ~400mW at λ = 532.8nm) as the light source. The incident light beam was vertically polarised with respect to the scattering plane, and the intensity was regulated with a beam attenuator (Newport M-925B) so as to avoid localised heating in the light scattering cuvette. Light scattering results from polysaccharide solutions have often been complicated by the presence of the aggregates [206]. Ultracentrifugation and filtration of the solutions have a significant effect on the results. Usually solutions in concentration range of 10^{-4} to 10^{-6}g/ml are used, but the lower the concentration the more reliable are the results obtained.

3.3.3 Fourier Transform Infrared Spectroscopy (FT-IR)

FT-IR spectroscopy is a well established analytical technique employed particularly in the identification and study of organic molecules and is concerned with the detection of transitions between vibrational energy levels in molecules, resulting from stretching and bending vibrations of interatomic bonds [207]. The frequencies of such vibrations are characteristic of specific functional groups and are affected by the molecular environment, chain conformation (in polymers), morphology and intermolecular interactions.

At room temperature, most molecules exist in their ground vibrational energy state. When molecular vibrations cause a change in the bond dipole-moment, resulting from a change in the electron distribution in the bond, it is possible to simulate transitions between energy levels by interaction with electro-magnetic radiation of the appropriate frequency. Molecular vibrations are enhanced when the electric sector of the incident radiation is in phase with the vibration dipole. When this happens,

energy is transferred from the incident radiation to the molecule and it is this absorption of energy which is the basis of FT-IR spectroscopy. In practice, spectral transitions are detected by scanning through the frequency range (typically 4000-400 cm^{-1}), whilst monitoring the intensity of the transmitted light.

An FT-IR spectrum represents a fingerprint of a sample with absorption peaks, which correspond to the frequencies of vibrations between the bonds of the atoms making up the material. FT-IR spectroscopy is widely used in both qualitative and quantitative analysis of polymers and additives [207]. It has also been applied to studies of the polymerisation process, end group analysis and investigations of mechanical deformation of material [208]. These techniques also allow information on chain conformations, stereochemical structure etc. of polymers to be obtained [208].

FT-IR can also be used to study physical interactions between the components of a mixture. Interactions between the molecules of two components in a polymer blend are often an important factor, which promotes miscibility, and such interactions can often be observed as a shift in the wavenumber of the bands relating to the groups involved.

Figure 3.3.4 shows the layout of a typical FT-IR spectrometer. There are three basic components: a source, a Michelson interferometer (consisting of a beam splitter, a fixed mirror and a moving mirror) and a detector. Collimated radiation from the broad-band source is directed into the interferometer and impinges on the beam splitter. Approximately 50% of the light is transmitted through the beam splitter and is directed onto the fixed mirror. The remainder of the light reflects off the beam splitter and is directed onto the moving mirror. The beams reflect off the surfaces of the two mirrors and recombine at the beam splitter. Here, constructive and destructive interference occur, and depending on the relative position of the moving and fixed mirrors, absorption takes place. Finally, the light beam continues onto the detector. In simple terms, what is happening is that the interferometer encodes the initial frequencies (by optically taking the Fourier transformation of the incoming signal) into a special form that the detector can observe in time. The inverse Fourier transformation is a mathematical means of resorting the individual frequencies for the final presentation of the infrared spectrum.

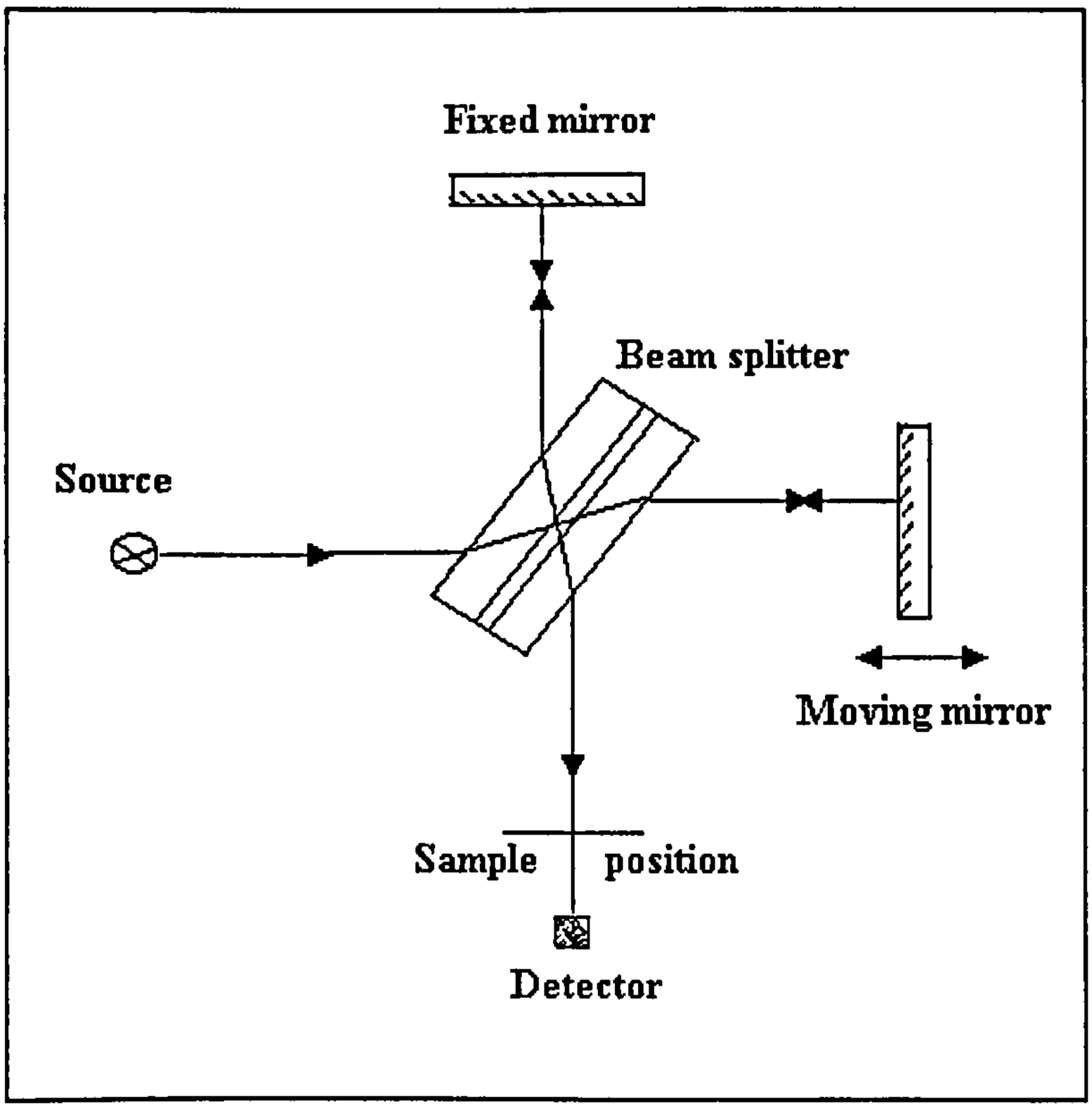

Figure 3.3.4 Schematic diagram of a f FT-IR spectrometer

In our experiments, transmission spectra of the films were recorded using a Mattson 3000 FTIR spectrometer for 64 scans at a resolution of $4cm^{-1}$. The specimen films were prepared as described in Section 3.2.1, except that the concentration of solution was 0.5wt.% instead of 1.5wt.%. The dried films were treated by immersing films in methanol for 24 hours to remove acetic acid and were then dried for 24 hours at 35°C. The samples for the study of the crosslinking process by FT-IR spectroscopy were prepared in the manner described in Section 3.2.4.

3.3.4 Differential Scanning Calorimetry

Structural changes are usually associated with changes in heat absorption or emission and are measured by means of calorimetry. Differential scanning calorimetry (DSC)

can measure the changes at constant heating or cooling rates. DSC is an invaluable tool in the characterisation of polymer materials [209-211], yielding information on such processes as the glass transition, reaction kinetics, melting behaviour, structure relaxation, degree of crystallinity and other aspects of polymer morphology. A DSC instrument is a simple device for measuring the heat flow into and out of a sample, usually while it is subjected to an isothermal or linearly rising temperature programme. The difference in heat loss or gain between the sample and reference cells is measured in a differential scanning calorimeter. In this case, the heat input needed to maintain both cells at the same temperature is measured. The principle of this technique is schematically illustrated in Figure 3.3.5.

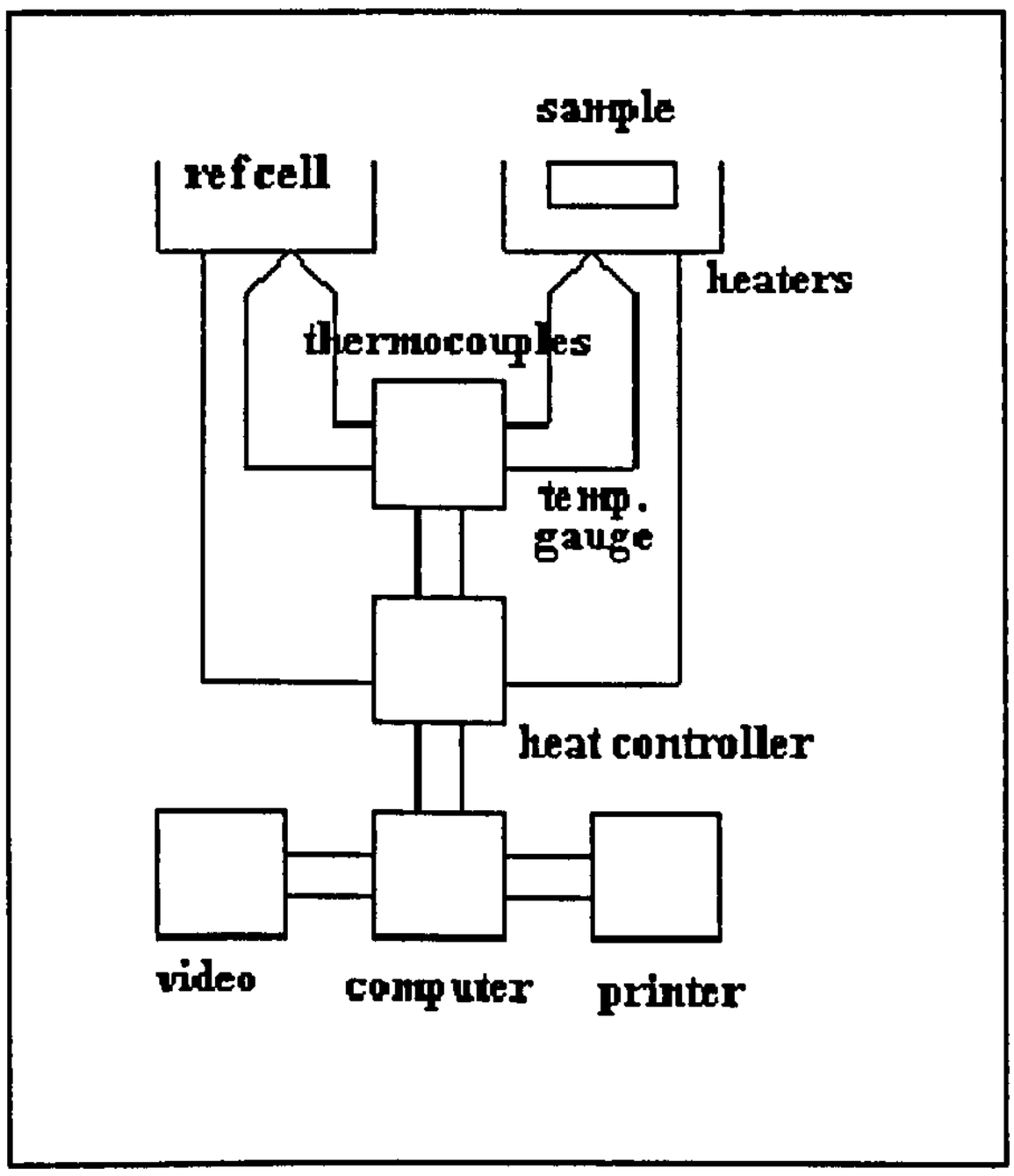

Figure 3.3.5 A schematic diagram of DSC

The cells are mounted in a metal block, which can be cooled for more efficient heat stability. The thermocouples measure the temperatures as well as differences in temperature. The difference is quickly compensated by the heat controller, and the amount of compensation is measured. DSC curves reflect the temperatures and heat flows associated with transitions in materials as a function of time and temperature.

From these measurements, the rate of heat absorbed by, or evolved from, the sample can be computed. The more detailed description of the utility and design parameters of differential scanning calorimetry can be found [211,212] elsewhere.

DSC has been used widely to characterise [209-211] the thermal properties of polymeric materials. DSC is a particularly useful tool in studying polymer-polymer miscibility and phase-separated polymer blends [210].

In this study, the thermal analysis was carried out using a TA Instruments differential scanning calorimeter, DSC, 2920. For each experiment, the sample had the same thermal history. LPEO, CS/LPEO blends, CS/LPEO blend networks, HPEO, CS/HPEO blends and CS/HPEO blend networks were heated to 80°C and kept at 80°C for 10min. After this, the samples were cooled to -10°C for CS/HPEO blends and their networks, to -35°C for CS/LPEO and their networks, respectively, at cooling rate of 10°C/min. Then, they were reheated at a heating rate of 10°C/min.

3.3.5 Ultraviolet/visible spectrometry (UV)

UV spectrophotometry is based on the fact that electrons in certain types of chemical bonds are excited from the ground state when exposed to radiation in the wavelength range of 200 – 800 nanometres (UV: 200-380nm; Vis: 380-800nm). The sample will absorb energy at wavelengths whose energies correspond to that required for the electronic transition. The spectrum corresponds to electronic excitation and the energy levels depend on the chemical bonds within the specimen. σ-electrons, involved in covalent bonds, absorb high energy photons in the UV region, whereas, π-electrons absorb photons at larger wavelengths, often in the visible region [213]. Absorption is determined by measuring the difference in the signal with and without the presence of the absorbing species. As a result, a typical electronic absorption spectrum is obtained [213].

UV-visible spectrophotometry consists in implementing Beer-Lambert's law. For a given sample, the light absorbed is a function of the concentration of its components:

$$A = kcl \qquad [3.3.5\text{-}1]$$

where A is the absorbance; k is the extinction coefficient and l is the path length. The measurement of light absorption at one, or several, wavelengths, thus allows quantification of the samples [213].

UV-visible spectrophotometry provides information on the multiple bonds and the aromatic conjugation with in molecules. The interaction between polymer molecules and the UV component in sunlight can lead to dissociation of σ-bonds and is principal cause of photodegradation of polymers [213]. Aromatic structures have delocalised electrons and exhibit strong UV absorption at very short wavelengths. The absorption in the far ultraviolet region, where wavelengths are shorter than 200nm, which involve the σ bonds and π electrons in a nonconjugated system, cannot be detected. Only polymers having a fairly high percentage of conjugated systems will show characteristic absorptions [213]. Hence, ultraviolet absorption spectra have limitations with respect to the analysis and identification of polymers. However, it can be extremely useful for the determination of impurity traces of highly conjugated or aromatic materials in polymers [213].

The commonly used UV-visible spectrometers measure absorption of light in the visible and near ultraviolet region, i.e. 190-750nm. The basic instrumentation consists of one or several light sources such as a tungsten filament lamp for >375nm and a deuterium discharge lamp for <375nm. A monochromator selects the desired wavelength; a compartment is accessible by the sample; a detector is used to feed the ratio of reference beam to sample beam intensities (I_0/I) to a pen recorder and a data processing system. Figure 3.3.6 illustrates the component parts.

Of the few sampling techniques for UV spectrometry, the solutions technique is the most commonly used and was adopted in this research. By this technique, the amount of material that can be detected in solution is very small. The choice of solvent is important as the possibility of reaction or solute-solvent associations will affect the spectra.

In this study, an Uvicam SP1800 spectrophotometer was used to record the UV spectra between 190nm and 400nm. The equipment settings are: absorbance meter range 0-2; slit width 0.34nm; scan speed 120nm/min. Deionised water was used as the reference.

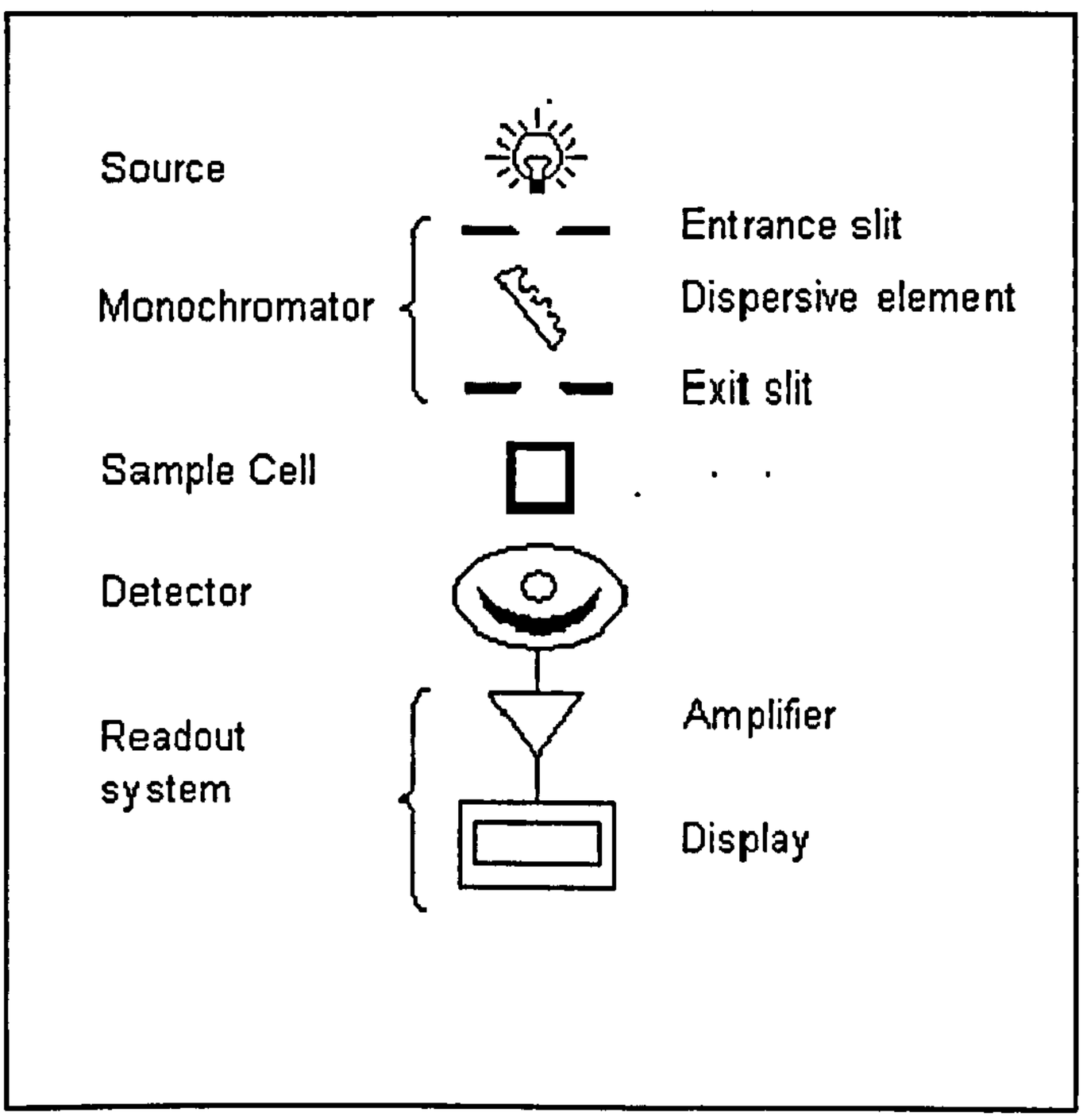

Figure 3.3.6 Schematic diagram of the component parts of a UV spectrophotometer

3.3.6 Tensile tests

The prime consideration in determining the general utility of a polymer is its mechanical behaviour: the deformation and flow characteristics under stress [214, 215].

Testing usually consists of securing a standard test sample between two sets of grips. One set of grips is fixed and the other is attached to a moving crosshead and load-cell arrangement. The sample used is usually of a dumb-bell shape (see Figure 3.3.7) so that breaking occurs in the central area away from the grip regions. Crosshead speed depends on the nature of the polymer material [214,215]. It should be noted that test speed influences tensile behaviour dramatically.

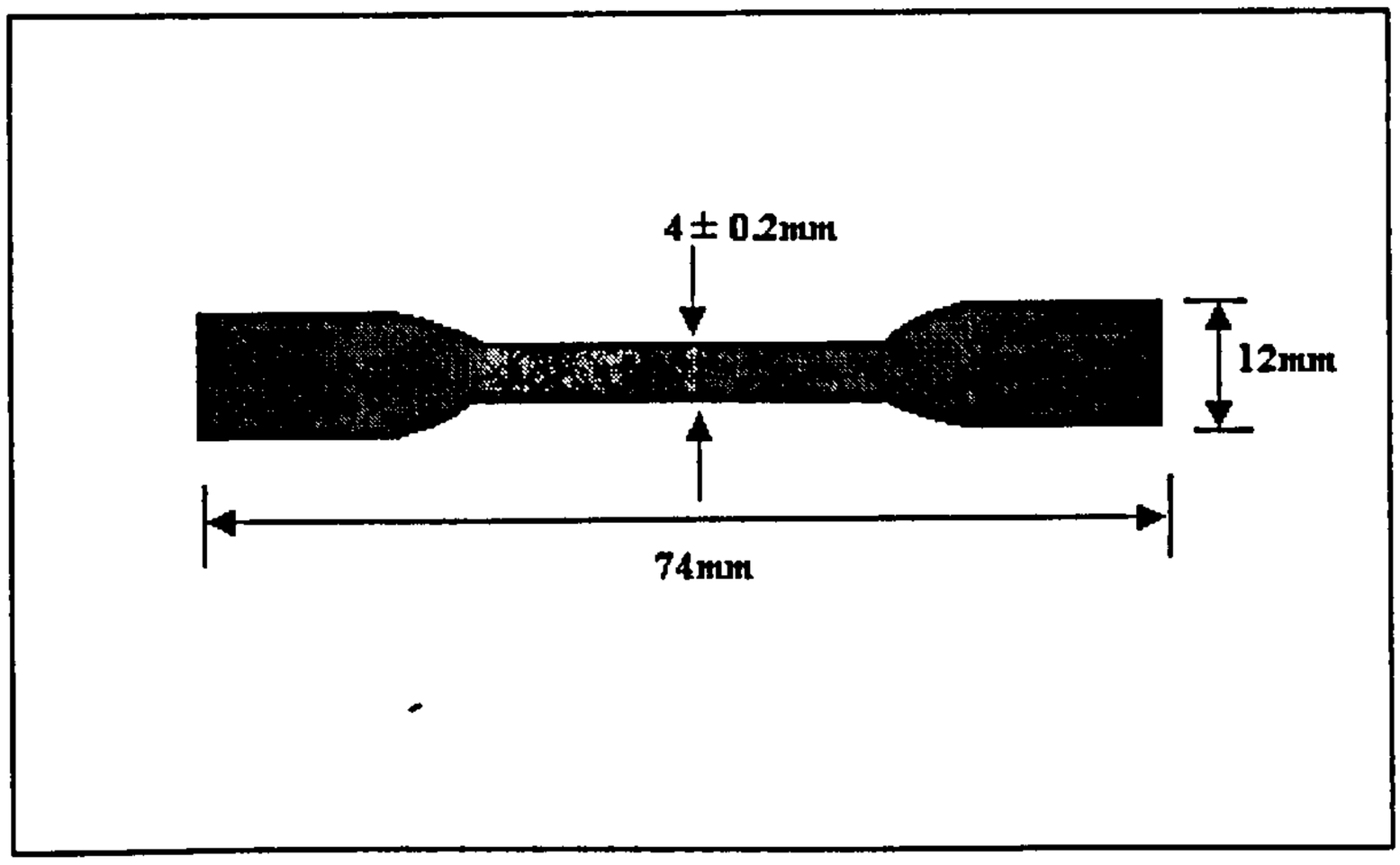

Figure 3.3.7 Dimensions of the dumbbell specimens that were used in this research

The tensile testing results are usually shown as a plot of the stress versus the elongation (strain) as shown in Figure 3.3.8. The following tensile parameters were calculated [214].

(1) Tensile strength (σ) - the maximum tensile stress which the test piece is capable of supporting.

$$\sigma = \frac{F}{A}(MPa) \qquad [3.3.6\text{-}1]$$

where F is the force, in N, and A is the initial cross-sectional area of the sample, in m^2

(2) Elongation at break (ε) –the extent of elongation when the sample ruptures.

$$\varepsilon(\%) = \frac{L - L_0}{L_0} \times 100 \qquad [3.3.6\text{-}2]$$

where L is length between reference marks at break, in mm and L_0 is initial gauge length in mm.

(3) Elastic modulus (modulus of elasticity or Young's modulus) – the ratio of applied stress to the strain it produces in the region where strain is proportional to the stress. Primarily a measurement of resistance to deformation, or the stiffness, of a material.

$$\text{Modulus} = \frac{\Delta\sigma}{\Delta\varepsilon}(\text{MPa}) \qquad [3.3.6\text{-}3]$$

where $\Delta\sigma$ is the difference in stress between two points on the straight line. $\Delta\varepsilon$ is the difference in strain between the same two points.

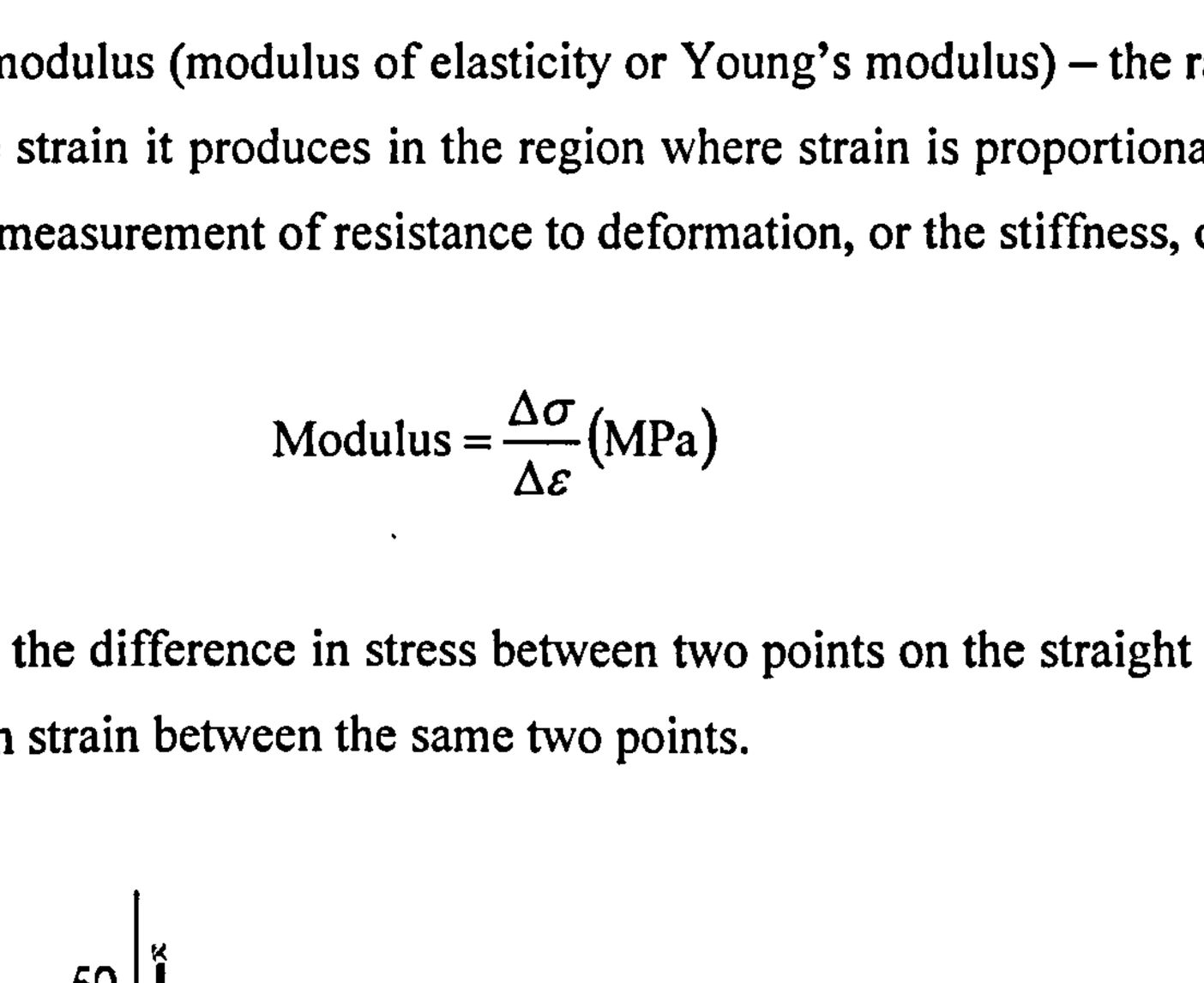

Figure 3.3.8 A typical tensile stress-strain curve for a polymer. (A) for a brittle polymer, (B) for a toughness polymer, (C) for an elastic polymer

The tensile strengths of the films were measured using a Lloyd Instruments L1000 tensometer and using a 500N load cell operated according to the D638 ASTM standard. The extension rate was 10mm/min. In order to examine the physical properties of the films as a function of moisture content, they were placed in relative humidity chambers over distilled water; and the moisture content was determined by drying to constant weight. Each test was repeated at least 5 times and the average taken.

3.3.7 Solubility and stability in neutral water

The crosslinked/un-crosslinked CS and CS/HPEO (LPEO) blend films were immersed in 100ml methanol for 24 hours to remove the acetic acid in the films, then they were taken out and dried for 24 hours at 35°C. The dried films were weighed accurately with an electronic balance. The dried films were then immersed in distilled water (pH 7) for 8 hours, and the remaining films were then taken out and dried for 48 hours in vacuum at 35°C. A second weighing was conducted to determine the amount of PEO extracted from blends. All the films used were from the samples used in the tensile strength measurements above. Stability, therefore, can be expressed by the following equation.

$$S = W_2/W_1 \times 100 \qquad [3.3.7\text{-}1]$$

where *S* is the percentage weight of the extracted films after immersion in neutral water. W_1 and W_2 are the weight of dried films before and after immersion in water, respectively. Each experiment was repeated three times and the average value taken.

3.3.8 Swelling experiments

The swelling behaviour of the crosslinked/un-crosslinked CS and their blend films with LPEO were determined by swelling the films in media of different pHs at room temperature and 38°C, respectively. The samples (approximately 0.05g) were first treated as described above to remove any acetic acid. Blends and networks were incubated for approximately 48 hours in buffer solutions ranging from pH 2 to 13. It

was confirmed experimentally that after a 48-hour incubation period, the films reached their swelling equilibrium. The films were withdrawn from the buffer solutions and their wet weights were determined by first blotting with a filter paper to remove absorbed water on the surface, followed by immediate weighing on an electronic balance. The percentage of specific solution content, or weight uptake, of the films is expressed by the following equation.

$$E_{sw} = [(W_s - W_d) / W_d] \times 100 \qquad [3.3.8\text{-}1]$$

W_d and W_s are the weights of the samples in the dry and swollen states, respectively.

In order to study the drug release mechanism, the volume fraction of water, *H*, in the swollen membrane was used. *H* value measurements where obtained by the swelling experiments in water at 23°C. The volume fraction of water is expressed by the following equation.

$$H = (W_s - W_d) / W_s \qquad [3.3.8\text{-}2]$$

3.3.9 Contact angle measurements

Information on the surface properties of a material can be readily obtained by a relatively fast and simple contact angle measurement. This method measures the extent to which a liquid interacts with a solid to promote wetting, characterized by the contact angle [216-218].

The surface energy of a solid can be estimated by the measurement of a contact angle formed at a three-phase interface. There are a number of possible methods of measuring the contact angle on a solid surface, including:

- Sessile drop
- Pendant and receding drop
- Advancing and receding bubble
- Drop on a tiled plane

When a drop of a liquid is placed on a solid surface, the system will try to establish a state of minimum total surface free energy. Depending upon the relative values of the interfacial tensions involved, the contact angle, θ, between the liquid and the solid phase will vary from 0° and 180°. Young [216] first proposed treating the contact angle of a liquid as the result of the mechanical equilibrium of a drop resting on a plane solid surface under the action of three surface tensions (see Figure 3.3.9).

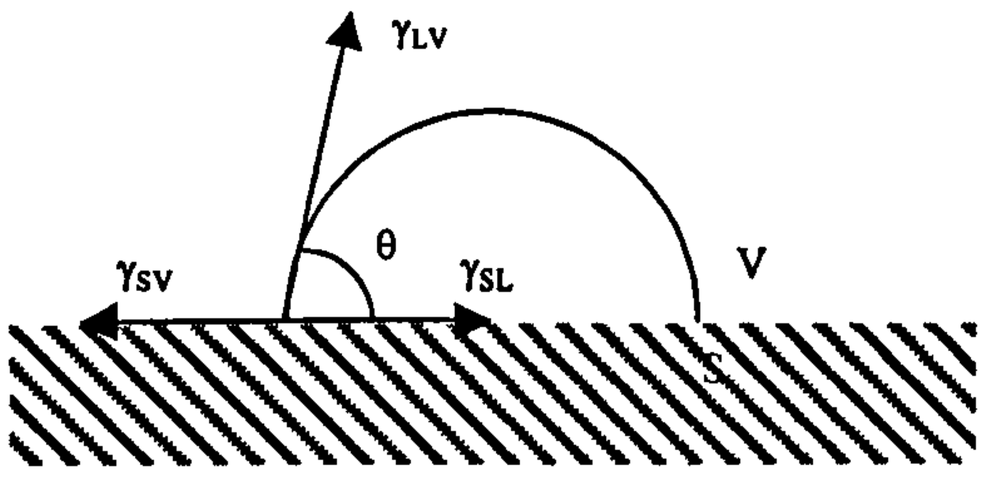

Figure 3.3.9 Schematic of a liquid drop on a surface and the forces acting at three-phase contact point.

The correlation between γ and θ is given by Young's equation [216].

$$\gamma_{SV} = \gamma_{SL} + \gamma_{LV} \cos\theta \qquad [3.3.9\text{-}1]$$

where γ_{SV} is the interfacial tension between solid and vapour, γ_{SL} is the interfacial tension between solid and liquid, γ_{LV} is interfacial tension between liquid and vapour and θ is the contact angle.

The contact angle used in Young's equation relates to the equilibrium angle of a liquid on a surface, because it is assumed that the surface is both smooth and chemically homogeneous. However, the simplicity of Young's equation is deceptive because there are conceptual and experimental difficulties.

The surface free energy is related to the following relationship

$$\gamma_{SV} = \gamma_S - \pi_\theta \qquad [3.3.9\text{-}2]$$

where γs is the true surface free energy of solid (equal to G^s). π_θ is a quantity known as the equilibrium spreading pressure. The term π_θ is a measure of energy released through adsorption of the vapour onto the surface of the solid, a process that lowers its surface free energy. π_θ is usually negligible when the contact angle is larger than 10°, but becomes significant when the contact angle is smaller than about 10°. When π_θ is negligible, γ_{SV} equals to γs.

Fowks [217] proposed a separation of the surface energy of a material into the potential energies of interaction between the liquid and the solid. He suggested that the surface tension of a phase could be divided up into independent component parts, such as London dispersion contribution γ^d and polar contribution γ^p as represented below:

$$\gamma = \gamma^d + \gamma^p \qquad [3.3.9\text{-}3]$$

Fowks [217] also make a fundamental hypothesis important to the study of interfaces and adhesion, namely that materials exhibiting only dispersion force interactions interact with other surfaces by only those interactions. It was also Fowks' contention that polar force and dipole-induced dipole forces were insignificant when one of the materials at an interface was non-polar. Mathematically, this can be stated as follows.

$$\gamma_{SL} = \gamma_s + \gamma_{SL}\gamma_L - 2\left(\gamma_S^d \gamma_L^d\right)^{1/2} \qquad [3.3.9\text{-}4]$$

The success of the Fowks hypothesis prompted others to develop a theory of fractional polarity. One such equation was developed by Owens and Wendt [218]

$$\gamma_{SL} = \gamma_S + \gamma_L - 2\left(\gamma_S^d \gamma_L^d\right)^{1/2} - 2\left(\gamma_S^p \gamma_L^p\right)^{1/2} \qquad [3.3.9\text{-}5]$$

By combining Equations. 3.3.9-1, 3.3.9-3 and 3.3.9 -5,

$$(1+\cos\theta)\gamma_L / 2\left(\gamma_L^d\right)^{1/2} = \left(\gamma_S^p\right)^{1/2}\left(\gamma_L^p / \gamma_L^d\right)^{1/2} + \left(\gamma_S^d\right)^{1/2} \qquad [3.3.9\text{-}6]$$

γ_L, γ_L^d and γ_L^p can all be found in the literature. γs^p and γs^d may also be denoted as G^s_p and G_d^s.

For contact angle analysis, solutions for both crosslinked and un-crosslinked chitosan and their blends with HPEO (or LPEO) were prepared as outlined in Section 3.2. Contact angle measurements were carried out using a Data Physics OCA20 instrument, which comes with an automatic image capture system. The advancing sessile drop method was employed where the needle remained immersed in the drop during measurements. This is to avoid unnecessary vibration or distortion of the drop. The volume of the drop was increased by 1μl at a dosing rate of 0.5μl/s. The liquids used were pure water, mixtures of 70% pure water and 30% ethanol and 50% pure water and 50% ethanol. Due to the rapid evaporation of ethanol and the need to maintain consistency of results, dynamic tracking was set up to capture the contact angle of the drop at every second for up to 1 minute. Plots of contact angle (θ) versus drop age (seconds) were generated for each sample with different liquid systems.

3.3.10 Permeability and drug release studies for Vitamin B_{12}

In order to estimate the usefulness of hydrogel membranes for a given application, knowledge of their transport properties is required. The diffusion rate of selected solute through the membrane can be measured. When no chemical interactions between the solute and the membrane take place, solute diffusion through a hydrogel membrane is described by Fick's first law [219].

$$J_s = \frac{P}{l}\frac{dC}{dt} = \frac{P\Delta c}{l} \qquad [3.3.10\text{-}1]$$

where J_s is the solute flux, P is the solute diffusion permeability coefficient in the membrane, l is the membrane thickness, and Δc is the solute concentration difference

across the membrane. The permeability coefficient is a product of the solute solubility coefficient in the membrane.

The solute diffusion in the gel membrane, D_{gel}, was evaluated using the following equation:

$$D_{gel} = P/K_d \qquad [3.3.10\text{-}2]$$

where K_d is a partition coefficient.

This partition coefficient is driven by interactions between the solute and the polymer chains. Here, the tendency of the magnitude of the partition coefficient may sometimes be contrary to that of the diffusivity. That is the polymer in which solute has a higher partition coefficient may sometimes show lower diffusivity.

The diffusion apparatus consisted of two cylindrical half-chambers 230cm^3 in volume. The chitosan membrane was placed between the compartments. The effective membrane area was 2.83cm^2. Each compartment was stirred continuously by an externally mounted constant-speed motor. The diffusion apparatus was placed in a water bath maintained at 37°C. Membranes were swollen to equilibrium in deionized water at 37°C before they were placed between the two chambers.

The donor compartment was filled with 2mg/ml vitamin B_{12} solution and deionized water was added to receptor side. Samples of the donor and receptor chambers were taken at various time points. The vitamin B_{12} concentration of the samples was determined using a UV spectrometer.

For diffusion cell experiment Equation 3.3.10-1 can be derived as following [220]

$$\ln(1-\frac{2c_t}{c_0}) = -\frac{2AP}{Vl}t \qquad [3.3.10\text{-}3]$$

c_t is the vitamin B_{12} concentration in the receptor cell at time t, c_0 is the initial vitamin B_{12} concentration in the donor compartment, A is the membrane surface area, V is the

volume of each cell, l is the membrane thickness and P is the permeability coefficient [221]. The permeability coefficient, P, was calculated from the UV absorbance data by Equation 3.3.10-3

The partition coefficient can be defined in two ways [222]. One is the ratio of solute concentration in the membrane to that in the surrounding solution. This can be determined by solute uptake experiments. The membrane, previously equilibrated in deionized water, was incubated in a vitamin B_{12} solution (1mg/ml, 20ml) at 37°C. After 48 hours, the membrane were taken out from the solution, blotted with a tissue to remove the excess aqueous solution on the membrane surface and immersed in 20ml deionized water at 37°C for 48 hours. The concentration of vitamin B_{12} released in the solution (C_2) was determined by UV spectrometry as described above. From the known concentration of solute after equilibration with the membrane (C_1), it was possible to estimate the amount of solute sorbed into the swollen membrane. The partition coefficient, K_d, was calculated according to Equation 3.3.10.4.

$$K_d = \frac{C_2 V}{V_p (C_1 - C_2)} \qquad [3.3.10\text{-}4]$$

where V and V_p refer to the volume of the buffer and swollen membrane, respectively.

The other is the ratio of the solute concentration in the membrane standardised by the water volume in the membrane to that in the bulk solution. If we express the former as K_d and latter as K', the two partition coefficients are related as follows.

$$K_d = HK' \qquad [3.3.10\text{-}5]$$

The diffusion coefficient (D) of vitamin B_{12} in the various the films was evaluated by Equation 3.3.10-2.

3.3.11 ES release from a drug carrier

Figure 3.3.10 shows the UV spectra of ES at different concentrations. It can be seen that the absorption peak at 200nm increased markedly with increases in the solution concentration. The value of absorption at 200nm vs. ES concentration is shown in Figure 3.3.11, where the value of absorption at 400nm was considered as the base line because it was independent of the concentration of ES. A linear relationship between the value of absorption at 200nm and ES concentration was obtained. In the ES release study, this figure was used as the standard curve for determining the fractional ES release.

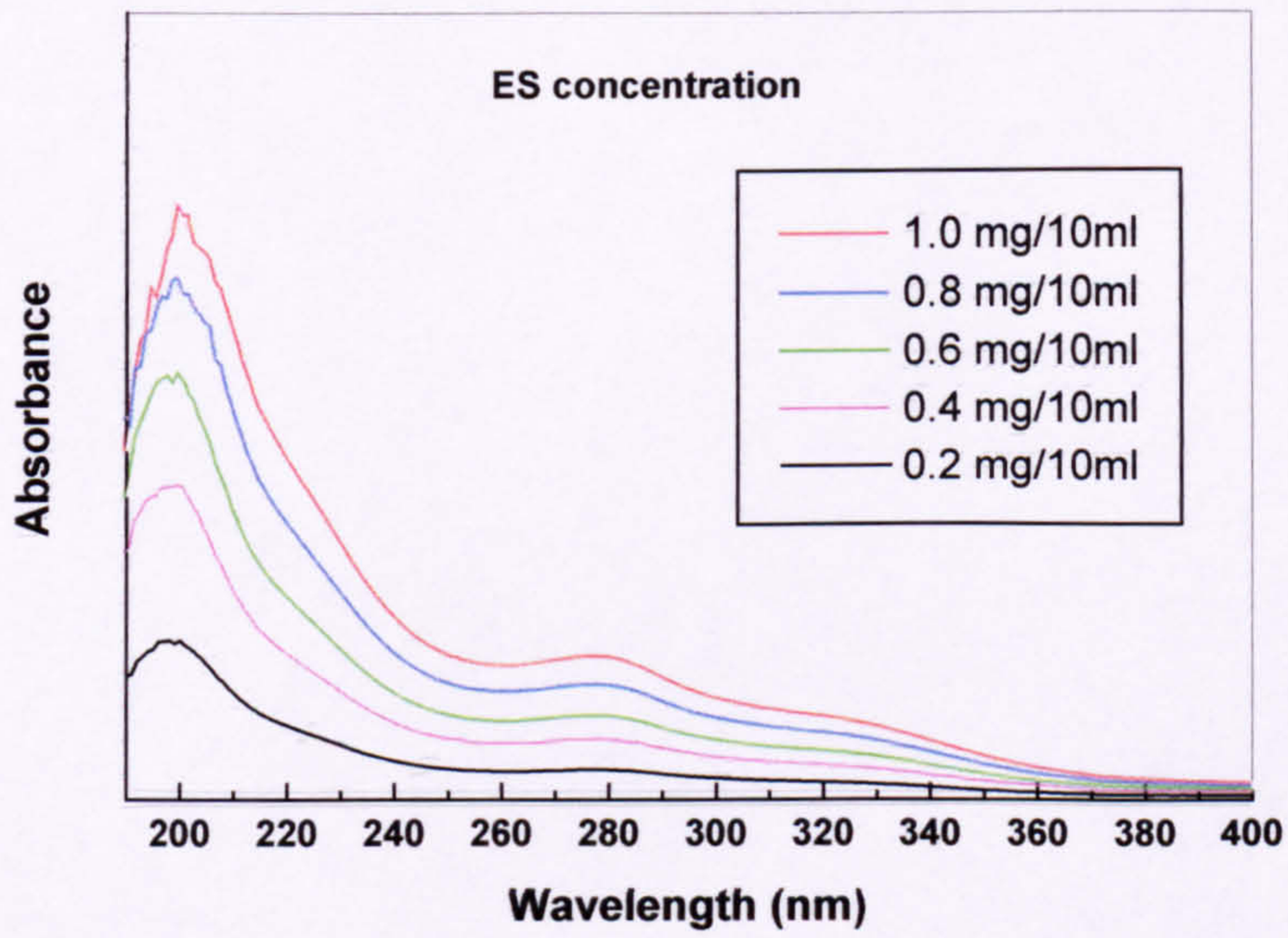

Figure 3.3.10 UV spectra of ES with different concentration

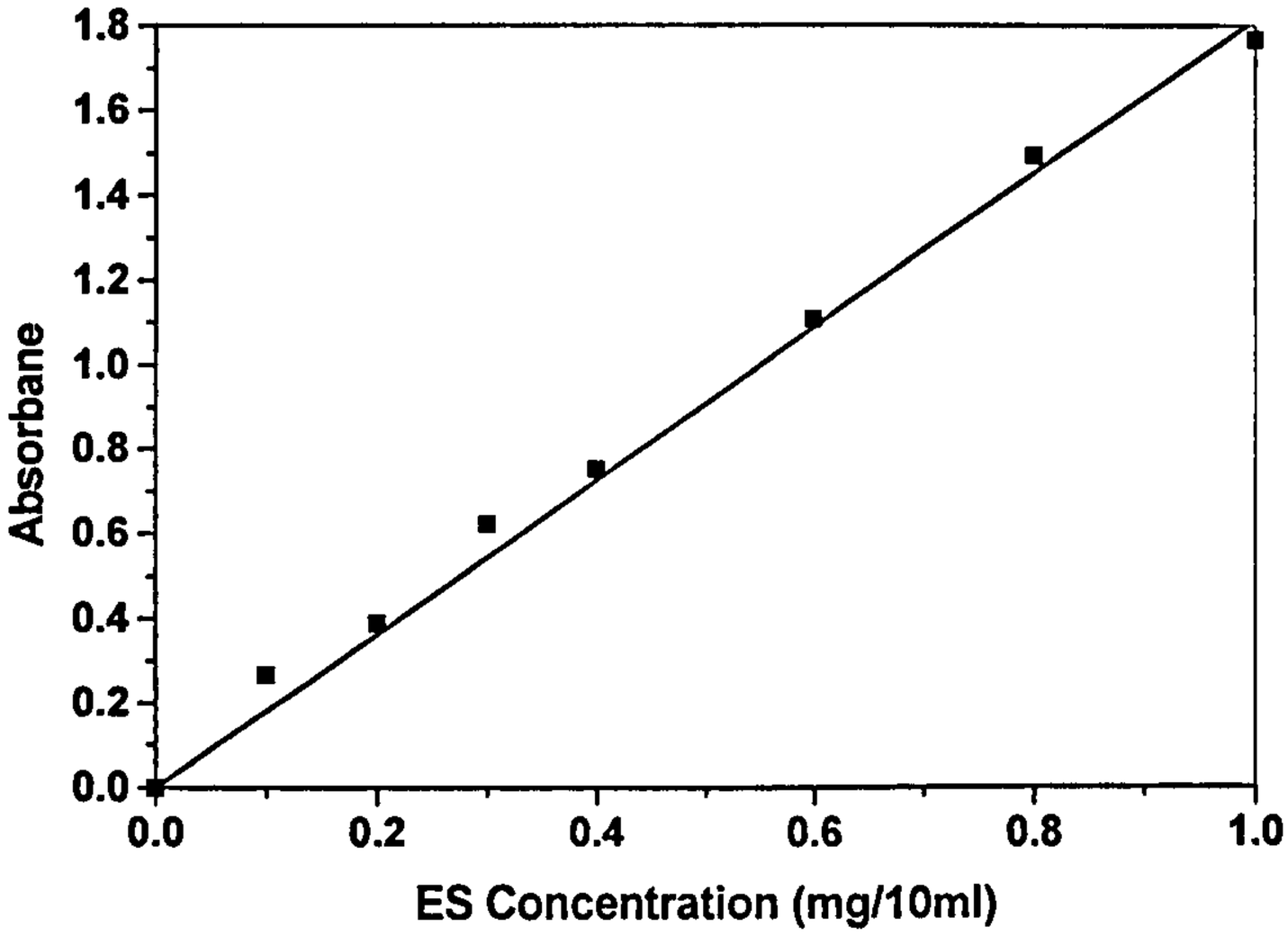

Figure 3.3.11 A standard concentration curve of ES

Samples of loaded drug were prepared (see Section 3.2.7). For the drug release study, two methods of drug release were employed: from fully hydrated samples (fixed boundary condition) and from dry samples (moving boundary condition).

For fully hydrated or dried samples, each film was immersed in a beaker containing 250ml of distilled water at 37°C and was well stirred with a magnetic stirring bar to minimise boundary layer formation around the film. Samples of solution were removed from the beaker at various time intervals. ES concentrations of the collected samples were measured at 200nm with a UV/VIS spectrophotometer as described above.

M_t, the amount of ES sorbate released at time t was calculated. M_∞, the amount of ES released after infinite time was taken to be the value at which the equilibrium was attained. M_t/M_∞, the fractional ES sorbate release value was plotted as a function of time. The calculation method has been outlined in the section on sample preparation.

3.3.12 Separation of protein from ES

In order to study absorption capacity, the films were cut into small pieces and immersed in PBS solution at pH 7.4 for 2h prior to adsorption. Protein and ES solutions were freshly prepared by dissolving egg white or ES powder in PBS at pH 7.4 to give a final concentration of 1mg/ml. Film substrates were incubated in glass bottles, containing 3ml protein solution, and the glass bottles were gently shaken overnight at 23°C. 48 hours after equilibrium, the protein concentration in ES was measured using a UV-vis spectrometer via at the absorbance at 280nm. By comparing the initial and final concentrations, the adsorption capacities could be calculated from mass balances and plotted against the final concentration in solution.

To study protein separation from ES solution, the same diffusion apparatus was used. The details of the method are described in Section 3.3.10.2.

CHAPTER 4

Morphology of Chitosan/PEO Blends and Networks

4.1 Introduction

One of the important factors affecting the physical properties of a material, including its mechanical, optical and thermal properties, is its morphology. The morphology of a material depends on the components present, the fabrication methods used in sample preparation and thermal history.

Polymer blending is a quite simple method by which a mixture of two or more polymeric components, which are not chemically bonded to each other, is produced. Generally, there are two main reasons for blending polymer together. The first is property modification of a given polymer to extend its range of applications or to tailor its properties to fit a special requirement. Indeed, depending upon the level of mixing of the components in a binary mixture, the blend can have properties that make it suitable to areas of application beyond consideration of either individual constituent.

The mixing of polymeric materials is not always predictable. The vast majority of polymer pairs when blended are not miscible, but form separate phases or domains within the mixture. Such blends are termed immiscible. Miscibility, therefore, implies a level of homogeneity within the mixture or is defined in terms of the behaviour of macroscopic properties. Miscibility determines phase structure of blend systems. Chitosan has many functional properties [30]. When chitosan is blended with PEO, the miscibility between their molecules is a very significant factor especially for determining the mechanical properties of the blends. It is, therefore, essential to study the miscibility in order to understand the morphology of chitosan/PEO blends.

In this chapter, the morphologies of chitosan/PEO blends and networks will be investigated by means of FT-IR spectroscopy, DSC and SAXS measurements.

4.2 Chitosan/HPEO Blends

4.2.1 Molecular interactions of chitosan/HPEO blends

An important consideration in the choice of components for a blend is the intermolecular interactions, which are considered to play a key role in polymer miscibility [91,223,224]. FT-IR spectroscopy has been proven to be a powerful tool for the study of specific interactions [91,223,224] between two components in blends through observing any shifts in the position of peaks corresponding to the functional groups involved in the interactions. The purpose of this section is to provide direct information on the molecular interactions between the two components in the chitosan/PEO blends.

The infrared spectra of pure PEO and chitosan have been reported [91,223]. The main characteristic bands are the following.

3480cm-^{1} C_6 - OH stretching band of chitosan

3447cm^{-1} C_3 – OH stretching band of chitosan

3264cm^{-1} N-H hydrogen bonding of amide

1652cm^{-1} amide I band of chitosan.

1558cm^{-1} amide II band of chitosan, overlaping with NH_3^+ band (1500cm^{-1})

PEO: the C-O-C stretching band at 1280cm^{-1}and 840cm^{-1}

The identification of these peaks allows us to investigate the influence of chain-chain interactions in the blend on the basis of band positions and relative intensities. The chain-chain interactions can be deduced from the shifts of the vibration frequencies of the group involved in the hydrogen bonding.

Figure 4.2.1, parts (A) and (B), shows the FT-IR spectra for pure chitosan and the blends in the composition studies. The hydroxyl (OH) stretching band for chitosan, and for chitosan/HPEO blends, is shown in Figure 4.2.1(A).

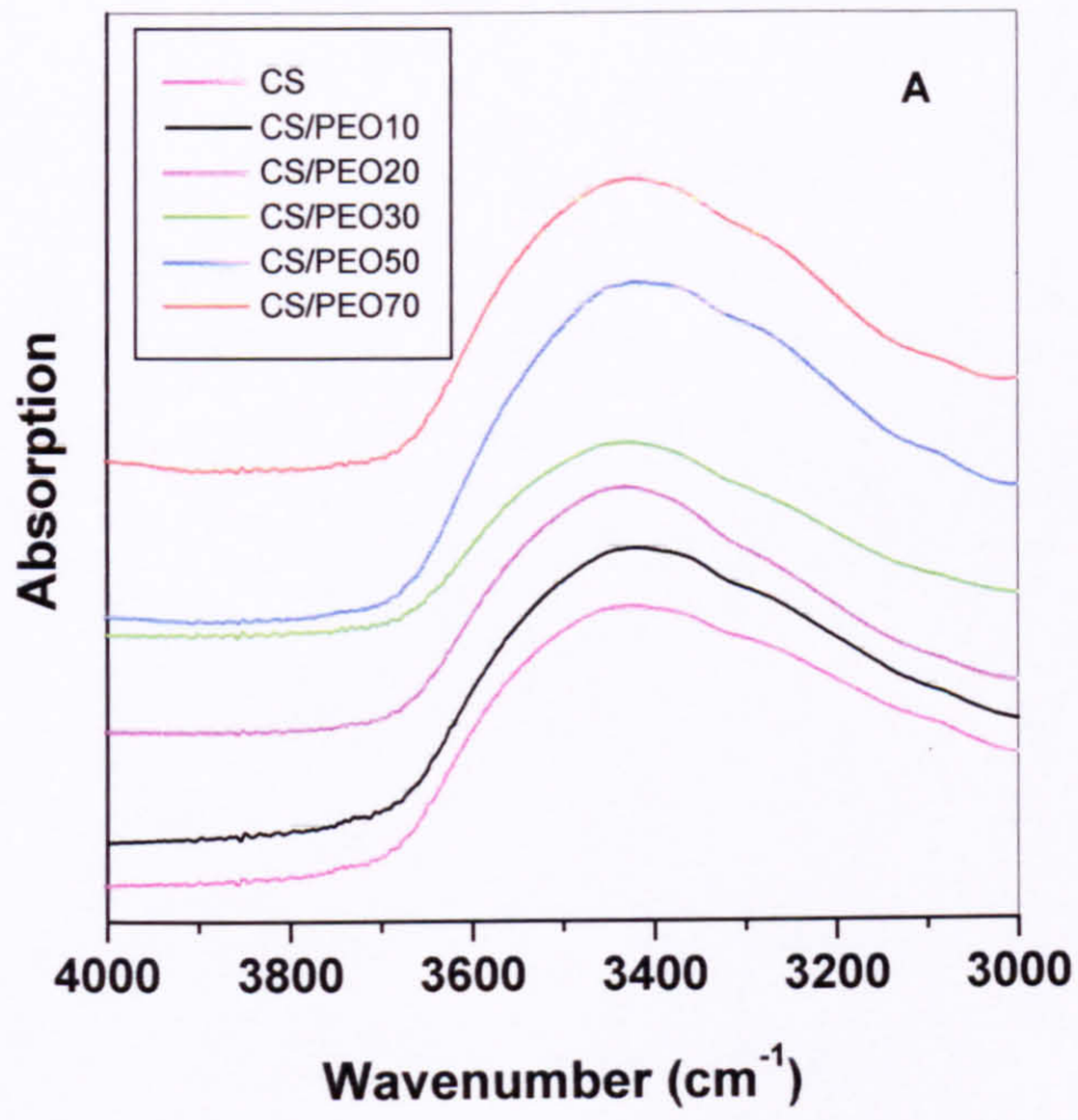

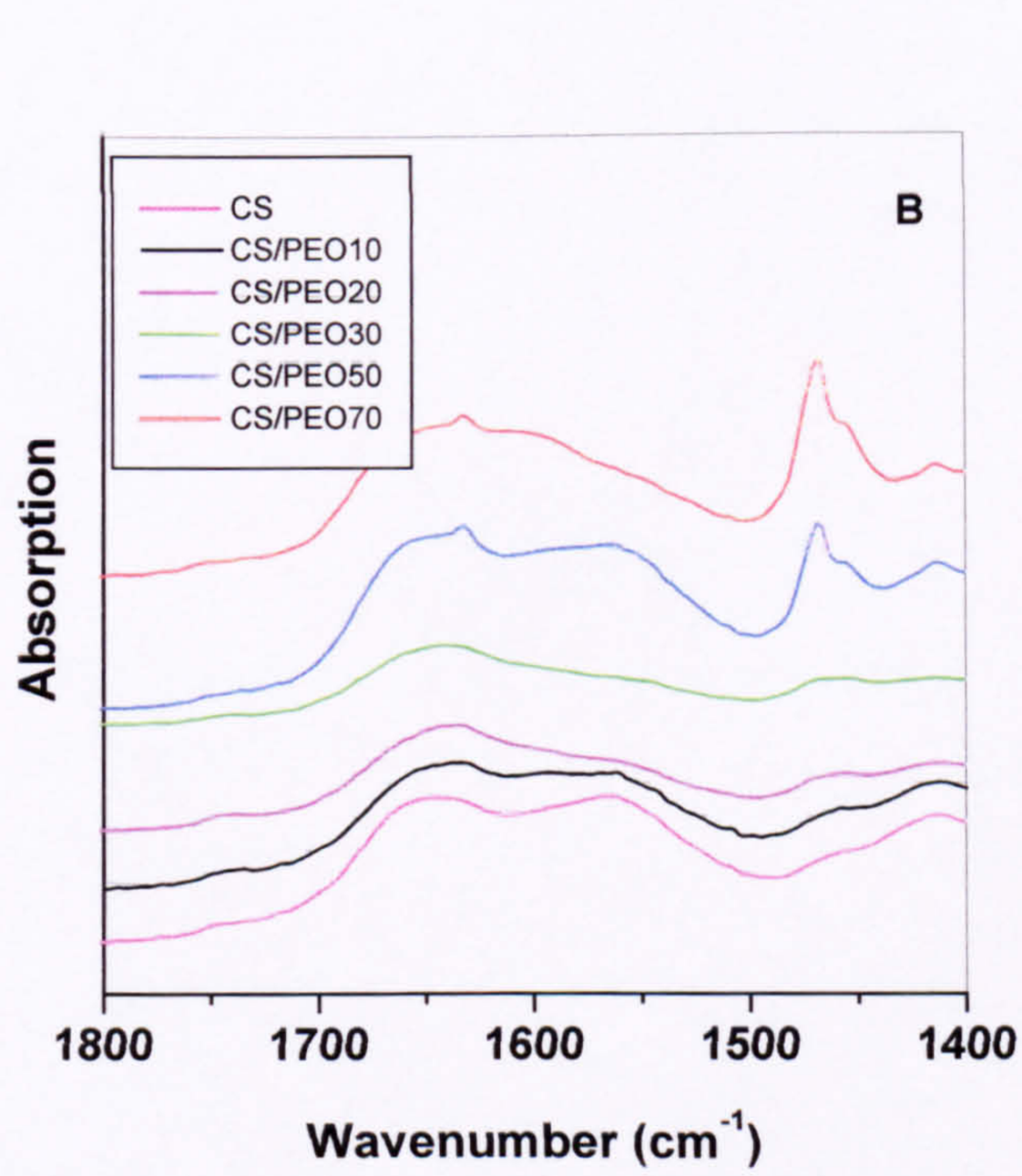

Figure 4.2.1 FT-IR spectra of chitosan and CS/HPEO blends:
(A) 4000-3000cm^{-1} and (B) 1800-1400cm^{-1} regions

It can be clearly seen that when compared with the respective chitosan, the OH vibration is shifted to a higher frequency. The greatest frequency shift from about 3424cm^{-1} to about 3438cm^{-1} was observed for the blend with 30% HPEO content.

The OH vibration also broadened with increasing HPEO content. Analysis of the spectra of these blends indicates that hydrogen bonding interactions were involved in all the blends, probably between the chitosan hydroxyl and the PEO ether groups [224] and the greatest interaction occurred in the CS/HPEO30 blend.

The frequency of the free amine band of chitosan/HPEO blends is shown in Figure 4.2.1 (B). It highlights that when HPEO content increased to 30% the amide I band shifts toward lower frequency from its original position at 1645cm^{-1} to about 1632cm^{-1}. The a amide II band it is not easily amenable to quantitative evaluation because of vibrational overlap and possible changes in absorption intensity. The figure clearly shows that the absorption intensity of amine II band (1563cm^{-1}) decreased when the HPEO content increased from 0 to 30%, but increased when the HPEO content was further increased to 50%. These correspond to hydrogen bonding interactions between the -O- in the HPEO repeat units and -NH side group in the chitosan repeat unit. Analysis of the spectra of these blends indicates that interaction between chitosan and PEO in the blends occurs and when the HPEO content was 30% the interaction between chitosan and PEO was the strongest. These results prove that two polymers are miscible.

4.2.2 Miscibility and the interaction parameter of chitosan/HPEO blends

For a polymer blend, it is important to understand the miscibility of its components. DSC is a particularly useful tool in studying polymer-polymer miscibility and phase-separated blends [211]. The most commonly used method for establishing miscibility in polymer-polymer blends, or partial phase mixing in such blends, is through the determination of the glass transition of the blend versus those of the unblended constituents. A miscible polymer blend will exhibit a single glass transition between the glass transition temperatures, T_g, of the components with a sharpness of the transition similar to that of the components [211]. In cases of borderline miscibility,

broadening of the transition will occur [211]. At the other extreme, a blend exhibiting essentially the glass transition behaviour of unmixed components is defined as immiscible [211]. Miscibility, therefore, implies, by this definition, a level of homogeneity within the mixture. In other words, miscibility also suggests a level of mixing adequate to yield the macroscopic properties expected a single-phase material. In practice, many polymer blends are neither completely miscible nor completely immiscible, but exhibit a degree of partial miscibility. However, when studying the miscibility of a blend using the single glass transition criterion, problems will arise if the two polymers have transitions at similar temperatures or very weak transitions. In this situation, it is very difficult to examine whether one or two transitions are present [211]. In such a case, it is necessary to use another method. Studying melting point depression [225-227] in the blends is another method for establishing miscibility in polymer-polymer blends. This method is usually employed in characterizing the miscibility of semi-crystalline/amorphous polymer blends [225]. From the melting point depression, it is possible to determine the Flory-Huggins interaction parameter, (x_{12}) [226,227], in polymer blends.

In this study, a thermal characterization of the chitosan/HPEO or chitosan/LPEO blends was undertaken as a macroscopic evaluation of the miscibility between the components.

In order to estimate the miscibility of chitosan/PEO blends the melting point depression was analysed.

Figure 4.2.2 shows heat flow vs. temperature plots for the chitosan/HPEO blends. The melting temperatures, T_m, and heats of fusion, ΔH, for various weight fractions of HPEO were compared and plotted against the volume fraction of chitosan in Figures 4.2.3 and 4.2.4. As shown in the later figures, a downward shift of melting temperature (T_m) and heat of fusion of HPEO (ΔH) were registered as the chitosan content was increased. This shift in the melting transition of the crystalline polymer in the blend can be taken as qualitative evidence of miscibility [225,226] of the chitosan/HPEO blends.

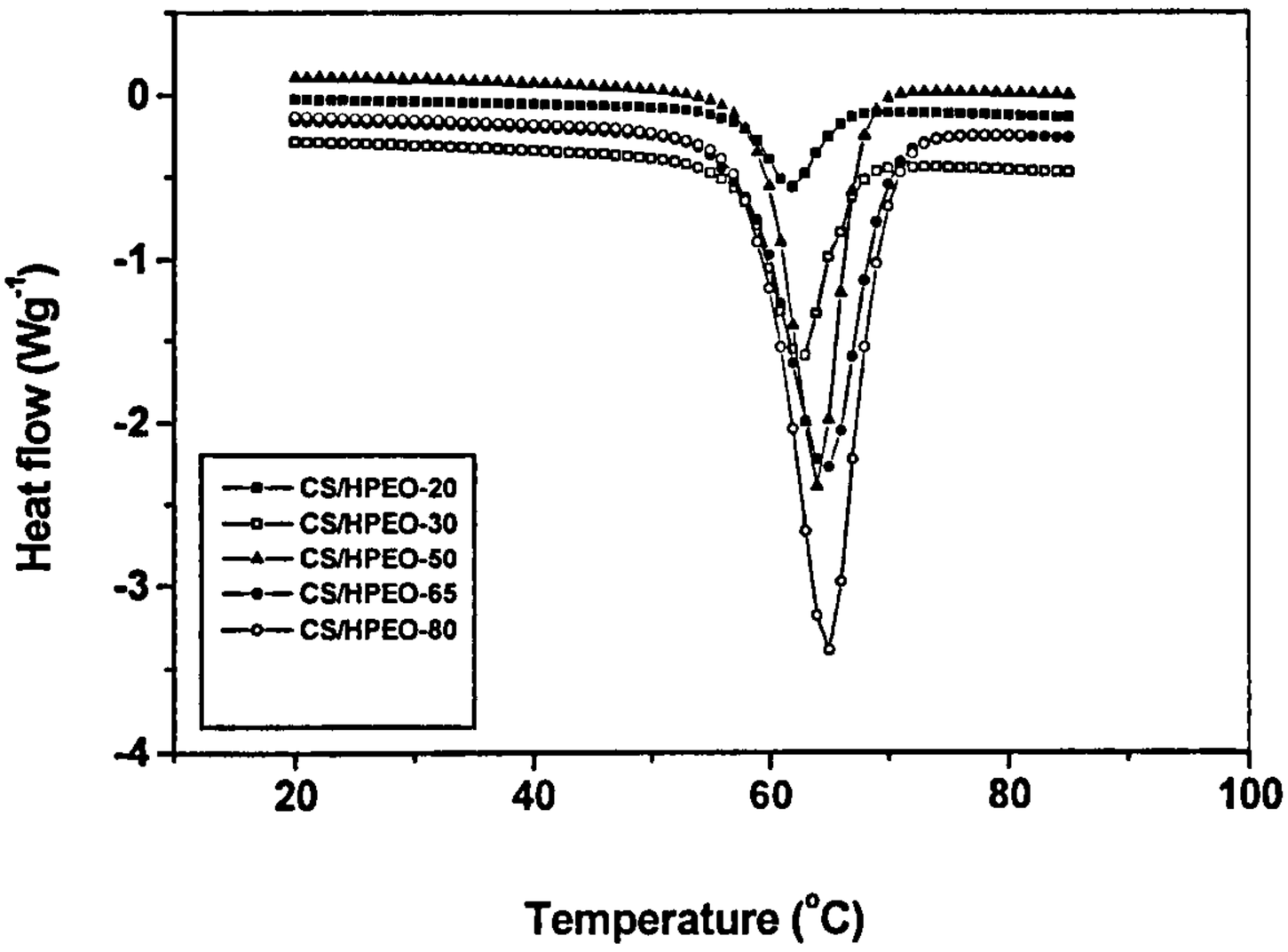

Figure 4.2.2 Heat flow vs. temperature curves for the chitosan/HPEO blends

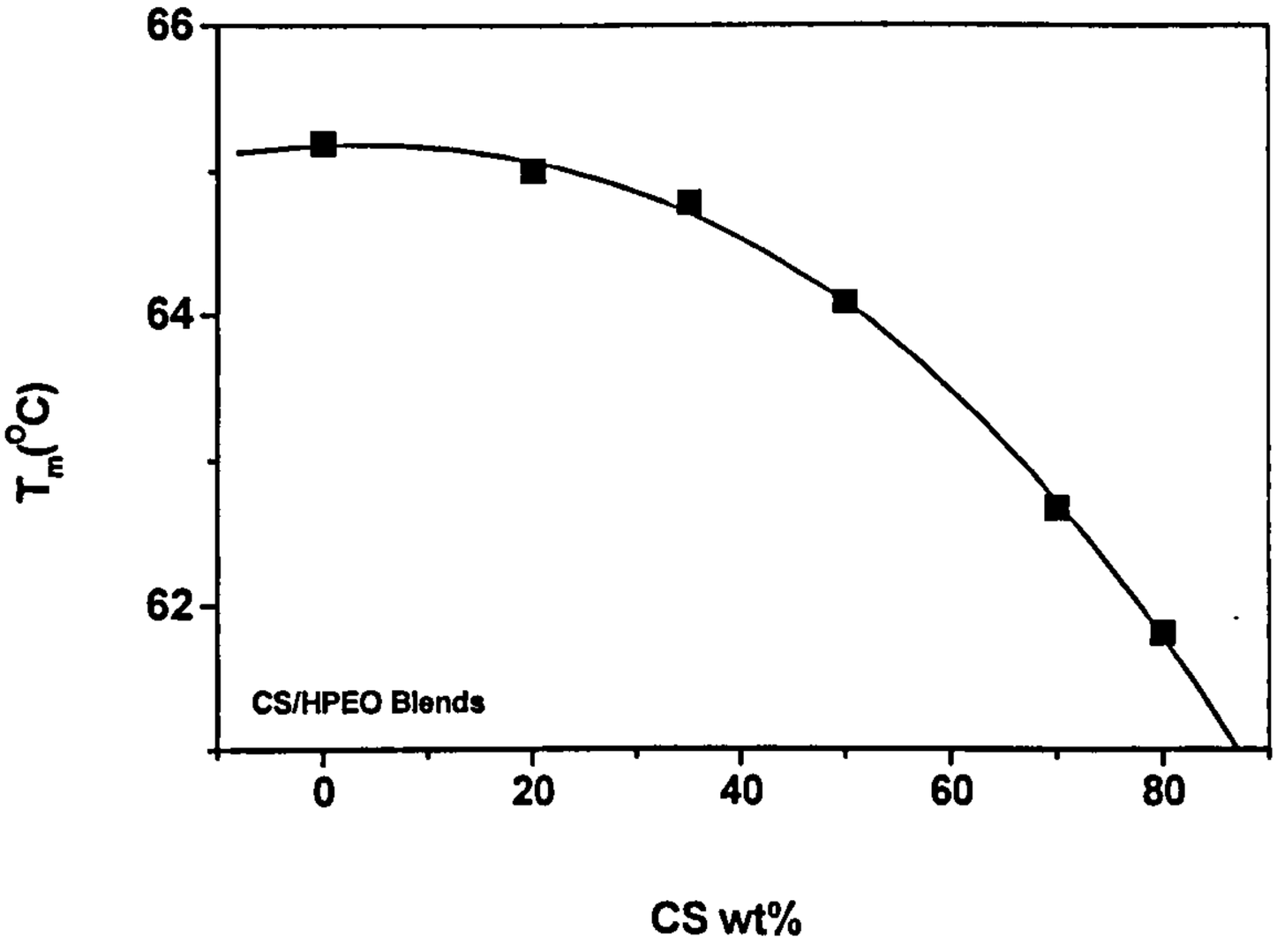

Figure 4.2.3 Melting temperatures (T_m) of HPEO versus the composition (wt%) of chitosan

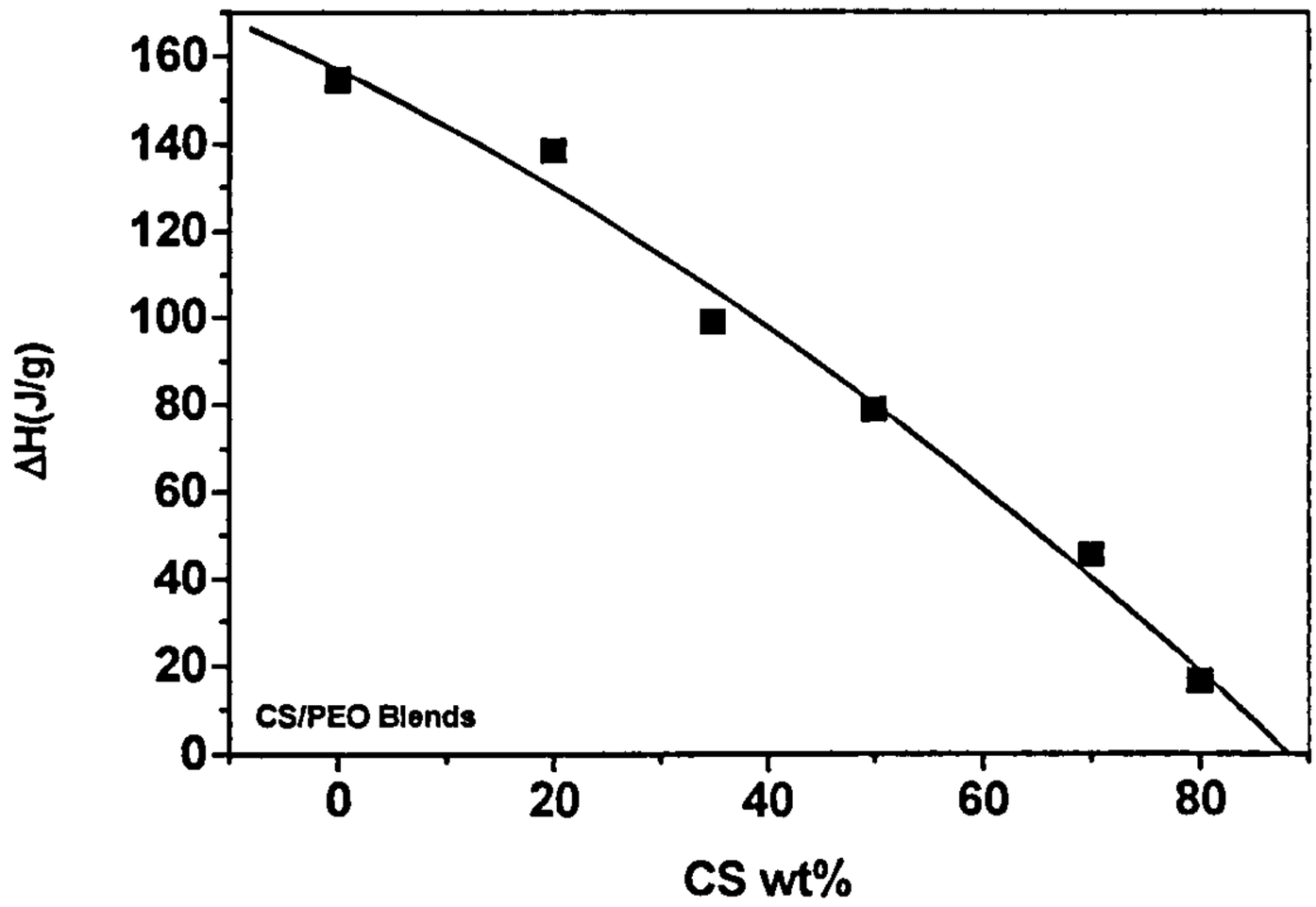

Figure 4.2.4 Heat of fusion (ΔH) of HPEO versus the composition (wt.%) of chitosan

Chitosan has been reported to impede PEO crystallization in chitosan/PEO blends [225]. This effect has been attributed to the retardation of the rate of crystal growth arising from the effect of the stiff chitosan molecular chains on the overall mobility in the blend. This was clearly seen in the chitosan/HPEO blends investigated here. Progressively increasing the chitosan component within the blends resulted in increasingly lower T_m value and more significantly, lower ΔH values. The ΔH values were lower, reflecting a lesser % crystalline phase in the PEO component of the blends.

It is known that miscibility of polymer blends is controlled by thermodynamic factors [226]. The Flory-Huggins thermodynamic interaction parameter, $\chi_{12,}$ characterises the interaction in free energy of mixing and is used as a measure of the excess enthalpy and entropy contributions to potentially favourable mixing. The more negative the parameter the stronger the interactions are. These are often called *specific interactions,* as they are not present in either component by itself, but only appear when both are present. Several techniques [227] have been used to determine the

Flory-Huggins interaction parameter for miscible polymer blends. The melting point depression of a crystalline component means that the re-growth of the crystalline phase is interrupted by the interactions in the blend, and can, therefore, be used to estimate the interaction parameter in the blend. The data obtained in these studies are usually analysed in terms of the equation derived by Nishi and Wang [228].

$$1/T^{o}_{m(b)} - 1/T^{o}_{m} = -(R\,V_{2u}/\Delta H_m\,V_{1u})\,\chi_{12}\,\phi_1^{2} \qquad [4.2.2\text{-}1]$$

where $T^{0}_{m(b)}$ and T^{o}_{m} are the melting temperature of the crystalizable polymer in the blend and in the pure state, respectively; ΔH_m is the enthalpy of fusion of the 100% pure crystalline material per mole of repeating units, which can be calculated by extrapolating the data of semi-crystalline samples; V_{1u} and V_{2u} are the molar volumes of the repeating units of the amorphous and the crystalline polymers; ϕ_1 is the volume fraction of un-crystallized component; R is the gas constant (8.314J/mol K); and χ_{12} is the interaction parameter.

In turn, Equation 4.2.2-1 is based on using the classic Flory-Huggins model [229,230].

$$\Delta H_m = N R T \chi_{12}\,\phi_1\,\phi_2 \qquad [4.2.2\text{-}2]$$

where N is the number of moles of segments in the system and T is the absolute temperature, ϕ_1 and ϕ_2 are the volume fraction of amorphous and crystalline components, respectively .

Obviously, χ_{12} is the key parameter for modelling phase behaviour, and is used as a measure of the excess enthalpy and entropy contributions to potentially favourable mixing.

Chitosan starts to degrade at above 80°C. It is very difficult to obtain the equilibrium melting point for HPEO in the chitosan/HPEO blends. From Equation 4.2.2-1, $T_{m(b)}$ and T_m were taken instead of $T^{o}_{m(b)}$ (the equilibrium melting temperature of pure PEO) and T^{o}_{m} (the equilibrium melting temperature of PEO in the blends with chitosan). In this analysis, the following values were employed: $V_{1u} = 132.5 cm^3/mol$

and V_{2u} = 39.3cm^3/mol are unit molar volume of chitosan and PEO, respectively, calculated from the densities and molecular weights and ΔH_m = 9782.2J/mol (enthalpy of fusion of completely crystalline PEO). A plot of $(1/T_{m(b)} - 1/T_m)$ versus ϕ_1^2 was constructed and fitted with a straight line (Figure 4.2.5). From it, the interaction parameter, χ_{12}, between the components of the blend was calculated as -0.16.

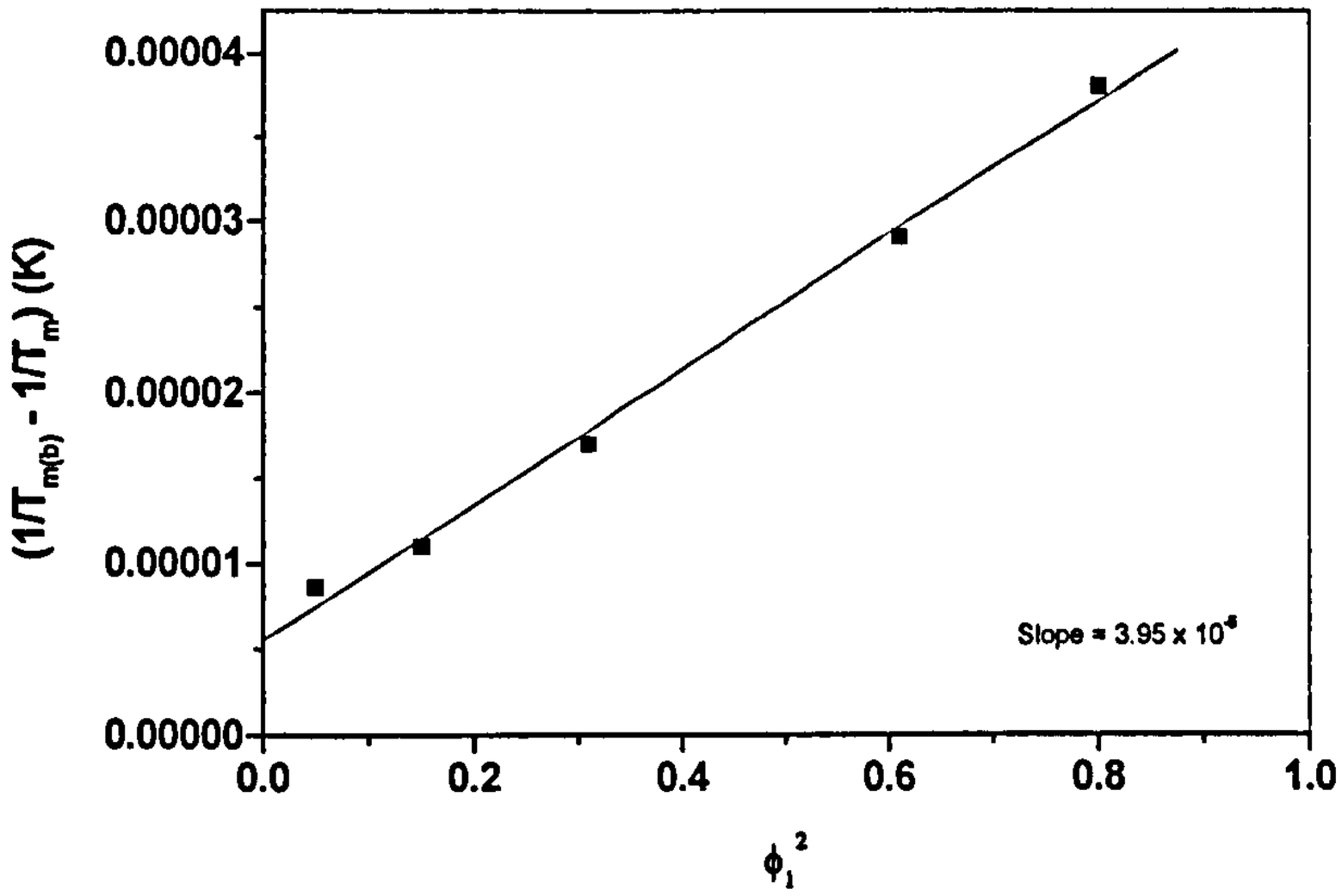

Figure 4.2.5 $(1/T_{m(b)} - 1/T_m)$ (K) versus volume fraction of chitosan (ϕ_1^2). The interaction parameter (χ_{12}) is obtained from the slope.

This negative value indicates that a certain degree of miscibility in the amorphous phase of the blends and that specific interactions are occurring between the components over the whole range compositions.

4.2.3 Crystallinity of chitosan/HPEO blends

The degree of crystallinity of the PEO in the blends can be determined from the following equation:

$$X_c = (1/fw)((\Delta H /(\Delta H_o) \qquad [4.2.3\text{-}1]$$

where ΔH_o is the heat of fusion for 100% crystalline sample of HPEO, ΔH is the heat of fusion of the HPEO component in the blend and *fw* is the weight fraction of HPEO in the corresponding blend.

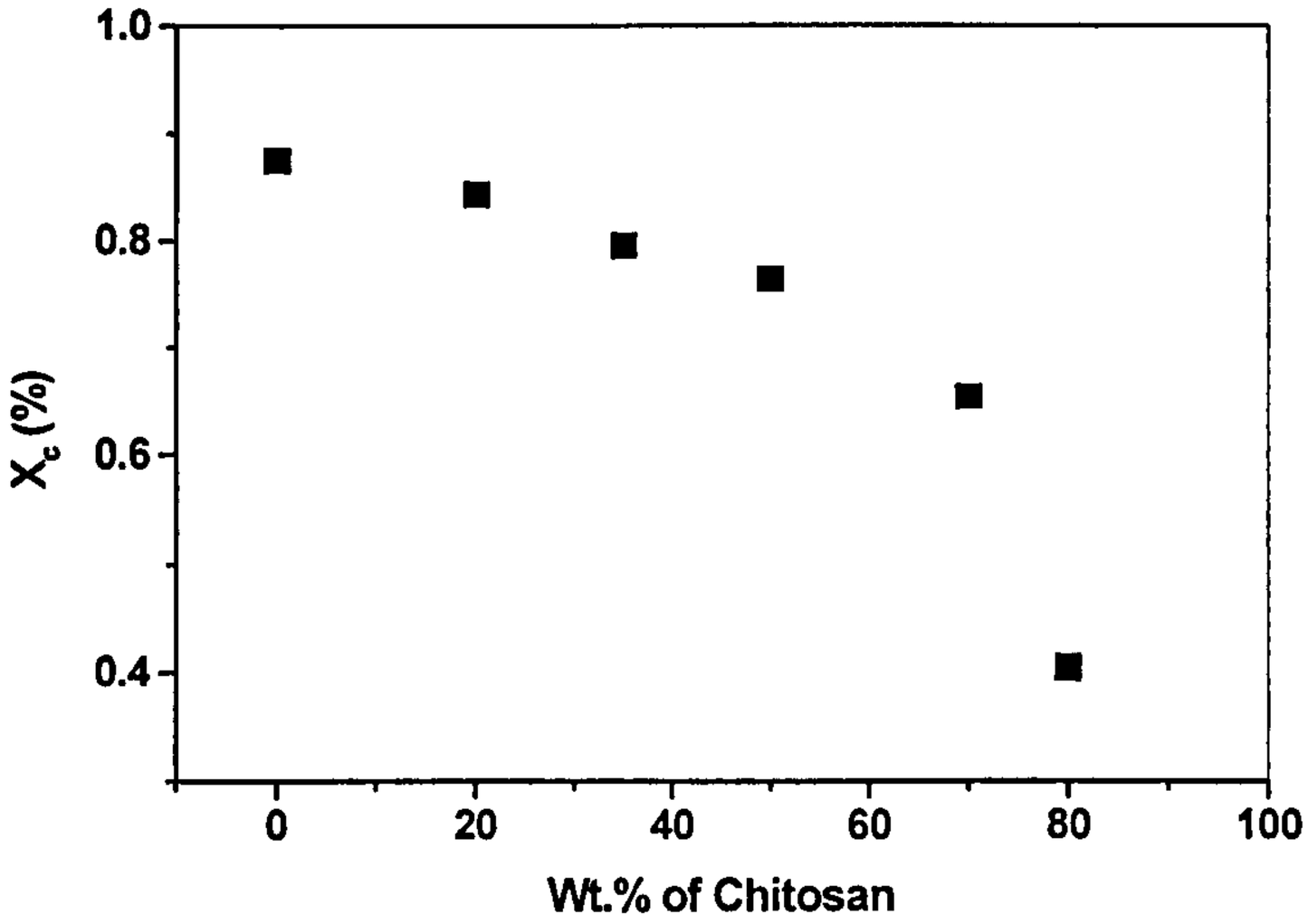

Figure 4.2.6 Effects of the composition in chitosan/HPEO blends on the degree of crystallinity

The X_c value obtained is illustrated in Figure 4.2.6. It can be seen in the figure that the crystallinity of the chitosan/HPEO blends decreased as wt.% of chitosan increased.

4.3 Chitosan/LPEO Blends

The molecular weight of PEO influences the morphology, and, therefore, the physical properties of chitosan/PEO blends. In this section, the molecular interaction and morphology of chitosan/LPEO (molecular weigh of PEO: 600) blends were studied using a number of techniques, including DSC, FT-IR spectroscopy and SAXS.

Figure 4.3.1 shows the DSC curves for chitosan and for the chitosan/LPEO blends. From these curves, the melting points (T_m) and heat of fusion (ΔH) of LPEO in the

corresponding blends were obtained. The melting temperatures and heats of fusion for various weight fractions of LPEO were collated and are illustrated in Figures 4.3.2 and 4.3.3.

It is notable that the melting point, closely related to the composition, initially increased with increasing chitosan content, peaked at 60% chitosan at 20°C and then decreased rapidly to 15°C by 80wt.% chitosan. The melting enthalpy, ΔH, of LPEO decreased as the chitosan content increased. A comparison between Figures 4.2.3 and 4.3.2 shows that chitosan/HPEO and chitosan/LPEO blends behaved differently as the wt.% of chitosan was increased. In the chitosan/HPEO blends, the melting point of HPEO decreased with increasing chitosan content in the blends. The chitosan/HPEO blends were miscible, as has been discussed previously. In the case of chitosan/LPEO, a similar effect was observed for blends where the wt.% of chitosan was greater than 60%. In the case of blends with wt.% of chitosan smaller than 60%, however, the melting points increased as wt.% of chitosan was increased.

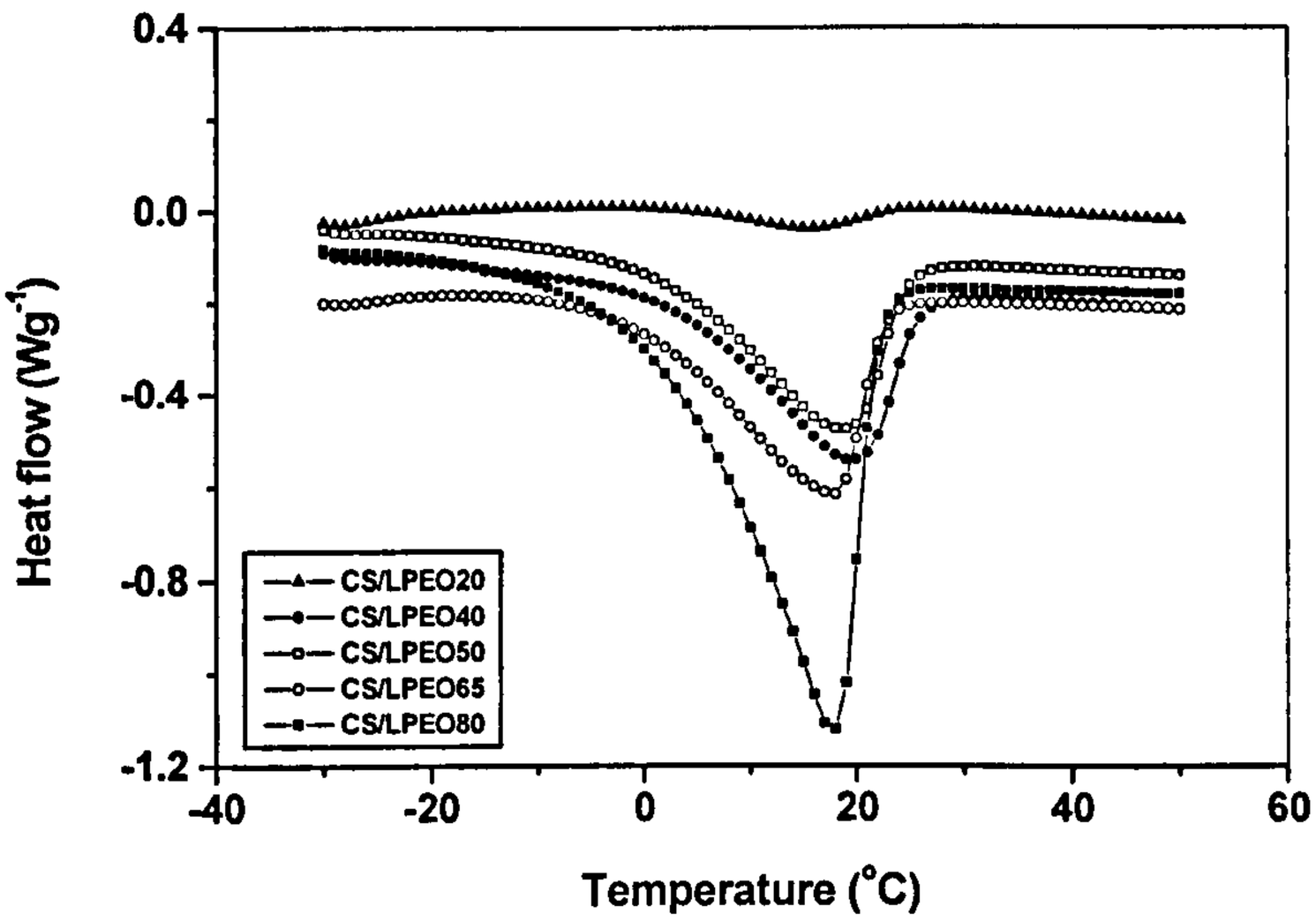

Figure 4.3.1 Heat flow vs. temperature curves for chitosan/LPEO blends

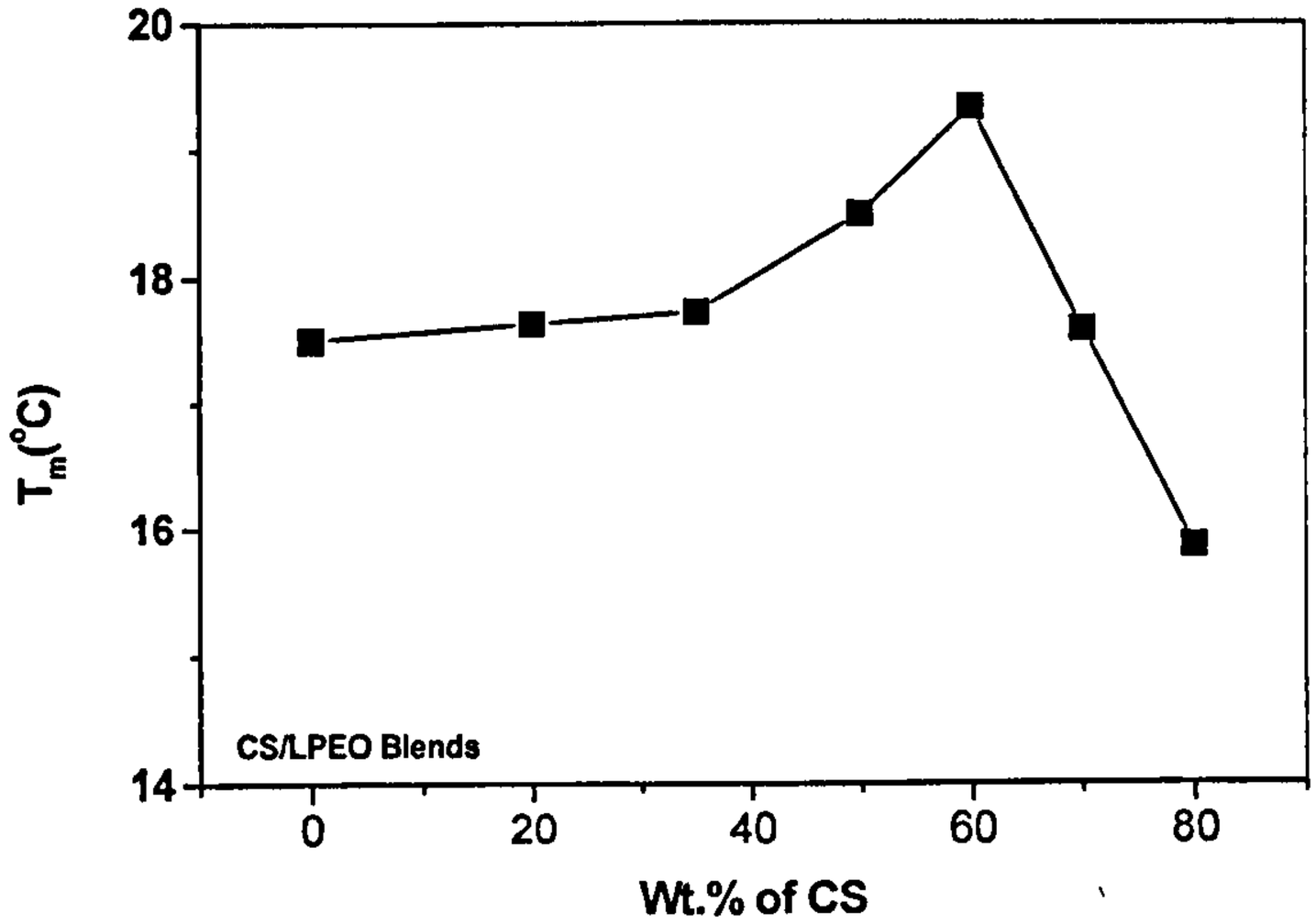

Figure 4.3.2 Melting temperature (T_m) curves for LPEO versus composition (wt%) of chitosan

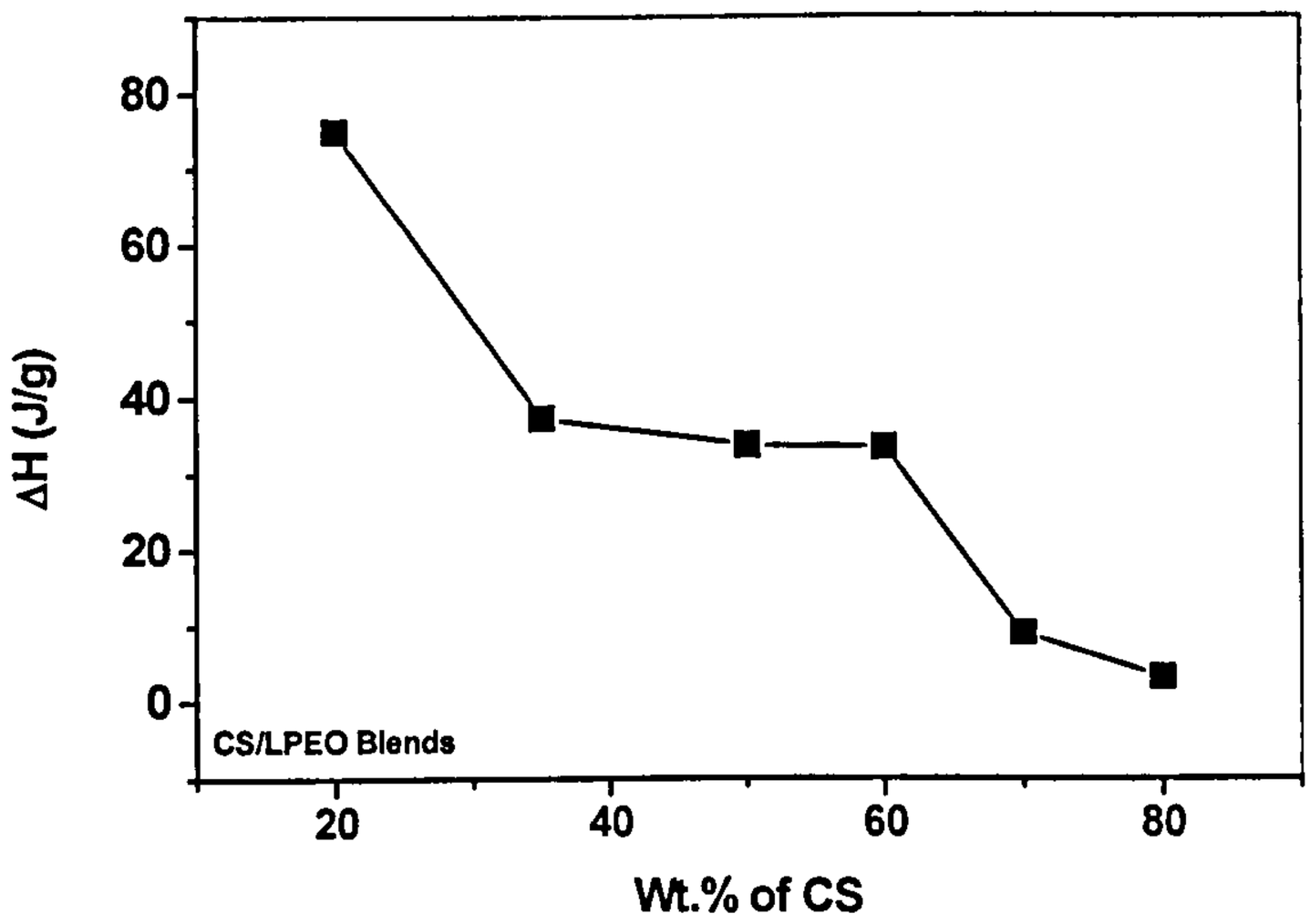

Figure 4.3.3 Enthalpy (ΔH) of LPEO versus various compositions (wt%) of chitosan

Generally, increases in the melting temperature of crystalline polymers are caused by increases in the lamellar thickness [231]. The melting behaviour of a polymer crystal is, therefore, sensitive to the lamellar thickness. For example, the relationship between melting temperature, T_m, and lamellar thickness, L, for polyethylene can be expressed as [171]:

$$T_m = 414.2(1 - 0.627/L) \qquad [4.3\text{-}1]$$

Hence, the larger the lamellar thickness, the higher is the melting temperature. In a miscible polymer blend, molecular interactions have an influence on the crystalline structure, which leads to a decrease of lamellar thickness. The decrease of lamellar thickness results in a depression of the melting temperature. However, for immiscible polymer blends, the lamellar thickness remains unchanged, giving rise to an unchanged melting temperature [232].

From a thermodynamic point of view, for a miscible polymer blend, its miscibility increases if the molecular weight of a constituent decreases [232,233]. The chitosan/HPEO blends are miscible, as has been discussed previously. Consequently, the chitosan/LPEO blend is certainly also a miscible system.

As Figures 4.2.3 and 4.3.2 show, when wt.% of chitosan contents was less than 60%, chitosan/HPEO and chitosan/LPEO blends behaved differently. Contrary to usual expectations, in the case of chitosan/LPEO blends, the melting points increased as wt.% of chitosan was increased. The rules of thermodynamics state that an increase in the melting point of a polymer blend is caused by the effects resulting from an increase in lamellar thickness. However, this explanation is in conflict with the above discussion – if a polymer blend, such as chitosan/LPEO, is miscible, its lamellar thickness should not increase. This is a finding which requests further investigation.

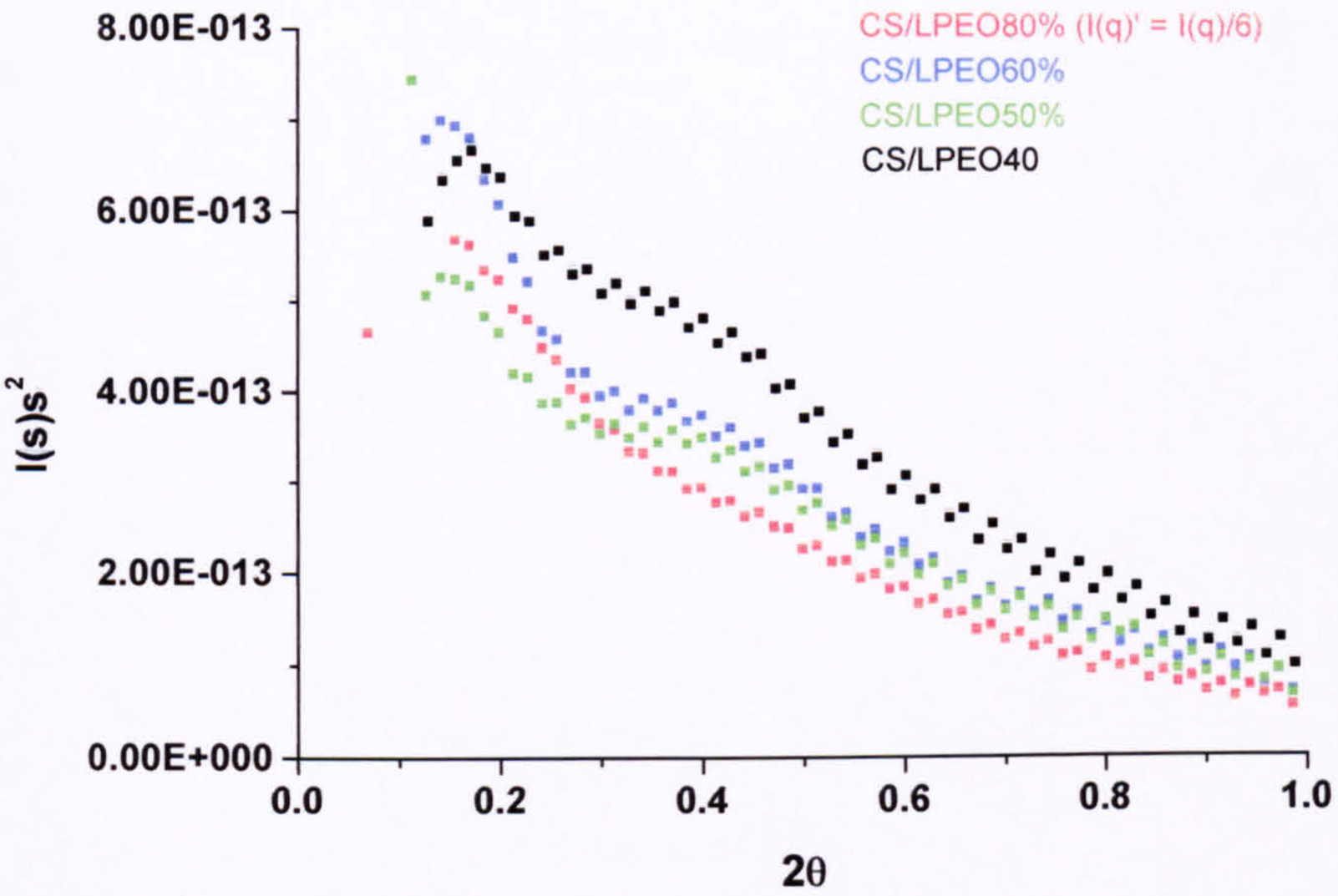

Figure 4.3.4 SAXS curves for the chitosan/LPEO blends showing the changes in long period

Figure 4.3.4 shows SAXS results for 20, 40, 50 and 60 wt.% of chitosan of the blends. (The theory behind and the discussion on the results obtained for long period analysis will be treated in detail in Section 4.4.2.) The long periods (peak position) did not increase, but decreased with increasing chitosan content, meaning that the lamellar thickness of LPEO in the chitosan/LPEO blends certainly did decrease. Given this, the issue remains what caused the increase in the melting points.

Molecular interactions between chitosan and LPEO in the blends were examined by FT-IR analysis. It can be seen, from Figure 4.3.5, that with increases in wt.% of LPEO, one observed an increase in the frequency shift of the free amine band, with the maximum shift of 30 units from 1563 cm^{-1} to 1593 cm^{-1} taking place at 60% chitosan content. This shows that there are strong intermolecular interactions in the chitosan/LPEO blends.

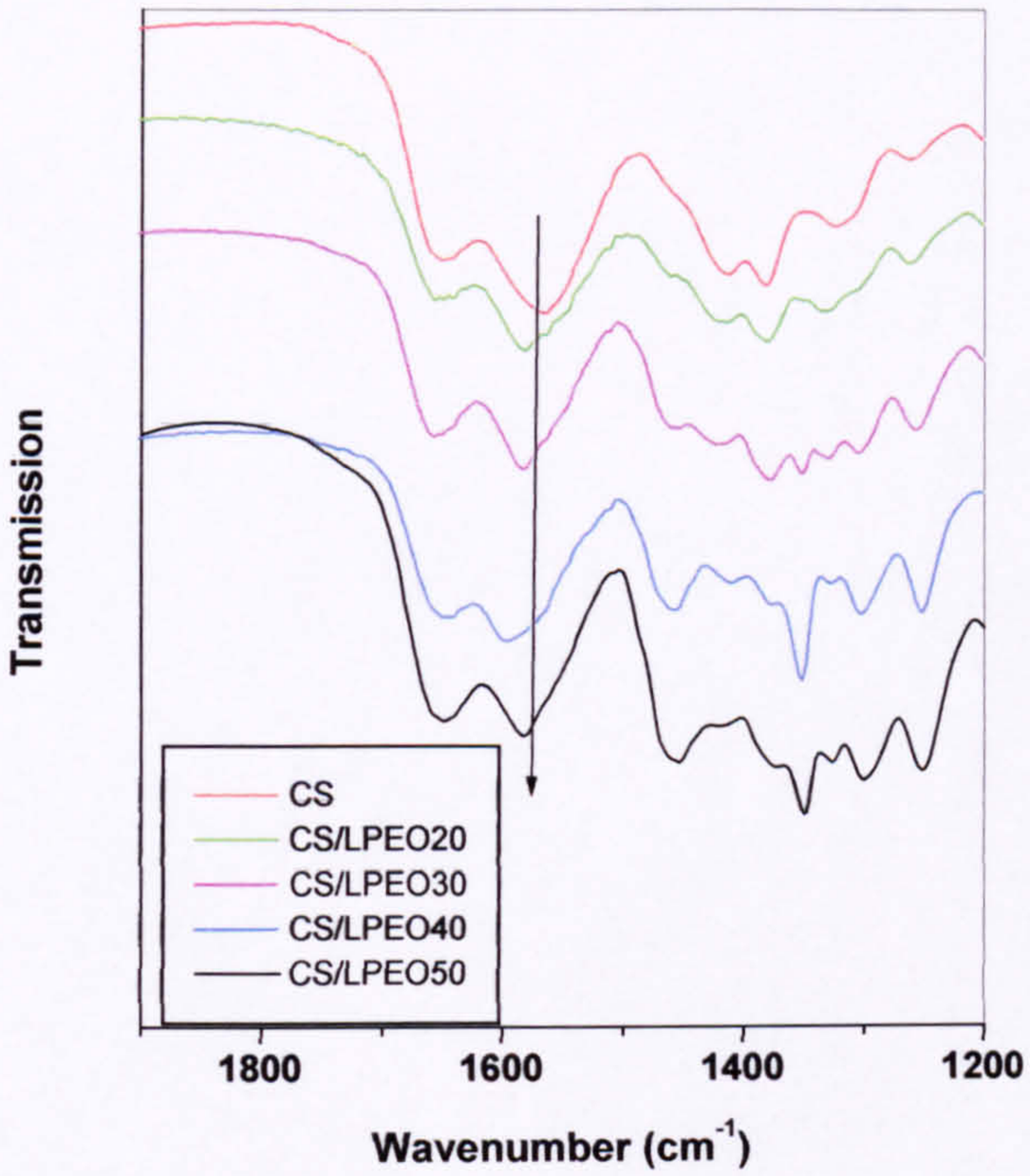

Figure 4.3.5 FT-IR spectra for chitosan and chitosan/LPEO blends

The morphology of crystalline polymer and amorphous polymer blends, in which crystallinity is not equal to zero, can be considered as a two-phase structure: one is the crystalline phase and the other is the amorphous phase. Generally, molecular interactions occur only between molecules in the amorphous phase and not between molecules in the amorphous with those in the crystalline phase [232,233]. The low molecular weight of PEO (600) must give rise to a small crystal. Due to the strong molecular interactions in the chitosan/LPEO blends, it is possible that molecular interactions between chitosan molecules and the molecules in the crystalline phase occur. It can be assumed that during melting, the crystalline phase must have the energy required for de-folding and to overcome the effect of the strong molecular forces. So, in the chitosan/LPEO blends, it is believed that the increase in the melting points could result from the strong molecular interactions. The FTIR and DSC results, as shown in Figures 4.3.2 and 4.3.6, are of particular use. When looked at

together at 60wt.% chitosan content, the molecular interaction was at its strongest and the melting point was at its highest.

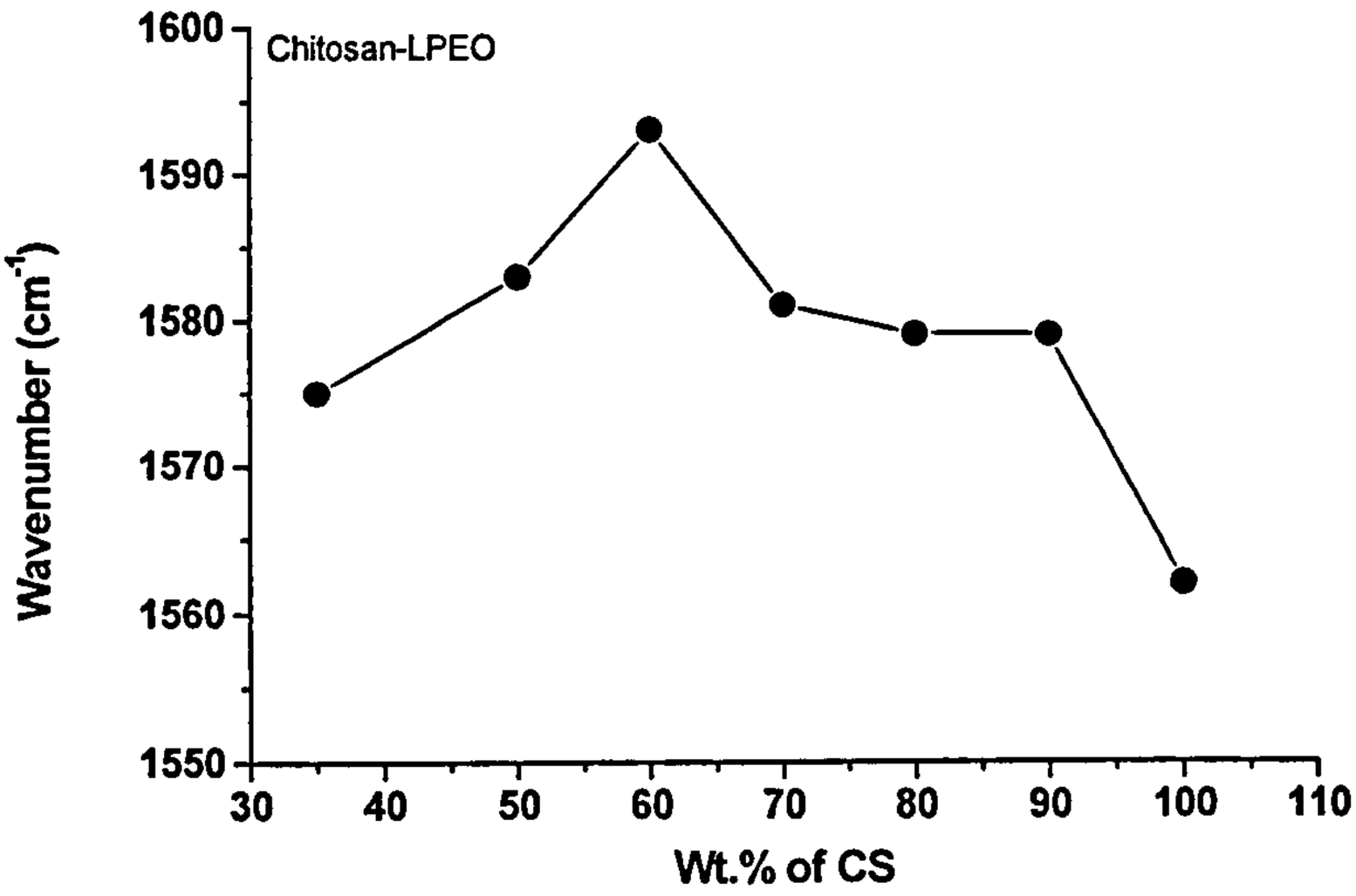

Figure 4.3.6 Change in the frequency of free amine band in chitosan/LPEO blends with varying chitosan content

Assume that the increase in melting point resulting from the strong molecular interactions between chitosan molecules and these molecules in the crystalline phase of LPEO is $\Delta T(I)$, and the depression of the melting point resulting from miscibility is $\Delta T(m)$. When $\Delta T(I) > \Delta T(m)$, DSC shows an postulated increase of melting points. In the chitosan/HPEO blends, with increasing chitosan content, the melting points decreased (see Figure 4.2.3). In the chitosan/LPEO blends, in some range, with increasing chitosan content, the melting points increased (see Figure 4.3.2). According to above analysis, it is believed that there is a molecular weight of PEO such that $\Delta T(I) = \Delta T(m)$ and the melting points are unchanged.

It is clear that the melting points of the chitosan/LPEO blends, at least, are sensitive to PEO molecular weight.

4.4 Chitosan/HPEO or LPEO Blends Crosslinked by Genipin

4.4.1 Phase separation behaviour of chitosan/HPEO (or LPEO) blends crosslinked by genipin

The miscibility and morphology of chitosan/HPEO and chitosan/LPEO blends were studied in the previous sections. The conclusion was that chitosan/PEO blends are miscible in the whole composition range. The issue that follows is whether that crosslinking by genipin affects the morphology of chitosan/PEO blend; in particular, whether it causes phase separation. SAXS is a particularly useful method of examining whether phase separation occurs in polymer system [205,234,235].

For a two-phase system, the structure factor, *F(q)*, is given by the Fourier transform of the electron density function $\eta(\mathbf{r})$ [234,235].

$$F(\mathrm{q}) = \int_0^V \eta(\mathbf{r}) \exp(-\mathbf{i}\mathbf{r} \cdot q) d\mathbf{r} \qquad [4.4.1\text{-}1]$$

where V is the volume irradiated by the x-rays; the variable **q** is a scattering vector defined as $(2\pi/\lambda)(\mathbf{s}_o\text{-}\mathbf{s}')$ where the unit vectors $\mathbf{s}_o$ and **s'** correspond to the propagation directions of the incident and scattered rays, respectively, and its magnitude is given by $h = (4\pi/\lambda)\sin\theta$, where 2θ is the scattering angle; and λ is the wavelength of the x-rays.

The scattered intensity, I, can be expressed in terms of the structure factor [234].

$$I = I_e FF^* = I_e \langle \eta^2 \rangle V \int \gamma(\mathrm{r}) \exp(-ir \cdot \mathrm{q}) dr \qquad [4.4.1\text{-}2]$$

I_e is the Thomson scattering intensity from an electron [234]. The mean square electron density fluctuation, $\langle \eta^2 \rangle$, is given for the ideal two-phase system by Equation 4.4.1-3.

$$\langle \eta^2 \rangle = (\rho_1 - \rho_2)^2 \varphi_1 \varphi_2 \qquad [4.4.1\text{-}3]$$

where ρ_i and ϕ_i are the electron density and volume fraction, respectively, of the i^{th} phase. The function $\gamma(\mathbf{r})$ is the correlation function of the density fluctuation, which is a function of r only for an isotropic system [205,235].

For an isotropic and ideal two-phase system, it follows from Equations 4.4.1-2 and 4.4.1-3 that

$$I(h) = I_e(\rho 1 - \rho 2)^2 \phi 1 \, \phi 2 V \int \gamma(\mathbf{r}) \exp(-i\mathbf{r}.\mathbf{q}) d\mathbf{r} \qquad [4.4.1\text{-}4]$$

From Equation 4.4.1-4, the difference in electron density between the crystalline and amorphous regions, thus, indicates the extent of the homogeneity of the system.

In this study, the morphology of chitosan/PEO blends and networks were examined by SAXS. Figure 4.4.1, parts (A) and (B), shows plots of the scattered intensity (**I**) versus the scattering vector, **q**, of chitosan/HPEO blends and networks, respectively. The scattering vector was calculated by:

$$q = 4\pi / \lambda \sin \theta \qquad [4.4.1\text{-}5]$$

where λ = 0.154nm. The scattering intensity of the networks was comparatively stronger than the blends. The same was seen with chitosan/LPEO blends and networks (Figure 4.4.2, parts (A) and (B)).

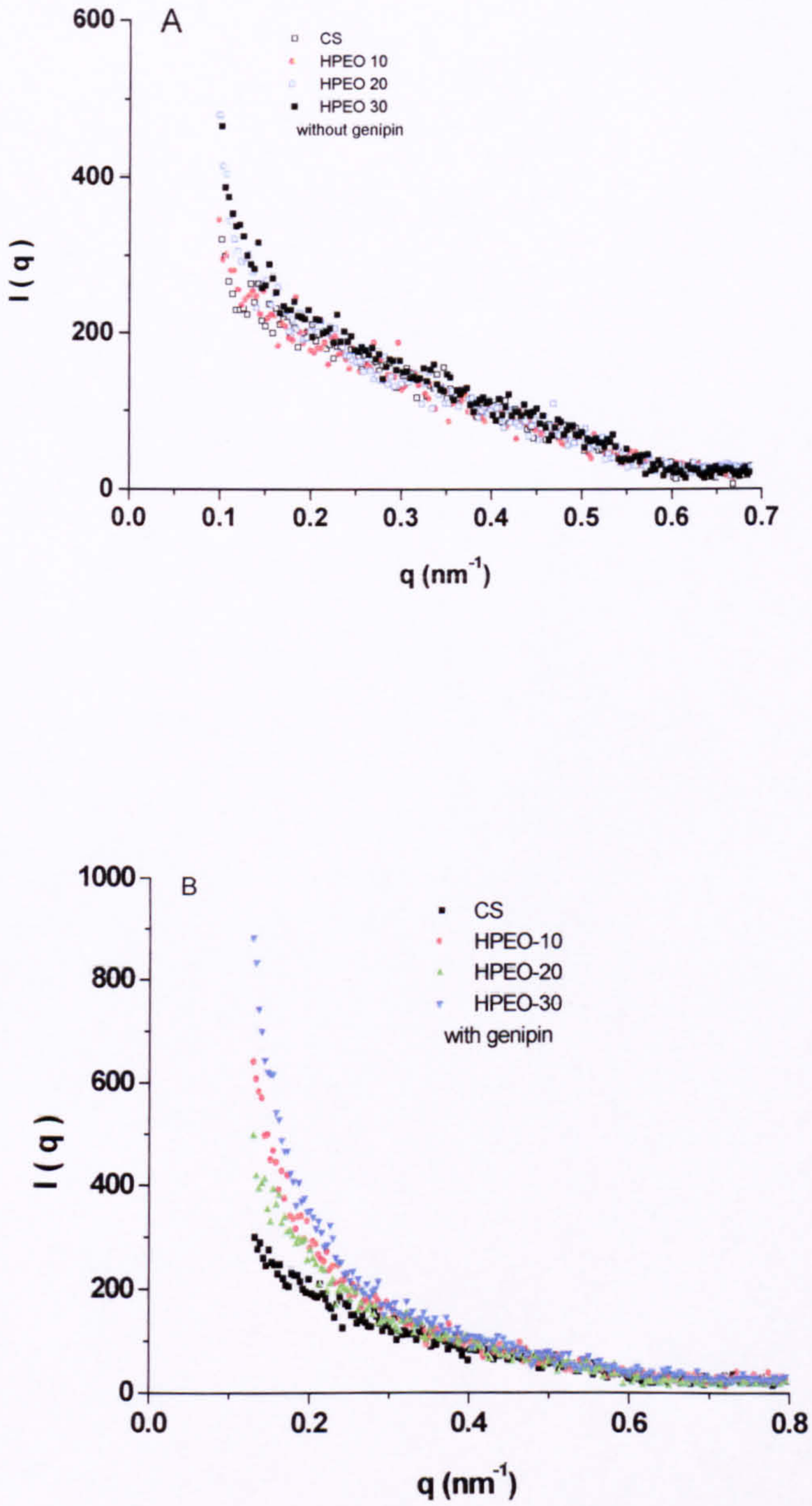

Figure 4.4.1 Scattered intensity versus scattering vector (q) for chitosan/HPEO blends (A) and for the blend networks (B)

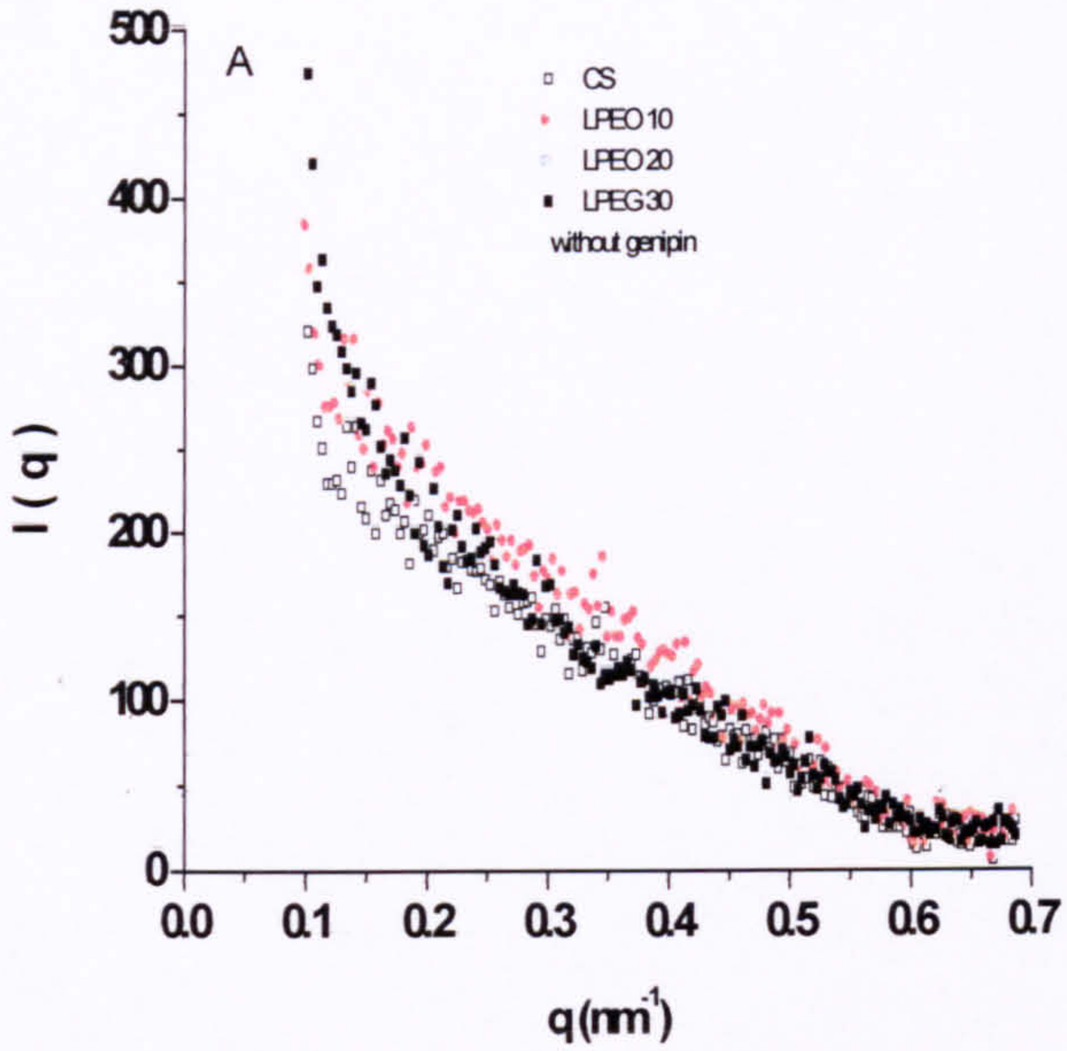

Figure 4.4.2 Scattered intensity versus scattering vector (q) for chitosan/LPEO (A) and for the blend networks (B)

SAXS measurements provide information regarding the electron density distribution of the material. Analysis of the angular distribution of the intensities reveals the periodicity and magnitude of that electron distribution. The principle of the technique is that in an ideal two-phase system, the scattered intensity is proportional to the mean square electron density fluctuation [234]. If there is non-phase separation in a system, in which the electron density is the same, the scattered intensity only represents for background scattering. For a phase-separated system, there is a difference in the electron densities, which results in higher scattering intensity. A comparison between Figure 4.4.1, parts A and B, and between Figure 4.4.2, parts A and B, shows that crosslinking by genipin increased the scattered intensity for the chitosan/HPEO and chitosan/LPEO systems. These can be regarded as evidence of differences in electron densities in each group of network. Such differences signify partial segregation in the blend. The stronger the intensity, the greater is the segregation. This result indicates that crosslinking resulted in phase separation.

As can be seen in Figures 4.4.1B and 4.4.2B, the chitosan network with 30% of HPEO (or LPEO) exhibits the strongest intensities – the stronger intensity the greater is the phase separation. The larger phase separation in the crosslinked chitosan/PEO blend leads to reduced molecular interaction between the chitosan and PEO and the network with the higher HPEO or LPEO contents produces a less than desirable blend.

4.4.2 Restrictions on crystallisation

Bragg's law states that the relationship between the long period and the scattering angle is given by:

$$D_m = 2\pi/q_m = \lambda/(2 \sin\theta_m) \qquad [4.4.2\text{-}1]$$

where D_m is the periodicity of the structure and θ_m is the scattering angle at the maximum intensity of the scattered rays.

Figure 4.4.3 shows SAXS results for 20, 40, 50 and 60 wt.% chitosan blends crosslinked by genipin. The maximum scattering angle increased as the chitosan content was increased. According to Bragg's law, therefore, the long periods decreased with increasing chitosan content. This means that the LPEO lamellar thickness in these chitosan/LPEO blends decreased.

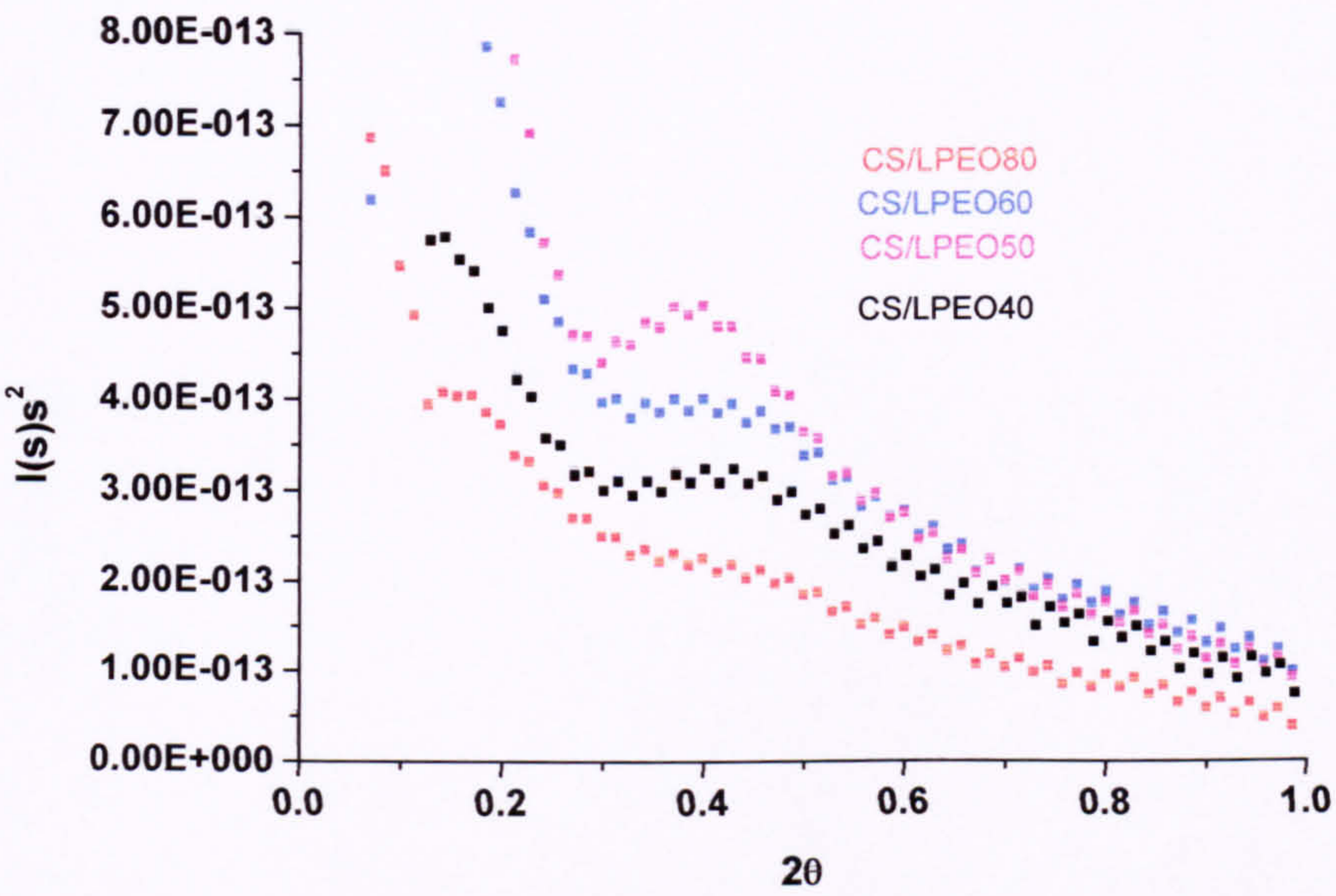

Figure 4.4.3 SAXS curves for chitosan/LPEO networks showing the changes of long period

A comparison of Figure 4.4.3 with Figure 4.3.4 shows that with increasing chitosan content there were decreases in the long periods of both the blends and the networks, but these decreases were more noticeable in the case of chitosan/LPEO networks (see Table 4.4.1). Crosslinking using genipin led to decreases in the crystallite size, meaning that the presence of networks restricts crystallisation.

Table 4.4.1: Comparison of the long periods of crosslinked and un-crosslinked chitosan/LPEO blends

LPEO content	**Crosslinked**		**Un-crosslinked**	
	Maximum scattering angle (θ_m), °	Long period (D_m), nm	Maximum scattering angle (θ_m), °	Long period (D_m), nm
40	0.215	20.5	0.0875	50.4
50	0.191	23.1	0.0775	56.9
60	0.213	20.7	0.080	55.1
80	0.0876	50.4	0.061	72.3

The results of DSC analysis are shown in Figure 4.4.4. After crosslinking, the melting point of the chitosan/LPEO blends decreased. Thermodynamically speaking, decreases in the lamellar thickness are responsible for the decreases in the melting points [171,232]. Consequently, DSC analysis also shows that crosslinking restricts crystallisation and leads to smaller crystals.

Figure 4.4.5 shows SAXS results for the 50 wt.% LPEO blend crosslinked by different amounts of genipin. The scattering angles (2θ) of the long periods for blends with genipin contents of 0.5% and 0.8% are 0.382° and 0.415°, respectively. The angles for the blend with genipin content of 0.01% and 0.1%, however, were not obtainable from the figure because their peaks occurred at very small angles.

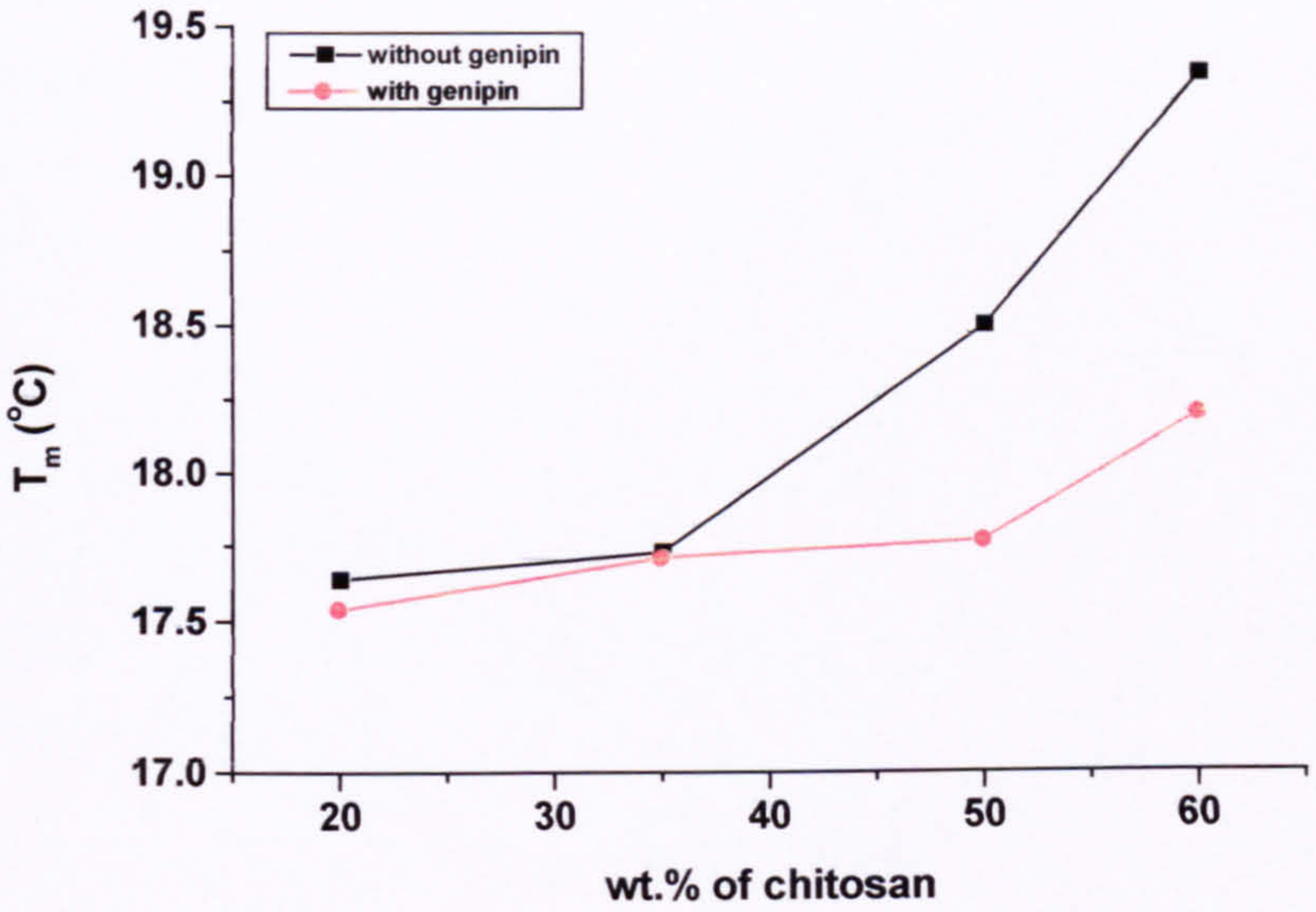

Figure 4.4.4 Comparison of T_m for chitosan/LPEO blends and networks

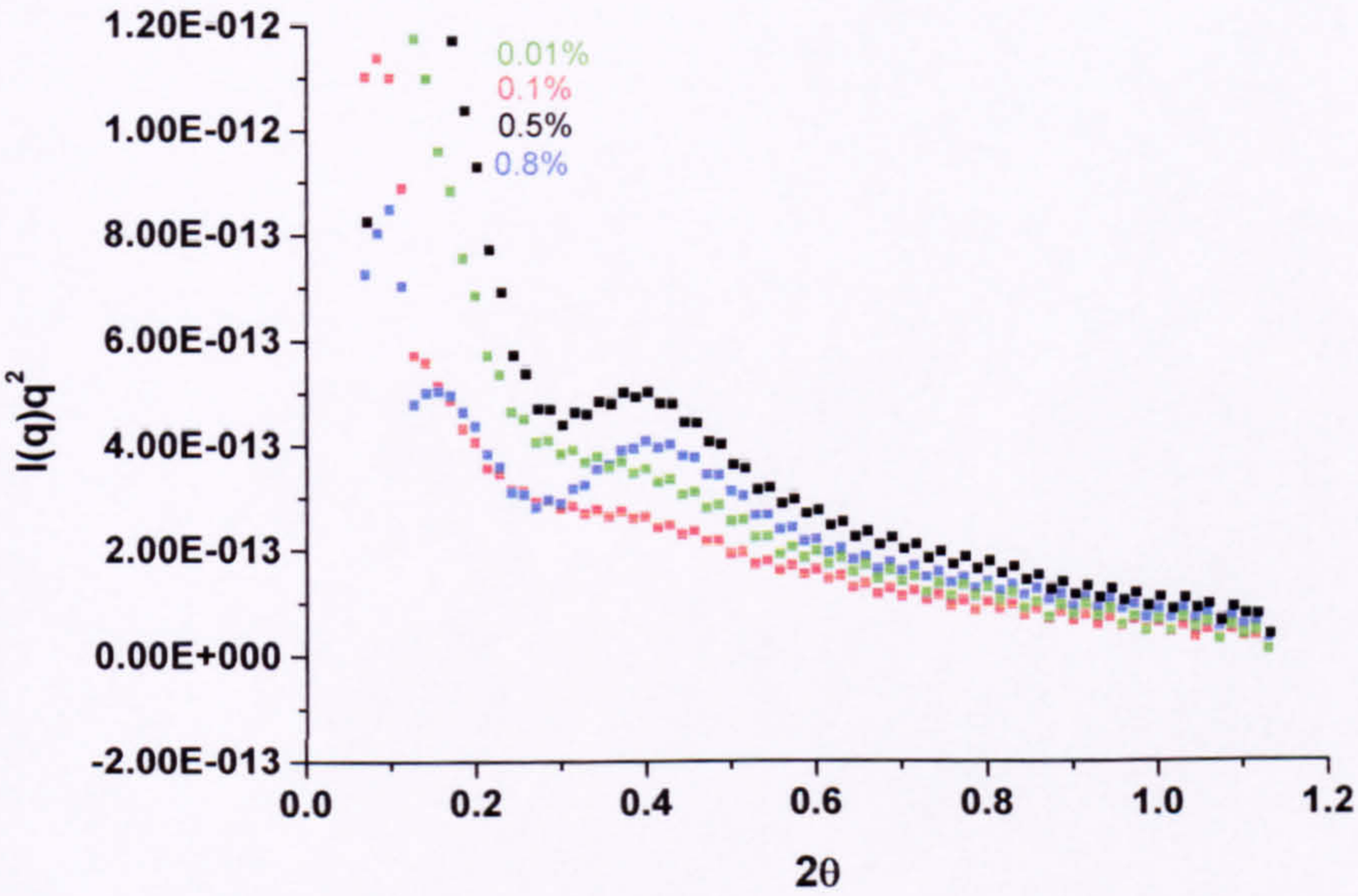

Figure 4.4.5 SAXS curves for chitosan/LPEO50% networks showing the changes of long periods with genipin content: 0.01, 0.1, 0.5 and 0.8wt.%.

The results clearly indicate that with increasing genipin content, the long period of LPEO in a chitosan/LPEO blend decreases. One can see from Bragg's law, stated above, that there is an inverse relationship between the size of the scattering angle and the magnitude of the long period. It has already been stated that crosslinking restricts crystallisation. This discussion shows that increases in the genipin content lead to greater restrictions on crystallisation, and, hence, to smaller crystals.

The above discussion on the morphology of chitosan/HPEO or LPEO blends and networks has shown that blending and crosslinking, especially the latter, leads to substantial morphological changes, including phase separation and reduction in the crystallite size. The effects of such changes in morphology on the mechanical and other physical properties of the polymer will be discussed in the following chapters.

4.5 Conclusions

The molecular interaction and miscibility of chitosan/PEO blends were examined. For chitosan/HPEO system, FT-IR spectra reveal hydrogen bonding interactions between the -O- group in the HPEO repeat units and -NH side group in the chitosan repeat unit of the blends. The results show that chitosan/HPEO blends are miscible over the whole composition range and the interaction parameter, χ_{12}, between both of components of the blend was -0.16. An interesting phenomenon was observed for chitosan/LPEO blends. When the composition of chitosan was less than 60% by weight, the melting points increased as the composition of chitosan was increased. It is believed that there are strong molecular interactions between chitosan molecules and the molecules in the crystalline phase of LPEO in these chitosan/LPEO blends.

The morphology of chitosan/PEO blend networks was investigated. SAXS results showed that a heterogeneous structure exists in the chitosan/HPEO (or /LPEO) blend networks. Crosslinking by genipin restricts crystallisation and leads to smaller crystals.

This information on the morphology of chitosan and chitosan/PEO blends and networks will be helpful in the understanding of the properties of their films.

CHAPTER 5

Mechanical Properties of Chitosan/PEO Blend Films and Networks

5.1. Introduction

As reviewed in the Chapter 2, chitosan, as a member of the family of β (1→4) linked polysaccharides, is a collective term applied to deacetylated chitin in various stages of deacetylation and depolymerisation. In contrast to most other polysaccharides, chitosan displays basic properties that impart it with unique physicalchemical characteristics [30,43]. Owing to the presence of reactive amino groups, chitosan can be modified [30,43]. Like many other polysaccharides, it manifests very good film-forming properties, which significantly extend its range of applications. The films are usually obtained from a solution of the polymer in the salt form. The mechanical characteristics of chitosan films depend on various parameters. Numerous studies have demonstrated that the salt-form [236], molecular weight [236] and degree of deacetylation [237] as well as the external conditions of film formation [236-238] influence the properties of this polymer. As some literature reports, the nature of the interactions, the concentration of chitosan and the nature of the acid used could influence the conformation of the polymer chains during the formation of the film and, as a consequence, the density of entanglement of the chains in the solid state. It is, therefore, these factors that must be considered carefully during film formation.

For biomedical applications, one of the most important physical properties of chitosan films is their mechanical properties in the hydrous state, because the films have to be in contact with the living body for long periods of time. For a un-crosslinked chitosan film in anhydrous conditions, the stress at break can be relatively high and close to 80MPa and the Young modulus near 3.6GPa [238]. However, after immersion in deionized water for a few hours, a tremendous loss of mechanical properties takes place: 99% for the Young modulus and 88% for the stress at break [239]. Clearly, the mechanical properties of a un-crosslinked chitosan film cannot meet the requirements for biomedical applications.

One of the main tasks in our research is to develop a novel chitosan/PEO blend film crosslinked by genipin with the optimisation of mechanical properties for biomedical applications. The aim of this chapter is to study the mechanical properties of the novel chitosan/PEO blend films in both the dry and wet states.

5.2 Effects of PEO Content, Molecular Weight of PEO and Crosslinking on Mechanical Properties of Chitosan/PEO Blend Films

The strength and elasticity of a polymer film can be reflected by its tensile strength and elongation at break, which are measured by tensile testing. Films suitable for biomedical applications should be strong, but flexible. Films prepared from pure chitosan are rather brittle [43]. Therefore, it is very important to improve their ductility. There are several ways to obtain films with better elastic and strength properties, for example, preparing them from blends[90-93] and or by crosslinking [4,7,8,]. In this study, PEO was introduced into chitosan and crosslinking with genipin was used to improve the flexibility and strength of chitosan.

The tensile strength and the elongation at break plotted against wt.% LPEO for dried films of both crosslinked and un-crosslinked chitosan and chitosan/LPEO blends are shown in Figures 5.2.1 and 5.2.2, respectively. It can be seen that the pure chitosan film is brittle: the tensile strength was 39MPa and the elongation at break 8%. The highest tensile strength was found in the blend with 20wt.% of LPEO (55MPa) and the greatest enhancement of elongation at break (38%) occurred at 65% LPEO content, the highpoint of a general trend of elongation increasing as LPEO content increased. Crosslinking with genipin gave rise to improvements in both mechanical properties. It was also observed experimentally that films containing more than 65% LPEO were opaque, while films with lower LPEO content were transparent and pale yellow to brown in colour. From this observation, it can be concluded that films with a low LPEO content are likely less heterogeneous than films with high LPEO content. This fact has already been confirmed by the study of miscibility in Chapter 4.

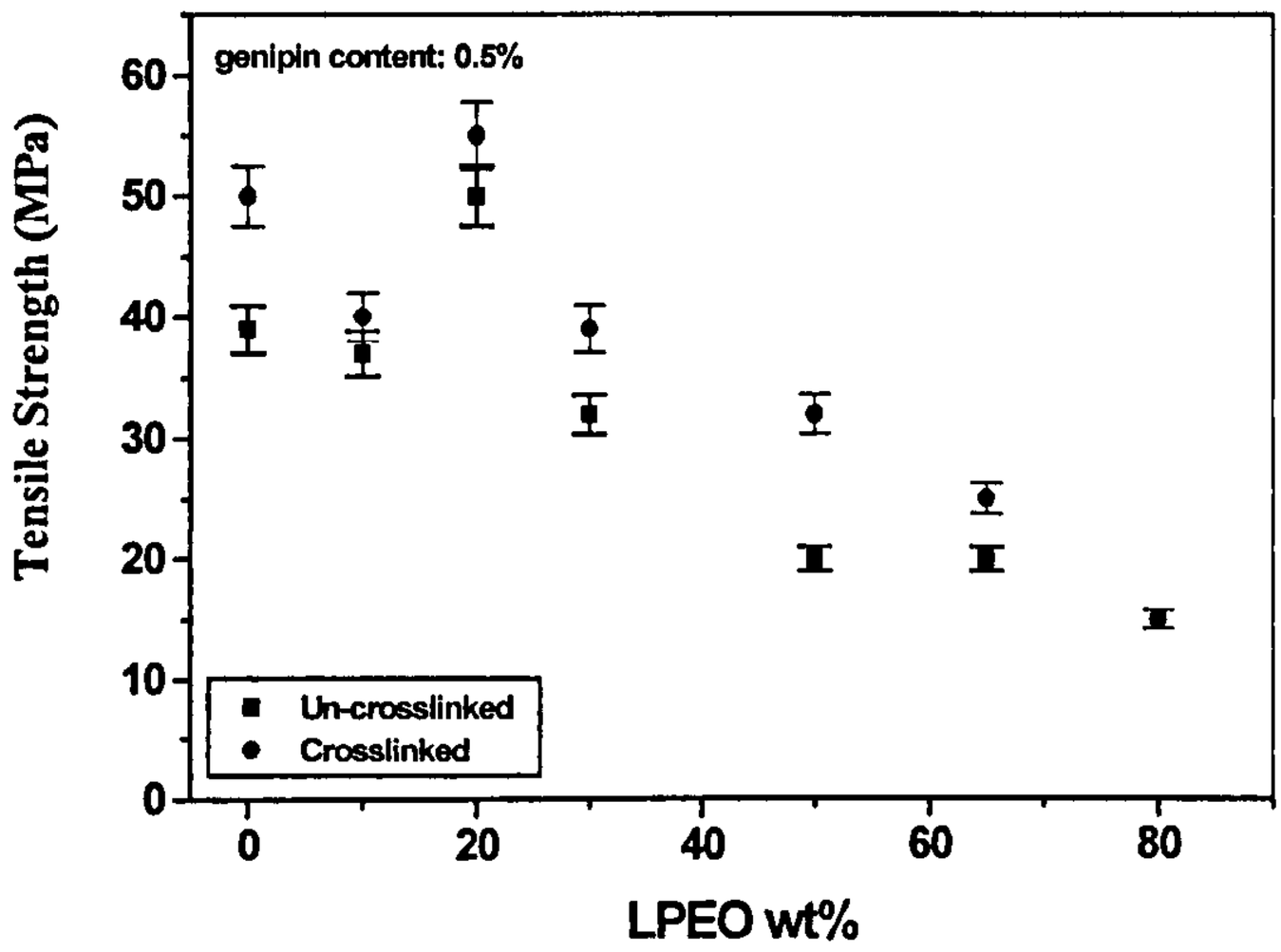

Figure 5.2.1 Tensile strength of crosslinked and uncrosslinked dried chitosan/LPEO blend films

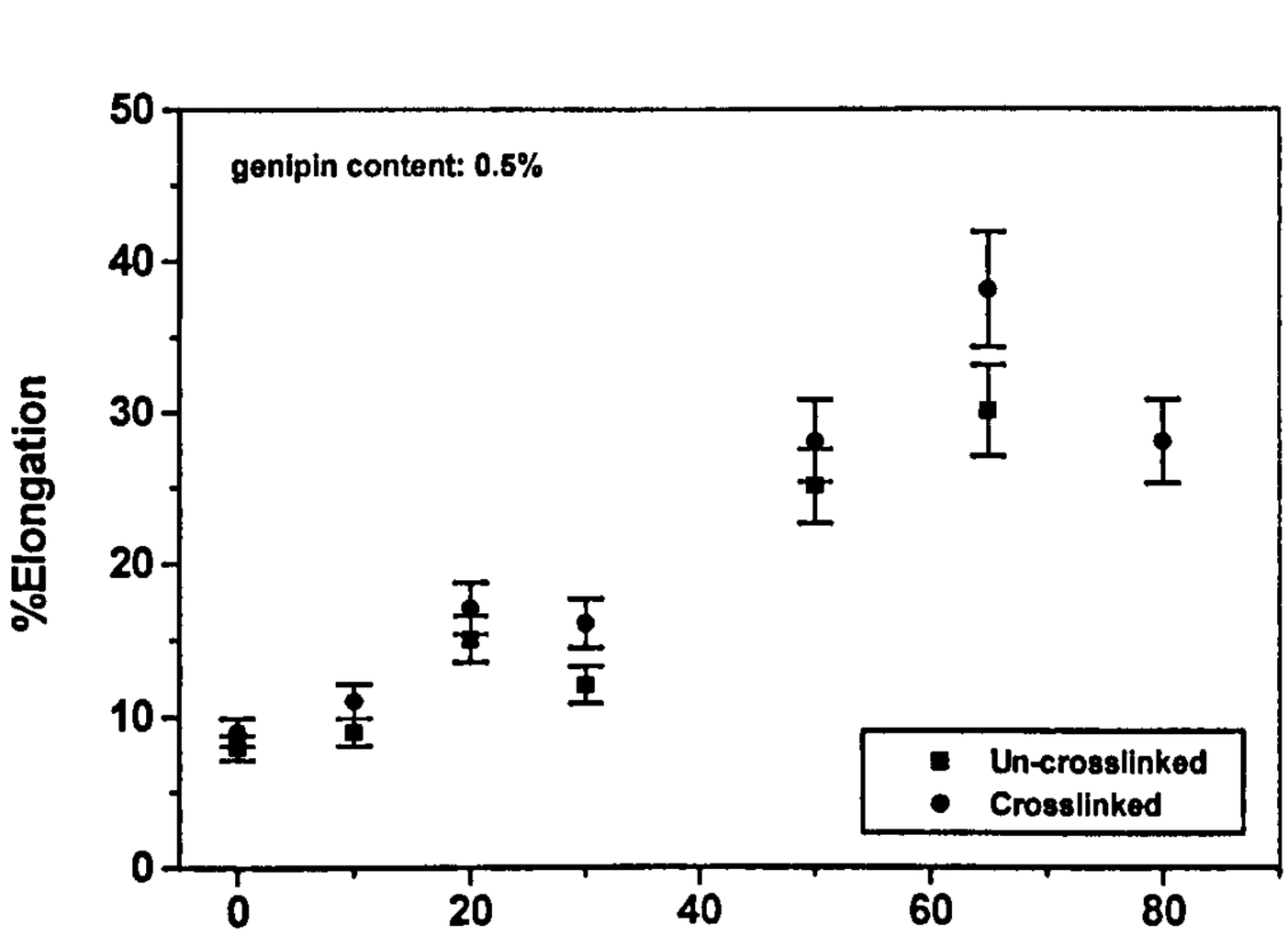

Figure 5.2.2 Elongation at break of crosslinked and uncrosslinked dried chitosan/LPEO blend films

Table 5.2.1. Tensile strength and elongation at break of the chitosan /HPEO blend systems (Genipin content: 0.5wt.%)

PEO (%)	Elongation at break (%)	Stress at break (MPa)
	Un-crosslinked CS/HPEO System	
10	19 ± 2.0	60 ± 1.2
20	25 ± 1.5	63 ± 1.7
30	14 ± 1.2	50 ± 1.9
	Crosslinked CS/HPEO System	
10	15 ± 1.5	55 ± 2.0
20	17 ± 1.2	70 ± 1.2
30	15 ± 1.9	58 ± 1.8

Table 5.2.1 shows the results of tensile strength and percentage elongation at break for chitosan/HPEO systems. The chitosan/HPEO blend films could not be prepared when the HPEO content was higher than 30%. It can be clearly seen, from the results shown in the table, that crosslinking with genipin did not give rise to improvement in either tensile strength or elongation at break for the chitosan/HPEO systems. This may be due to the low miscibility of chitosan with HPEO as indicated previously in Chapter 4.

5.3 Effects of Crosslinking Density and Water Content on Mechanical Properties of Chitosan/LPEO Blend Films

It is clear from Section 5.2 that for all films containing LPEO crosslinking gave rise to increases in the tensile strength and elongation at break of the films. From the results shown in Figures 5.2.1 and 5.2.2, it can be seen that there is an optimal content of LPEO, 50/50 by weight, for elongation and tensile strength in the chitosan/LPEO blend films. In discussing the effects of crosslinking density and water content on the mechanical properties of the chitosan/LPEO blend films, the focus is, therefore, on the results of chitosan/LPEO (50/50 by weight).

Figures 5.3.1 and 5.3.2 give the stress-strain curves for un-crosslinked and crosslinked CS/LPEO50 blend films (genipin content: 0.5%) with different water contents.

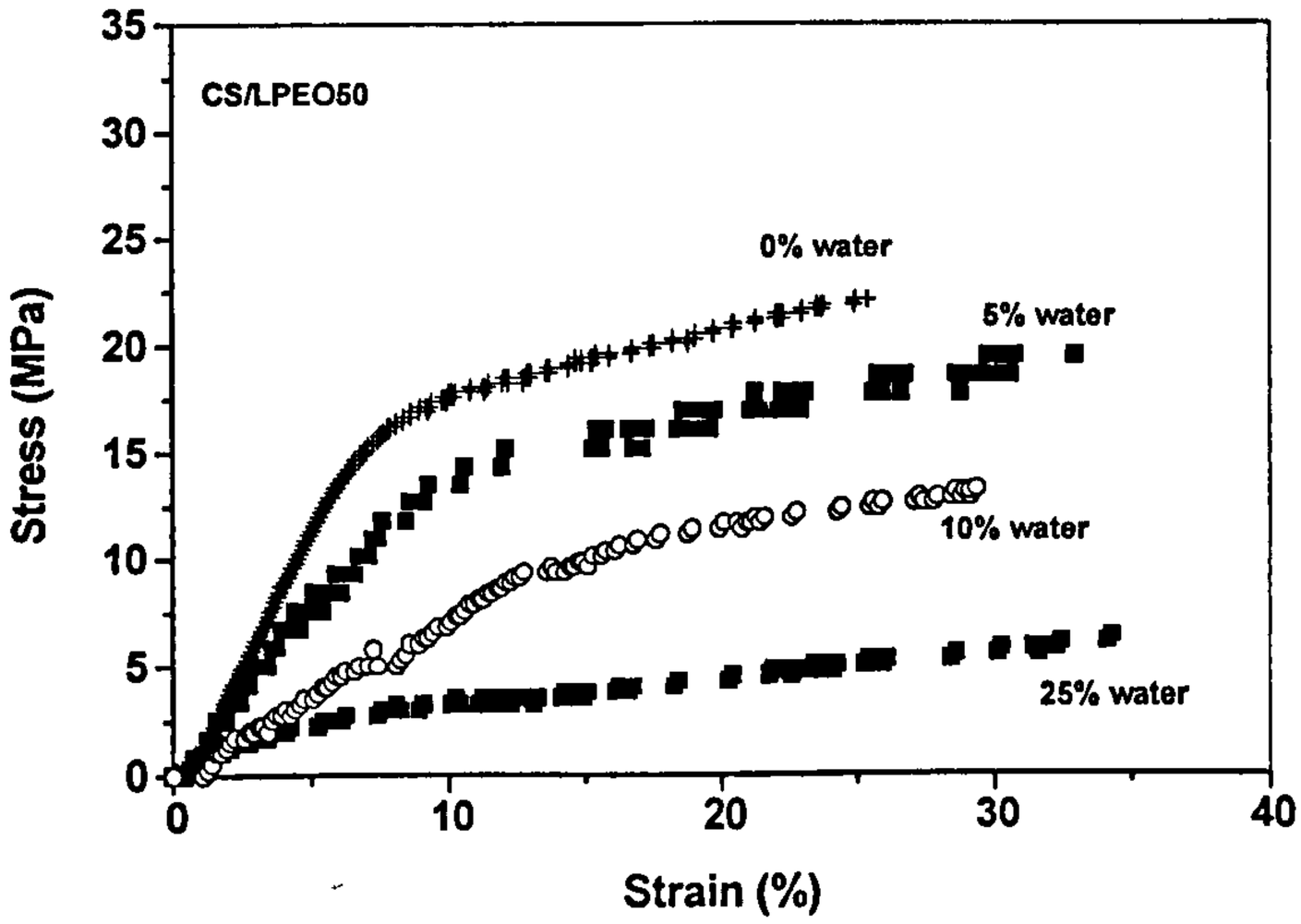

Figure 5.3.1 Stress vs. strain curves for un-crosslinked CS/LPEO50 blend films with different water contents

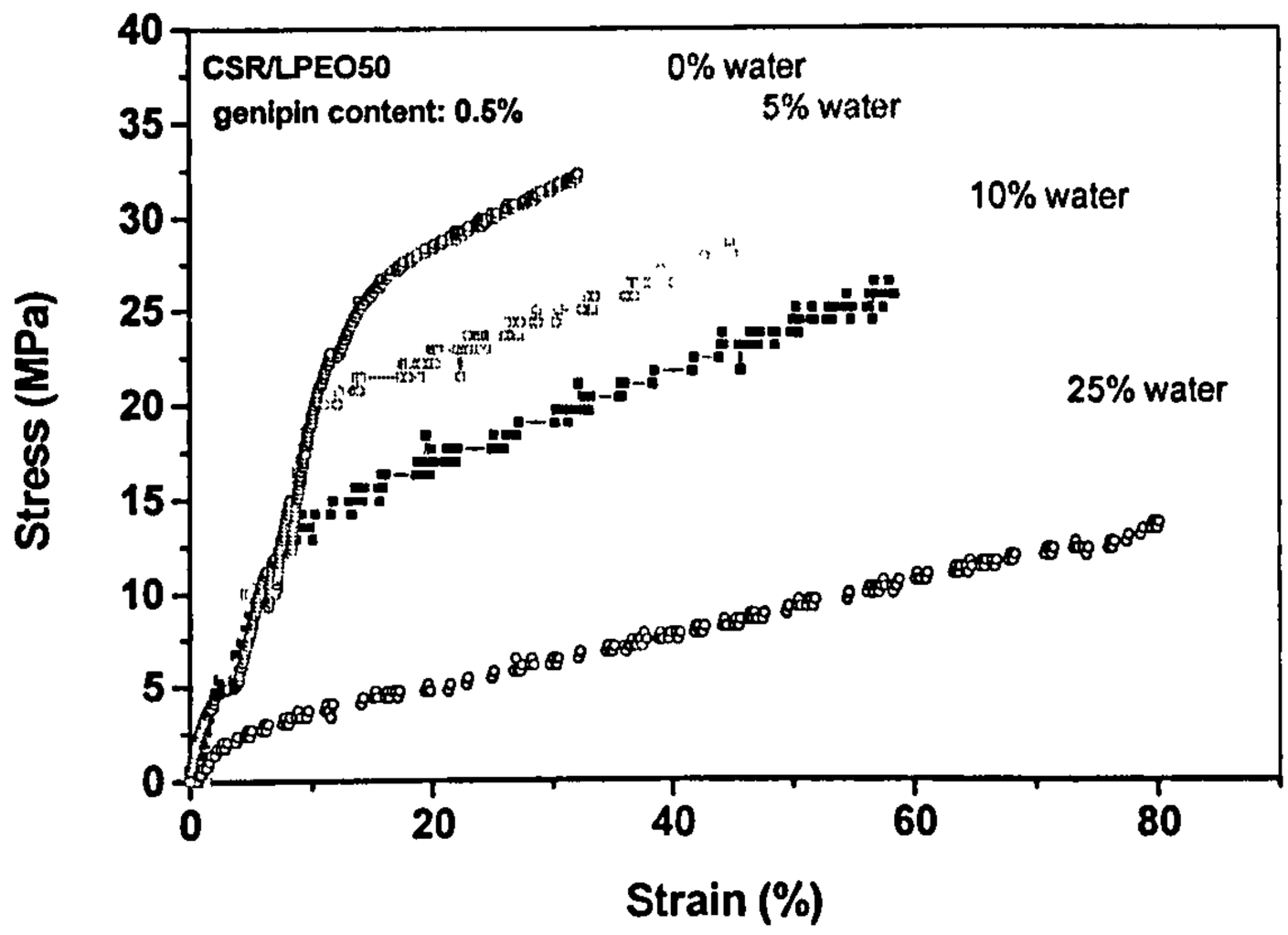

Figure 5.3.2 Stress vs. strain curves for crosslinked CS/LPEO50 blend films with different water contents

It can be seen in both cases that with increasing water content in the films, elongation at break increased whereas tensile strength decreased. However, crosslinking gave rise to greater increases in both tensile strength and elongation at break than the equivalent dried samples. At 15% water content, the increase in tensile strength of the crosslinked film was more than twice that of the un-crosslinked one. At 25% water content, for the crosslinked film, the elongation at break reached 80% and the tensile strength was at about 15MPa, and for the uncrosslinked film, the elongation at break was 35% and the tensile strength was at about 6MPa.

Table 5.3.1 Comparison of the modulus and elongation at break of un-crosslinked and crosslinked CS/LPEO50 films with different water contents (genipin content:0.5%)

Sample	Water content (%)	Modulus (MPa)	Elongation at break (%)
CS/LPEO50	0	2114 ± 105	25.4 ± 1.2
	5	1586 ± 80	29.0± 1.6
	10	1117 ± 40	32.9 ± 1.8
	25	547 ± 30	34.5 ± 1.8
CSR/LPEO50	0	2341 ± 102	28.0 ± 1.4
	5	1942 ± 98	45.1 ± 2.4
	10	1567 ± 78	58.5 ± 3.0
	25	627 ± 35	80.1 ± 3.2

Table 5.3.1 gives a comparison of the modulus and elongation at break of un-crosslinked and crosslinked CS/LPEO50 blend films with different water contents. With increasing water content, the modulus of the CS/LPEO50 films decreased and the elongation at break increased. However, crosslinking with genipin produced significant increases in the modulus when the water content was less than 25%. As the water content increased from 0 to 10%, the modulus for the un-crosslinked film reduced by 47%, but the modulus for the crosslinked film reduced only by 33%. As the water content increased from 0 to 25%, the increase in elongation at break for the

crosslinked film was more than 6 times that of the un-crosslinked film. These enhanced properties were more noticeable in films with higher water contents. The importance of preventing the carrier in a drug delivery system from disintegrating when the water content of its surrounding environment increases means that these improvements in the mechanical properties are of real significance.

The stress-strain plots of the crosslinked CSR/LPEO50 blend film with different genipin contents are shown in Figures 5.3.3 (where the water content of the film is 5%) and 5.3.4 (where the water content of the film is 13%). Both indicate that the increment in elongation at break was tremendous when the genipin content was 0.1%: the increase in elongation was 200% at 5% water content and 450% at 13%. When the genipin content was increased further to 0.5% and then 0.8%, the improvement in elongation at break were not as significant as that for 0.1% genipin. The reasons for this are not yet clear. It may have resulted from the effect of crosslink density.

Table 5.3.2 shows a comparison of the modulus (as well as elongation at break) of crosslinked CSR/LPEO50 blend films with different genipin contents, when they contain 5 and 13% water. Crosslinking reduced the loss in modulus of the films as the water content increased, in particular where the genipin content was high.

As expected, films crosslinked by genipin became more elastic and maintained their strength when they were in wet state.

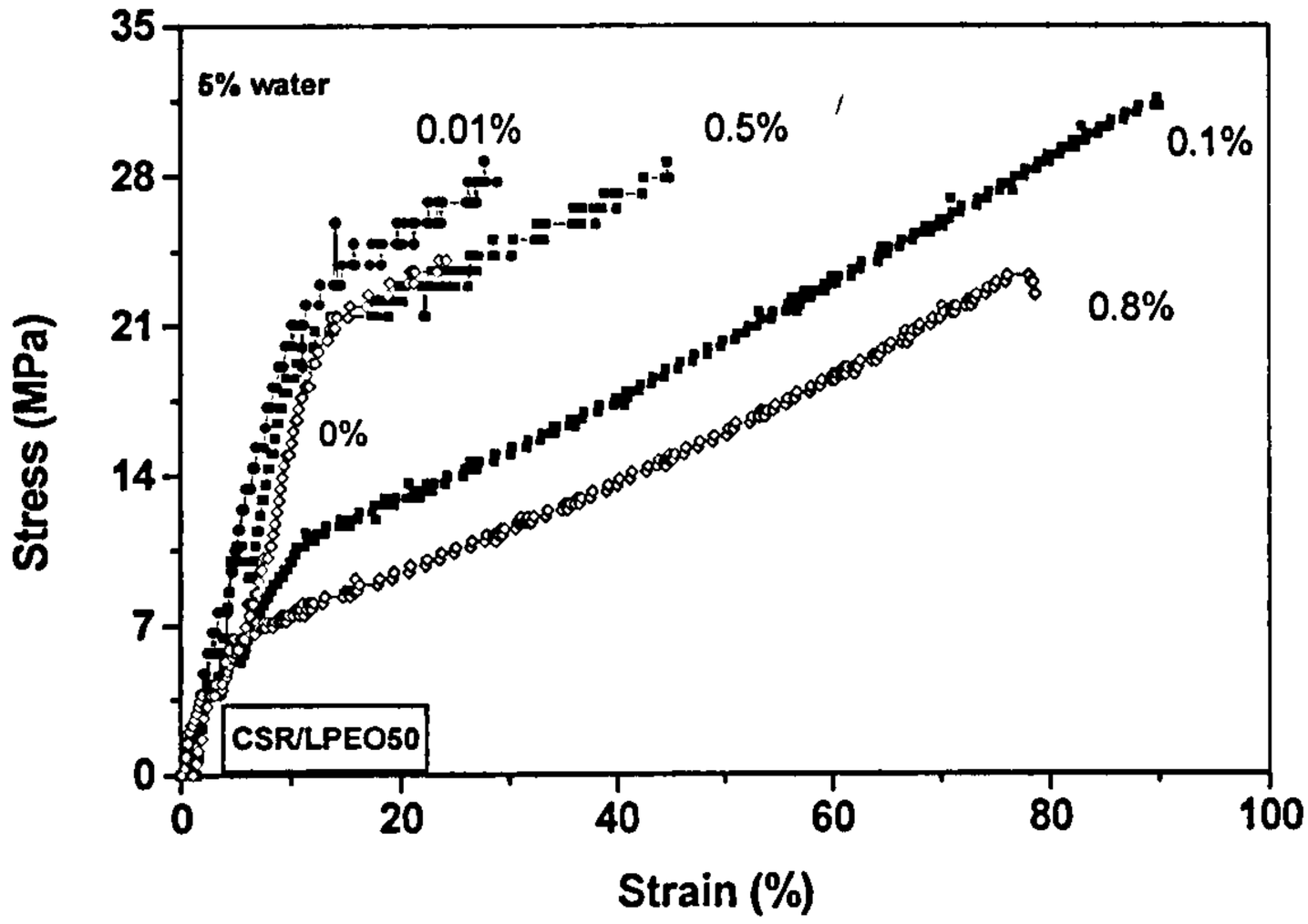

Figure 5.3.3 Tensile stress versus strain of the CSR/LPEO50 blend films with 5% water content and with a range of genipin contents

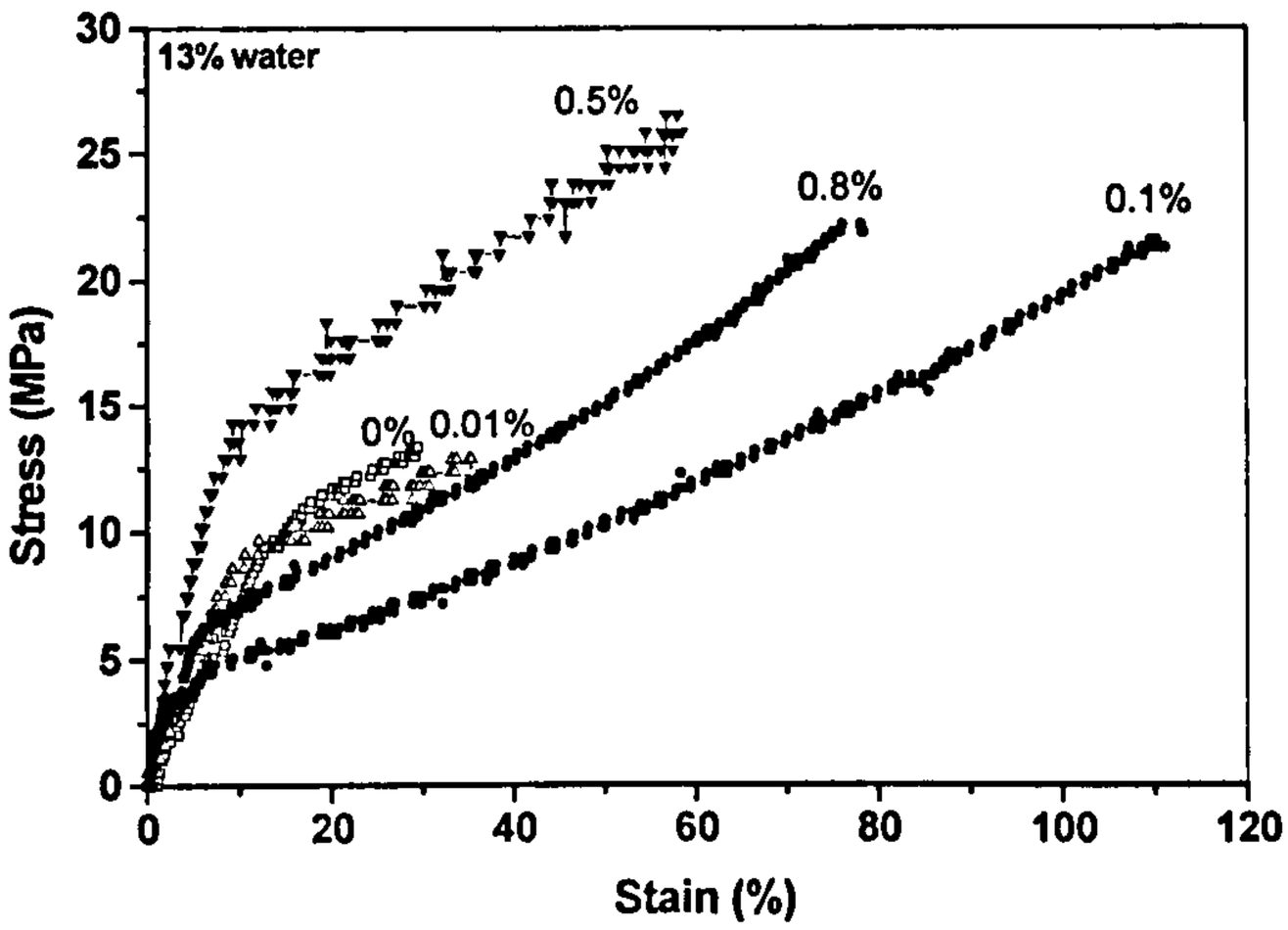

Figure 5.3.4 Tensile stress versus strain of the CSR/LPEO50 blend films with 13% water content and with a range of genipin contents.

Table 5.3.2 Modulus for crosslinked CSR/LPEO50 blend films

Sample	Genipin content (%)	5% water		13% water	
		Modulus (MPa)	Elongation (%)	Modulus (MPa)	Elongation at break (%)
CSR/LPEO50	0	1586 ± 80	29.0 ± 1.6	870 ± 80	20.1 ± 1.8
	0.01	2096 ± 102	29.1± 1.7	978 ± 50	35.6 ± 1.8
	0.1	2143 ± 60	90.1 ± 3.1	1120 ± 56	111.2 ± 3.3
	0.5	1942 ± 98	45.1± 2.4	1720 ± 90	58.4 ± 2.9
	0.8	2025 ± 55	78.6 ± 3.5	1447 ± 70	78.4 ± 3.5

Chitosan has been described in terms of the degree of deacetylation and average molecular weight in conjunction with its film-forming properties [175]. It has been observed that the film formation of un-crosslinked blends is closely related to their composition. Above 50wt.% of HPEO or 65wt.% of LPEO content, no useful films could be formed. Similar results have been reported by Zhao [225]. However, crosslinked blends at 80wt.% of LPEO or above overcame this problem. These indicate that using genipin as a crosslinker can improve the mechanical properties of chitosan/PEO blend films.

Such improvements are in agreement with the previous discussions about changes in morphology. Crosslinking reduced crystal size and the degree of crystallinity and it gave rise to improvements of the mechanical properties.

5.4 Effect of Solution pH on the Mechanical Properties of Chitosan Films

Chitosan exists in the solid state in various forms such as films, yarns, flakes, powder etc [43]. Most of them arose by regeneration from a solution or gel. The mechanical properties of chitosan in the solid state obviously depend on the conditions of preparation, i.e. the solution or gel properties of this polymer.

Chitosan is an acidic soluble polymer. pH has an influence on the solution properties [30,43]. Solution behaviour of chitosan reflects the role of the superamolecular organizations and also allows us to understand various interactions in which this polymer can be involved. The gelation of chitosan solutions depends on the molecular mobility of the polymer chains in the media and the extent of acetylation. The first important point is the initial media [43]. Indeed, gel formation can only be achieved if chitosan is initially in the form a salt obtained with a weak acid [30,43]. The behaviour must be related to the fact that the reaction of acetylation is performed on free amine functions, and, therefore, favoured in presence of a weak acid. As a consequence, solution pH plays an important role in relation to the occurrence of gelation [30,43].

It is clear from the above that film formation conditions, such as solvent pH and the type of solvent used can certainly affect the mechanical properties of chitosan films. Thus, in this section, the mechanical properties of chitosan films, which were formed with different pH values, are discussed.

Un-crosslinked and crosslinked chitosan films were prepared when solution pHs were 2.5, 3.0, 4.0 and 5.0, respectively. The tensile strength and elongation at break plotted against pH value of solution for both films are shown in Figures 5.4.1 and 5.4.2, respectively. The results for the un-crosslinked chitosan films clearly indicate that solution pH has a significant influence on both tensile strength and elongation at break. The more acidic the solution, the greater the tensile strength and the larger the elongation at break. When the solution pH was 2.5, the values of both properties were double that when the solution pH was 5.0. For the crosslinked chitosan films, the results indicated that when the solution pH was 3.0 the elongation at break was the greatest, but that the solution pH did not have a substantial effect on the tensile strength.

From the above results, it can be seen that the tensile stress and elongation of crosslinked and uncrosslinked chitosan films at break are influenced by the solution pH. From tensile tests alone, it is difficult to understand why solution pH has a significant influence on stress and elongation of chitosan films at break.

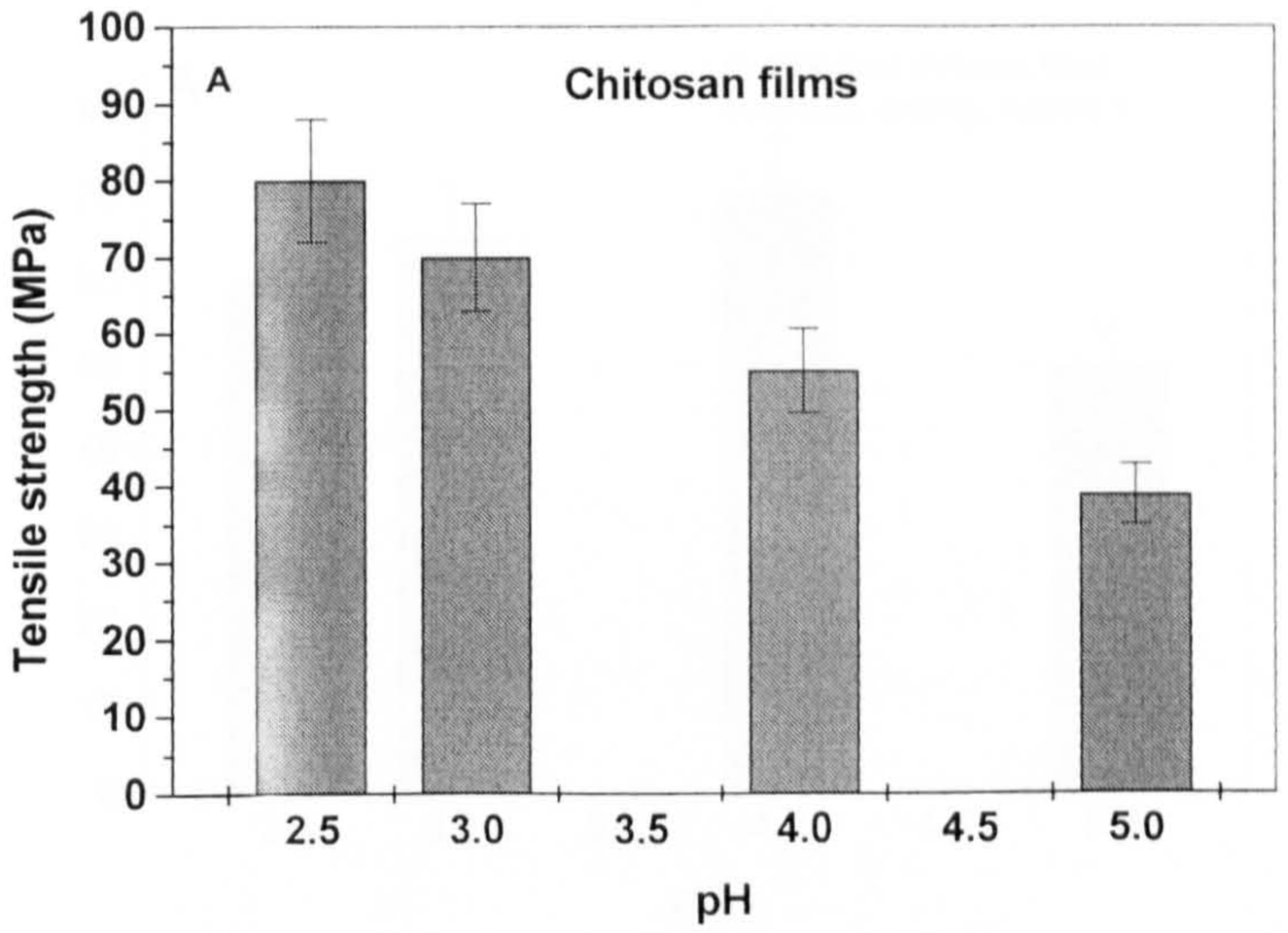

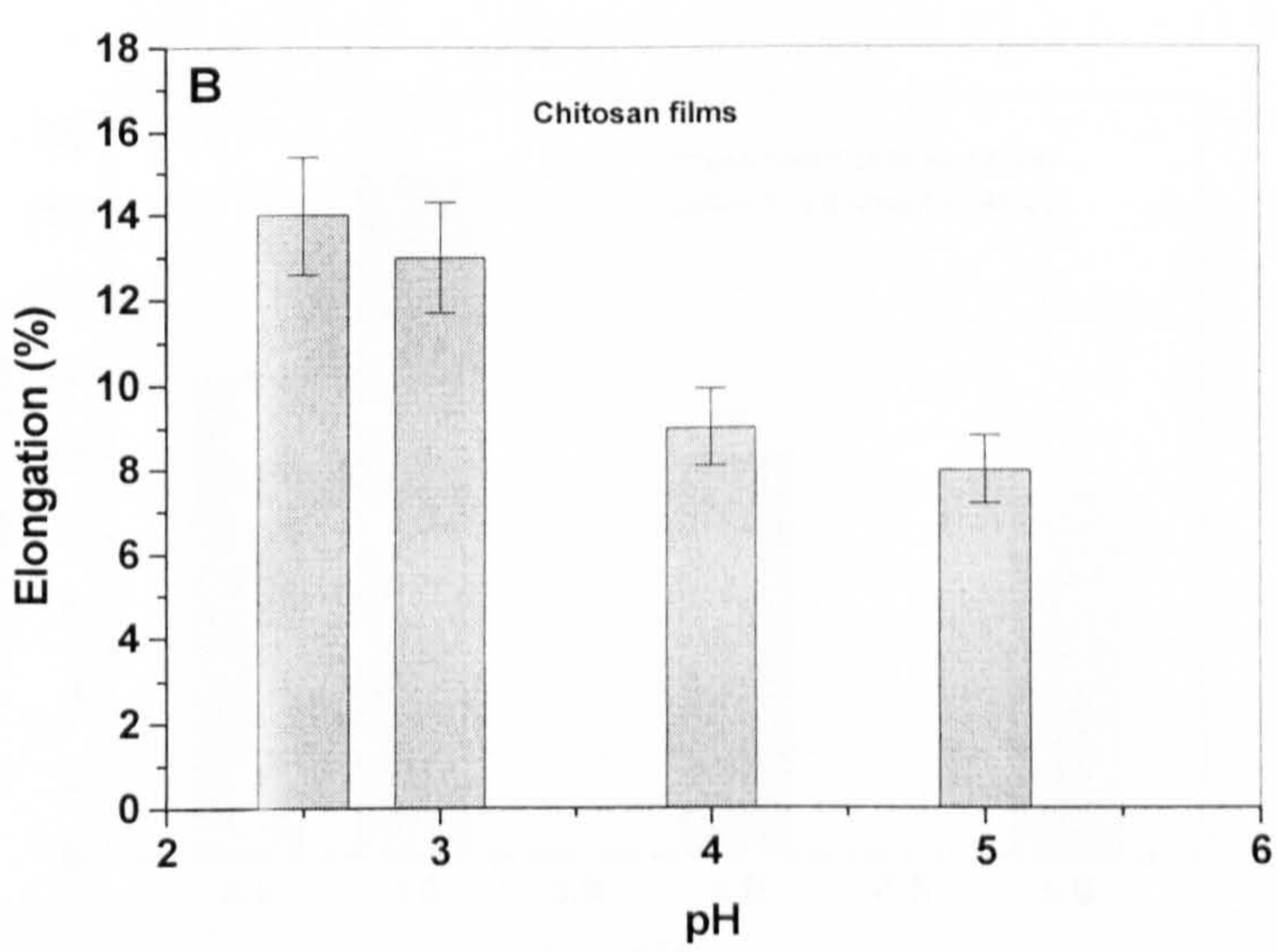

Figure 5.4.1 (A) tensile strength, (B) elongation at break for the un-crosslinked chitosan films versus the solution pH.

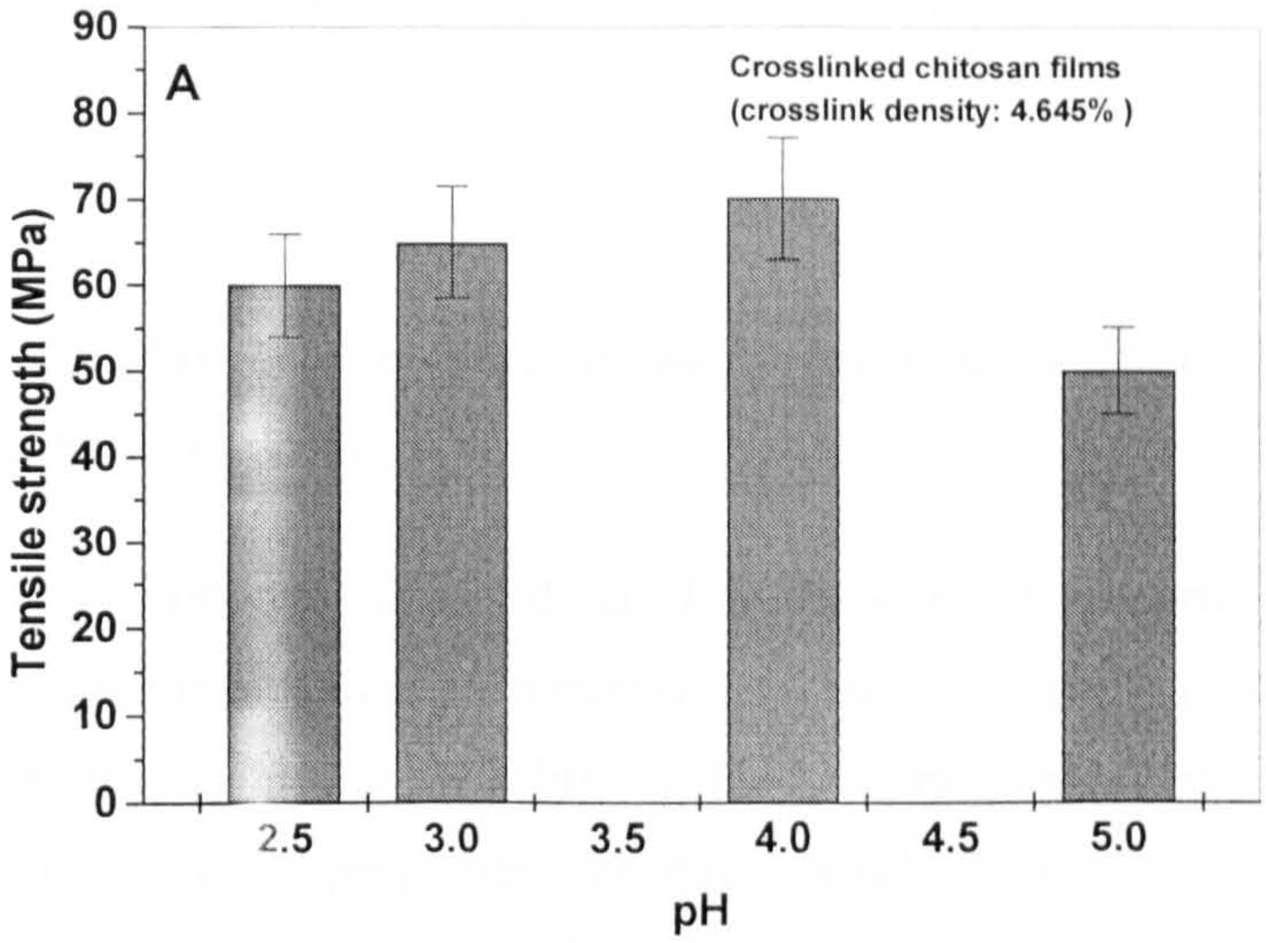

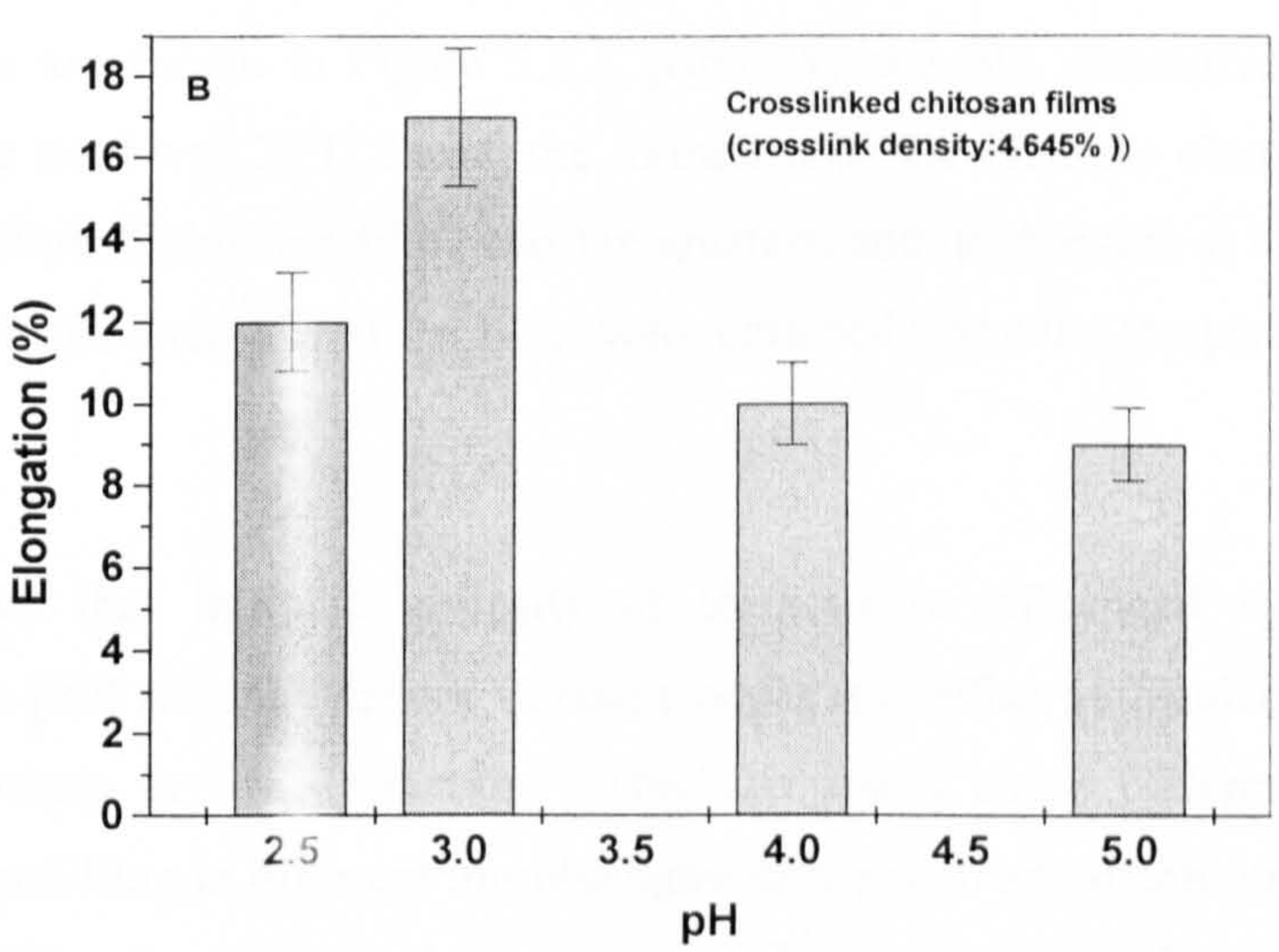

Figure 5.4.2 (A) tensile stress, (B) elongation at break for the crosslinked chitosan films versus the solution pH.

In order to understand this effect, it is necessary to investigate the aggregation behaviour of chitosan macromolecules during film formation. In Chapter 8, the results of this investigation are discussed and the issue of why solution pH has a significant influence on tensile strength and elongation at break of chitosan films is addressed.

5.5 Effect of Film-forming Temperature on the Mechanical Properties of Crosslinked Chitosan Films

Temperature is an important factor of affecting the solution properties of chitosan, which determine the mechanical properties of the chitosan films. It is because during film formation the molecular mobility of the polymer chains in the media is influenced by the solution properties [30, 43]. In this section, the effect of film-forming temperature on the mechanical properties of crosslinked chitosan films was studied. The film-formation temperatures used are 25°C, 40°C and 60°C, respectively.

The tensile strength and elongation at break plotted against the film-forming temperature are shown in Figure 5.5.1, parts (A) and (B), respectively. When the temperature used was 25°C during the formation of the film, the elongation at break of the crosslinked chitosan films was the greatest, and double that at 40°C. However, the better tensile strengths of the films were obtained when the temperature was 40°C and 60°C.

It is known that intrinsic viscosity of chitosan is influenced by the solution temperature [29] and the intrinsic viscosity could also affect molecular motion during the crosslinking or film-formation. This fact could cause different crosslinking processes, resulting in different morphologies of the network in chitosan films, giving rise to different mechanical properties. The temperature-dependence of the crosslinking reaction of chitosan and genipin (Chapter 7) will answer the question of why film-forming temperature affects the mechanical properties of crosslinked chitosan films.

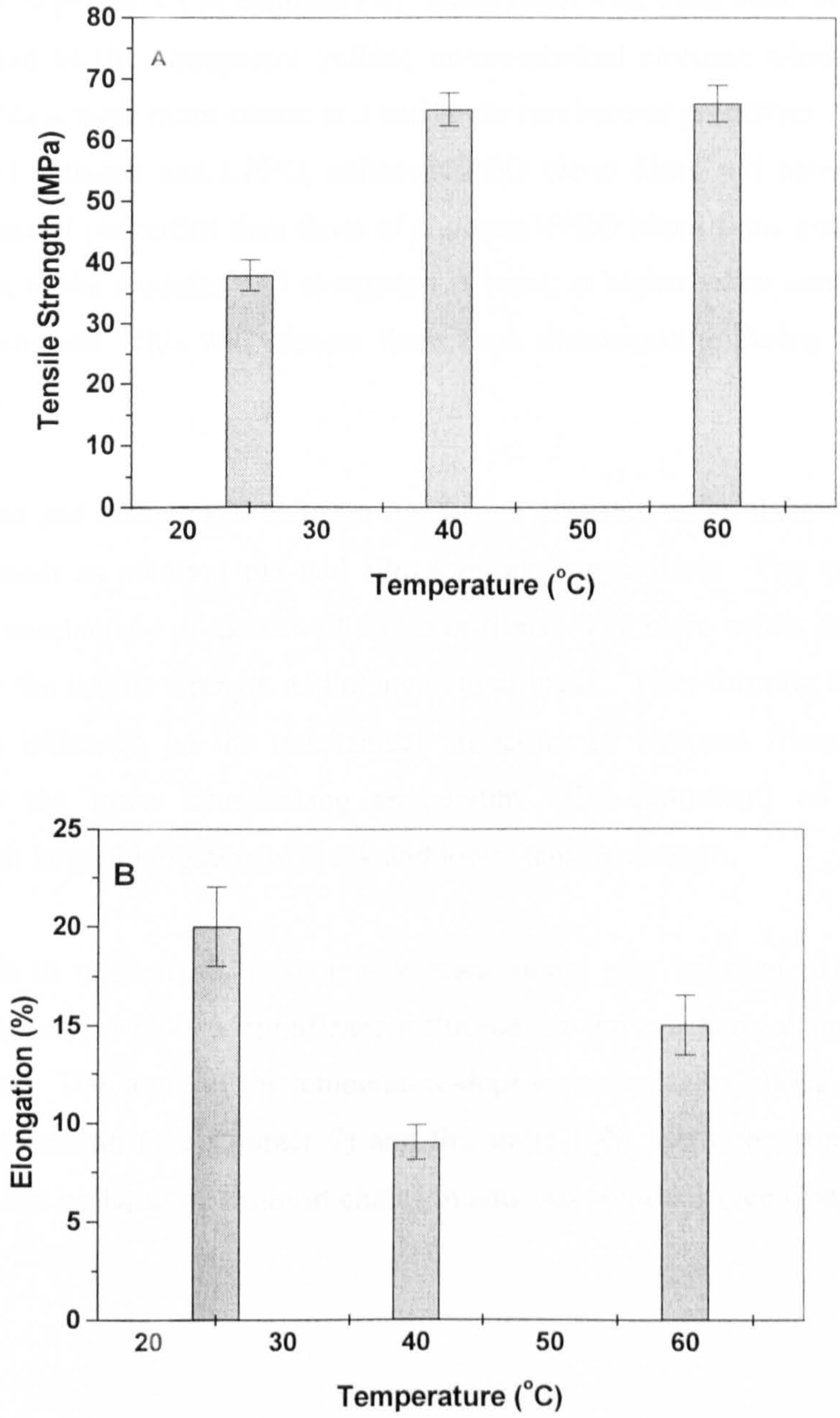

Figure 5.5.1 (A) tensile stress, (B) elongation at break of crosslinked chitosan films versus film-forming temperature

5.6 Conclusions

The mechanical properties of chitosan/PEO blend films were examined. It was found that, compared to the transparent yellow, un-crosslinked chitosan films, the blue, crosslinked films were more elastic and had better mechanical properties. Due to the miscibility of chitosan and LPEO, chitosan/LPEO blend films and networks show better mechanical properties than those of chitosan/HPEO blend films and networks. Improvement in the modulus and elongation at break at higher water contents in the films was achieved. This will prevent them from disintegrating during biomedical applications.

Uncrosslinked and crosslinked chitosan films were prepared under different external conditions, such as solution pH and film-forming temperature. The solution pH affected the mechanical properties of chitosan films. The more acidic solution, the greater were the tensile strength and elongation at break. Film-forming temperature also had an influence on the mechanical properties of chitosan films. The film obtained by the lower crosslinking temperature (film-formation) of 25°C was endowed with larger elongation at break and lower tensile strength.

It is difficult to understand, from tensile tests alone, why solution pH and film-forming temperature have a significant influence on the mechanical properties of chitosan films. The study of the temperature-dependence of crosslinking reaction of chitosan and genipin (see Chapter 7) and the static light scattering studies on the aggregation and collapse of chitosan chains in aqueous solutions (see Chapter 8) will answer this question.

CHAPTER 6

Swelling Behaviour and Surface Properties

6.1 Introduction

It is known [239-241] that drug release from carriers depends on their physical and chemical properties in response to the surroundings. For drug delivery, materials have to be mechanically satisfactory and stimuli-responsive, because they are expected to reside in the body for a long period of time and modulate drug release by responding to local environmental stimuli [239].

Some polymers undergo strong conformational changes when only small changes occur in the environment, such as temperature, pH and ionic strength [240-244]. They can provide the tools for creating functional materials with a wide variety of uses because environmental changes induce structural changes. These polymers are called stimulus-responsive polymers. In particular, hydrogels exhibit dramatic changes in their swelling behaviour in response to surrounding environmental conditions, such as temperature [240,241], pH [242]], ionic strength [243], electric field [244] etc, both internal and external to the body [245]. These can result in the release of an entrapped drug in a controlled manner. Various stimuli that have been explored for modulating drug delivery are represented in Figure 6.1 [246].

Changes in pH are the most useful signal in the human body because they occur naturally in some areas of the body. For example, as the pH of the gastric condition is much lower than that of the enteric condition, a pH-sensitive hydrogel is a candidate as an intelligent device to deliver drugs to the small intestine while avoiding release in the stomach. In the pH system, the ionic group within polymer gels control polymer chain interactions. Recently, hydrogels based on chitosan have been developed for controlled drug delivery systems. The chitosan-based hydrogels, which swell and contract in response to external pH have potential uses in site-specific drug delivery systems [247,248]. Changes in temperature are another important signal in the human body. In the temperature system, the thermosensitive hydrogels swell and collapse in

response to temperature variations. Okano and Kim *et al.* [249,250] have synthesised cross-linked copolymer hydrogels, which achieved on-off regulation of drug release in response to step-wise temperature changes. As the hydrogel was swollen at high temperature, the drug could be release from it. Recently, temperature–responsive crosslinked chitosan microspheres coated with lipid for intelligent drug delivery systems have been reported [251]. The drug release rate was controlled by the phase transition temperature of the lipid. The amount of drug released increased when the temperature was raised to 42°C and decreased when the temperature was lowered to 37°C: the phase transition temperature was 41.4°C.

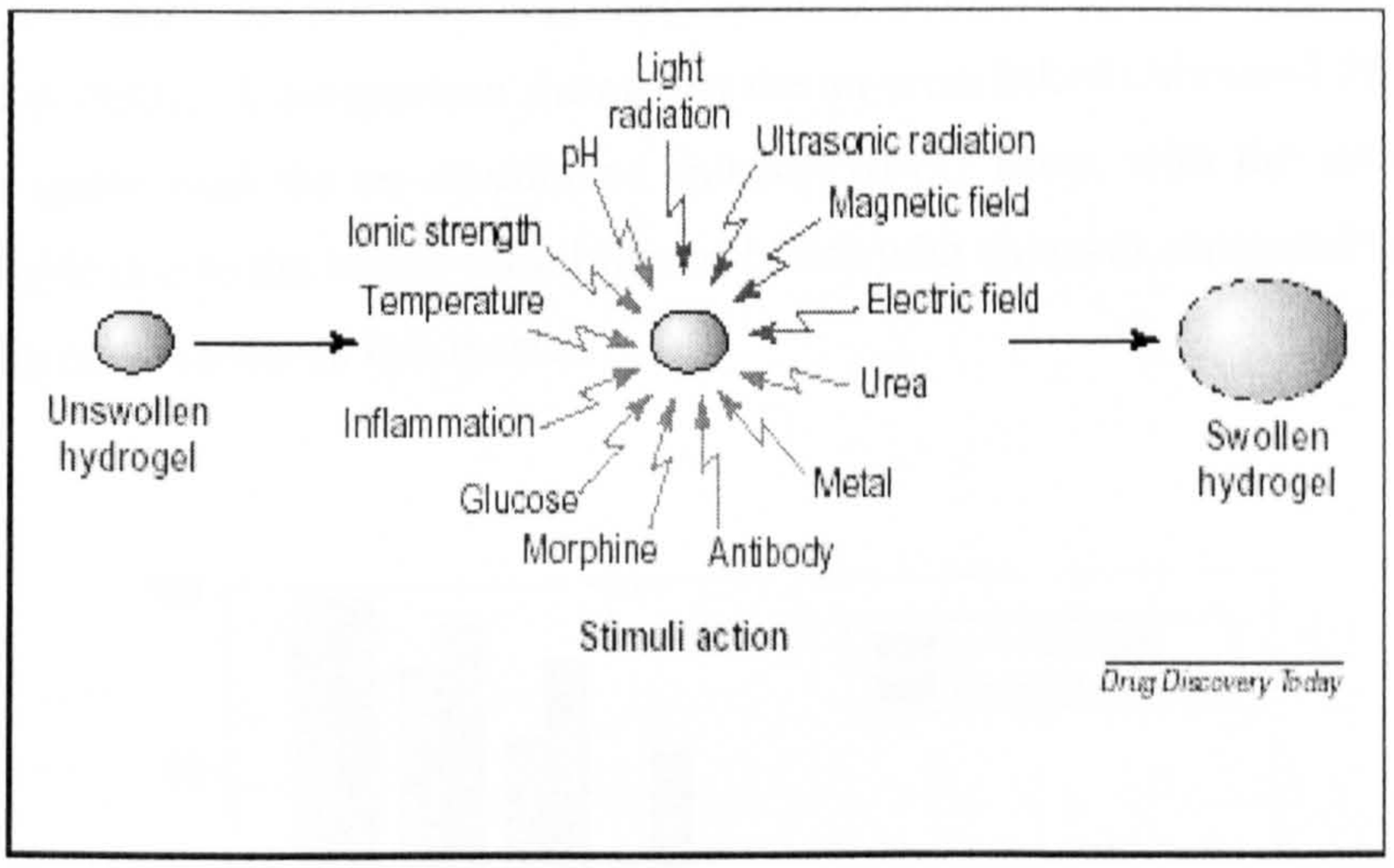

Figure 6.1 Stimuli responsive swelling of hydrogels for drug delivery

As seen from the above overview, temperature and pH are the most widely utilised triggering signals for intelligent drug delivery systems. In our research, it is proposed to study the novel chitosan/PEO film crosslinked by genipin as a material for potential biomedical uses such as in drug delivery systems. The mechanical properties of the films have been improved by blending and crosslinking methods and these have been discussed in the preceding chapters. Now, it is very important to examine the nature of the systems in their environmental conditions. In this chapter, the stability, swelling behaviour and surface properties, which respond to changes in environmental conditions, are investigated.

6.2 Stability of Crosslinked Films in Water

From the point of view of medical applications, because materials have to reside in the body for long periods of time, their mechanical properties in the wet state are more important than those in the dry state. It is known that chitosan is insoluble in water (pH 7), whereas both HPEO and LPEO are water-soluble. In order to develop optimum novel films for medical purposes, in this section, the stability of both crosslinked and un-crosslinked blend films in neutral water were investigated.

Figures 6.2.1 and 6.2.2 show the degrees of stability of the films plotted against wt.% of HPEO (LPEO). A comparison shows that the un-crosslinked chitosan/LPEO films are more stable than the un-crosslinked chitosan/HPEO films, with the latter being very unstable due to the higher miscibility of LPEO with chitosan compared to that of HPEO (reported earlier in this thesis).

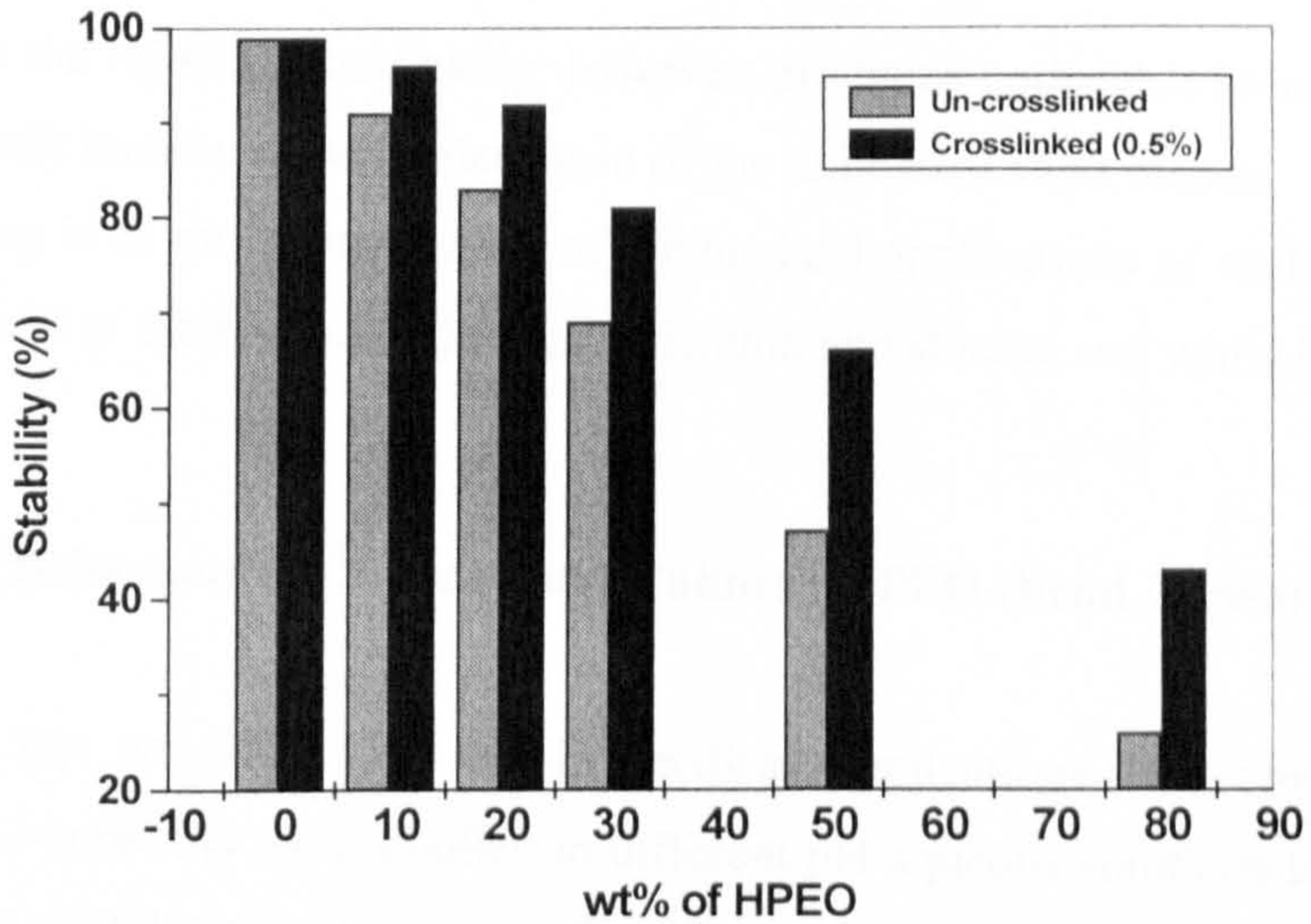

Figure 6.2.1 Comparison of the stability of cross-linked and un-cross-linked chitosan/HPEO blend films (0.5% genipin) in water at pH7

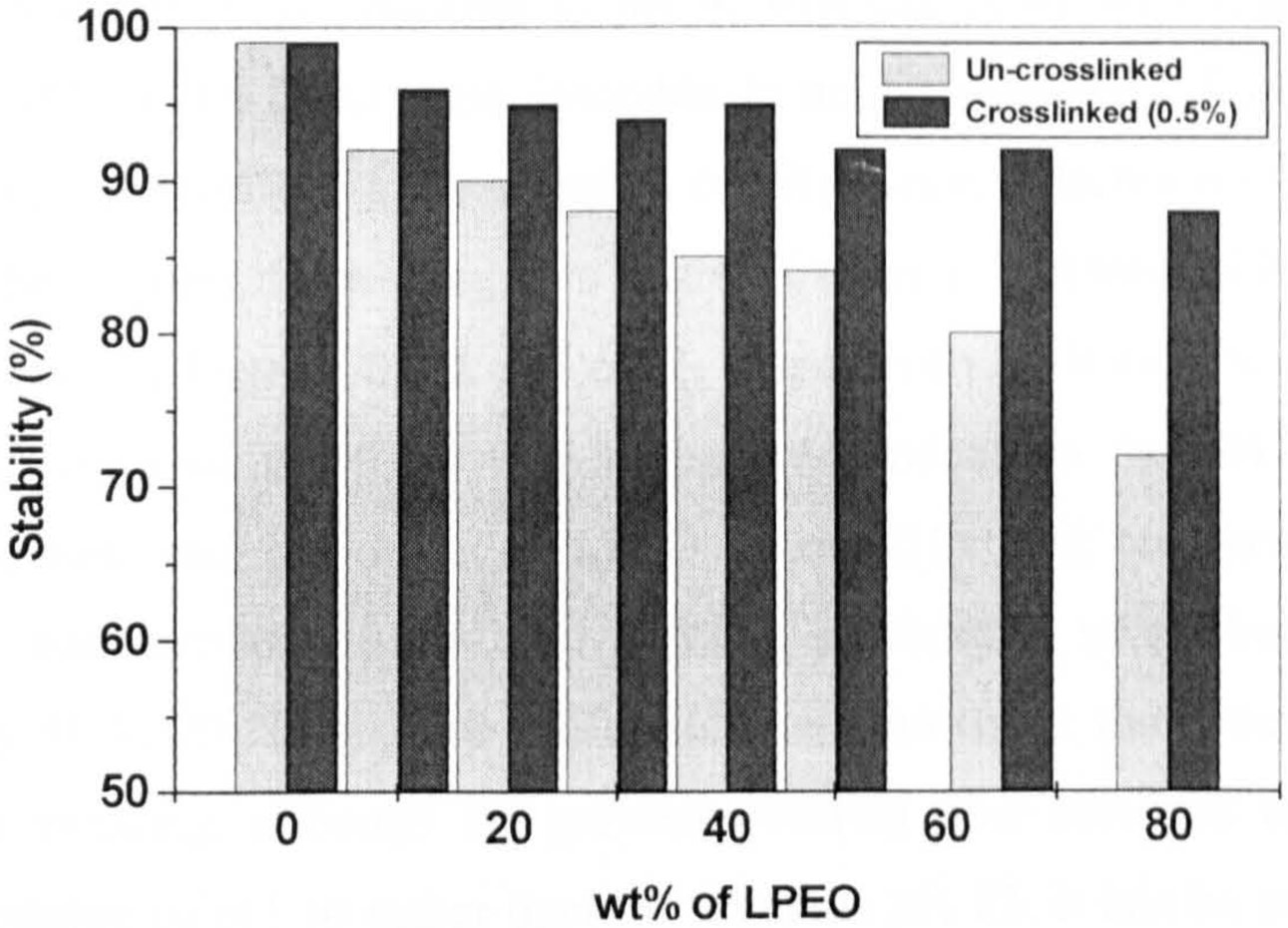

Figure 6.2.2 Comparison of the stability of cross-linked and un-cross-linked chitosan/LPEO blend films (0.5% genipin) in water at pH7.

As seen from the figures, crosslinking, however, produced noticeable increases in the stability of both blends, in particular those of the chitosan/LPEO blends. This effect of crosslinking is of much importance to the medical applications of such materials, since it is linked to their stability during fabrication and storage and while in service.

6.3. Swelling Behaviour of Chitosan and Chitosan/LPEO Blend Networks

To examine the possibility of use in medical applications, the chitosan and chitosan/LPEO networks were swollen in different pH aqueous solutions to simulate the conditions of GI (gastrointestinal) tract delivery. It is known that when the macromolecular chains of a polymer are fixed by chemical crosslinking, the swelling ability of the polymeric network is reduced.

Chitosan is soluble at pH $\leq$ 6.5. Crosslinked chitosan networks have the advantage of being insoluble in acidic and alkaline solutions and has the ability to swell in these aqueous media. Figure 6.3.1 shows that the swellability of pure chitosan films was

affected by the crosslink density. From the figure, it can be seen that films with a low crosslink density (0.26%) dissolved at pH 4, whereas films with higher crosslink densities (4.65% and 9.22%) were insoluble in acidic solutions. Furthermore, for insoluble films, an increase in the crosslink density meant a decrease in the extent of swelling. The degrees of swelling of a series of films in different pHs at 23°C and 38°C are shown in Figures 6.3.2 and 6.3.3, respectively. It can be seen that the swelling behaviour of the films was strongly dependent on the pH value of the swelling medium and the wt.% of LPEO in the film and temperature. When temperature was increased from 23°C to 38°C, swelling in pH≤7 buffer solutions increased by 50-100%. In alkaline buffer solutions, however, there were no notable increases in swelling, although the greatest swelling now occurred under the less alkaline condition of pH 10 rather than the previous pH 12. It can be concluded that the genipin-crosslinked chitosan network resulted in significantly different swelling characteristics in various pH buffer solutions. The increased swelling of the crosslinked films at pHs lower than 7 may be ascribed to the hydrolysis of the amide linkage of the crosslinked chitosan network by acid and the regeneration of amine groups in the networks [252].

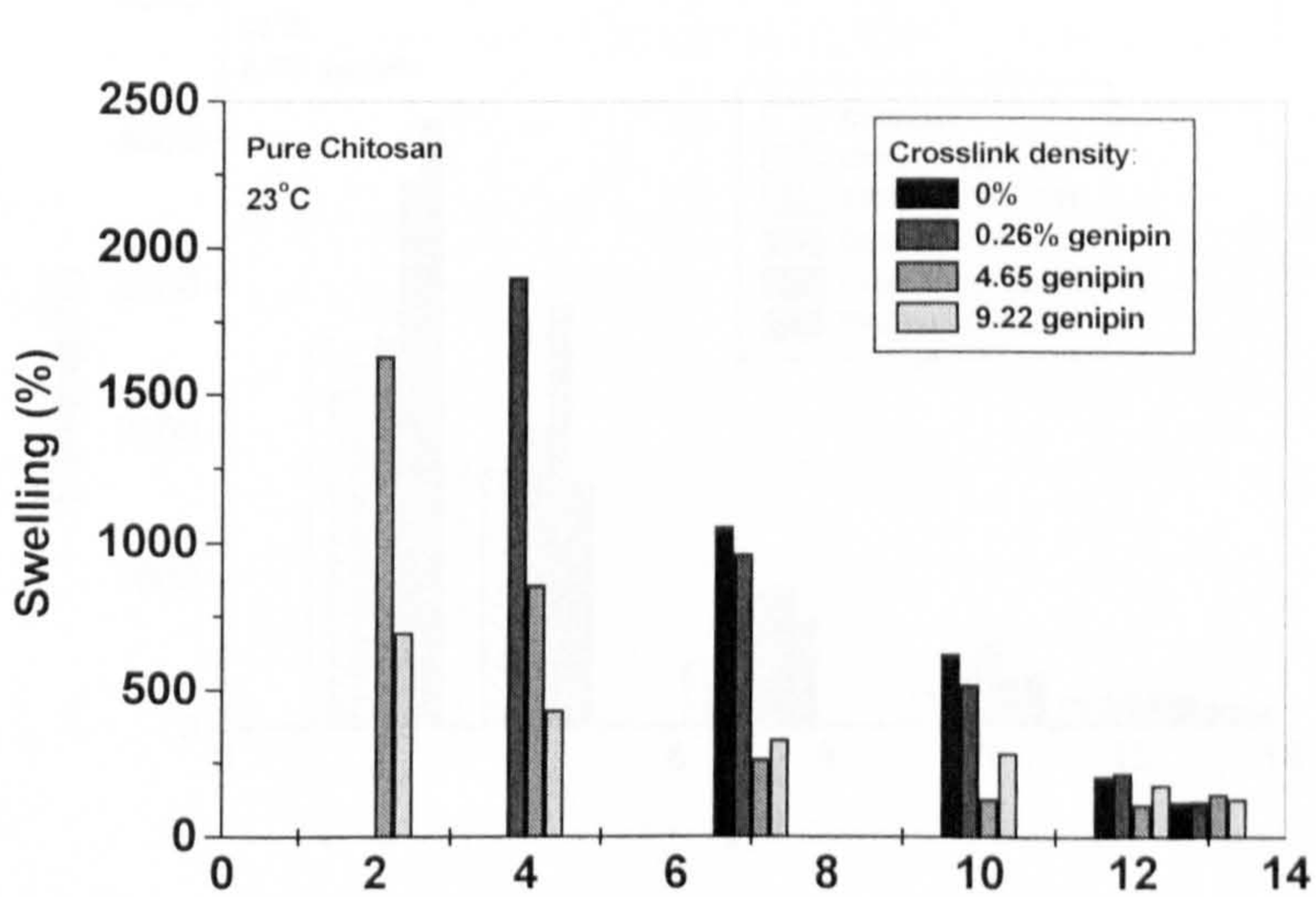

Figure 6.3.1 Swelling behaviour of chitosan films at 23°C with different crosslink density.

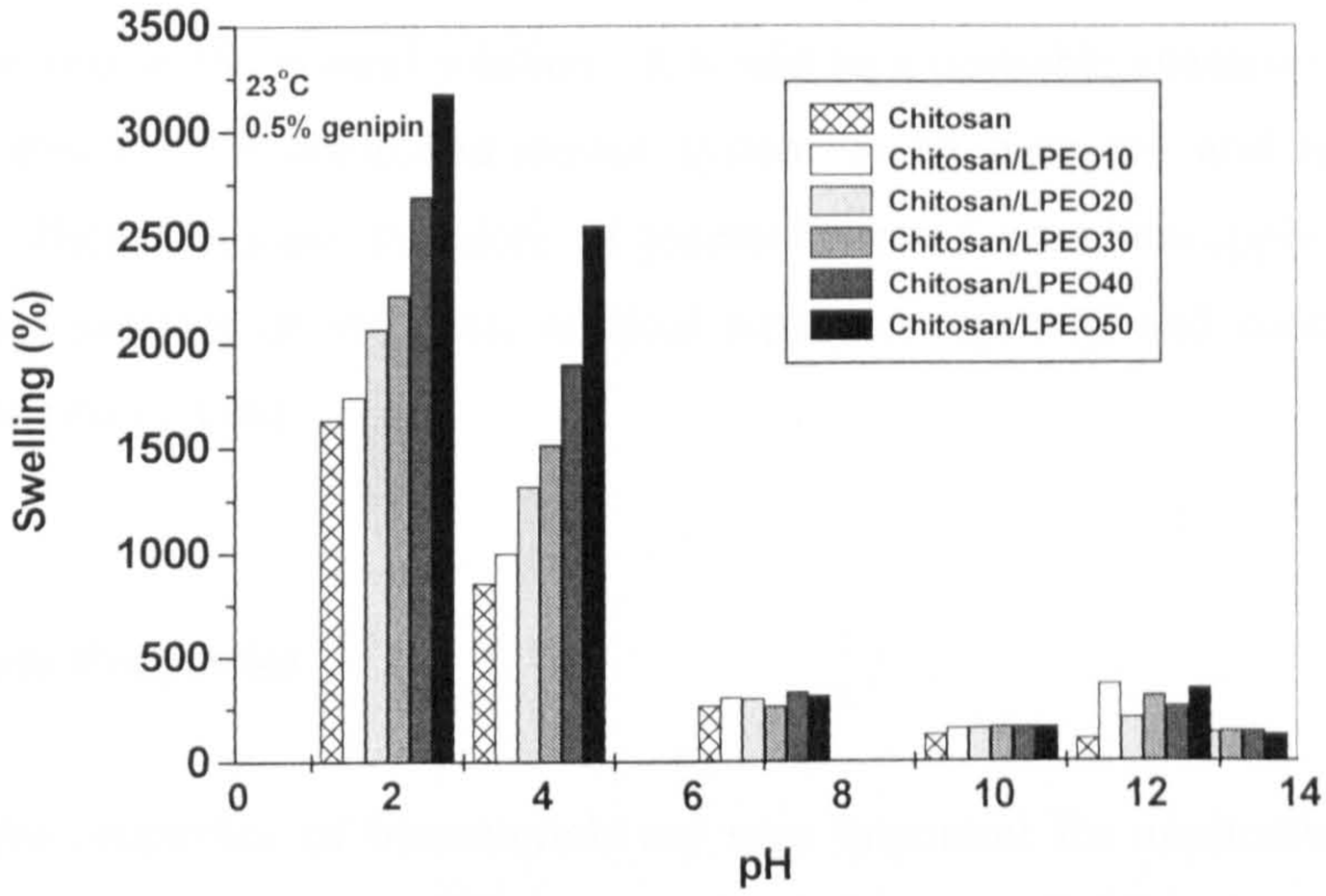

Figure 6.3.2 Swelling behaviour of cross-linked chitosan/LPEO blend films at 23°C.

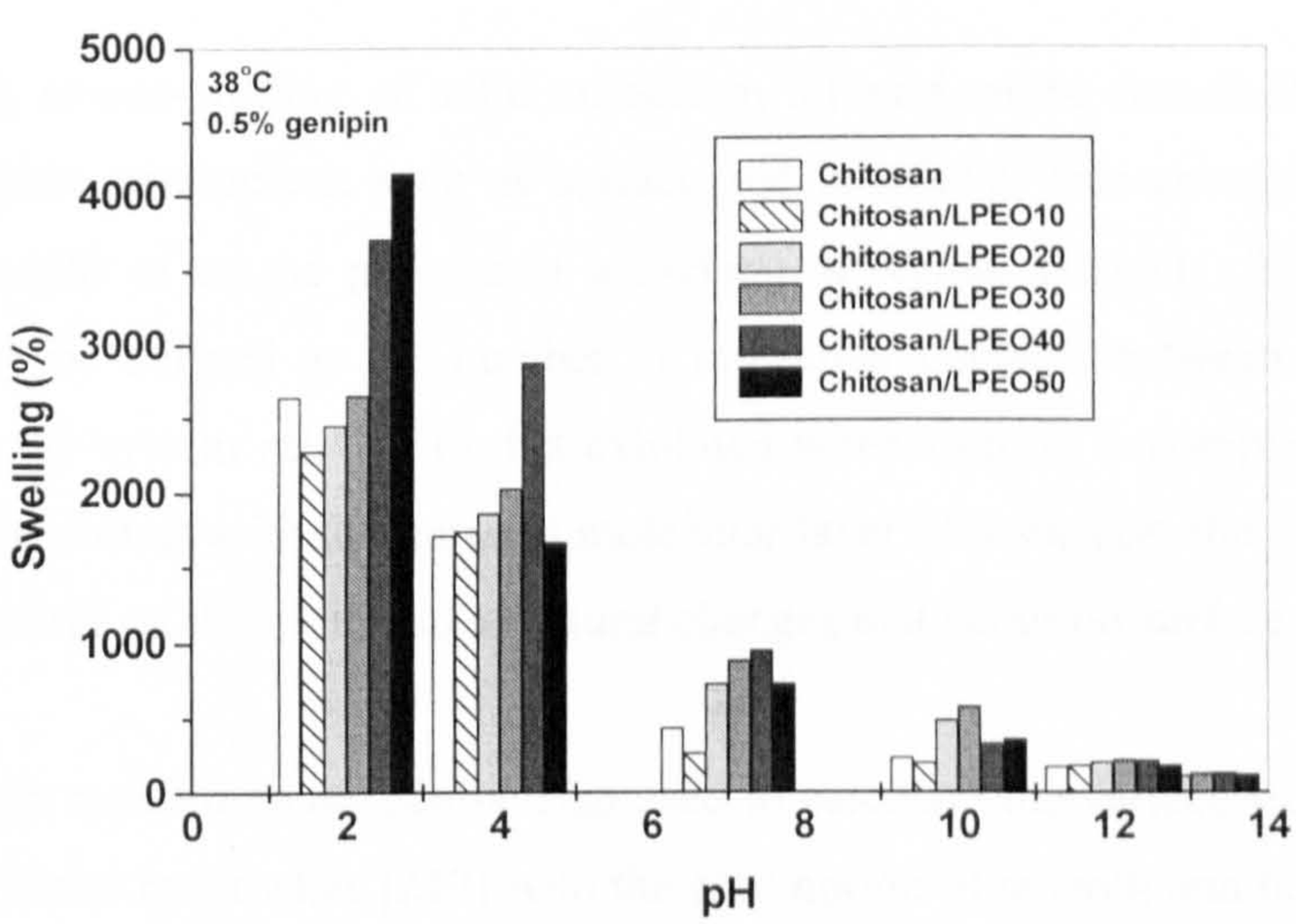

Figure 6.3.3 Swelling behaviour of cross-linked chitosan/LPEO blend films at 38°C.

Because of the fact that the amino groups reformed in the network could be protonated in acid, the equilibrium ratio of swelling of the chitosan film in acid was larger than that in the neutral solution. It would be a desirable characteristic for the swelling ability of a controlled-release system to be both pH and temperature-sensitive. These films are, therefore, of general interest for medical applications such as artificial muscles or switches, medical separation systems and controlled drug release systems [5,176].

6.4 Surface Properties

The surface properties of biomaterials are very important for applications ranging from solute separation to controlled drug delivery because of the surface interactions between the materials and the solutes [253,254]. The surface behaviour can minimise interfacial problems with host tissues and fluids. Generally, when PEO is introduced into polymer blends it contributes to their high water content and special surface properties because of their hydrophilic and biocompatible properties [62,63].

The wetting, or non-wetting, of solid surfaces by a liquid can be described in terms of thermodynamic parameters, such as surface and interfacial free energies. Wetting may be thought of as the process of achieving molecular contact. The extent of wetting may be defined as the number of molecular contacts between two phases comprising the system relative to that exhibited when wetting is complete. Since a liquid makes contact with the outmost molecular layer of a surface, the contact angle is more sensitive to chemical and structural changes that occur on surface.

Contact angle measurements can be also used to calculate the surface free energy of solid, as outlined by Fowkes [217] with the assumption of smooth and homogeneous surfaces and under conditions where a state of equilibrium with the environment has been reached. The equilibrium contact angle is a function of the surface free energies of the solid substrate and liquid in contact with it and of the free energy of the interface between the two phases [216,217]. In this section, therefore, further characterisation of the surface properties of the chitosan films and the blends for both crosslinked and un-crosslinked samples were carried out by contact angle analysis.

6.4.1 Water contact angles on the surface of the films

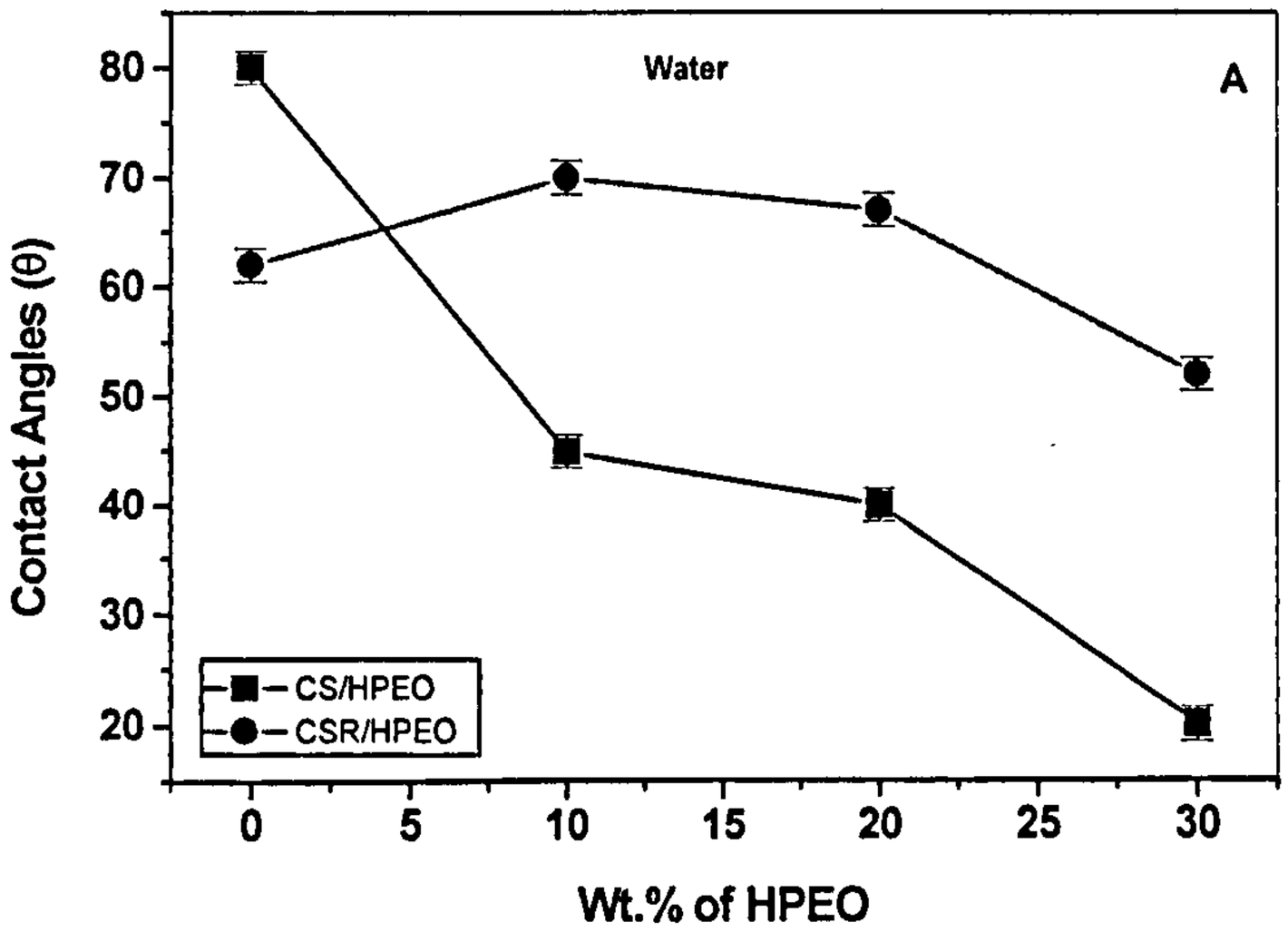

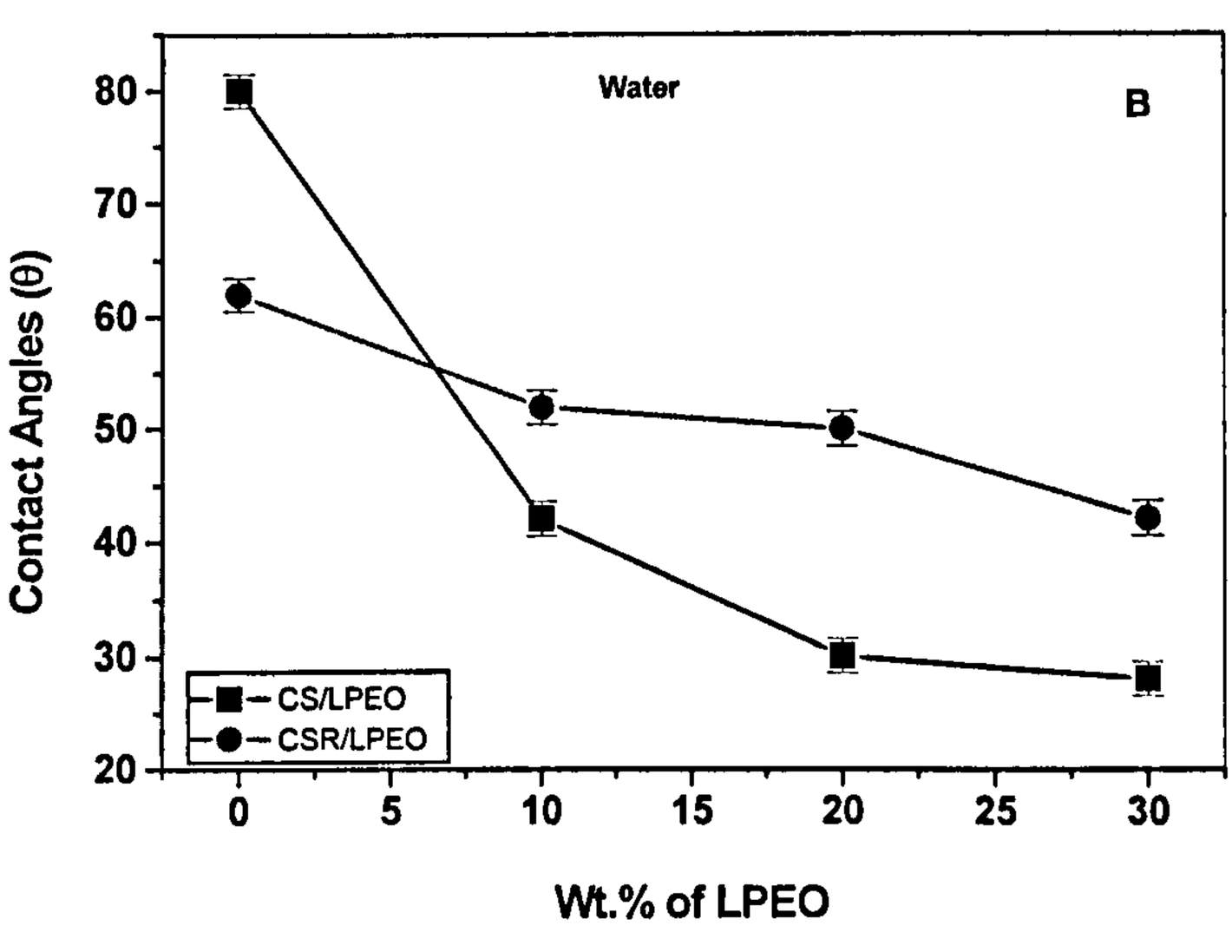

Figure 6.4.1 Contact angles for crosslinked and un-crosslinked chitosan and blend films for water: (A) CS and CS/HPEO, (B) CS and CS/LPEO

Figure 6.4.1, parts (A) and (B), shows the contact angle for water media when a drop was placed on the surface of the chitosan and the chitosan/PEO blends and their networks. The contact angles for chitosan and the network films were found to be 80° and 62°, respectively. Crosslinking resulted in an improvement in the wettability of the chitosan films. As seen from the figure, the angle decreased gradually when 10, 20 and 30wt.% of HPEO (or LPEO) were introduced into the films, and in most cases the contact angle for crosslinked blends were much higher than for the un-crosslinked ones. In order to understand the wettability of the films, the surface free energy was investigated.

Table 6.4.1 Surface free energies for diiodomethane (DIM), water and water/ethanol mixtures at 20°C [255]

Liquid	γ_L (mJ/m^2)	γ^p_L (mJ/m^2)	γ^d_L (mJ/m^2)
DIM	50.8	0	50.8
water/ethanol (100:0)	72.8	51.0	21.8
water/ethanol (70:30)	35.5	17.0	18.5
water/ethanol (50:50)	29.7	12.1	17.6

Table 6.4.2 DIM contact angles for chitosan, CS/PEO blends and networks at 25°C

Sample	Contact angle (θ°)	Sample	Contact angle (θ°)
CS	40.2 ± 2.2	CSR	40.6 ± 2.5
CS/HPEO10	44.0 ± 1.5	CSR/HPEO10	29.1 ± 6.4
CS/HPEO20	32.2 ± 2.6	CSR/HPEO20	36.6 ± 1.5
CS/HPEO30	45.1 ± 2.2	CSR/HPEO30	38.6 ± 2.5
CS/LPEO10	40.6 ± 2.7	CSR/LPEO10	44.8 ± 1.5
CS/LPEO20	34.0 ± 2.4	CSR/LPEO20	36.8 ± 1.2
CS/LPEO30	38.4 ± 3.7	CSR/LPEO30	35.8 ± 2.6

In this experiment, two types of liquid with known surface energy, namely triply distilled water and diiodomethane (DIM), which represent polar and non-polar liquid media, were used. DIM was chosen as a reference medium and its contact angles on the surface of uncrosslinked and crosslinked chitosan and chitosan/PEO films were measured as shown in Table 6.4.2. The surface energies of triply distilled water and DIM, at 20°C, are given in Table 6.4.1 [255]. The surface free energy of a film and its dispersion and polar components can be estimated from the contact angle of a liquid by means of Equation 3.3.9-6. The surface free energy (γ) with its respective dispersion (γ_s^d) and polar (γ_s^p) components of un-crosslinked and crosslinked chitosan and chitosan/PEO blendes are listed in Table 6.4.3.

Table 6.4.3 Water contact angles and surface free energies of crosslinked and uncrosslinked chitosan and CS/LPEO (or CS/LPEO) blends and networks

Sample	**Contact angle** (θ^o)	γ^d_s (mJm^{-2})	γ^p_s (mJm^{-2})	γ_s (mJm^{-2})
CS	80.2	39.3	3.5	42.8
CS/HPEO 10	45.2	37.6	21.9	59.5
CS/HPEO 20	40.1	43.4	22.9	66.3
CS/HPEO 30	20.3	37.1	34.8	71.9
CS/LPEO 10	42.1	39.2	22.9	62.1
CS/LPEO 20	30.4	42.4	27.6	70.0
CS/LPEO 30	28.1	40.3	29.6	69.9
CSR	62.0	39.2	11.5	50.7
CSR/HPEO 10	70.0	43.7	6.3	50.0
CSR/HPEO 20	68.1	41.2	7.8	49.0
CSR/HPEO 30	52.2	40.2	16.7	56.9
CSR/LPEO 10	52.4	37.1	18.1	55.2
CSR/LPEO 20	50.6	41.1	17.4	58.5
CSR/LPEO 30	42.3	41.6	21.7	63.3

*The average experimental errors: contact angle ± 1.5°, surface energy: ± 1.2 mJm^{-2}

The effect of crosslinking by genipin on the contact angle and surface free energy of chitosan films can be clearly seen in a comparison between the data in Table 6.4.3. The decline of contact angle for chitosan film indicates that the hydrophilicity increased as a result of crosslinking. This finding was confirmed by the calculation of surface free energy. The surface free energy of a crosslinked chitosan film was 50.7mJ/m^2, which was significantly greater than that of an uncrosslinked chitosan film (42.8mJ/m^2). This means that the surface of the crosslinked chitosan film has better wetting capability compared with the surface of the un-crosslinked chitosan film. The increases in surface energy were due to increases in the polar component (γ_s^p) of the film, rather than its dispersion (γ_s^d) component.

Figure 6.4.2, parts (A) and (B), shows the surface free energies of un-crosslinked and crosslinked chitosan/HPEO blend films and chitosan/LPEO blend films. It can be seen from both figures that as the wt% of PEO increased, the surface free energy also increased. Also, crosslinking the blends by genipin resulted in decreases in the surface free energy. As Table 6.4.3 indicates, the changes in the dispersion energy were smaller when 10, 20 and 30 wt% of HPEO were introduced into chitosan. In consideration of the margin of experimental error, it can be ignored such changes. However, for the CS/HPEO20 blend film, the dispersion energy increased by only about 4 mJm^{-2}. With increasing wt.% of HPEO, the polar energy had a significant increase from 3.5 (CS) to 34.8mJm^{-1} (CS/HPEO30). It is, therefore, clear that increases in the surface energy must be principally attributed to increases in the polar energy. From experimental data, it was also observed that crosslinking with genipin mainly resulted in changes in the polar energy component. For uncrosslinked and crosslinked chitosan/LPEO blend films, similar results were obtained. However, there was a difference in that a much greater impact on the surface free energy of the films was induced by crosslinking when the PEO was of a higher molecular weight.

The polarity of both the liquid as well as the solid substrate is a factor to be considered in contact angle analysis. If both the liquid and solid are polar, then interactions will be formed at the interface between them, which means that there is better adhesion at the interface. This will result in a smaller contact angle being measured, which is due to the better wettability, or spreading, of the polar liquid on the polar solid substrate. On the other hand, if one of the liquids or solids is polar and

the other is non-polar, then interactions will not exist at the interface between them, and, therefore, a larger contact angle will be measured.

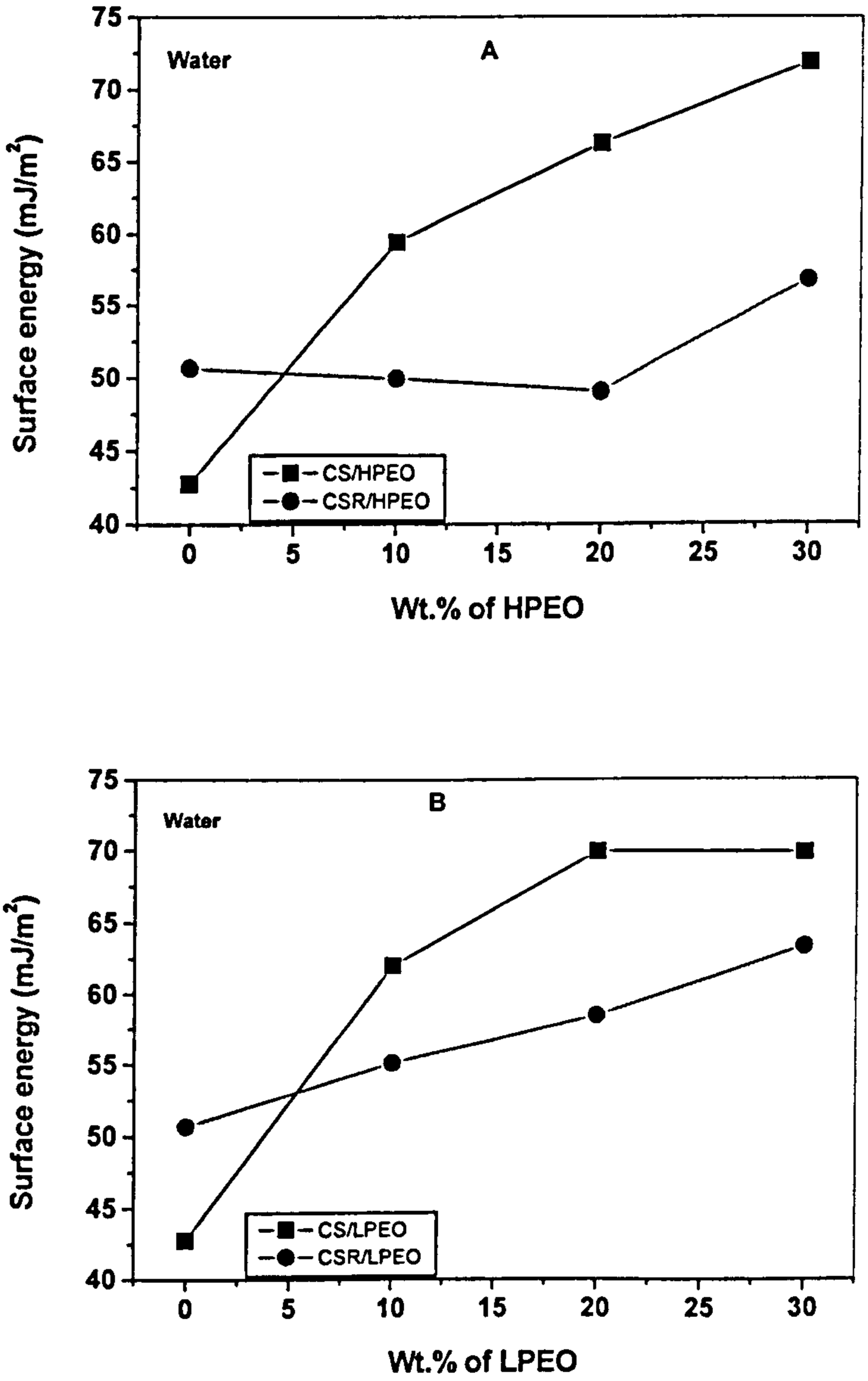

Figure 6.4.2 Surface energy of un-crosslinked and crosslinked CS/PEO blend films: (A) for CS/HPEO; (B) for CS/LPEO

PEO is a polar polymer and its chemical structure is shown in Section 2.3.1 (Chapter 2). When water, a polar liquid, interacts with PEO, interactions will be formed between -H atoms in water and -O- groups in PEO. The interactions formed between the liquid and solid substrate are stronger bonds than van der Waals forces. There is, therefore, more attraction (or "adhesion") between water and PEO, which is manifested as surface free energy.

The lower surface free energy of the uncrosslinked chitosan films can be understood from its chemical structure and soluble nature. When the glucosamine residues are in the free amine form, these structures are strongly involved in the formation of three-dimensional networks by hydrogen bonding, hydrophobic and van de Waals interactions [30]. Under acid conditions, the amino groups of chitosan are protonated, and solubility of chitosan which is dependent on the nature of the anion is involved. At neutral or basic pH, chitosan contains free amino groups (NH_2), which are neutral and so it is insoluble in water. In this case, the surface of an uncrosslinked chitosan film is, thus, more hydrophobic.

However, as evident from the chemical structure of genipin (Figure 2.5.2 shown in Chapter 2), genipin contains the -COH group, which may form hydrogen bonds with water molecules. This may make the surface of crosslinked chitosan films more hydrophilic than that of the un-crosslinked ones. These –COH groups in genipin have relatively high polarity, which may significantly increase the polar component (γ_L^p) of the surface free energy of the crosslinked chitosan films.

The morphology of materials is another factor to be considered in contact angle measurements [255]. The surface free energy of a semi-crystalline polymer should vary with its crystallinity. The crystalline density is usually higher than the amorphous density. Therefore, the crystalline surface tension is usually much higher than the amorphous tension [255]. The homogeneity of a material has a significant effect on its surface free energy when it is in contact with liquid. Blends of compatible and incompatible polymers show different surface interactions [256]. The surface interactions of incompatible blends are further complicated by their phase structure [256]. Surface interaction of blends of poly(ethylene oxide)/poly(propylene oxide) and of poly(propylene oxide) and polyepichlorohydrin were studied by Rastogi

[257]. The surface energy decreases with increasing molecular weight, apparently because of increased incompatibility, i.e. phase separation.

As discussed in Chapter 4 on the morphology of crosslinked chitosan/PEO blend films, crosslinking with genipin leads to phase separation. Phase separation results in the film becoming less homogenous. Furthermore, the higher the PEO content the more significant the phase separation and the less homogenous the film. Hence, crosslinked and uncrosslinked films have different wetting properties. The decline, after crosslinking, in the surface free energy for the crosslinked chitosan/HPEO and chitosan/LPEO films, as shown in Figures 6.4.2, can, therefore, be explained here. Additionally, a greater change in the surface free energy will be observed where the molecular weight is greater [255].

On top of this, from the above discussion, it is clear that the addition of PEO and crosslinking by genipin led to the existence of polar forces between the film and water, and, therefore, increases in the polar energy contributed to increases in the surface energy.

6.4.2 Contact angles of water/ethanol mixtures on the surface of the films

In recent years, studies on anti-cancer drugs, anti-AIDS drugs [4,38], gene therapies and anti-sense drugs have made much progress. Generally speaking, most drugs dissolve in water or water/ethanol mixtures, which are high performance solvents in pharmacy applications. However, it has been reported that some of the anti-cancer drugs, such as Taxol®, are insoluble in water, but soluble in ethanol [4,40]. Controlled drug-release is particularly important to the success of such a drug, given its highly sensitive activities. In order to develop the novel chitosan/PEO films as anti-cancer drug carriers, the surface properties of the films with water/ethanol mixtures were studied.

Figures 6.4.3 and 6.4.4, parts (A) and (B), show the contact angles for all of the chitosan and chitosan/HPEO (LPEO) blends and networks in two water/ethanol mixtures (70%/30% and 50%/50%). As seen, the contact angles of the crosslinked chitosan and blends exhibited higher values than that of the un-crosslinked films.

Similarly, the contact angle of the blend film deceased gradually when 10, 20 and 30 wt.% of HPEO (or LPEO) were incorporated. The lower contact angles corresponded well to the fact that HPEO (or LPEO) has high chain mobility and hydrophilicity.

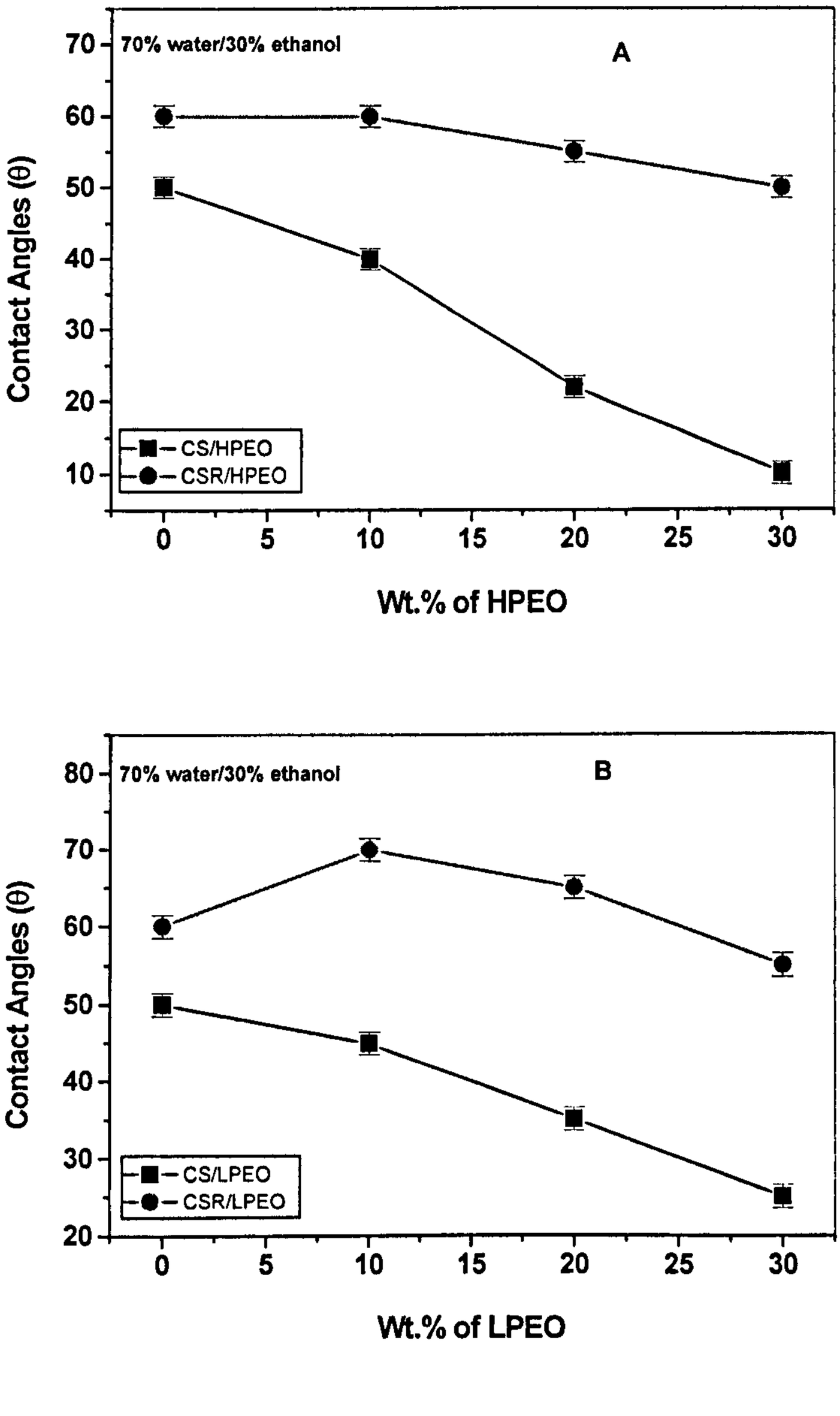

Figure 6.4.3 Contact angles of the cross-linked and un-cross-linked chitosan and CS/PEO blend films with a mixture of 70% water/30% ethanol: (A) for CS/HPEO; (B) for CS/LPEO

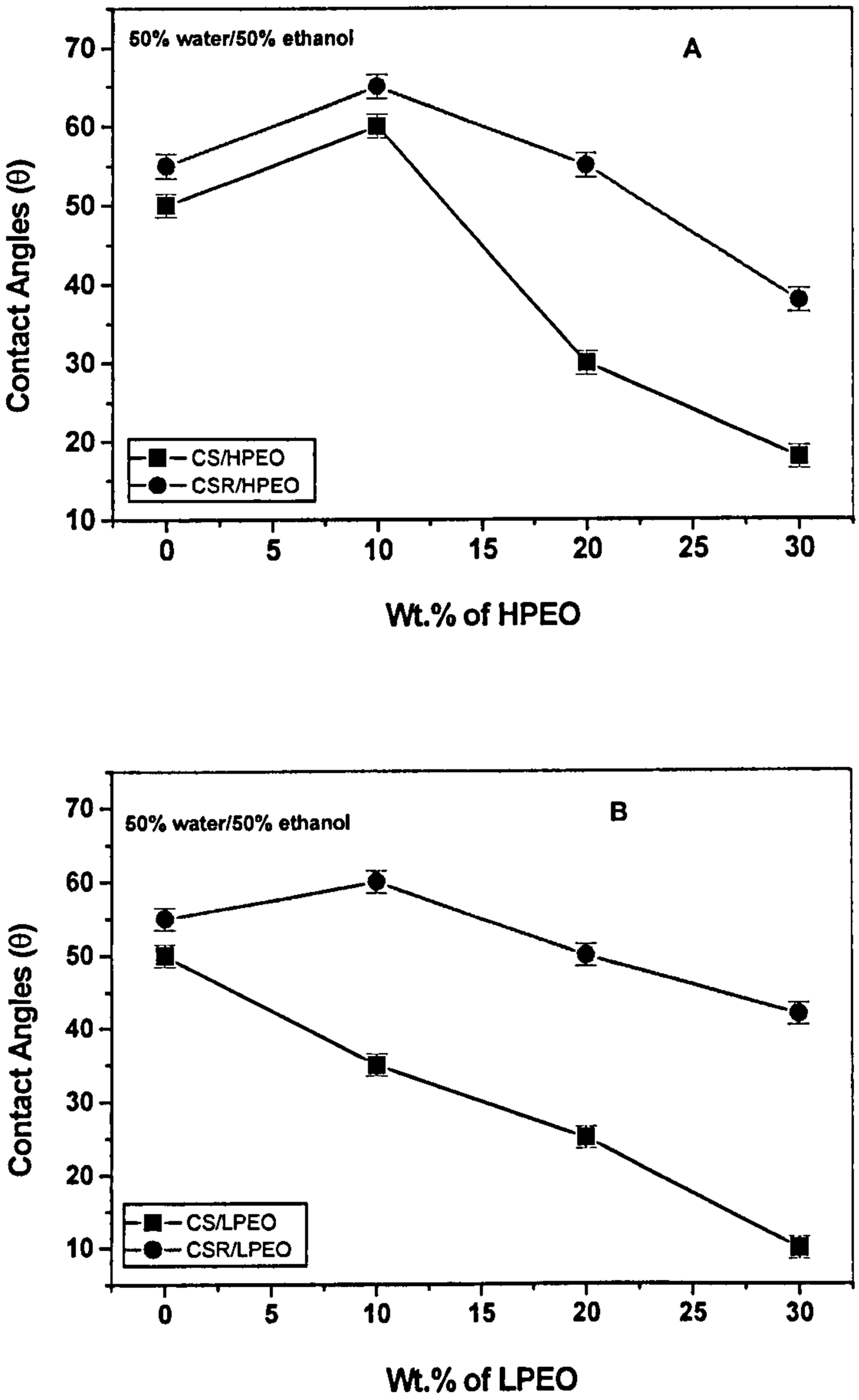

Figure 6.4.4 Contact angles of the cross-linked and un-cross-linked chitosan and CS/PEO blend films with a mixture of 50% water/50% ethanol: (A) for CS/HPEO; (B) for CS/LPEO

It can be observed from a comparison between Figures 6.4.1, 6.4.3 and 6.4.4 that a slight, but gradual, decrease in contact angles took place when water was diluted with 30 and 50% of ethanol. In aiding the understanding of the surface properties of the

blends and networks, the surface free energy with its respective dispersion and polar components were analysed.

The values of the surface free energies for the water/ethanol mixtures (70:30, 50:50) at 20°C are given in Table 6.4.1. From the contact angle measurements, the surface free energies of the films were calculated with DIM as a reference liquid. All results are listed in Tables 6.4.4 and 6.4.5.

Table 6.4.4 Contact angles and surface free energies of the films with the 70%water/30%ethanol mixture

Sample	Contact angle (θ^o)	γ^d_s (mJm^{-2})	γ^p_s (mJm^{-2})	γ_s (mJm^{-2})
CS	50.2	39.3	0.3	39.6
CS/HPEO 10	40.4	37.6	1.5	39.1
CS/HPEO 20	22.6	43.4	2.0	45.4
CS/HPEO 30	10.1	37.1	4.8	41.9
CS/LPEO 10	45.0	39.2	0.7	39.9
CS/LPEO 20	35.3	42.4	1.1	43.5
CS/LPEO 30	25.2	40.3	2.5	42.8
CSR	60.4	39.2	0.0	39.2
CSR/HPEO 10	60.0	43.7	0.2	43.9
CSR/HPEO 20	55.1	41.2	0.0	41.2
CSR/HPEO 30	50.6	40.2	0.2	40.4
CSR/LPEO 10	70.8	37.1	0.3	37.4
CSR/LPEO 20	60.4	41.1	0.1	41.2
CSR/LPEO 30	55.2	41.6	0.0	41.6

*The average experimental errors: contact angle ± 1.5°, surface energy: ± 1.2mJm^{-2}.

Table 6.4.5 Contact angles and surface free energies of the films with the 50%water/50%ethanol mixture

Sample	Contact angle (θ^o)	γ^d_s (mJm^{-2})	γ^p_s (mJm^{-2})	γ_s (mJm^{-2})
CS	50.5	39.3	0.2	39.5
CS/HPEO 10	60.3	37.6	1.0	38.6
CS/HPEO 20	30.2	43.4	0.0	43.4
CS/HPEO 30	18.0	37.1	1.0	38.1
CS/LPEO 10	35.4	39.2	0.1	39.3
CS/LPEO 20	25.4	42.4	0.1	42.5
CS/LPEO 30	10.2	40.3	0.7	41.0
CSR	55.0	39.2	0.7	39.9
CSR/HPEO 10	65.6	43.7	3.6	47.3
CSR/HPEO 20	55.3	41.2	1.1	42.3
CSR/HPEO 30	38.4	40.2	0.0	40.2
CSR/LPEO 10	60.6	37.1	0.9	38.0
CSR/LPEO 20	50.2	41.1	0.5	41.6
CSR/LPEO 30	42.3	41.6	0.1	41.7

*The average experimental errors: contact angle ± 1.5°, surface energy: ± 1.2mJm^{-2}

The results show that the polar component of the surface energy has a greater influence when water/ethanol mixtures were used. As Table 6.4.5 indicates, the polar energy induced by 50%water/50%ethanol was much smaller. In consideration of the margin of experimental error, we can ignore such figures. It is, therefore, clear that the surface free energy can be principally attributed to the dispersion energy. This fact of surface behaviour of the films is very important in developing drug delivery systems. As a carrier of anti-cancer drug, the surface of the carrier has to have lower polarity, and moreover, to achieve controlled drug-release there must be no interactions between the drug and the carrier. These surface properties can meet the delivery requirements for anti-cancer drugs. The issue that has to be addressed now is the reasons why water/ethanol mixtures bring about a significant difference in the surface free energy when compared to using water.

Ethanol is a very common polar solvent, but its polarity is much less than water. The chemical structure of ethanol is C_2H_5OH.

The effect of the ethanol content in the mixture on the surface free energy of the films may come from two sides. Firstly, ethanol influences the film surface properties by changing the properties of the solvent. The increase of ethanol content reduces the average interaction between molecules of the solvent, which leads to a decrease in the surface free energy of solvent mixture, as indicated in Table 6.4.1 (the surface energies at water/ethanol volume ratios of 100:0, 70:30 and 50:50 are 72.8, 35.5 and 29.7mJm^{-2}). This effect must induce a reduction of surface tension in the system. Hence, the surface free energy of the film tends to decrease as the ethanol content in mixture increases [257,258]. Secondly, where there are two or more surface active compounds in a solution, mixed absorption films are generated [257,258]. These parameters, which determine their surface behaviours are dependent both on the solvent (chemical structure, polarity etc.) and on the solid. Ethanol as a kind of surface-active liquid absorbs at the air/solvent interface and competes with the solid for the position of surface layer. Moreover, with increases in the ethanol content, the hydrophilicity of the films is reduced, inducing the weaker absorption tendency of the films. Both of them make the absorption of the film in water/ethanol mixtures lower [259]. From the above discussions, it is clear that the lower surface energy of the films in water/ethanol mixtures is due to the lower polarity of ethanol in comparison to water.

6.5 Conclusions

With the use of crosslinking, there were noticeable increases in the stability of the chitosan/HPEO (or LPEO) blends. The swelling behaviour of the films exhibited pH and temperature-dependent characteristics. However, the swelling extent can be regulated by the crosslink density.

In terms of the wettability of chitosan, chitosan/PEO blends and networks, with the one exception of crosslinked chitosan in 100% water, the crosslinked chitosan/PEO blends of both molecular weights were more hydrophobic than the uncrosslinked

ones. Although crosslinking resulted in decreases in the wettability of the films surfaces in some cases, this unwanted effect was negated to some extent by the addition of PEO. The addition of PEO and crosslinking by genipin led to the existence of polar forces between the film and water, and therefore, the increases in the surface free energy were mainly contributed by increases in the polar component. However, the reduced surface free energy for the crosslinked chitosan/HPEO and chitosan/LPEO films resulted from the phase separation in the system. Also, a greater change in the surface free energy was observed where the molecular weight was greater.

In water/ethanol mixtures, the surface free energy of the films is lower than that in water due to the lower hydrophilicity of ethanol.

These novel films are sensitive to the environment and the surface properties of chitosan/PEO blends and networks in water/ethanol mixtures have provided some particularly important information regarding their potential success as drug carriers.

CHAPTER 7

Temperature-Dependence of Crosslinking Reaction

7.1 Introduction

The crosslinking mechanism of chitosan with genipin has been investigated by Sung and co-workers [252]. From a series of spectra analysis, it was confirmed that genipin could go through a ring-opening reaction to form an intermediate aldehyde group due to nucleophilic attack by the amino group in chitosan. A heterocyclic compound of genipin-crosslinked chitosan was formed by a nucleophilic attack by the amino group on the olefinic carbon atom at C-3 of deoxyloganin aglycone, followed by the opening of the dihydropyran ring and attack by the secondary amine group on the intermediate aldehyde group. Additionally, secondary amide linkages could be established in the genipin-crosslinked chitosan network by the reaction of the ester group of genipin with the amino groups of chitosan. These bifunctional linkages of genipin with the amino group of chitosan lead to the formation of crosslinked networks. Genipin reacted with a nucleophilic reagent such as chitosan could further go through polymerisation to form an oligomer-bridge in the crosslinked networks. The suggested schematic [252] of the reaction mechanism for the synthesis of chitosan network using genipin as a crosslinker is given in Figure 7.1.1.

Although this figure gives a clear picture of the reaction mechanism, the details of the crosslinking process in relation to the passage of time and changes in temperature are still unknown. Differences in the crosslinking temperature may affect crosslinking characteristics and result in different mechanical properties of the networks. From the studies of the mechanical properties of crosslinked chitosan films (see Chapter 5), it was found that the mechanical properties, such as tensile strength and elongation at break, were influenced by the crosslinking temperature. In particular, when the temperature is at about 25°C, the films have larger elongation at break and lower tensile strength compared with those at crosslinking temperatures of 40°C and 60°C. This chapter facilitates the understanding of the effect of crosslinking temperature on the mechanical properties of the films by investigating the reaction process of

crosslinking networks at different temperatures by means of FT-IR and UV spectroscopies.

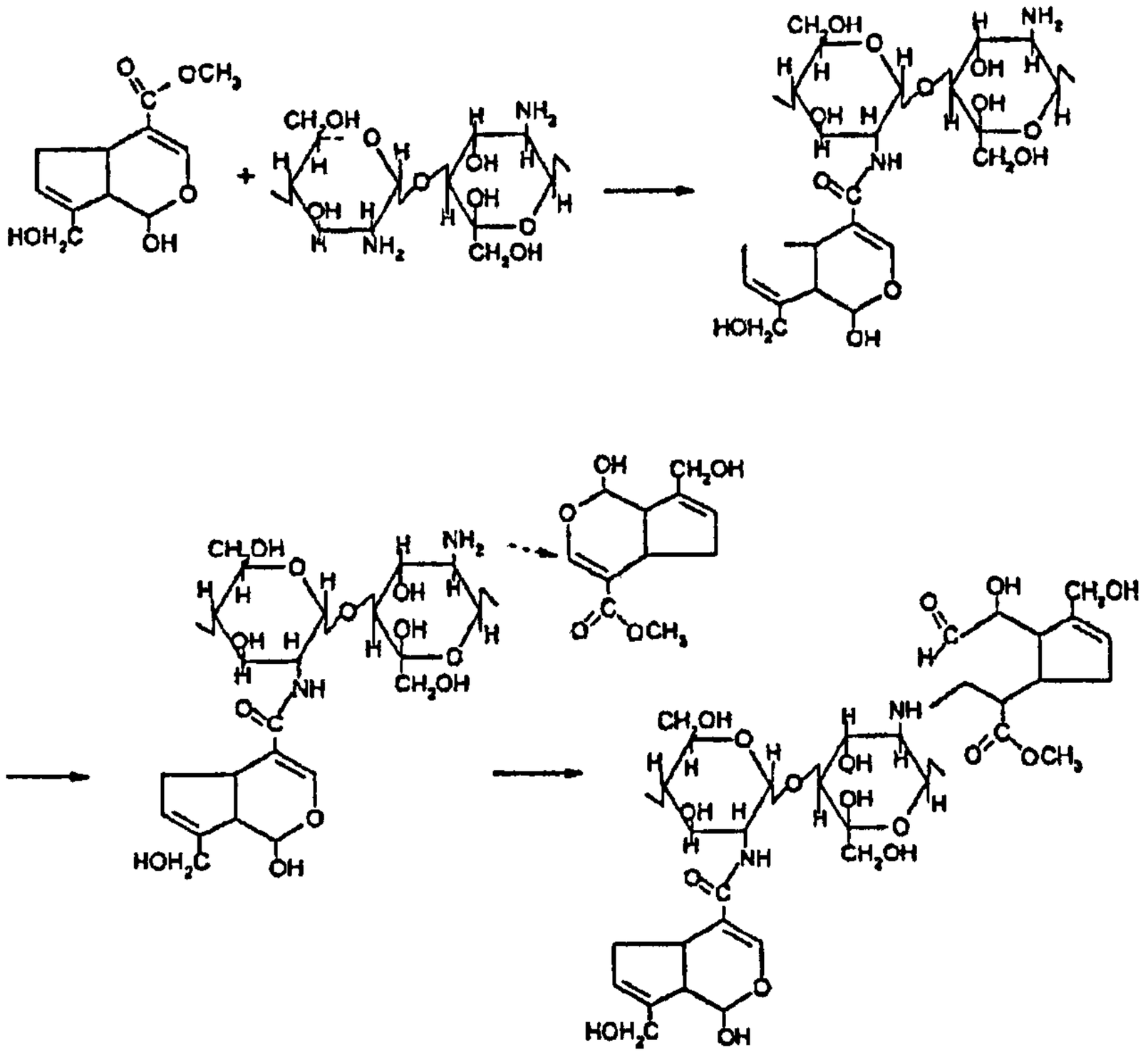

Figure 7.1.1 Schematic of the reaction mechanism for the synthesis of genipin crosslinked chitosan [252]

7.2 FT-IR Study

Figure 7.2.1 displays the FT-IR spectra of crosslinked chitosan with progress of time. The reaction temperature was 25°C. From Figure 7.2.1(A), it can be seen that the broad band of the hydroxyl group at 3400cm^{-1}, one of the characteristics of chitosan, became narrower with time. This indicates that the crosslinking reaction occurred after the addition of genipin, where the initial broadness is attributable to the abundance of hydroxyl interaction sites. As crosslinking proceeded, there was a more uptake of these interaction sites and the width of the absorbance band was thus reduced.

For the amide region shown in Figure 7.2.1(B), it was found that the intensities of the carbonyl stretching peak at 1645cm^{-1} (amide I) and 1560cm^{-1} (amide II), representing the N-acetyl functional group of chitosan, decreased with time. This suggests an increase in the crosslinking activity of the amide group in chitosan. As the reaction time exceeded 48 hours, the amide band disappeared relative to the absorbance band at 1560cm^{-1}, and the absorbance band at 1645cm^{-1} appeared as a shoulder. This again suggests that most of the free amino groups in chitosan had reacted.

Figure 7.2.2, parts (A) and (B), displays the FT-IR spectra of crosslinked chitosan with genipin at a reaction temperature of 40°C. Similar FT-IR spectra were observed for the hydroxyl band at 3400cm^{-1} and in particular the broad band became narrower with time. However, for the amide region the absorbance bands at 1645cm^{-1} and 1560cm^{-1} decreased gradually over 10 hours. Then they appeared again and the absorbance band at 1560cm^{-1} acquired a strong shoulder after 48 hours reaction.

Figure 7.2.3, parts (A) and (B), shows the FT-IR spectra of chitosan crosslinking by genipin at a reaction temperature of 60°C. There is very little difference between these results and those shown in Figures 7.2.1 and 7.2.2. Figure 7.2.4, parts (A) and (B), shows the spectra of chitosan when crosslinking time was 10 and 48 hours at different crosslinking temperatures. These results indicate the reaction characteristics were quite different due to the effect of temperature. The relationship between the mechanical properties of crosslinked chitosan films and different temperatures for crosslinking cannot, at the moment, be determined on the basis of the FT-IR study. We, therefore, have to turn to UV spectroscopy study.

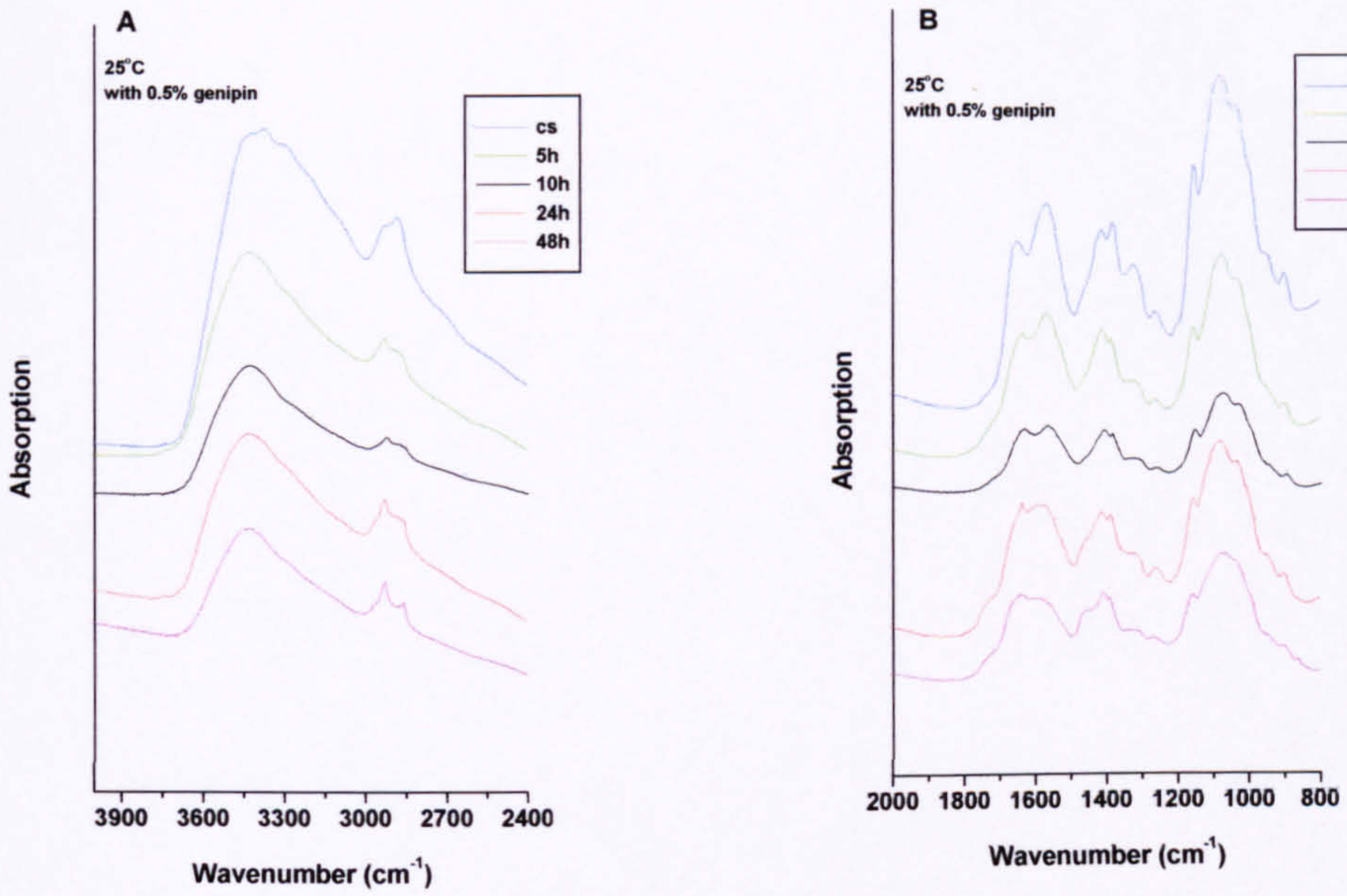

Figure 7.2.1 FT-IR spectra showing the hydroxyl region (A) and the amide region (B) of chitosan crosslinked with genipin at 25°C as a function of time

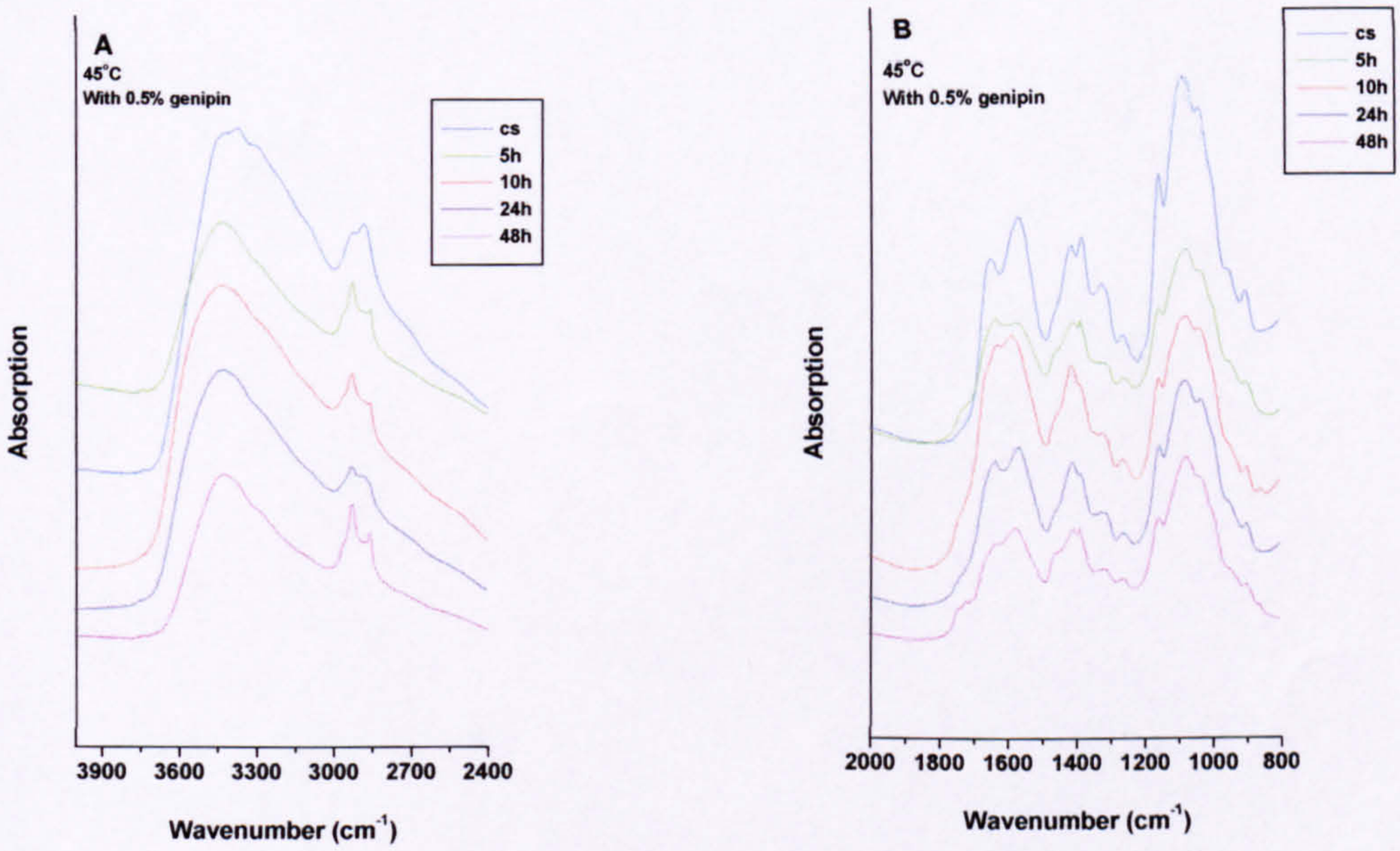

Figure 7.2.2 FT-IR spectra showing the hydroxyl region (A) and the amide region (B) of chitosan crosslinked with genipin at 45°C as function of time.

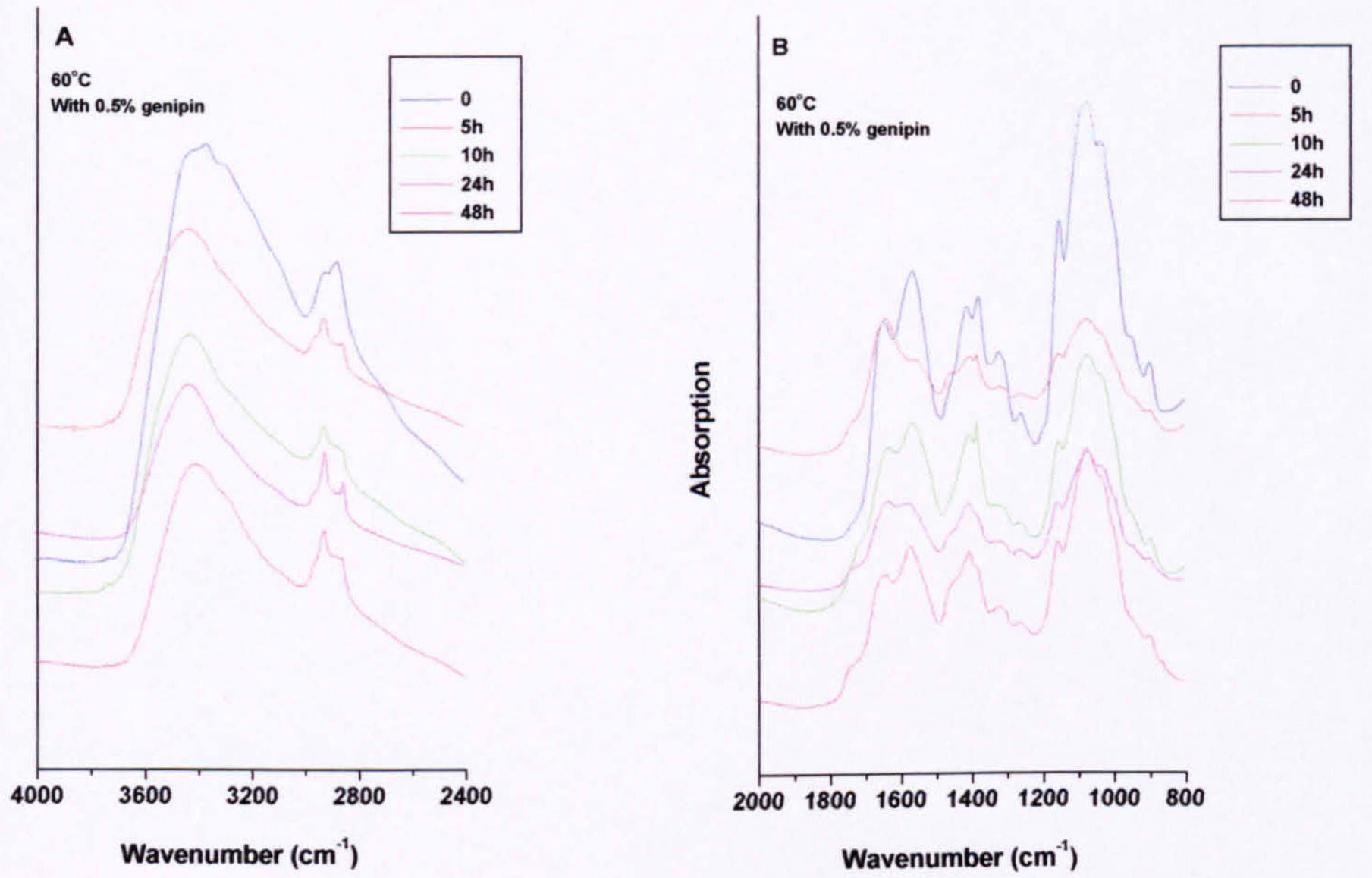

Figure 7.2.3 FT-IR spectra showing the hydroxyl region (A) and the amide region (B) of chitosan, crosslinked with genipin at 60°C as function of time.

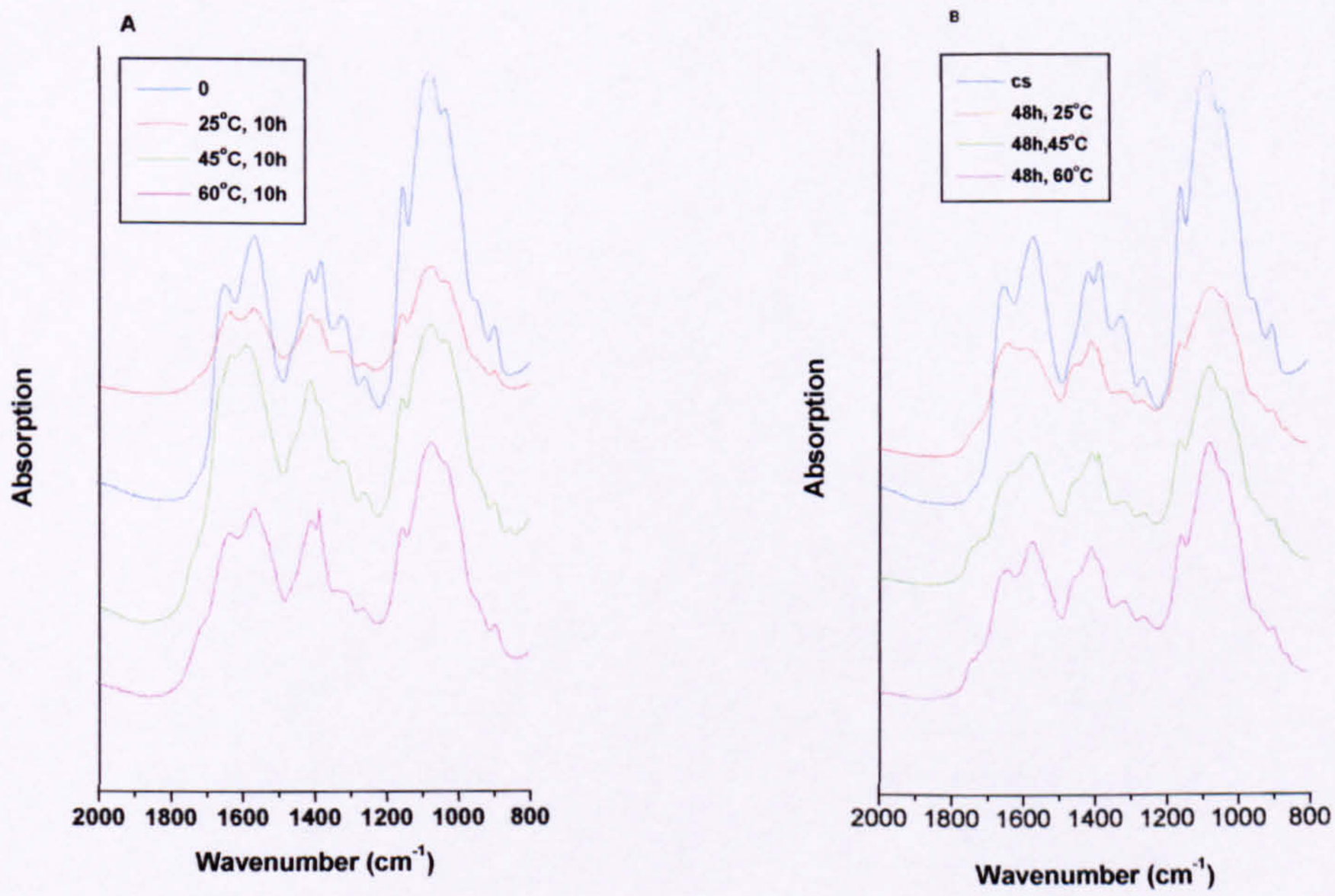

Figure 7.2.4 FT-IR spectra for comparing the temperature effect on the crosslinking process

7.3. Crosslinking Study by UV Spectra Analysis

7.3.1 Characteristics of UV spectrum of chitosan and genipin

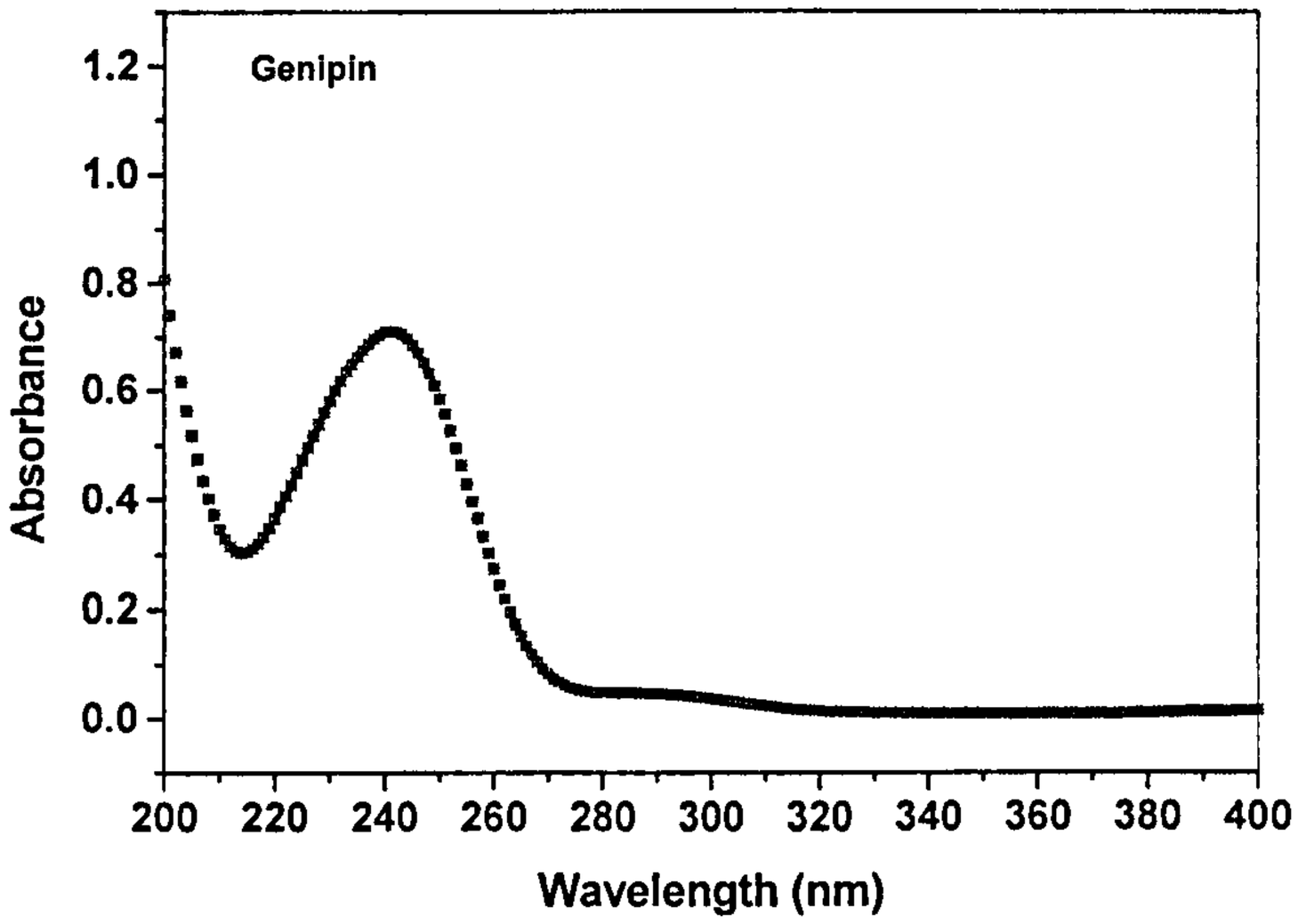

Figure 7.3.1 UV spectrum of genipin

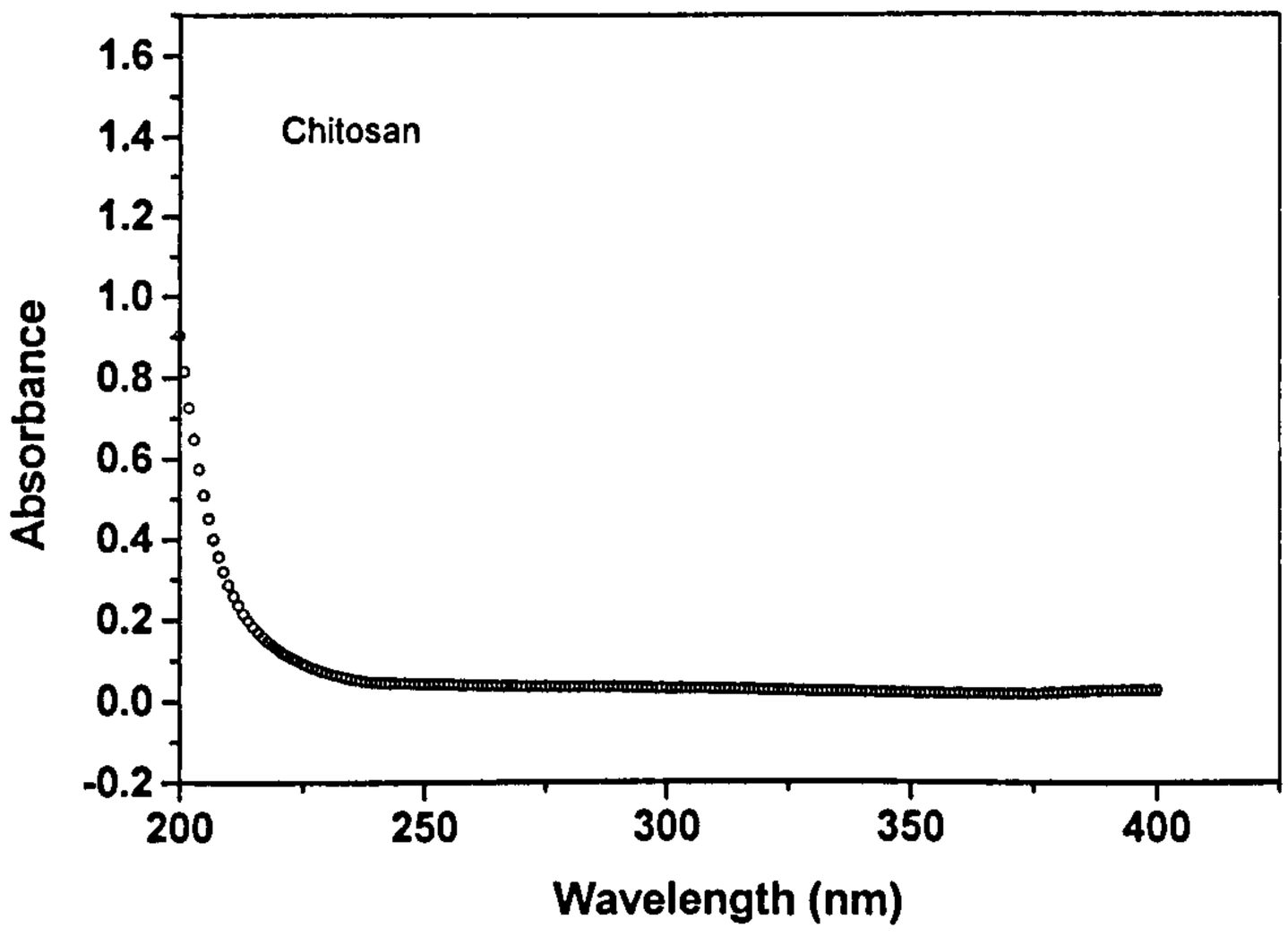

Figure 7.3.2 UV spectrum of chitosan

One of the most useful applications of UV-visible spectroscopy to polymers is for the characterisation of conjugated or aromatic materials [213]. Polymers with aromatic structures have delocalized electrons and exhibit strong characteristic UV absorption at very short wavelengths.

Figures 7.3.1 and 7.3.2 show UV spectra of genipin and chitosan. It was found that genipin dissolved in water and displayed a single ultra-violet absorption peak at 240nm. The chemical structures of genipin and chitosan are shown in Figures 2.2.1 and 2.5.1. Genipin is a heterocyclic compound with a conjugation bond. The UV spectrum of genipin was very compatible with the chemical structure of genipin.

Figure 7.3.3 shows UV spectra for a series of concentrations of genipin. The spectra illustrate that the intensity of the absorption peak at 240nm increased with increasing concentration of genipin. The relationship between the area of the absorption peak and the concentration of genipin was found to be linear, and the dependence of the former on the latter is shown in Figure 7.3.4.

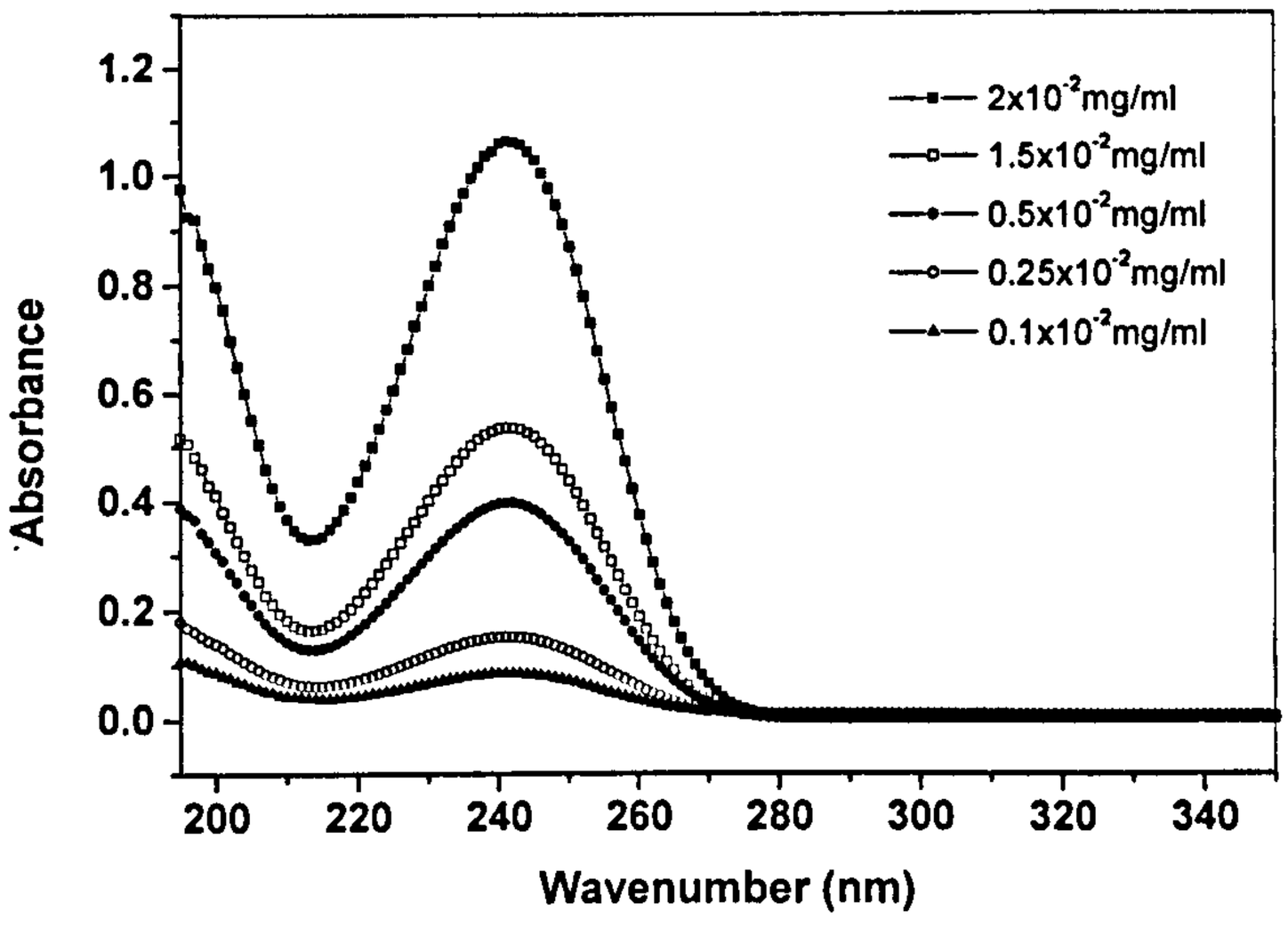

Figure 7.3.3 UV spectra of genipin at different concentrations

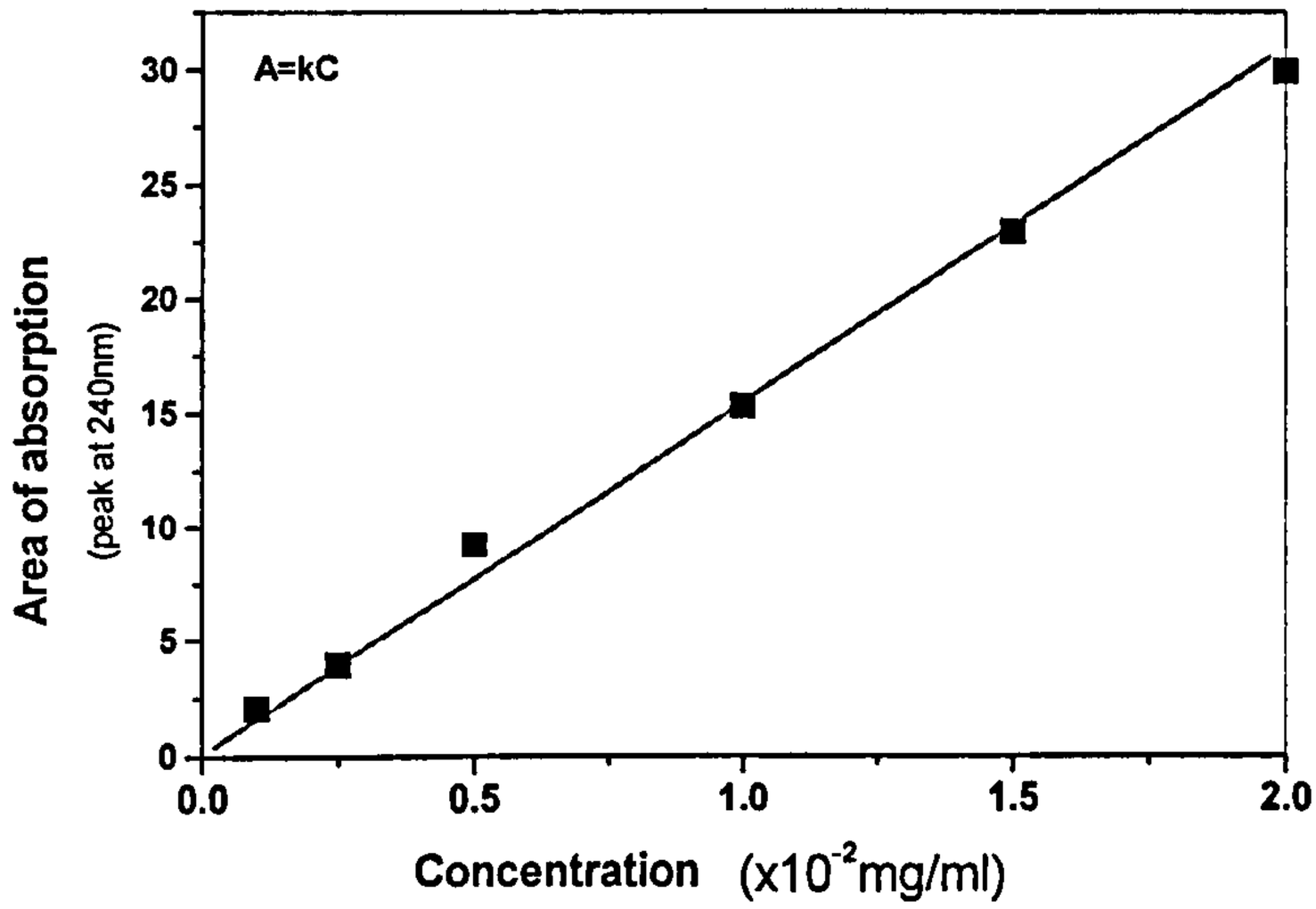

Figure 7.3.4 Area of absorption peak at 240 nm vs. concentration of genipin

The concentration of genipin, which represents the ester group content, is related to the area of absorption at 240nm. Based on this result, a new method of analysing the crosslinking process as time progresses can be introduced. This method will be used later in the study of the crosslinking of chitosan by genipin.

7.3.2. UV spectra study on temperature-dependence of crosslinking reaction

Various amounts of genipin were added to the chitosan solutions to monitor the crosslinking reaction process with time.

It has been confirmed that genipin reacts with chitosan via covalent bonding to form chemically crosslinked networks [200,252]. In this study, the extent of chemical crosslinking can be examined by UV spectra analysis. Figure 7.3.5, parts (A), (B) and (C), shows the variation of UV spectra of chitosan reacted with genipin (genipin content: 0.1%, 0.5% and 1%) at a reaction temperature of 25°C with time. They display the characteristic absorption peak at 240nm for the ester group of genipin and

at 280nm for reaction of genipin and the amino group of chitosan [252]. This suggests that genipin reacted chemically with chitosan. As can be seen from the figures, the two peak positions shifted during crosslinking, and, therefore, it is very difficult to use the intensity of the absorption peak to analyse the results. However, the area of characteristic absorption peak at 240nm decreased and the area of absorption peak at 280nm increased with increasing reaction time. This suggests the ring-opening of genipin via crosslinking, which is in agreement with Sung's studies [252]. With increasing genipin content, the changes in both areas of absorption peak at 240nm and 280nm became greater. This means that the crosslinking reaction became more extensive.

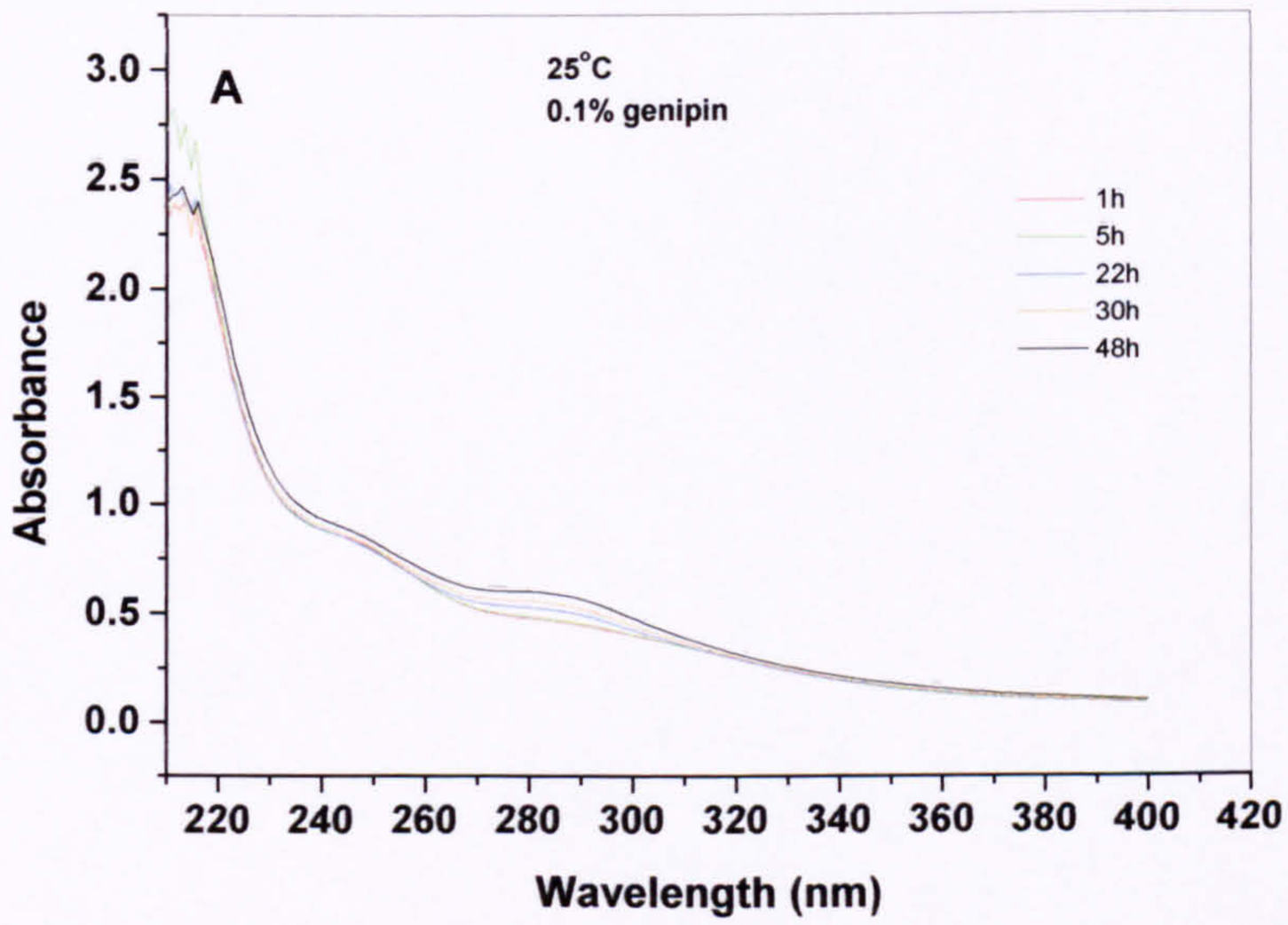

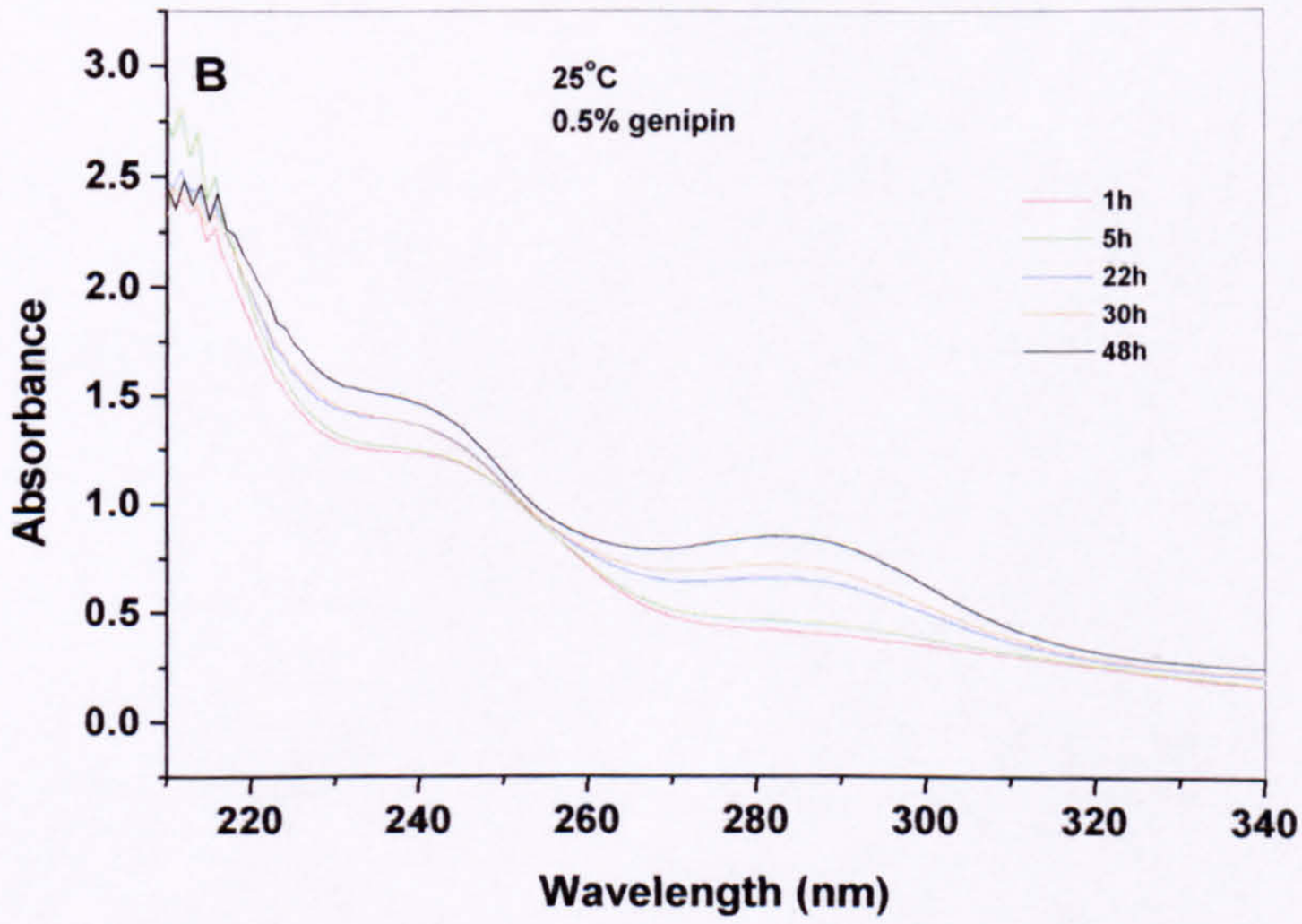

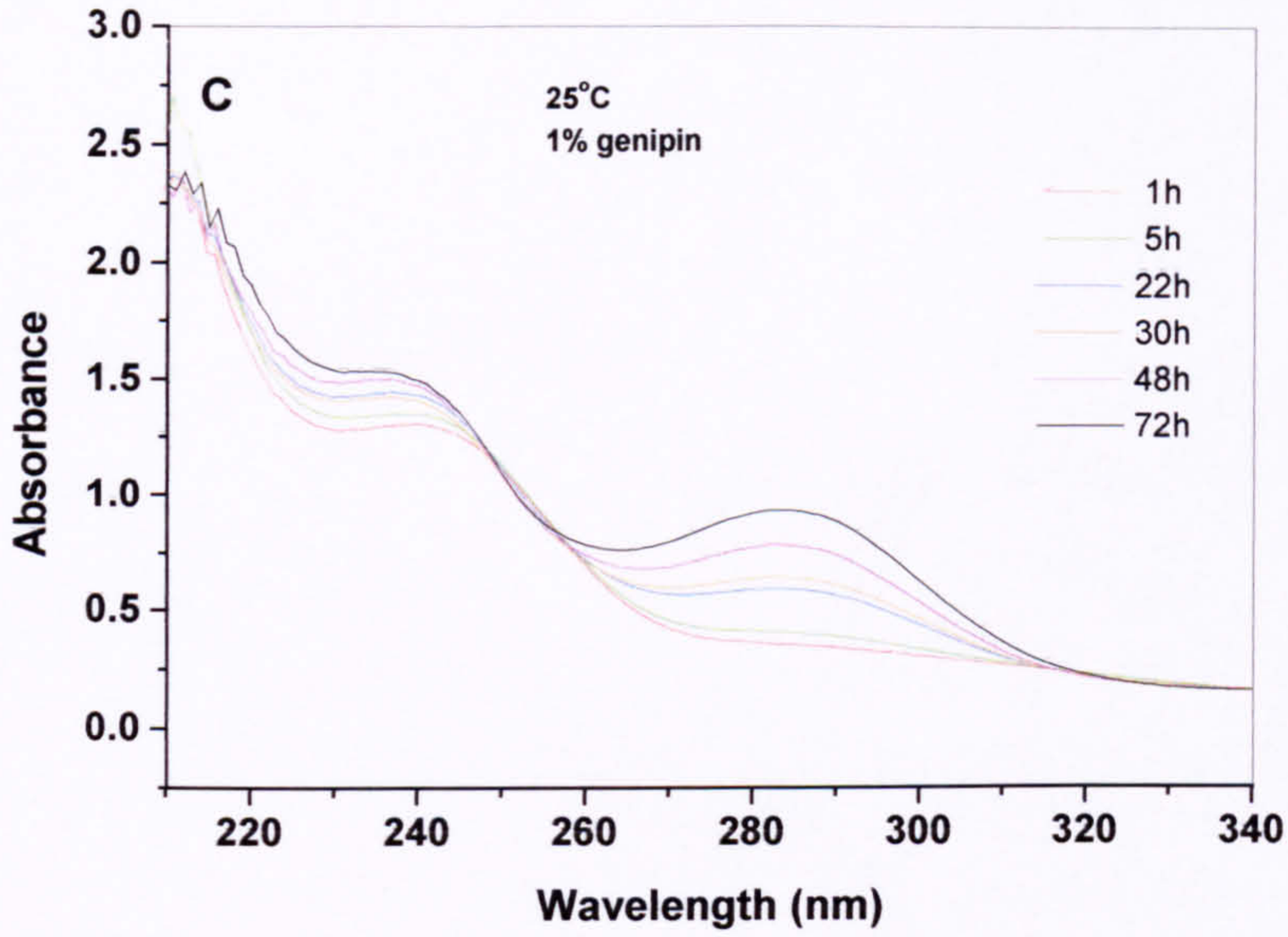

Figure 7.3.5 UV spectra showing the time-dependence of the crosslinking reaction at 25°C (A) 0.1% genipin, (B) 0.5% genipin, (C) 1% genipin

Figures 7.3.6 and 7.3.7 show the UV spectra of chitosan crosslinked by genipin at the reaction temperature of 40°C and 60°C, respectively. The concentration of genipin, which represents the ester group content, is related to the area of absorption at 240nm, as discussed above. We can now use this new method to analyse the reaction process. Table 7.3.1 lists the value of two areas of absorption peak at 240nm and 280nm as reaction time proceeded. A comparison of these data shows that the total value of the two areas was constant. This suggests the conversion of the ester groups of genipin to amide linkages. The increased area of absorption peak at 280nm is attributed to the formation of a heterocyclic amino compound. The smaller area of the absorption at 240nm the greater the conversion of the ester group to the amide linkage was. The extent of the crosslinking reaction at different times can be examined using these conversion characteristics.

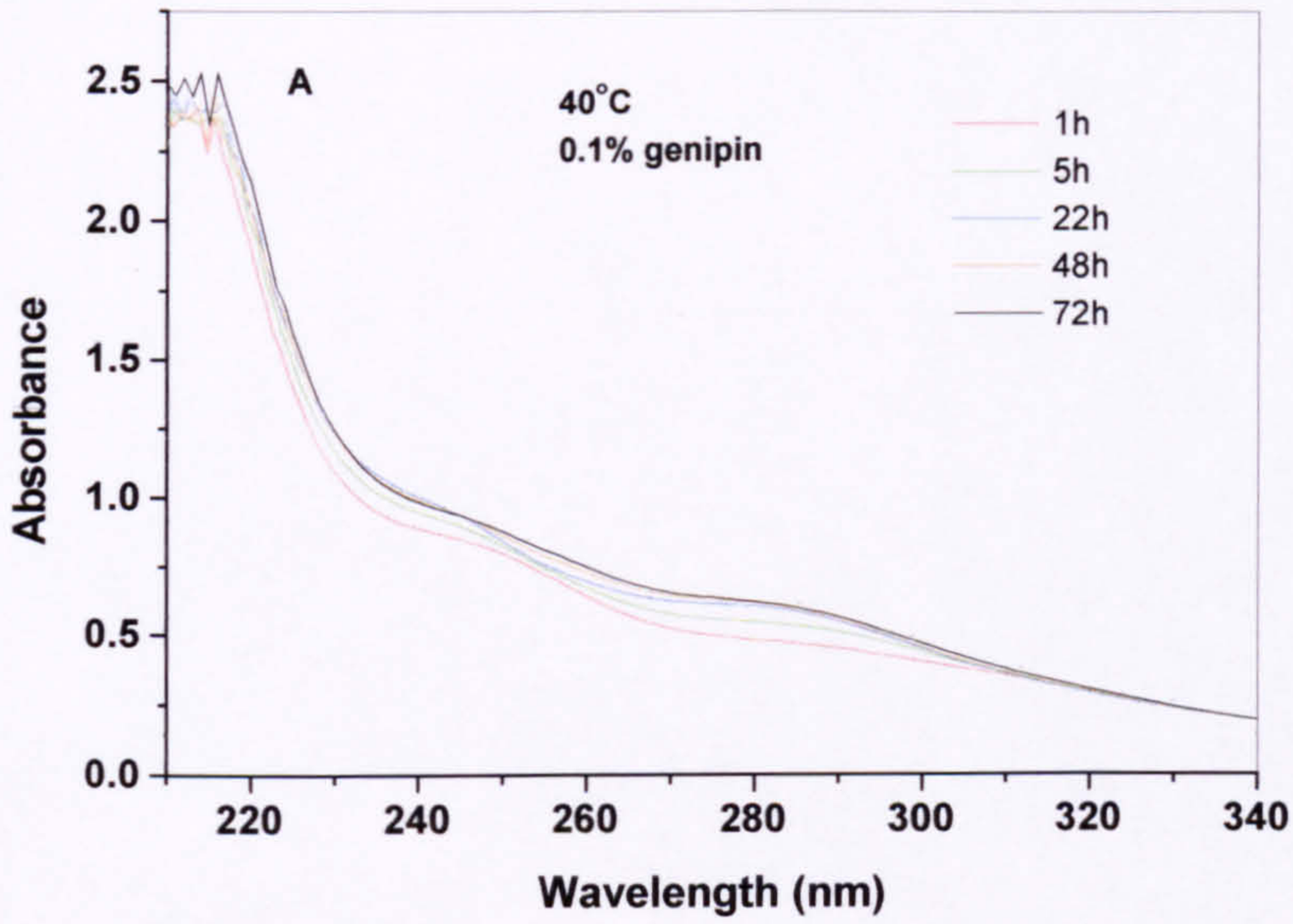
A
40°C
0.1% genipin
1h
5h
22h
48h
72h
Absorbance
2.5
2.0
1.5
1.0
0.5
0.0
220
240
260
280
300
320
340
Wavelength (nm)

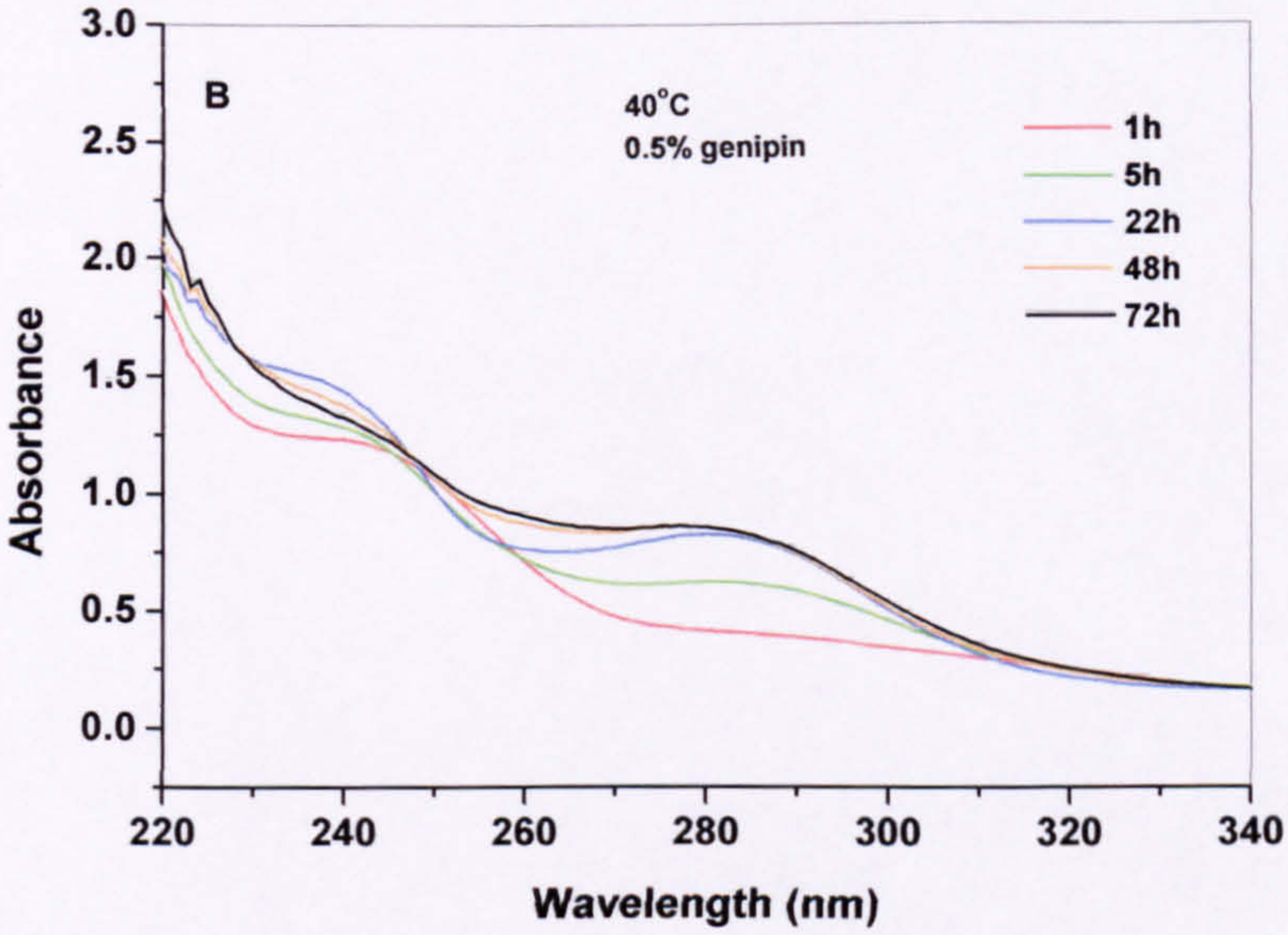
B
40°C
0.5% genipin
1h
5h
22h
48h
72h
Absorbance
3.0
2.5
2.0
1.5
1.0
0.5
0.0
220
240
260
280
300
320
340
Wavelength (nm)

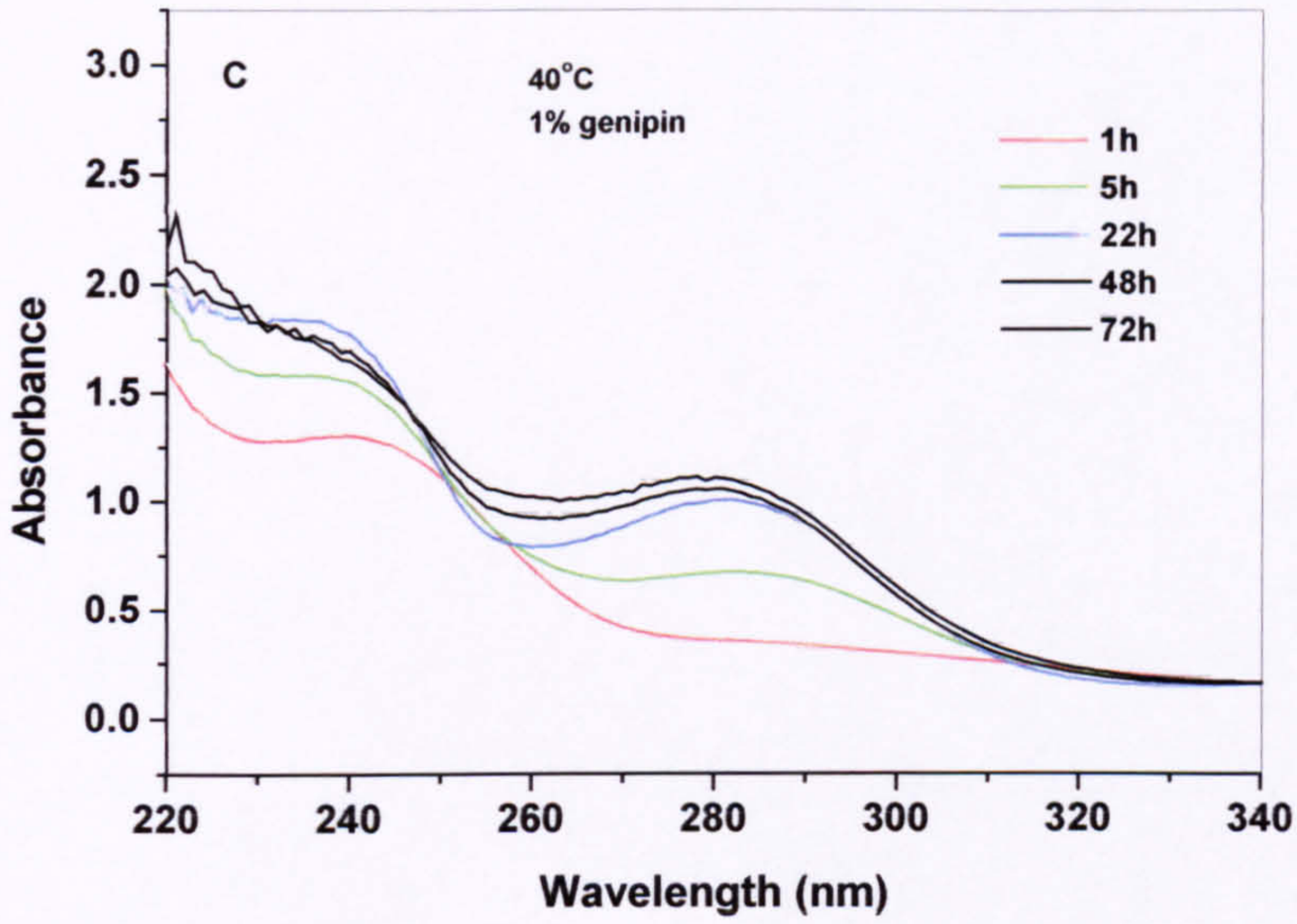

Figure 7.3.6 UV spectra showing the time-dependence on crosslinking reaction at 40°C: (A) 0.1% genipin, (B) 0.5% genipin, (C) 1% genipin

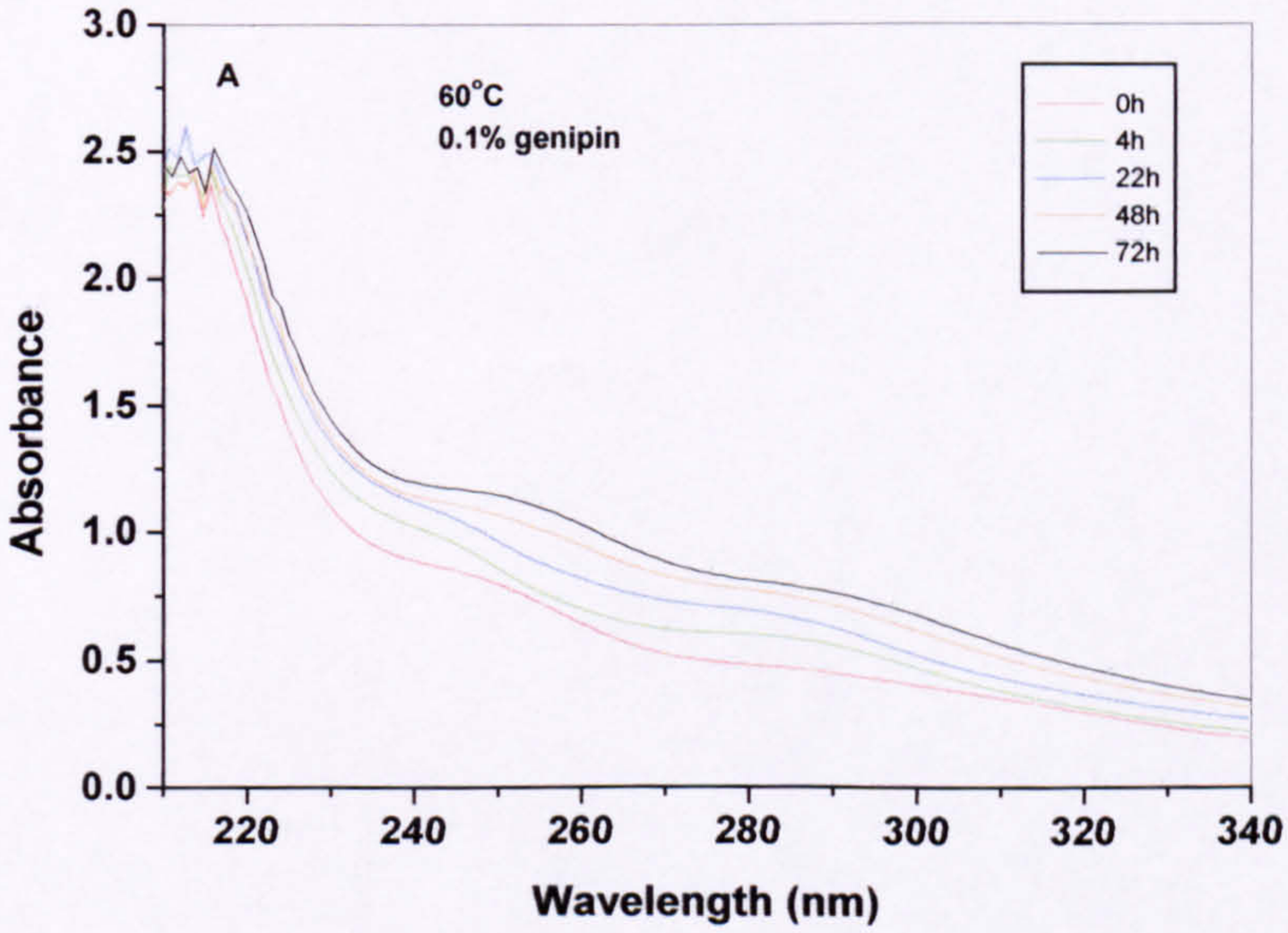

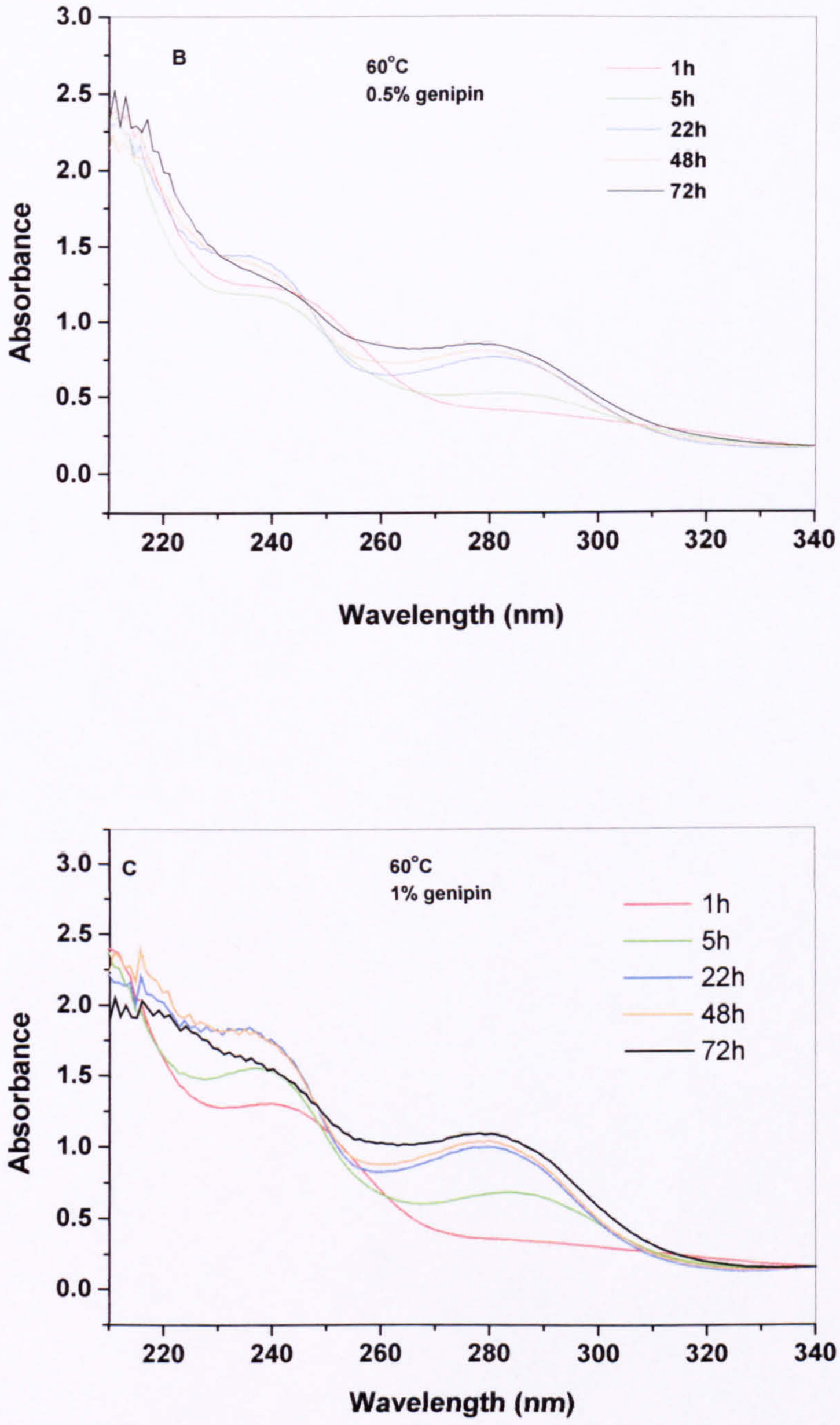

Figure 7.3.7 UV spectra showing the time-dependence of the crosslinking reaction of chitosan at 60°C: (A) 0.1% genipin (B) 0.5% genipin, (B) 1% genipin

Table 7.3.1 The two areas of absorption peaks

Genipin content (wt.%)	Temperature (°C)	Reaction time (hr)	A (at 240 nm)	A' (at 280 nm)	A+A'
1	60	1	13.12	2.94	16.06
		5	7.36	9.28	16.65
		22	4.07	12.30	16.37
		48	2.56	14.62	17.18
		72	1.47	13.87	15.29
1	45	1	14.95	2.46	17.41
		5	11.75	5.70	17.45
		22	5.28	11.61	16.89
		48	3.13	14.08	17.21
1	25	1	15.00	1.36	16.36
		5	13.07	2.68	15.75
		22	10.80	6.21	17.01
		48	7.95	8.62	16.57
0.5	25	1	7.27	3.76	11.03
		5	6.89	5.07	11.96
		22	5.50	6.25	12.05
		48	3.63	8.14	11.77
0.5	45	1	8.61	3.34	11.95
		5	4.42	7.22	11.66
		22	2.75	9.04	11.79
		48	2.24	9.69	11.99
0.5	60	1	8.79	3.18	11.97
		5	6.13	5.89	12.07
		22	3.45	8.32	11.78
		48	2.76	9.89	12.65
		72	2.02	10.07	12.09

Figure 7.3.8 plots the percentage area of absorption peak at 240nm (calculated from the combined area of the absorption peaks at 240nm and 280nm), which represents the extent of the crosslinking reaction, against reaction time (genipin content 1%). The percentage area of the characteristic absorption peak at 240nm decreased with increasing reaction time due to the ring-opening of genipin via the crosslinking reaction. Furthermore, within the first 5 hours, the extent of crosslinking reaction increased slowly at the lowest temperature of 25°C, but far more quickly at 40°C. This proves that the conversion of the ester group of genipin into amide linkage was quickest at 40°C. It can be seen from the figure that a linear relationship between the extent of the crosslinking reaction and time was obtained at 25°C. This means that at this temperature the reaction rate was constant. At 40°C, the reaction rate was fastest in the initial stages, but then changed sharply to a much slower rate. In the later stages, the reaction rate was nearly constant, which can be observed from the straight line indicated in the figure. At 60°C, the rate of reaction was fast within the initial 5 hours, and then became slower. In the whole crosslinking process, the reaction was heterogeneous, which was confirmed by the non-linear relationship between the deceased area of absorption peak at 240nm and the reaction time (as shown in Figure 7.3.8). From the experimental data, the area value can be extrapolated to zero, as shown in the figure, to estimate the end time of the crosslinking reaction at different temperatures.

From Figure 7.3.8 the time of crosslinking reaction at different temperatures can be estimated. Although this method could not give an accurate estimate of the time needed for the crosslinking reaction, the details of the reaction process were obtained. This information may be very important in helping us to understand the effect of crosslinking reaction temperature on the mechanical properties of crosslinked chitosan films.

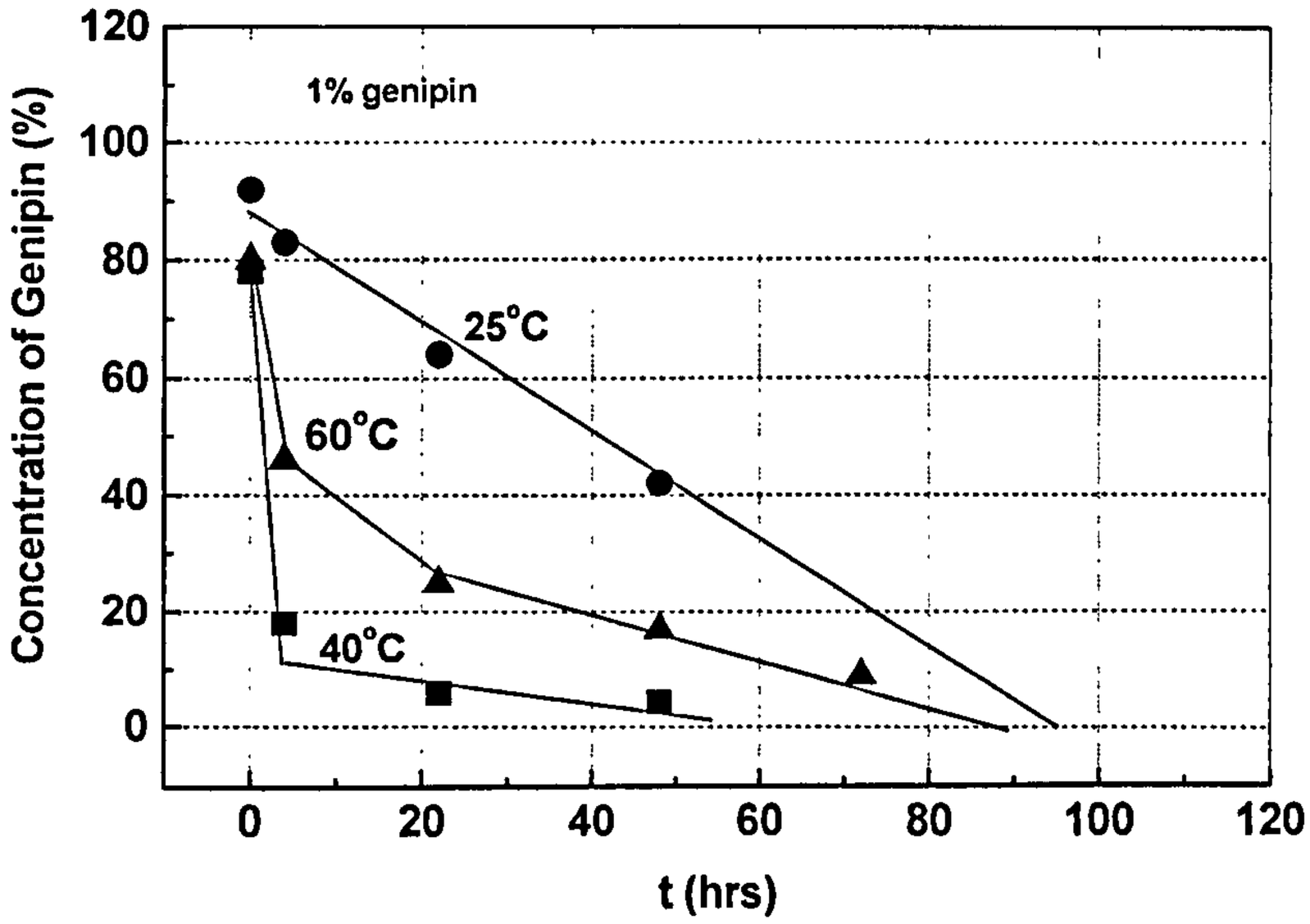

Figure 7.3.8 Concentration of genipin as a function of time during crosslinking reaction of chitosan

7.4 Effect of Crosslinking Reaction Temperature on the Mechanical Properties of Crosslinked Chitosan Films

The mechanical properties of crosslinked chitosan films were investigated at the different temperatures of 25°C, 40°C and 60°C, which were used for film-formation (or crosslinking). As concluded in Chapter 5, the crosslinking temperature has an influence on the mechanical properties of chitosan films. When the temperature used for film formation was 25°C, the elongation at break of the crosslinked chitosan films was the largest, and double that at 40°C. However, better tensile stresses for the films were obtained when the temperature was 40°C and 60°C.

From the above FT-IR and UV spectra studies, it is clear that using different crosslinking temperatures for the formation of chitosan films leads to significant differences in the crosslinking process, particularly in terms of the reaction rate, reaction homogeneity and the necessary reaction time. These factors may have an

effect on the morphologies of chitosan films, which is seen through different mechanical properties.

The above analysis suggests that in order to understand the mechanical properties of chitosan films that are formed by a process in which chitosan solution turns to gels and then films, we have to understand the effect of the temperature on the solution properties of chitosan, the effect of these properties on the crosslinking process and the morphology of the chitosan films obtained.

The intrinsic viscosity of chitosan solutions is influenced by temperature. With increasing temperature, the intrinsic viscosity of chitosan decreases linearly [30,43]. The intrinsic viscosity can affect on the molecular mobility in solution. During the formation of crosslinked chitosan film at lower temperatures, the molecular mobility of genipin may be restricted due to the higher intrinsic viscosity of the chitosan solution. The crosslinking reaction is, therefore, slower, which has been confirmed by previous studies when the temperature used was 25°C.

During film-formation of crosslinked chitosan, the temperature causes changes in the solvent quality as well as affecting the intrinsic viscosity of the solution. Hydrogen bonding plays an important role in the gelation process of chitosan and a significant influence on the mechanical properties of chitosan [260]. If the solution temperature is high, it can decrease chitosan solubility by the disruption of hydrogen bonding with water and reduce junction points on the chains in the solution [30,260]. At such temperatures, the molecular motion of genipin is, therefore, easier, causing a faster crosslinking reaction. The UV spectra results studied above are in agreement with this analysis.

As crosslinking proceeded with time, the solutions gradually formed chitosan gels, a process obviously dependent on the molecular mobility of the polymer chains in the media and in which there is an increasing density of physical crosslinking reticulation. In the initial stages, the density of crosslinking reticulation increased quickly due to the faster crosslinking reaction. However, the reticulation could also cause reductions in the contact opportunities between chitosan and genipin molecules and restriction of molecular mobility (or penetration) of genipin. As a result, the reaction rate

subsequently decreased. It can be seen from Figure 7.3.8 that after the first 5 hours the rates of crosslinking reaction were slower at temperatures of 40°C and 60°C. The higher the temperature and the stronger the effect was. At 25°C, by contrast, no such effect was observed. At this lower temperature, the reaction was homogeneous during the whole crosslinking process, resulting in homogenous crosslinked chitosan networks. This result explains the better elongation at break.

At the higher temperature, the rate of the crosslinking reaction changed from very fast to slow. As a result, this could lead to a heterogeneous density of crosslinking reticulation and phase separation in the films. Figure 7.3.9 is a schematic diagram of the heterogeneous density of crosslinked chitosan films. The more highly crosslinked and localized networks formed due to the faster crosslinking reaction can be treated like fillers, thereby explaining the mechanical properties of the films: greater tensile strength and lower elongation at break.

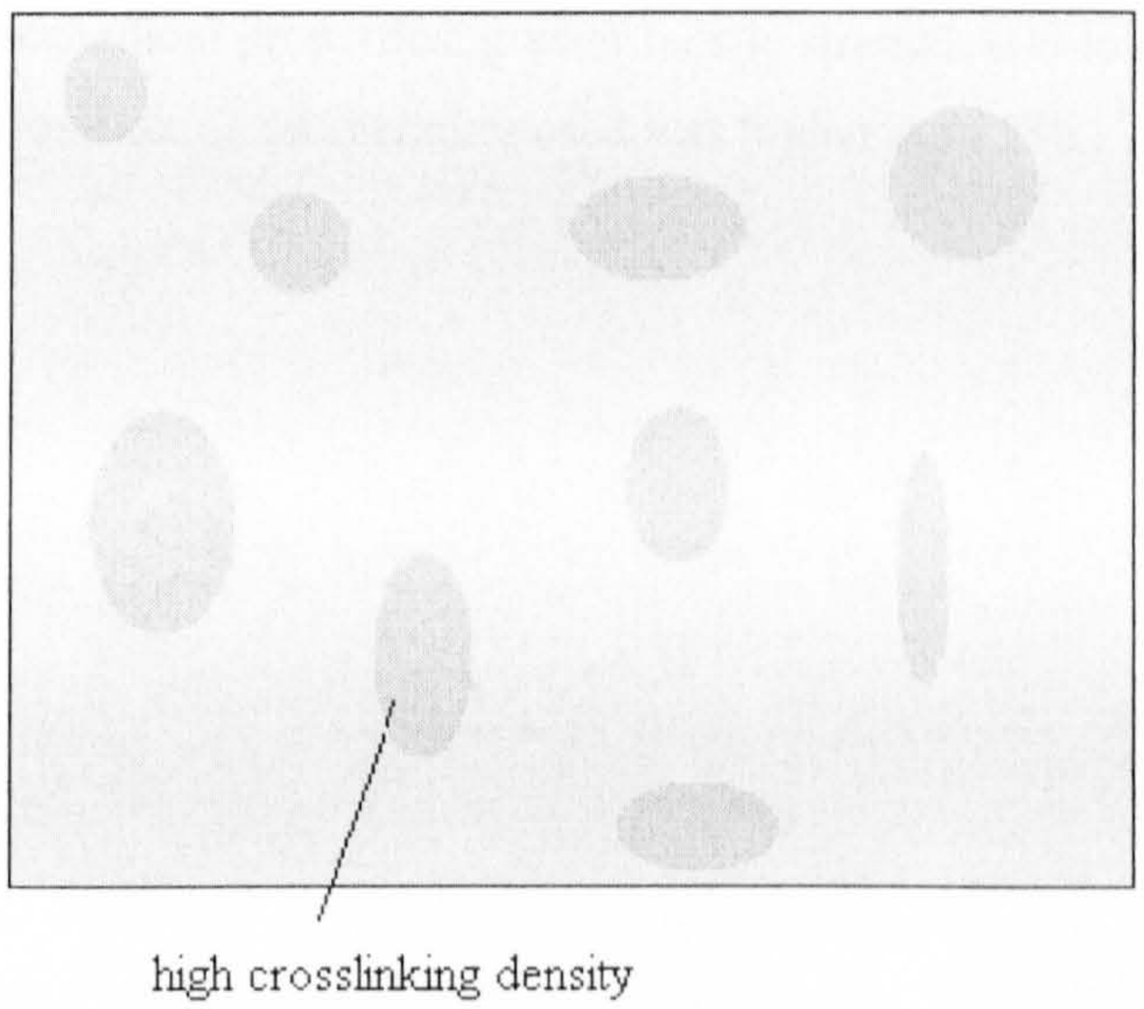

Figure 7.3.9 Schematic diagram showing the areas with high crosslink density as fillers in the chitosan films formed at high temperatures

7.5 Conclusions

The temperature dependence of the crosslinking reactions was studied by means of FT-IR and UV spectra analysis. The results of FT-IR spectra analysis indicated that the crosslinking reaction occurred after the addition of genipin, which is confirmed by the amino group of chitosan reacting with the ester group of genipin. The decrease in the number of amino group resulted in the change of intra-hydrogen bounding interactions. Information about the temperature dependence of the crosslinking reaction of chitosan was obtained by the UV study. The results show that at the lowest temperature of 25°C a homogeneous crosslinking reaction occurred and this resulted in better elongation at break of the chitosan films. At higher temperatures, heterogeneous crosslink density in the films formed due to the effect of the intrinsic viscosity of chitosan solution and crosslinking reticulation during film-formation on the molecular mobility of genipin. The localised high crosslinked density region can be treated as fillers in the film and from this result it is, therefore, possible to understand the mechanical properties: greater tensile strength and lower elongation at break when the crosslinking temperature used was higher than 25°C.

CHARPTER 8

Aggregation and Collapse of Chitosan Chains in Aqueous Solutions

8.1 Introduction

Chitosan belongs to a family of linear cationic polymers and it is also an acidic soluble polymer. pH has a significant effect on the solution properties of chitosan. These properties are also influenced by the degree of deacetylation and average molecular weight. Factors that affect the solution properties also affect its film-forming properties [236,237]. Film-making conditions, including solution pH, ionic strength, type of solvent (acid) used and annealing treatment, are parameters often manipulated to alter the physical and mechanical properties of chitosan films, which are particularly important to their medical applications. The results of Chapter 5, where the mechanical properties of chitosan films were discussed, indicate that tensile strength and elongation at break were affected by the pH of the solution used for film-making. In particular, when the solution was of pH 2.5 the mechanical properties of the film formed were at their optimal. Ionic strength, or pH, can be used to adjust the inter- and intra-molecular electrostatic repulsions between chitosan chains, thus allowing the chains to approach each other and enhancing the inter- and intra-molecular hydrogen bonding, and, therefore, resulting in changes in the molecular conformation [261]. Although several publications on the rheological and fluorescence properties of chitosan solution have been produced [261,262], the effect of the interactions on microscopic behaviour is still not yet fully understood. Hence, in order to understand the effect of solution pH on film formation of chitosan solution, which has an influence on the mechanical properties of chitosan films, there is a need to use an appropriate technique to investigate the molecular-level behaviour of chitosan solution.

Laser light scattering has been proven to be a particularly useful method of studying molecular conformation, especially in very dilute solutions [30, 263, 264]. In this chapter, the effects of pH on chitosan macromolecular conformation in solution were

studied by means of static laser light scattering and an understanding of the impact of chitosan solution pH on the mechanical properties of the film was developed. The dilute solution properties of chitosan with various acetic acid concentrations were investigated. Based on the experimental data, the dependence of the conformation of the chitosan macromolecules on acetic acid concentration will also be discussed.

8.2 Background to the Theory of Static Laser Light Scattering

Figure 8.2.1 shows relative position of the observer $Q(x_a)$ and the scattering volume $v(x_a)$. The scattered intensity is the square of the scattered electric field [207]. The incident light field, $E_{INC,}$ is polarized in the z-direction and is propagated in the k_I-direction. The vector R is defined from the origin of the scattering volume to the idealized point detector. φ is the scattering angle.

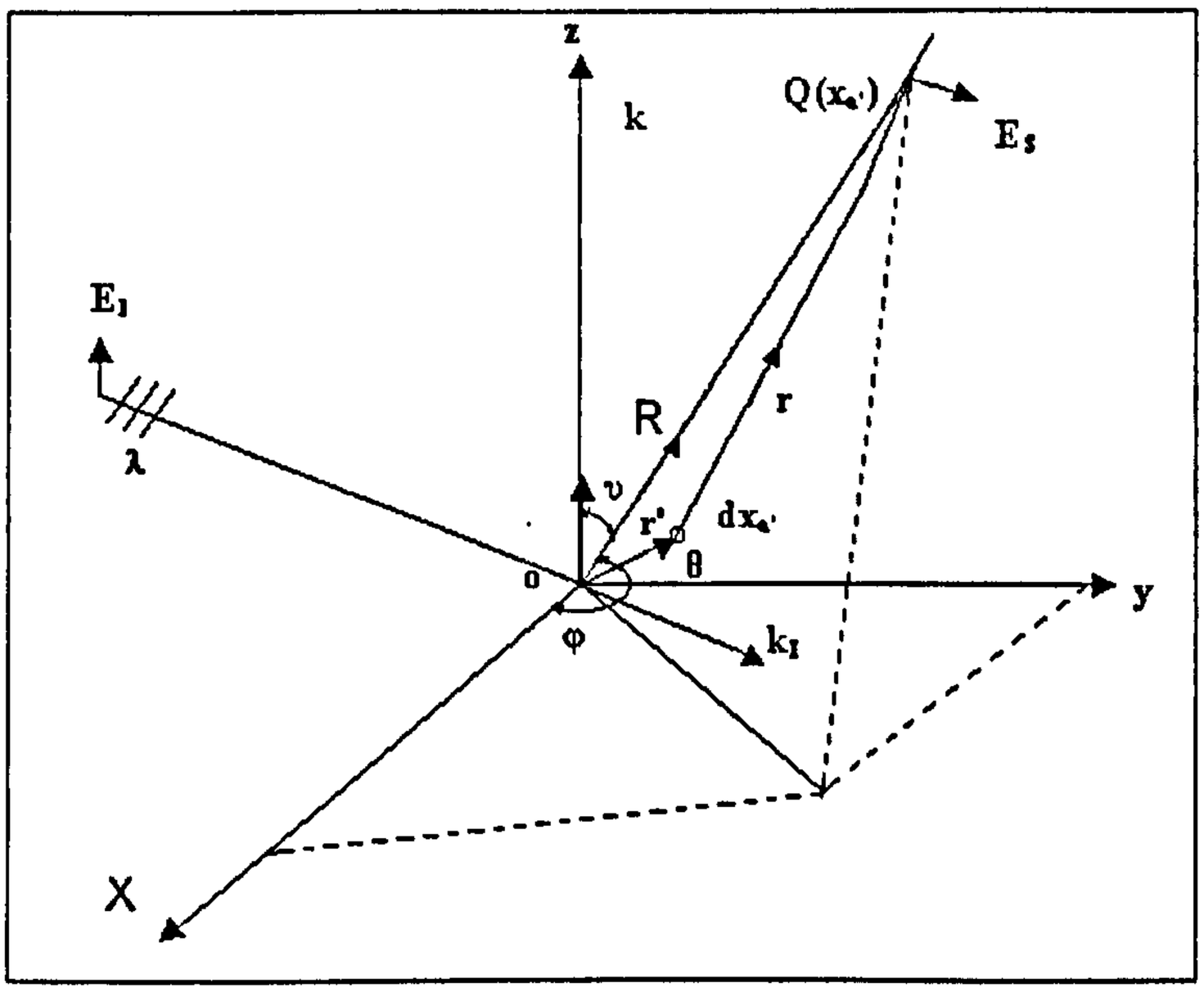

Figure 8.2.1 Relative position of the observer $Q(x_a)$ and the scattering volume $v(x'_a)$.(Index of refraction = n) [207]

For a single small particle with polarisability α, the scattered electric field E_s is proportional to the polarisability, which is related to the volume of the particle (V_p). Thus, the intensity of scattered light from a single particle (i_s), is proportional to E_s^2 and also to α^2. For an incident beam I_{INC}, the scattered intensity of a single small particle i_s is

$$\frac{i_s}{I_{INC}} = \frac{k^4 \alpha^2}{d^2} \qquad [8.2\text{-}1]$$

where $k = 2\pi/\lambda_0$ and d is the distance between the particle and the observer. For N identical particles in a solvent of refractive index n_o and polarisability α_o, the background scattering of the solvent has to be subtracted. Namely, α in Equation 8.2-1 has to be replaced by $\alpha_{ex} = \alpha - \alpha_o$ as follows.

$$n^2 - n_0^2 = 4\pi N_{ex} \qquad [8.2\text{-}2]$$

$$\alpha_{ex} = \frac{n_0}{2\pi}\left(\frac{n - n_0}{C}\right)\frac{M}{N_A} \qquad [8.2\text{-}3]$$

where $N = CN_A/M$ with C being the weight concentration. M is the mass of a particle. The excess scattered intensity, I_{ex}, for a dilute solution with N identical small particles in volume V without both intra-particle interference and inter-particle interactions is

$$\frac{I_{ex}}{I_{INC}} = \frac{k^4 \alpha_{ex}^2 N}{d^2} \qquad [8.2\text{-}4]$$

Correspondingly, the excess Rayleigh ratio $\Delta R_{VV}(K)$ ($=I_{ex}\ d^2/I_{INC}$) of the solute particle for vertically polarised incident and scattering light has the form

$$\Delta R_{VV}(K) = \frac{k^4 n_0^2}{2\pi^2 N_A}\left(\frac{\partial n}{\partial C}\right)^2_{T,P} MC = HCM \qquad [8.2\text{-}5]$$

In the presence of intra-particle interference and inter-particle interaction, the scattered intensity of a single particle i_s, where there is uniform polarizability, α, due to a phase shift, is

$$\frac{i_s}{I_{INC}} = \frac{k^4\alpha^2}{d^2V_p}\int V_p\rho(r)\exp(iK\cdot r)dv = \frac{k^4\alpha^2}{d^2}P(K) \qquad [8.2\text{-}6]$$

which can also be written as

$$\Delta R_{VV}(K) = HMCP(K) \qquad [8.2\text{-}7]$$

where $\exp(iK \cdot r)$ is the phase factor, with $\mathbf{r}$ ($=\mathbf{r}_i - \mathbf{r}_j$) being the vector distance between the two scattering elements inside the particle volume V_p; and $\rho(r)$ is the radial distribution function for the scattering elements inside the particle, which may be defined by the statement that $\rho(r)dv/V_p$ is the probability of finding the i^{th} scattering element within the volume element dv at a distance r from the j^{th} scattering element. A normalized intra-particle scattering factor of a single particle of uniform density and finite size is

$$P(K) = \frac{1}{V_p}\int_{V_p}\rho(r)\exp(iK\cdot r)dv \qquad [8.2\text{-}8]$$

In general, for a randomly oriented particle with an arbitrary shape, the probability that K and r have an angle between φ and $\varphi + d\varphi$ is $2\pi \sin\varphi\, d\varphi$, and, thus, the average value of the phase factor is

$$\langle\exp(K\cdot r)\rangle = \frac{\int_0^{\pi}\cos(Kr\cos\phi)\sin\phi d\phi}{\int_0^{\pi}\sin\varphi d\varphi} = \frac{\sin(K\cdot r)}{Kr} \qquad [8.2\text{-}9]$$

Therefore, for a single particle with a radial distribution function ρ(r) and finite size, the normalized intra-particle scattering factor can generally be defined as

$$P(K)=\frac{\int_{v_p}\rho(r)\frac{\sin(Kr)}{Kr}dv}{\int_{v_p}\rho(r)dv} \qquad [8.2\text{-}10]$$

For a uniform sphere, $\rho(r)=1$ and $\int_{V_p}\rho(r)\,dv=V_p$, so that,

$$P(K)=\frac{1}{V}\int_0^{2\pi}d\varphi\int\sin\varphi d\varphi\int_0^R r^2\frac{\sin(Kr)}{Kr}dr=\frac{4\pi}{V_p}\int_0^R r^2\frac{\sin(Kr)}{Kr}dr \qquad [8.2\text{-}11]$$

where R is the particle radius. At small values of Kr, and with the mass density dependent on r, we then have for the normalized particle scattering factor

$$P(K)=\frac{\varphi(K)}{\varphi(0)}\approx 1-\frac{K^2}{3}\frac{\int_{v_p}\rho(r)r^2dv}{\int_{v_p}\rho(r)dv}=1-\frac{K^2R_g^2}{3} \qquad [8.2\text{-}12]$$

where R_g is the radius of gyration, which for a particle can be defined as

$$\left\langle R_g^2\right\rangle=\frac{\int_{v_p}\rho(r)r^2dv}{\int_{v_p}\rho(r)dv} \qquad [8.2\text{-}13]$$

For a uniform solid sphere, $\int_v\rho(r)dr=1$

$$\left\langle R_g^2 \right\rangle = \frac{\int_0^R 4\pi r^4 dr}{\int_0^R 4\pi r^2 dr} = \frac{3}{5} R^2 \qquad [8.2\text{-}14]$$

Particle sized distribution can be obtained by the inverse Fourier transform from the time-average correlation function. Figure 8.2.2 shows a schematic representation [207] of the correlation between a particle, its observable experimental data, I(t), and its distance distribution function, ρ(r). From the particle sized distribution function, the radius of the particle can be calculated according Equations 8.2-13 and 8.2-14.

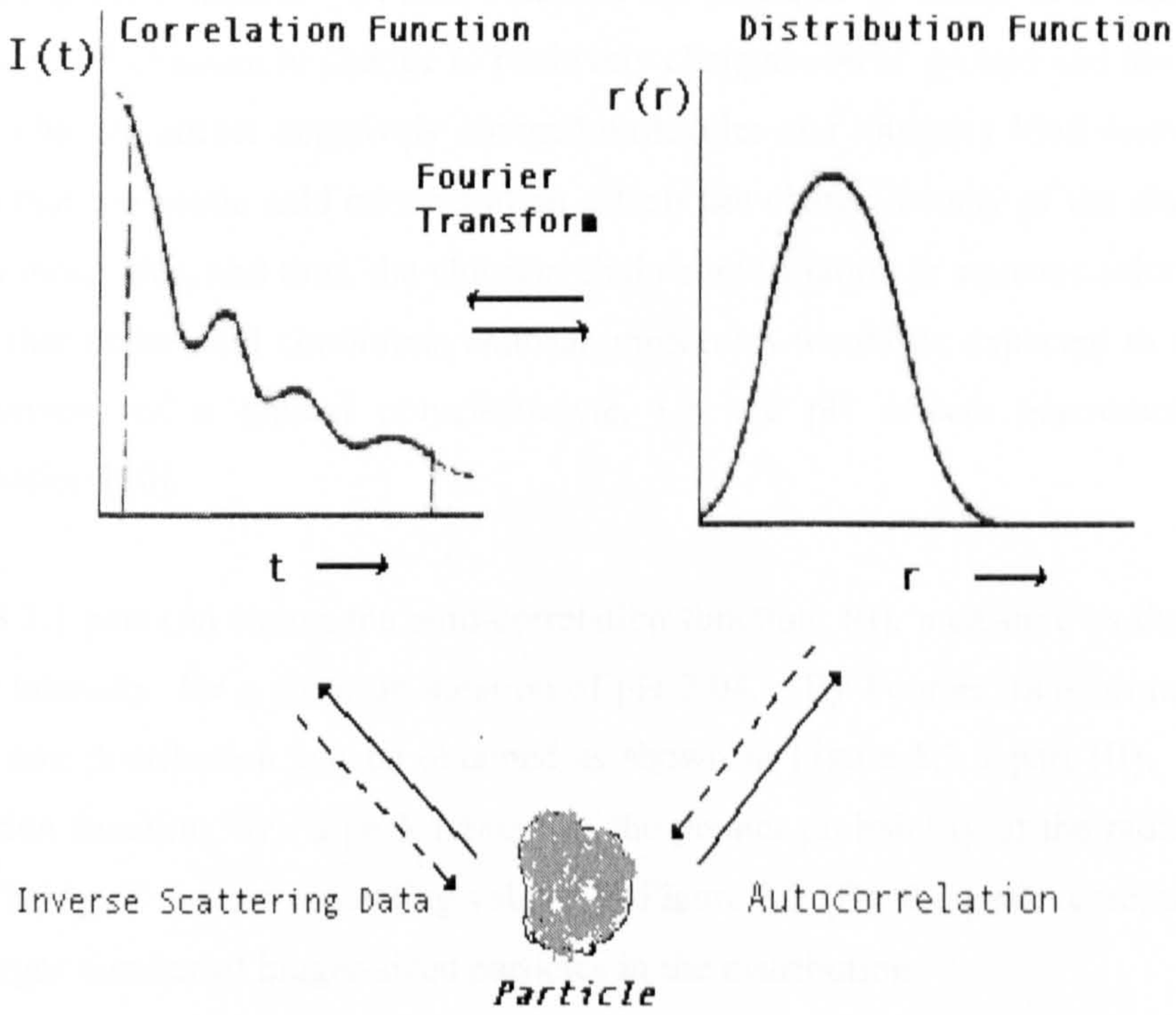

Figure 8.2.2 Schematic diagram of the correlation between a particle and the experimental data [207]

8.3 Effect of the Solution pH on the Conformation of Chitosan Macromolecules

8.3.1 Multi-chain aggregation phenomenon for chitosan in aqueous solution

Static laser light scattering was carried out at 25°C with a scattering angle, θ, of 30° for chitosan/acetic acid/water solutions with a chitosan concentration of 10^{-4}g/mL and at various pH values.

It is known [263] that the association behaviour of semi-dilute systems of chitosan can be affected by pH. As a linear polyelectrolyte, chitosan has both reactive amino groups and hydroxyl groups that can interact with the surroundings. Thus, it is expected that the physical and solution properties of chitosan will change with the surrounding environment. In acid solution, the presence of acetic acid causes the NH_2 groups of chitosan to change to positively charged $-NH_3^+$ groups and the strong positive charges attract negatively charged molecules and ionically bind them. It is obvious that the acetic acid concentration affects the charge density of the dissolved chitosan molecules, and thus, the chitosan chain conformation in aqueous solution. It follows that under acid conditions chitosan molecules would be expected to exhibit the behaviour of a typical polyelectrolyte, i.e. the pH affects macromolecular conformation [30].

Figure 8.3.1 part (A) shows the auto-correlation function, I(t), measured as the time-average intensity, for a chitosan solution of pH 2.04. By Fourier transformation, a particle size distribution can be obtained as shown in Figure 8.3.1 part (B). In the distribution function, r(r), a peak represents the greater probability of the radius of a particle being of the corresponding value. In Figure 8.3 (B), the peak represents the much larger number of bigger-sized particles in the distribution.

In low pH chitosan solutions, the chitosan molecules have higher $-NH_3^+$ charge densities and are expected to exist as random coils having a relatively extended conformation [30,263]. This is due to the high intra- and inter-molecular electrostatic repulsions.

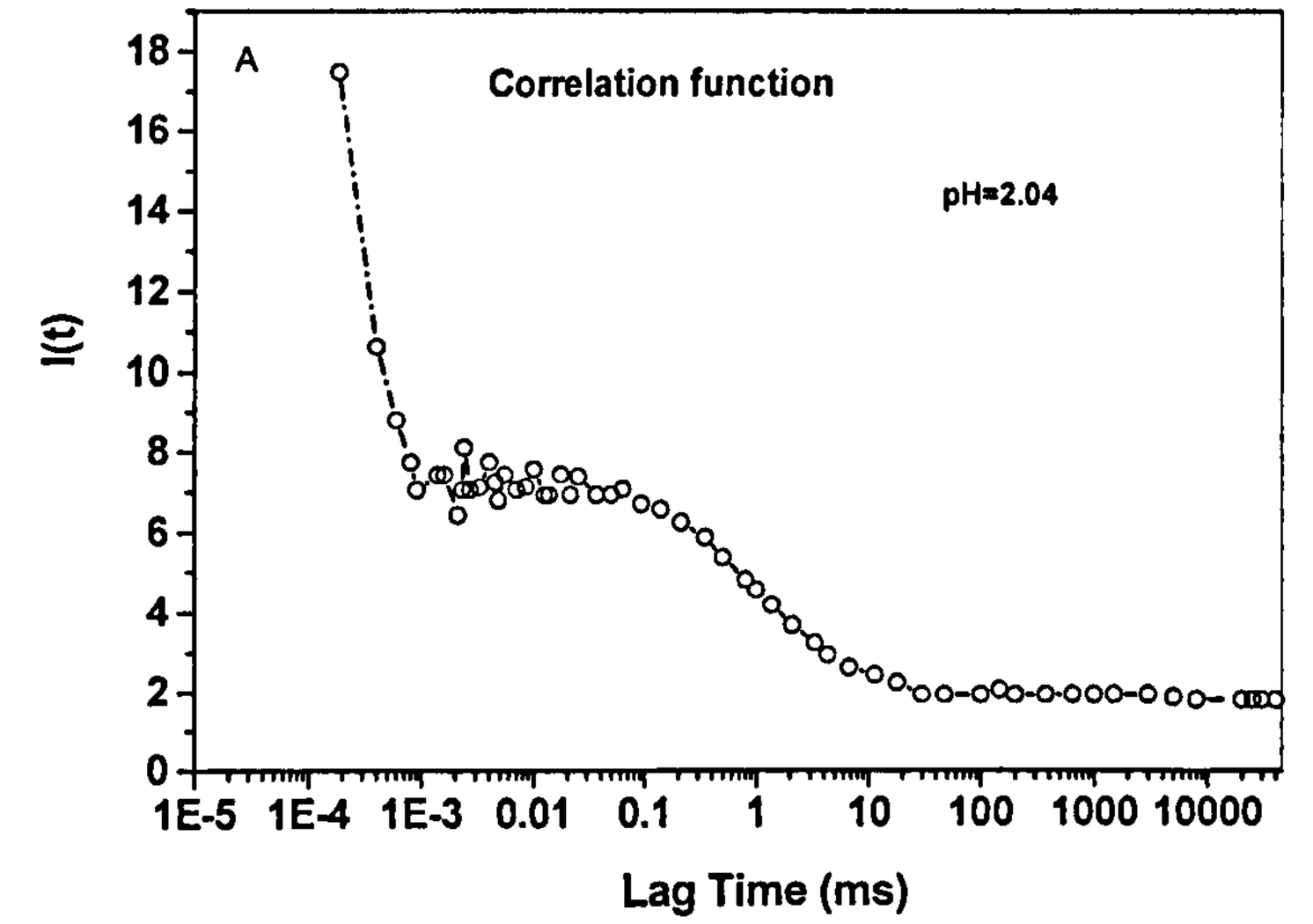

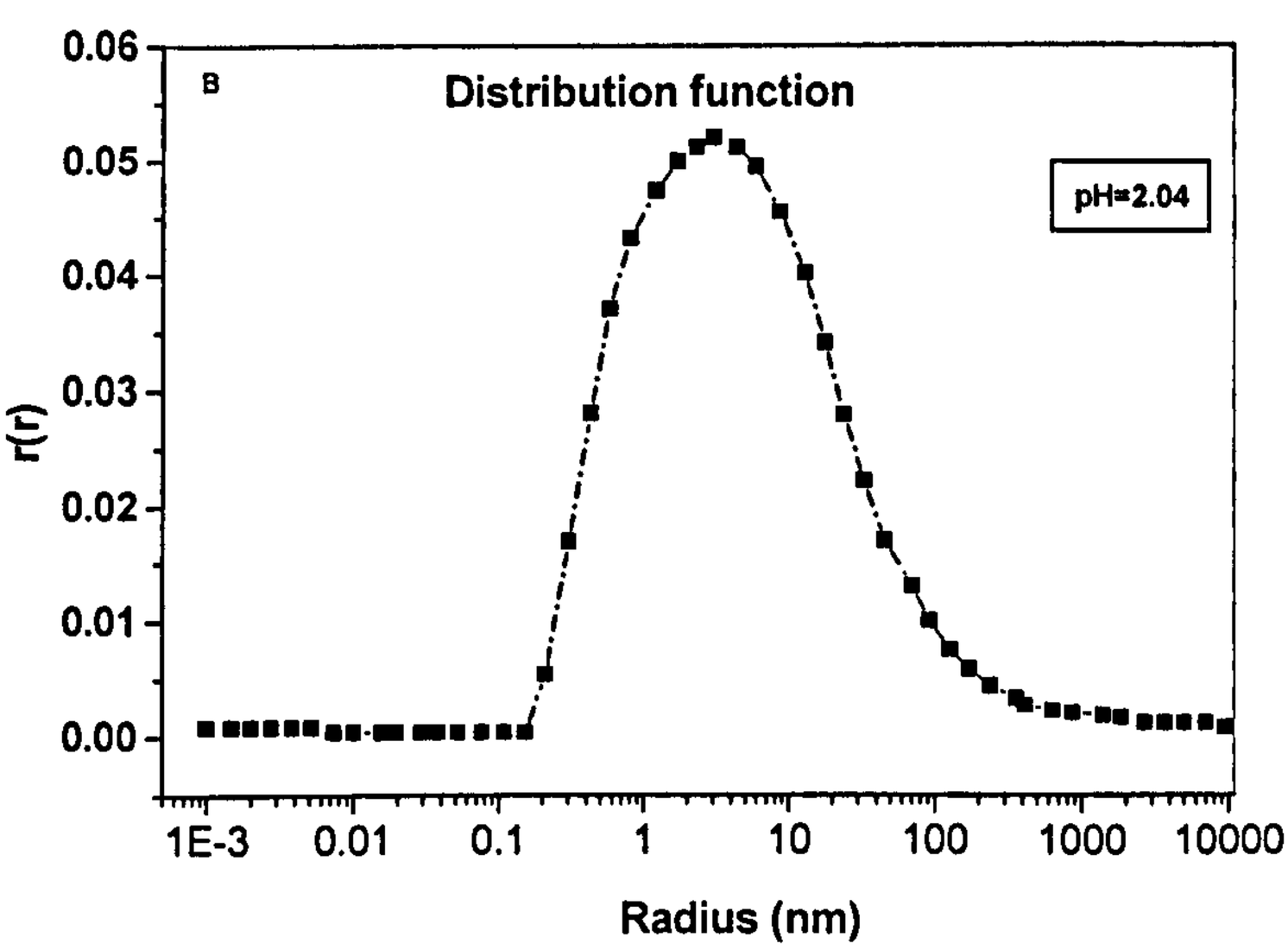

Figure 8.3.1 (A) The time-average intensity auto-correlation function and (B) particle size distribution in a solution of pH 2.04

Figure 8.3.2, parts (a), (b), (c), (d) and (e), shows particle size distribution functions of chitosan in solutions with pH values ranging from 2.53 to 5.49. Once the pH value of the chitosan solution reached 2.53, the main peak in the distribution function split into two peaks. This result indicates that multi-chain aggregation of chitosan in aqueous solution took place, which can be explained by the increase in the pH value of chitosan solution causing a decrease in the inter-chain electrostatic repulsion by the $-NH_3^+$ group, and also shows that the weak phase separation occurred in the solution. A comparison of the distribution functions for chitosan solutions of pH 2.53 and 3.10 shows that the larger peak moved to the right, indicating an increase in multi-chain aggregation. As the pH increased to 4.45, there was a noticeable decrease in the height of the second peak. This indicates that the majority of chitosan molecules have aggregated. As the pH increased to 5.49, there was a further decrease in the height of the second peak, so much so that it has almost merged with the larger, first peak. The larger peak, on the other hand, moved further to the right and became wider. The relationship between the pH of the solution and the strength of the inter-chain electrostatic repulsion has already been explained. Here, it is important to emphasise that there comes a point where the inter-chain electrostatic repulsion is so weak that they become insignificant compared to the van der Waals and dispersion forces. The effect of these latter forces is greater inter-chain attraction and the greater aggregation of the chitosan molecules. Overall, having regard to Figure 8.1 part (b) as well, one can see that as the pH increased from 2.04 to 4.45, the particle size increased steadily. As the pH increased to 5.49, the second peak continued to decrease in height. Furthermore, the experimental results showed that as the pH increased, the solubility of chitosan became poorer and the solution turned milkier.

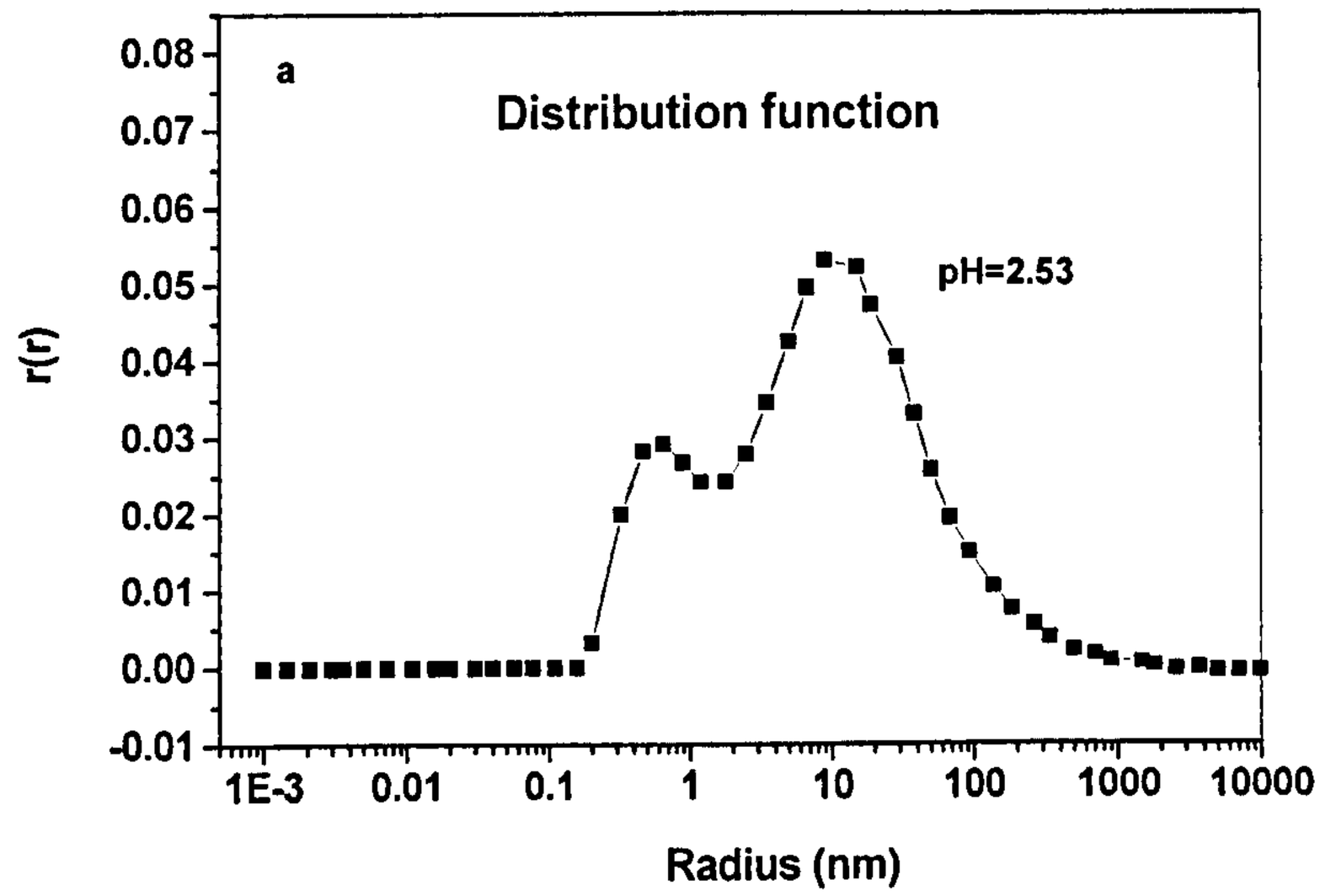
a
Distribution function
pH=2.53
r(r)
0.08
0.07
0.06
0.05
0.04
0.03
0.02
0.01
0.00
-0.01
1E-3
0.01
0.1
1
10
100
1000
10000
Radius (nm)

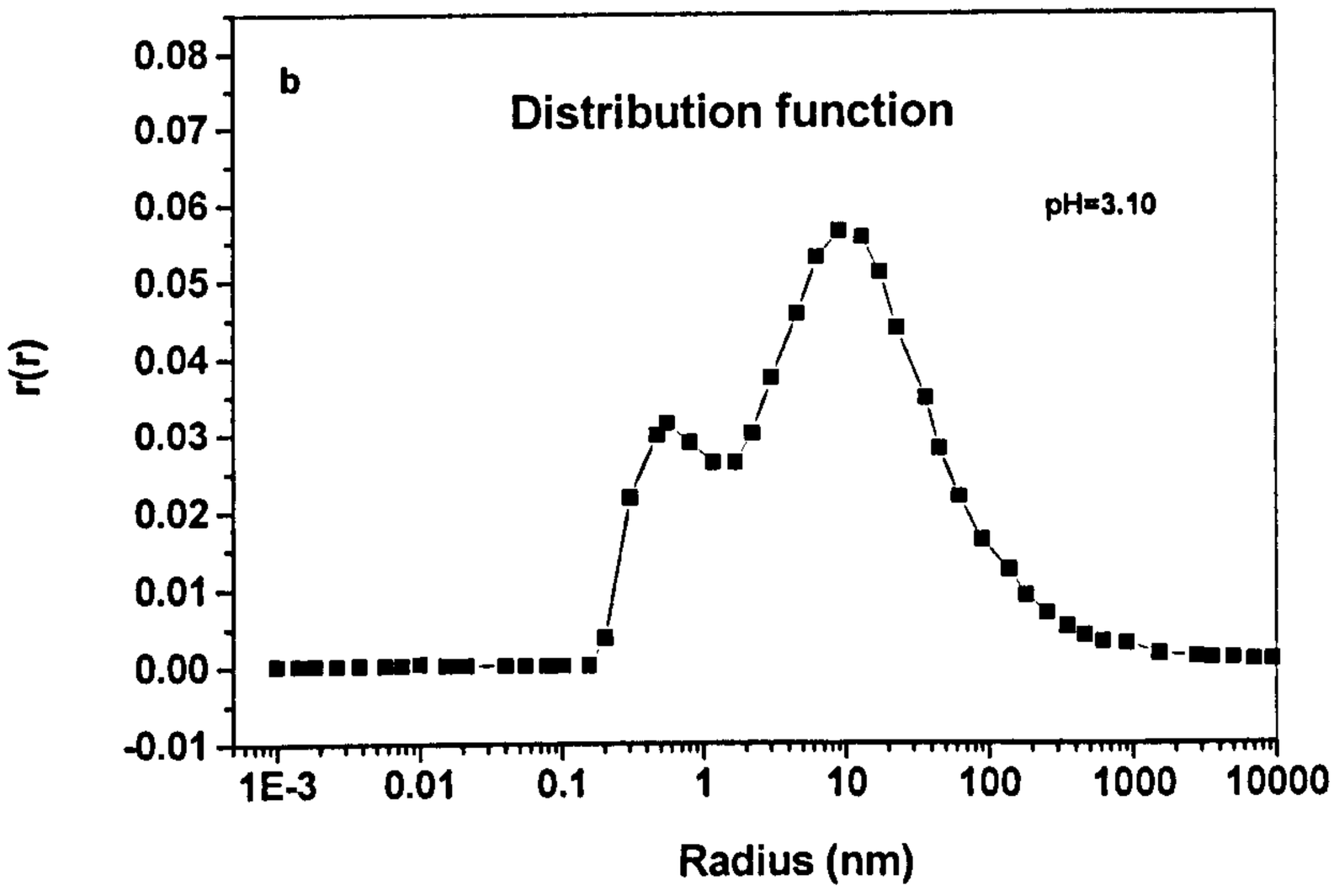
b
Distribution function
pH=3.10
r(r)
0.08
0.07
0.06
0.05
0.04
0.03
0.02
0.01
0.00
-0.01
1E-3
0.01
0.1
1
10
100
1000
10000
Radius (nm)

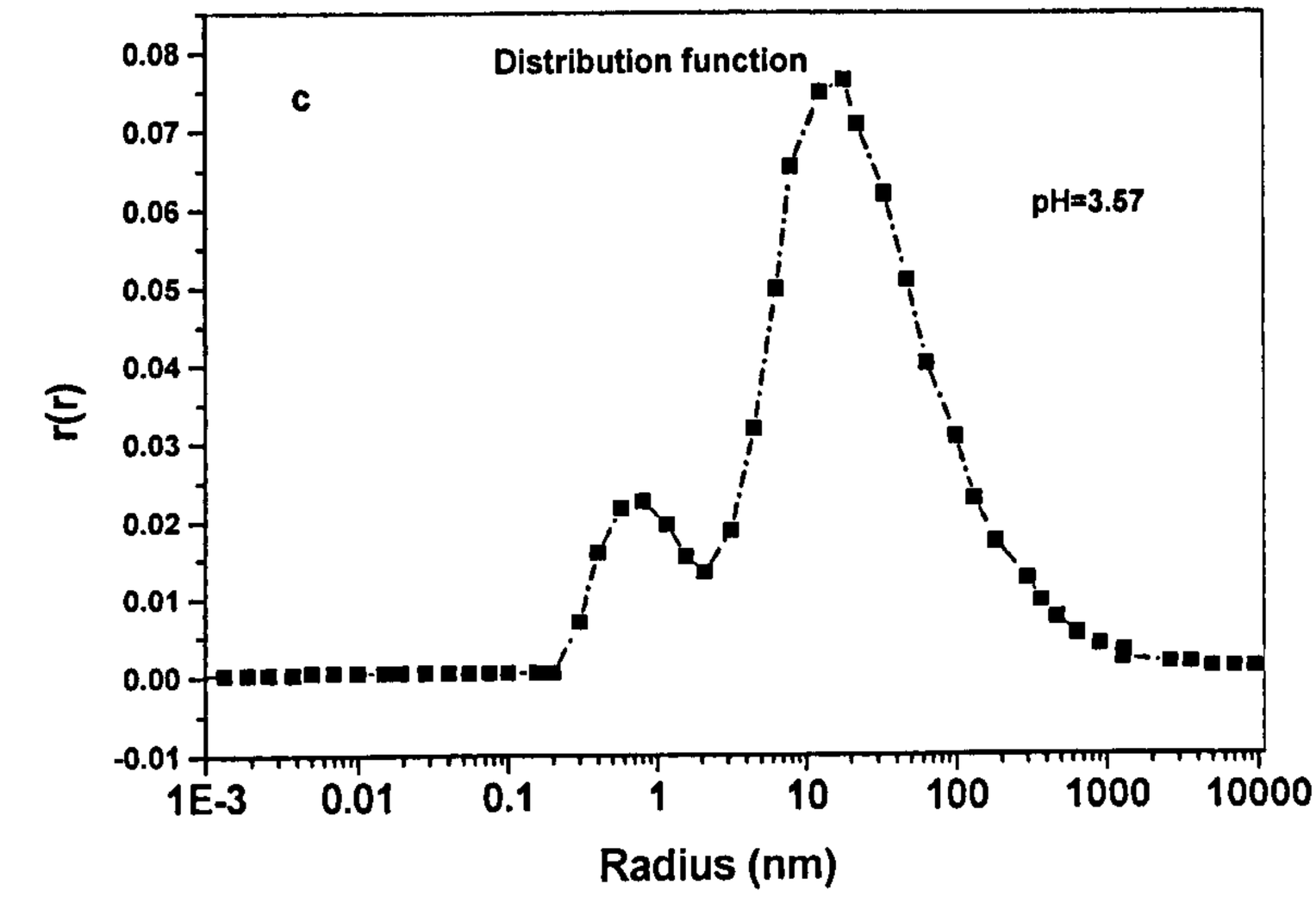
c
Distribution function
pH=3.57
r(r)
0.08
0.07
0.06
0.05
0.04
0.03
0.02
0.01
0.00
-0.01
1E-3
0.01
0.1
1
10
100
1000
10000
Radius (nm)

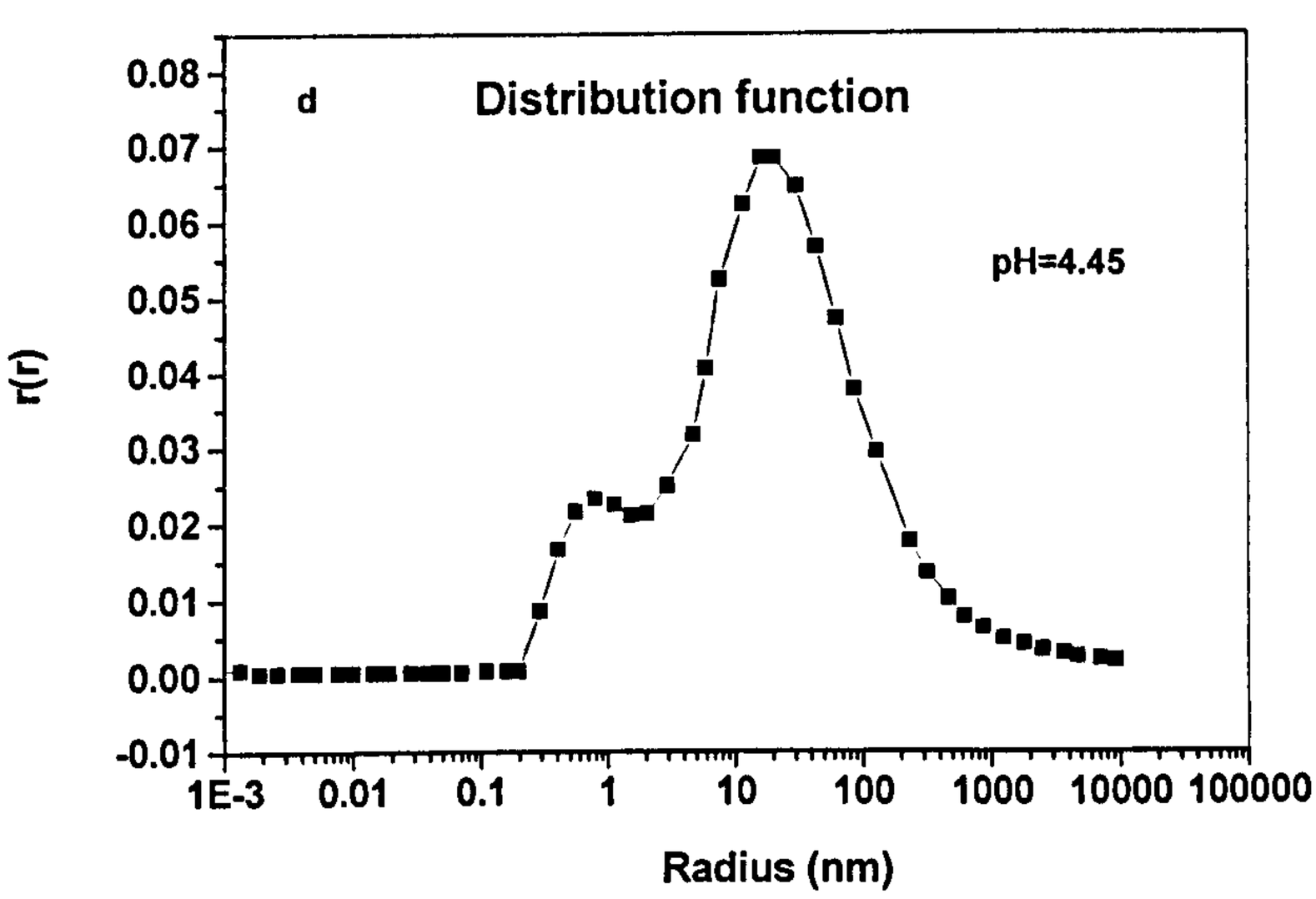
d
Distribution function
pH=4.45
r(r)
0.08
0.07
0.06
0.05
0.04
0.03
0.02
0.01
0.00
-0.01
1E-3
0.01
0.1
1
10
100
1000
10000
100000
Radius (nm)

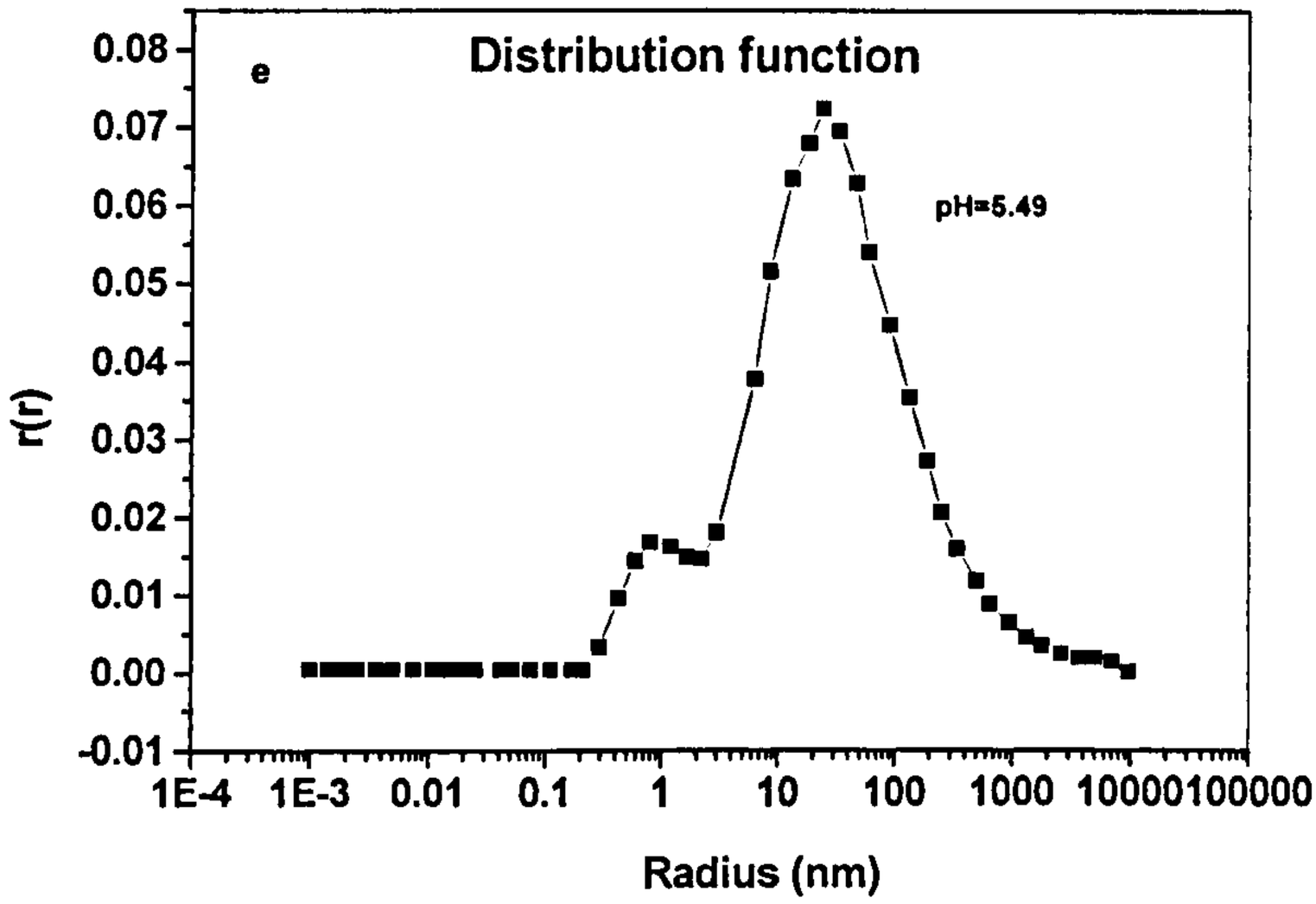

Figure 8.3.2 The effect of pH on chitosan macromolecular conformation in solution

The average radius of the particle can be calculated using Equations 8.2-13 and 8.2-14. The average particle size for chitosan macromolecules in the each solution with various pH values are summarised in Table 8.3.1.

Table 8.3.1 Summary of the results of particle size (R_s) for chitosan macromolecules in different pH solutions.

Sample No.	pH value	R_s (nm)	Ws (nm)*
1	2.04	65.5	39.0
2	2.53	123.7	89.8
3	3.10	113.7	69.5
4	3.57	189.2	145.7
5	3.89	212.5	173.2
6	4.45	280.2	204.4
7	5.49	356.5	242.2

* Half width of particle size distribution function.

It can be seen that the particle size of the chitosan macromolecules, R_s, increases as the pH value increases (see Figure 8.3.3). However, it can be seen that in lower pH values, the increase in particle size is smaller. Higher pH resulted in a stronger aggregation of the chitosan macromolecules.

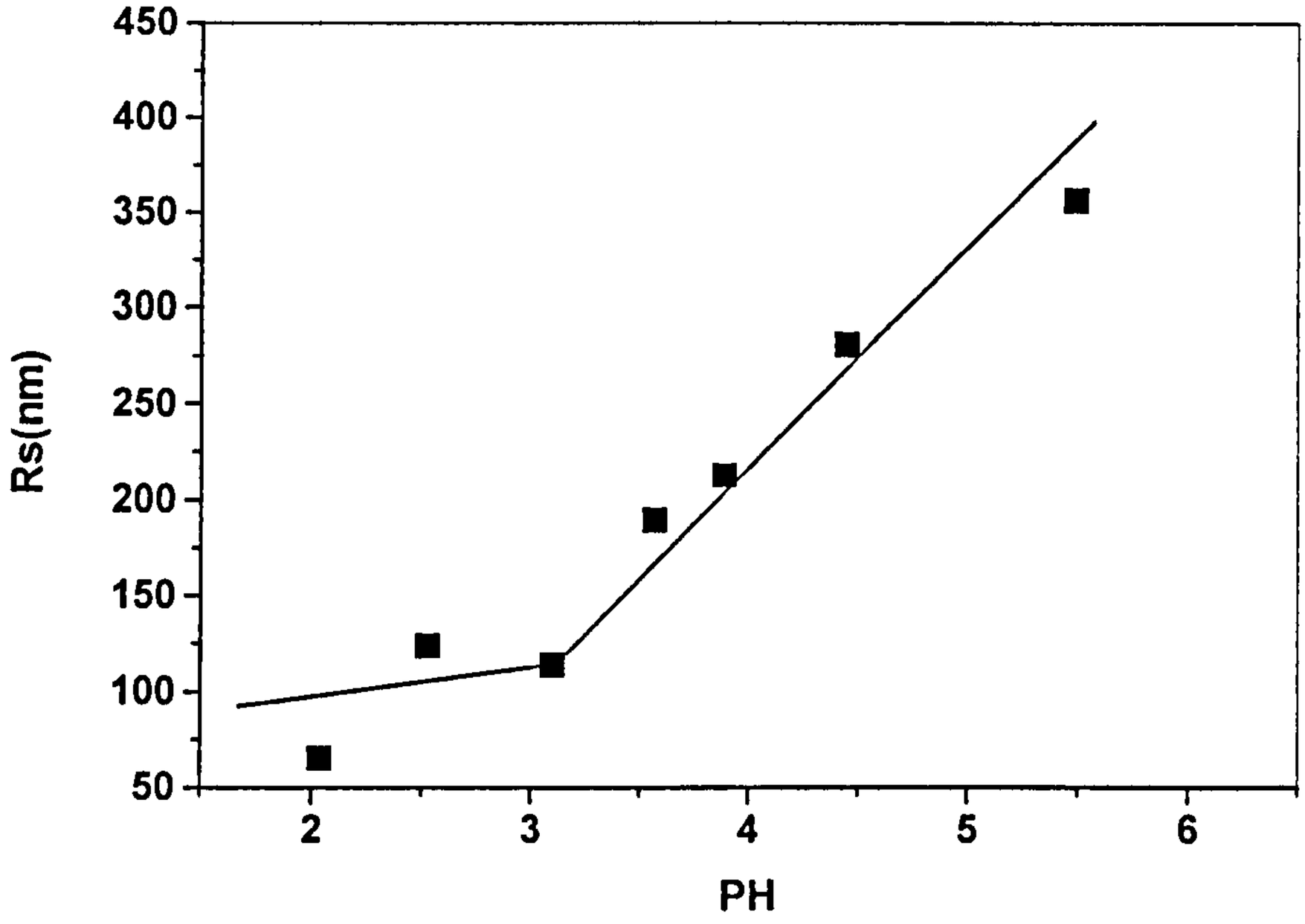

Figure 8.3.3 pH-dependence of the radius of chitosan particles in aqueous solution.

Based on polyelectrolyte solution theories [265], the intramolecular interactions along the chains are directly affected by the electrostatic repulsion arising from charges on the polymer chains. These interactions contribute to the local stiffness of the chain (i.e. the persistence length in the worm-like model of a chain molecule), affect the excluded volume in a good solvent and also impact upon the intermolecular interactions. The strength of the electrostatic interactions may be moderated by increasing the concentration of the $-NH_3^+$ groups, which screens the electrostatic repulsion on the polymer chains. However, excessive amounts of $-NH_3^+$ may significantly alter the solvent quality, which eventually leads to the weak phase separation of the polymer from the solution.

These results lead to the conclusion that the chitosan-solvent interactions must play an important role in the conformation of chitosan chains in acid solutions. The polymer chains in solution exhibit different conformations, which are mainly dependent on the chitosan-solvent interaction. In a good solvent, chitosan chains exist as a more extended coil, while in a poor solvent, inter-macromolecular aggregation occurs easily.

8.3.2 Single chain coil-to-globule transition (chain collapse)

A flexible polymer chain can change from an expanded coil to a collapsed globule, as first predicted by Stockmayer [266]. Since then, this prediction has been extensively studied both theoretically and experimentally [267,268]. It was concluded that there is a two-stage kinetics for the collapse of a single chain; a fast crumpling of the un-knotted chain followed by a slow knotting of the collapsed polymer chain. The transition between the coil and globule conformations of a polymer chain depends on the properties of both solvent (molecular structure) and polymer (molecular weight and structure) [268]. For a given polymer solution, the solvent can change from a good to a Θ solvent and finally to a poor solvent. When the solvent quality is poor, a flexible polymer chain collapses [269, 270]. Grosberg *et al.* [269] stated that there is a two-stage process of collapse. At the first stage, the chain density in its occupied volume quickly increases as the chain collapses, while at the second stage the chain density increases much more slowly during the rearrangement of the collapsed chain into the globule.

On the basis of the above concepts, to detect the globule state of isolated chains it is necessary to work at low concentration, so that the formation of multiple chain aggregates, which mask the coil-to globule transition, can be avoided, and where it is easier for individual chitosan chains to reach a collapsed state. For these reasons, a solution concentration of 10^{-6} g/ml was used instead of 10^{-4} g/ml. The scattering angle of 45° was used in this experiment due to the long distance between macromolecules in the dilute solutions.

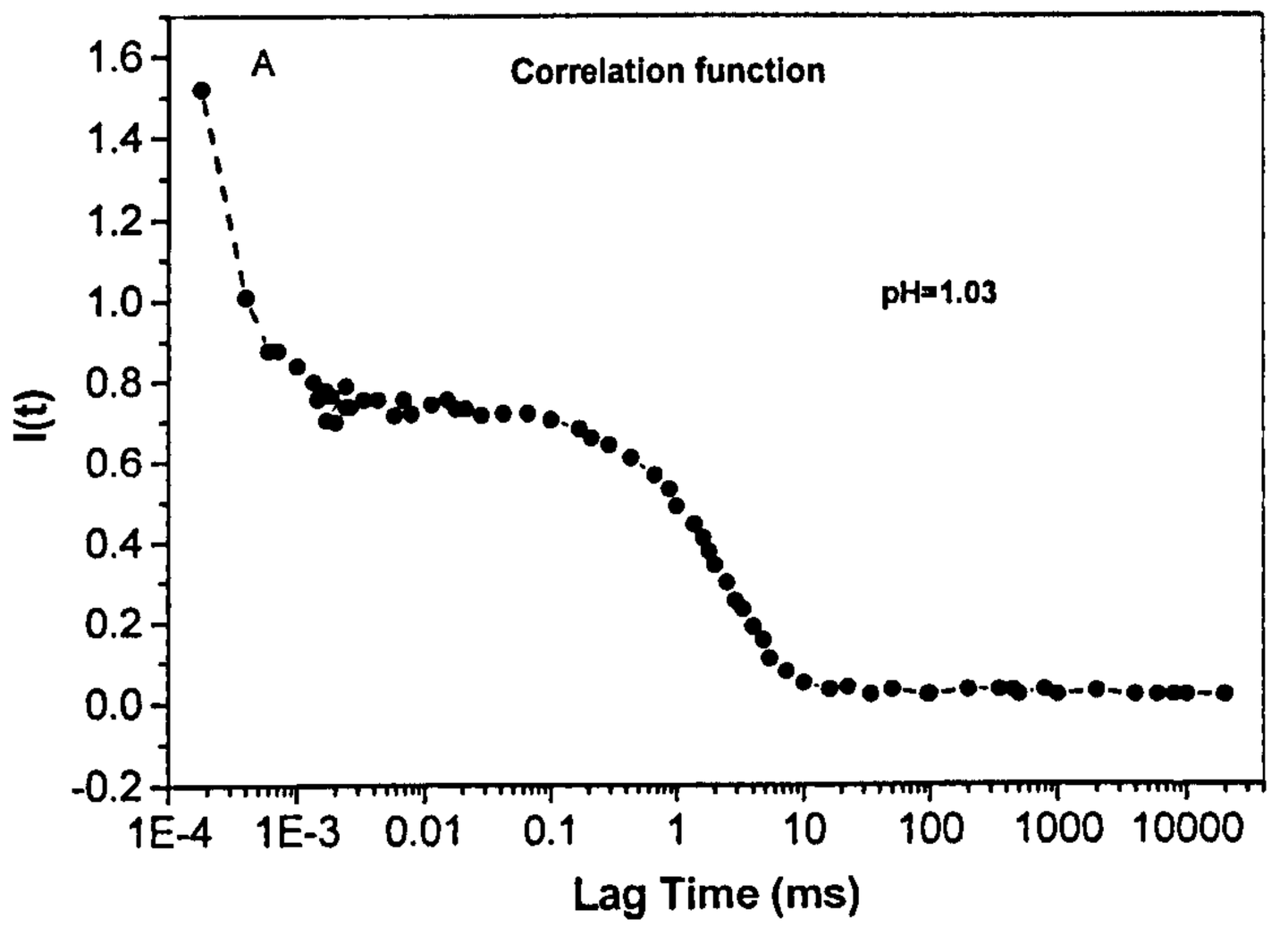

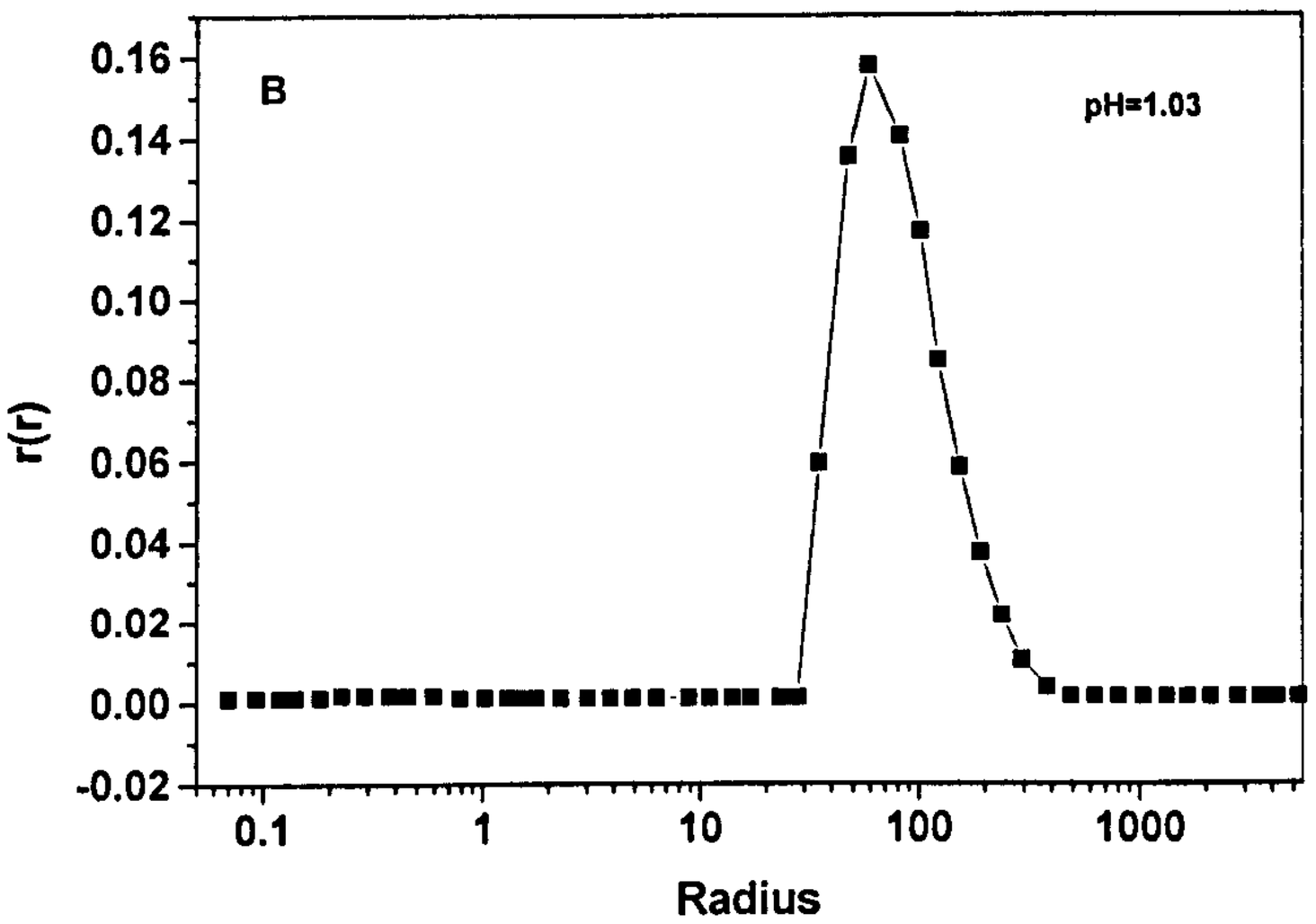

Figure 8.3.4 (A): the time-average intensity auto-correlation function and (B) particle-size distribution of chitosan macromolecules in a dilute solution of pH 1.03.

It is well known for a polydisperse sample that the species with the higher molecular weight will undergo phase transition first, which makes the whole solution into a thermodynamically unstable region [268-270]. It is also known that for a polyelectrolyte polymer the coil-to-globule transition is easier because of a relatively strong electrostatic interaction [268-270].

Figure 8.3.4, parts (A) and (B), shows, respectively, the correlation and particle-size distribution functions of chitosan macromolecules in a dilute solution of pH 1.03. It is clear that there is basically one peak in the distribution function. Figure 8.3.5 parts (a), (b), (c) and (d), shows the particle-size distribution function of chitosan macromolecules in various pH solutions.

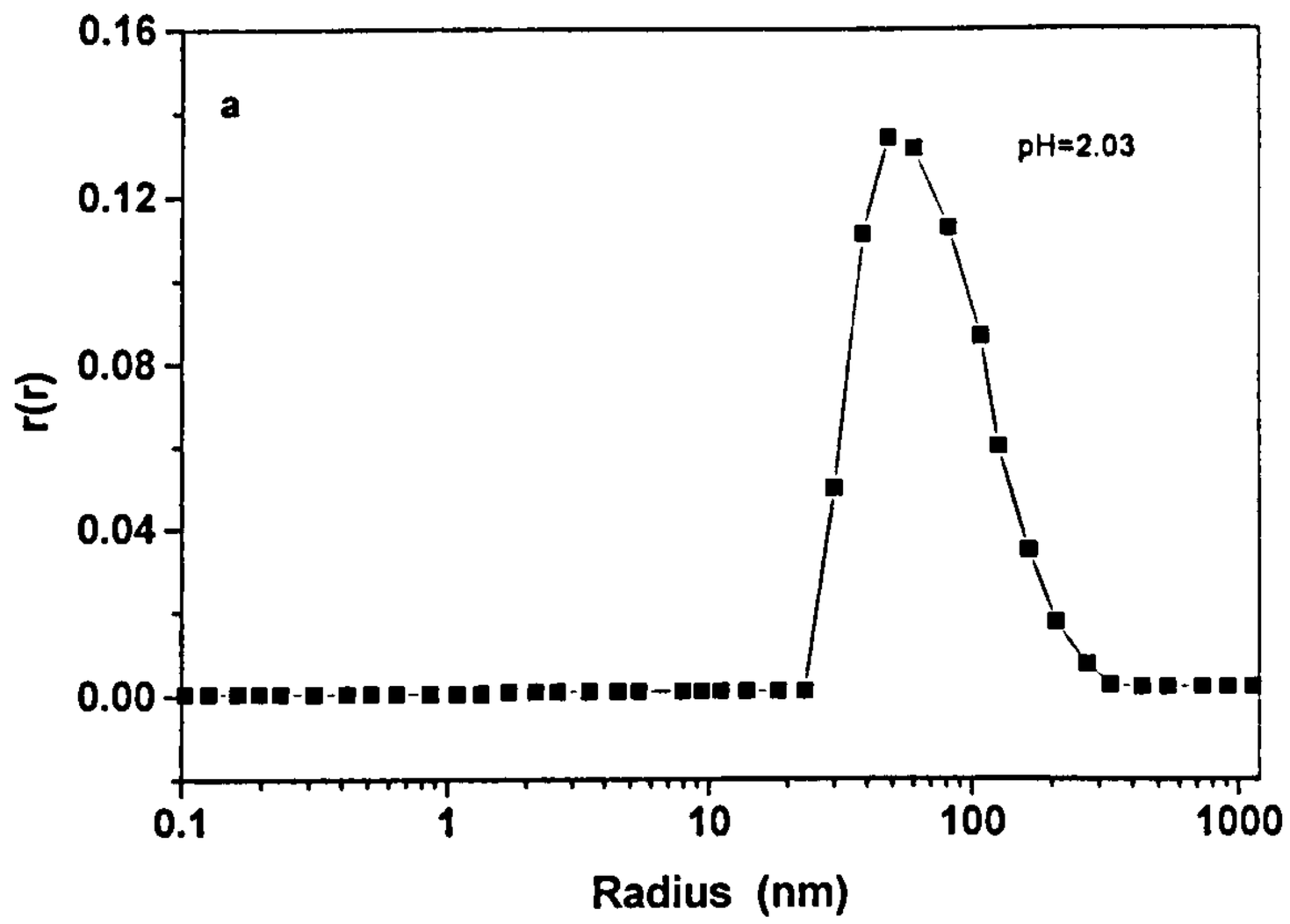

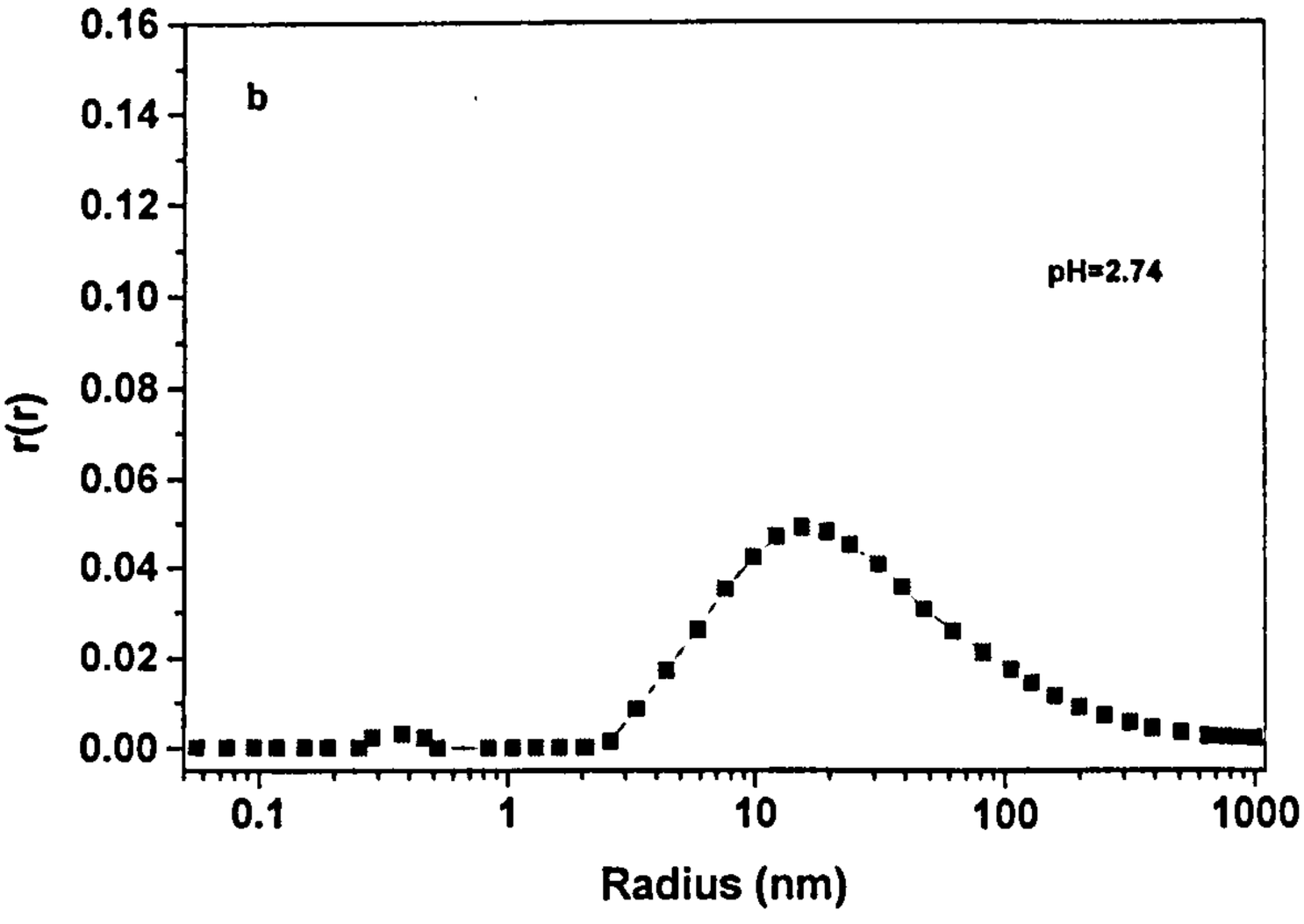

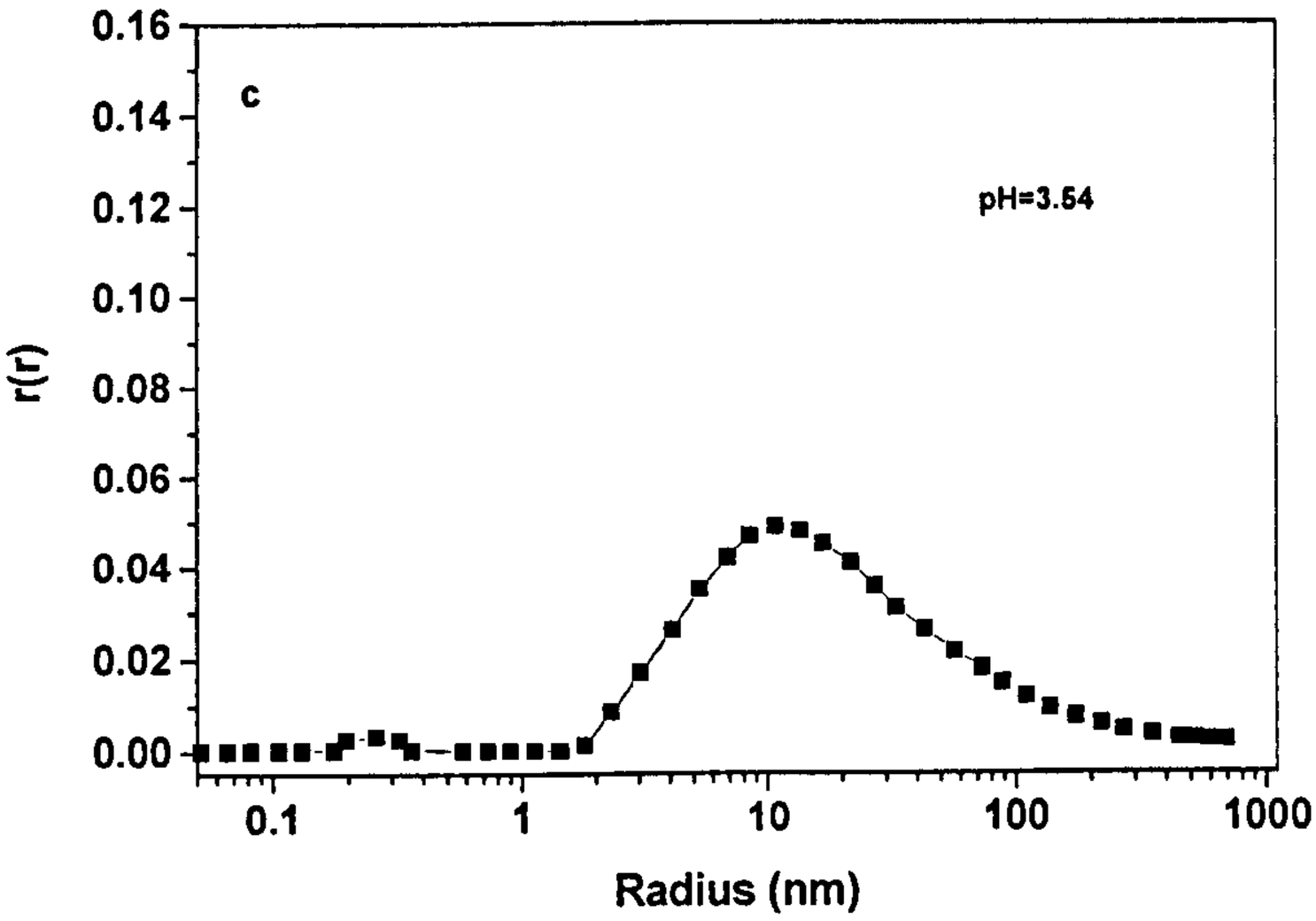

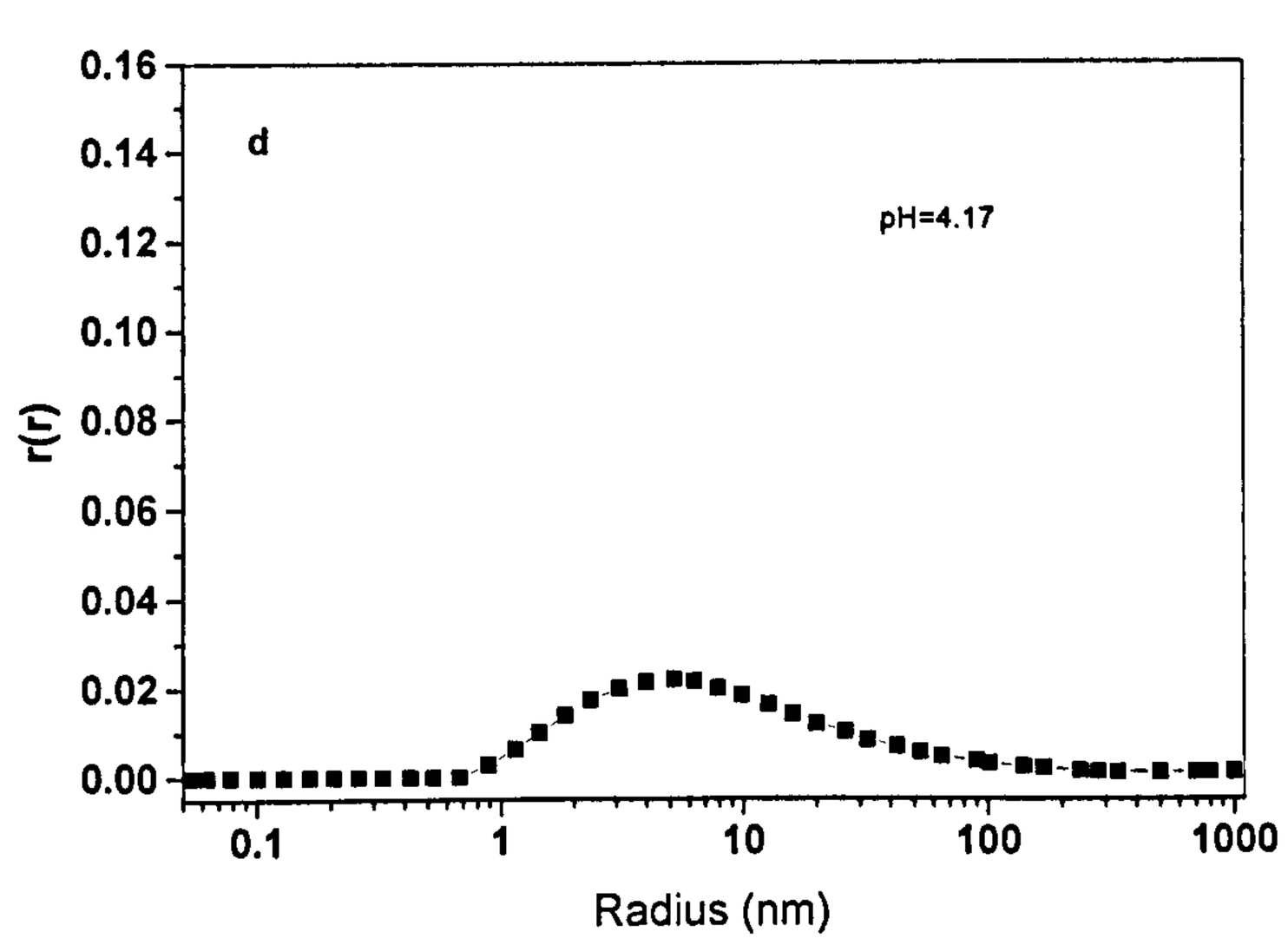

Figure 8.3.5 Effect of pH on chitosan macromolecular conformation in very dilute solutions.

A comparison of the data sets in Figure 8.3.5 clearly shows a leftward movement of the peak. This indicates a decrease in the radius of the chitosan macromolecules. The phenomenon of the single chain collapse of chitosan molecules has occurred [271,272].

The dilute nature of the chitosan solution leads to the existence of long distances between molecules and the only a small possibility of molecular aggregation taking place. For a particular chitosan macromolecule, the increase in the pH of the solution resulted in a decrease in the concentration of the $-NH_3^+$ groups, which caused a decrease in the solubility of chitosan in acetic acid solution. The decrease in $-NH_3^+$ concentration also led to a decrease in intra-molecular electrostatic charge repulsion, which gave rise to the single chain collapse. The end result of this was the reduction in the radius of chitosan macromolecules.

It is obvious from Figure 8.3.5 that when the pH of the chitosan solution increased from 2.03 to 2.74, there was a further leftward movement of the peak. This indicates an increase in the severity of the single chain collapse phenomenon. A further increase in the pH of the solution led to a further decrease in the concentration of the $-NH_3^+$ ions, and, therefore, one in the intra-chain electrostatic charge repulsion. As the pH of chitosan solution increased to 3.45 and then to 4.17, the leftward movement of the peak continued and there was an increase in the width of the peak, indicating further reduction in the size of the individual chains. This reflects the inter-chain coil-to-globule transition.

From the above experimental data, the particle sizes of chitosan macromolecules were calculated and are summarised in Table 8.3.2. Figure 8.3.6 shows the dependence of the radius of chitosan macromolecules on pH. The particle size of the chitosan macromolecules decreased with increasing pH value. When pH value increased from 2.74 to 3.54 and then to 4.17, the radius decreased sharply to 98.76nm and 50.73nm, respectively. In low-pH dilute solutions, the chitosan chains adopt an extended random coil conformation, because of electrostatic repulsion by the NH_3^+ groups, which result in the larger radius of chitosan chains. The solution is transparent. In

high pH solutions, the chains adopt compact coils because of the poor solvent quality. The solution is milky. These results suggest that in dilute solution the main driving force of the chitosan phase transition is the intra-chain forces, which can be much stronger than the inter-chain forces. Thus, in dilute solution, it should be easier for the individual chitosan chains to reach a collapsed state. The inter-chain association is relatively less likely than inter-chain collapse.

Table 8.3.2 The summary of the results for single chain collapse

Sample No.	pH value	Rs (nm)	Ws (nm)
1	1.03	196.1	90.2
2	2.03	194.0	82.6
3	2.74	205.1	98.1
4	3.54	127.2	50.3
5	4.17	76.4	25.2

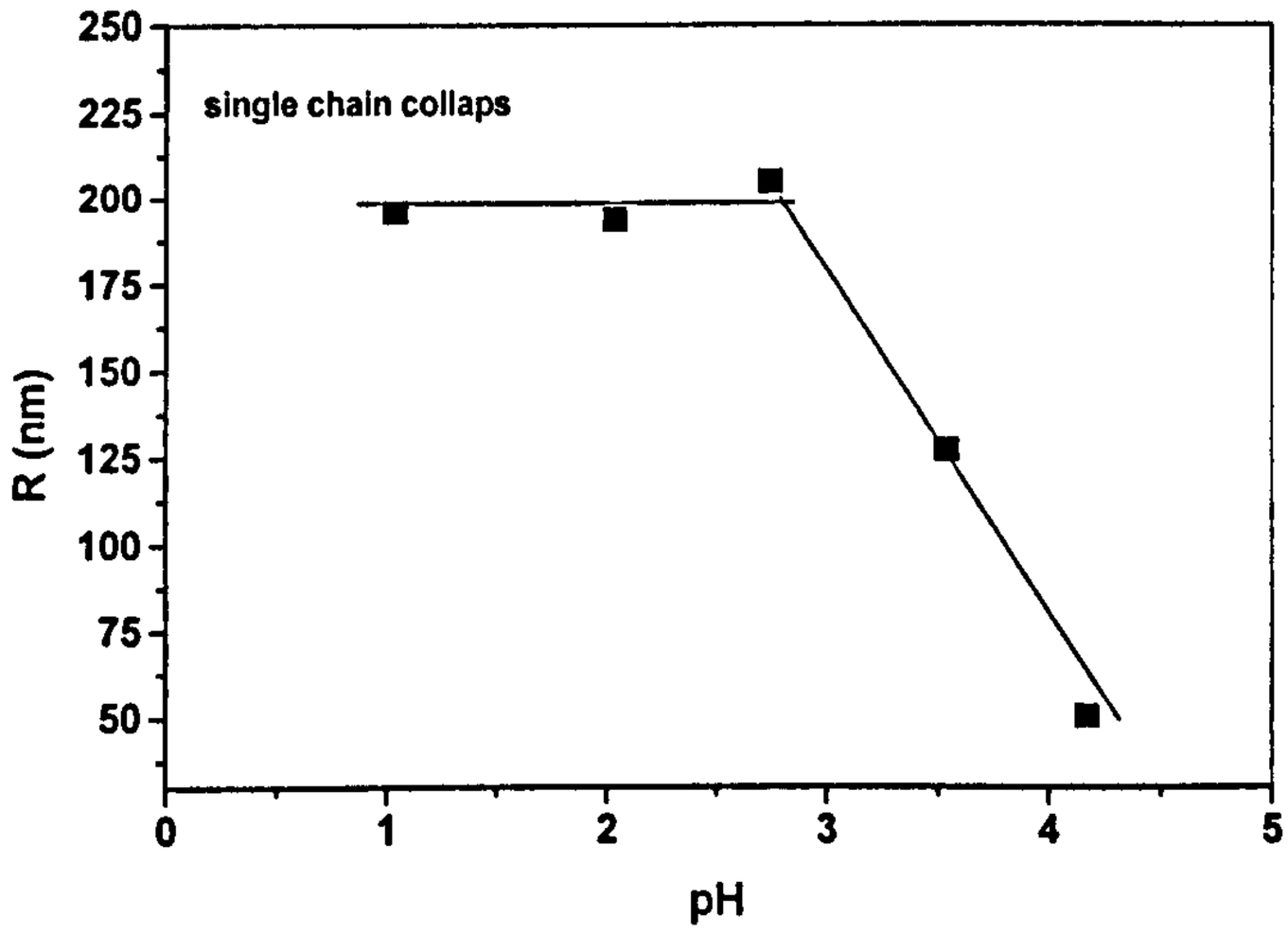

Figure 8.3.6 pH-dependence of the radius of chitosan particles in dilute solution.

There was a transition in the single chain conformation of chitosan molecules from coil to globule. It was found that the coil-to-globule transition depends on the pH of the dilute chitosan solution.

Figure 8.3.7 is a schematic diagram of the intra-chain collapse of chitosan chains in solution when the pH is changed. It can be seen that the greater the pH the smaller the size of the chitosan molecules and the greater the chain density.

Changes in the rheological properties of chitosan solutions with pH, ionic strength, and type of anion have been studied [262]. Between pH 2.0 and 5.0, the apparent viscosity increased with the decrease of pH in chitosan-organic acid solutions. Recently, Pa [263] studied the intrinsic viscosity of chitosan in dilute acetic acid solutions. These results show that the intrinsic viscosity increased with decreasing pH. This suggests the chain expansion of the chitosan molecules with increasing acetic acid concentration in water solution, which is in agreement with our results.

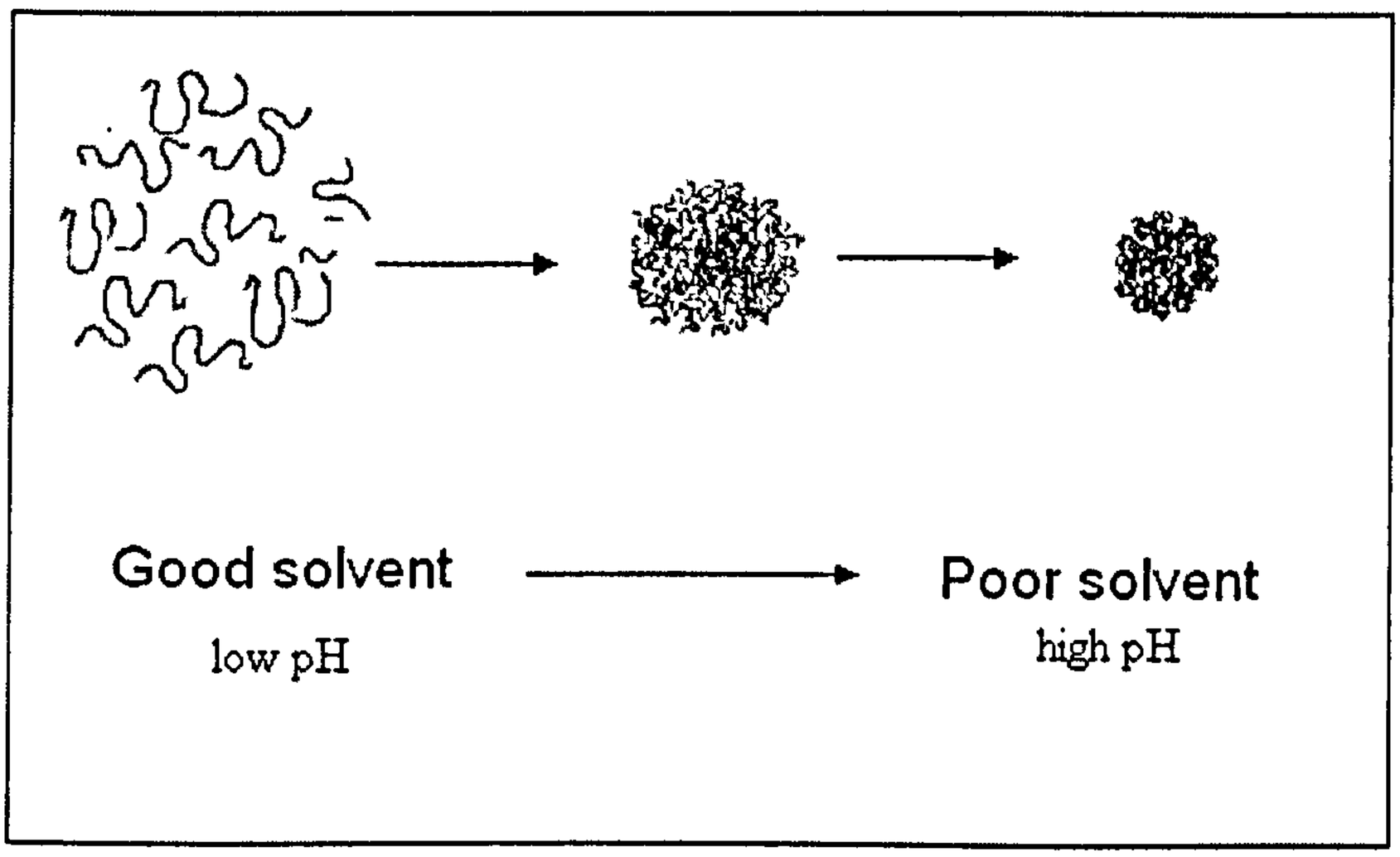

Figure 8.3.7 Schematic diagram of the single chain collapse of chitosan macromolecules in solution when the pH value is changed [263]

From the above discussion, it can be concluded that at a low pH, chitosan chains are homogenous in solution without liquid-liquid phase separation, and that when the pH increased, the chitosan chains became heterogeneous in the solution: the transition being the result of the collapse of the chains to globules. Phase separation also occurred.

8.4 Effect of Aggregation Behaviour on Mechanical Properties of Chitosan Films

The effect of the pH of the chitosan solution used in the preparation of the chitosan films on the films' mechanical properties were investigated in Chapter 5. The pHs of the solutions were 2.5, 3.0, 4.0 and 5.0. The results clearly indicate that there is a direct relationship between the two: the more acidic the solution, the greater the tensile stress and the larger the percentage elongation at break. When the solution was of pH 2.5, the values of both properties were double those when the solution was of pH 5.0.

One of the important factors affecting the physical properties of a material, including its mechanical properties, is its super-macromolecular structure or morphology. The morphology of a material depends on the components present, the fabrication methods used in sample preparation and so on. To get a better insight into the mechanical behaviour of the chitosan films in terms of tensile strength and elongation at break, a more detailed knowledge of morphology of the chitosan solution at different pH is required.

Figure 8.3.1 (B), part of the above discussion on the light scattering results, clearly shows that only one peak exists at pH 2.04 in the distribution function. As the pH increased from 2.04 to 2.53, the peak split into two peaks (as seen in Figure 8.3.2). This points to the chitosan backbones folding up to form compact coils and the chitosan chains becoming more favourable to intermolecular aggregation, which is caused by the poor solubility in solutions of high pH values. This also means that

phase separation in the solution existed. The higher pH the stronger was the degree of phase separation in solution. When the pH 2.04 solution was used to prepare a chitosan film, a homogenous solution structure may be obtained, and the chitosan chains became more expanded as a result of the mutual repulsions by the $-NH^{+}_{3}$ ions along the chitosan backbone. This expansion leads to easier interpenetration, or entanglement, of chitosan chains. The effect of this is to increase the opportunity for intermolecular association, resulting in the end in a homogenous gel network. When the solution pH was higher it means that a comparatively heterogeneous networks have formed. Applying a force to these films may lead to crack propagation along the phase boundaries (formed because of phase separation), which could explain the poor tensile strength and the low elongation at break of these chitosan films. However, for crosslinked chitosan films, the interfacial boundaries may be smeared by crosslinking. The fracture behaviour could be the same for the crosslinked films formed at lower and higher pHs. The pH will have little influence on stress at break (See Figure 5.4.2 (A) in Chapter 5). Although crosslinking can smear the interfacial boundaries, the morphology of networks formed at lower pHs are different from that formed at higher pHs. The structure of networks formed at lower pHs was homogeneous, but heterogeneous structures formed at higher pHs were revealed by the results of static light scattering. The homogeneous networks led to higher elongation at break (See Figure 5.4.2 (B) in Chapter 5).

The preceding discussion indicates that the pH of a chitosan solution can control the degree of the chain aggregation or phase separation. Therefore, by changing the solution pH, it is possible to control the mechanical properties of chitosan films in a way which is now clear.

8.5 Conclusions

The aggregation behaviour of chitosan macromolecules and the coil-to-globule transition of a single chain of chitosan in solution at different pHs were examined by the static light scattering technique. The results show that the conformation of chitosan macromolecules in solution was influenced by pH values. In chitosan solutions of a low pH, the chitosan chains exhibit a more extended conformation and

in high pH solutions, they have a tendency to aggregate. In the dilute chitosan solutions, the coil to globule transition of single chains exists when solubility of chitosan in the solvent became poorer. The aggregation behaviour of chitosan macromolecules in solution has a clear influence on mechanical properties of chitosan films. In low pH solutions, a homogenous gel network was formed due to intermolecular chain association during gelation, resulting in better mechanical properties (tensile strength and elongation at break) of these chitosan films.

CHAPTER 9

Evaluation of Chitosan/PEO Blend Films Crosslinked by Genipin for Controlled Drug Release and Protein Separation

9.1 Introduction

Controlled drug release technology first emerged in the 1980s as a commercially sound methodology of extending existing ways of administering pharmaceutical therapies [4]. Conventional dosage forms often lead to wide swings in serum drug concentrations [133-136]. The safety and therapeutic efficacy of current treatments may be improved if their delivery rate, biodegradation, and site-specific targeting can be predicted, monitored and controlled.

In recent years, considerable research efforts have been directed towards the development of safe and efficient drug delivery systems with the use of polymers as agents for the controlled release of drugs from various types of formulated products, such as tablets, implants, and adhesive strips. Evidence of the high degree of interest in the design of such dosage forms is provided by the number of reviews [273,274] and books [275, 276] that have been concerned with the subject. The release of drugs, absorbed or encapsulated by polymers, involves their slow and controlled diffusion from, or through, polymeric materials. Drugs covalently attached to biodegradable polymers or dispersed in a polymeric matrix of such macromolecules may be released by erosion or degradation of the polymer [273-276]. Therapeutic molecules, complexed by polymers, may also be released from gels by diffusion [273-276].

Chitosan is a naturally occurring polysaccharide with excellent biodegradable and biocompatible characteristics. Because of its unique polymeric cationic character, gel and film-forming properties, chitosan can be a suitable matrix, available in different forms, for sustained release of various drug formulations

Hydrogels based on chitosan have been widely used in controlled-release systems [277,278]. Hydrogels are highly swollen, hydrophilic polymer networks that can absorb large amounts of water and drastically increase in volume, while maintaining

their three-dimensional structure [277,278]. The three dimensional structure is often described as a mesh, with spaces between the polymer chains filled with water. The crosslinks can be formed by covalent or ionic bonds, van der Waals forces, hydrogen bonds, or physical entanglements [279]. It is well known that the physicochemical properties of hydrogels depend not only on the molecular structure, the gel structure, and degree of crosslinking, but also on the content and state of water in the hydrogel.

Based on chitosan, pH-sensitive hydrogels have been developed. They have potential use in site-specific delivery of drugs to specific regions of the gastrointestinal tract [5,40,137.]. These polymers are expected to reside in the body for a longer period and respond to local environmental stimuli to modulate drug release [239].

As indicated in the previous literature review, conscious of the limiting effects of the poor mechanical properties of chitosan upon its application, drug delivery formulations based on chitosan (such as films, beads, microspheres etc.) have been prepared by chemical crosslinking with glutaraldehyde etc [4]. However, the chemical crosslinking agents may induce toxicity and other undesirable effects, for example, chemically synthesized glutaraldehyde can cause irritation to mucosal membranes due to its toxicity [15,182,183,280].

In the preceding chapters, we have discussed chitosan/PEO blend films crosslinked by genipin that are pH-sensitive and have desirable mechanical properties. These characteristics and the film's non-poisonous nature [15], make it ideal for development as a controlled drug release delivery system. In this chapter, the potential for such development is investigated.

9.2 Vitamin B_{12} Release Through Chitosan and Chitosan/PEO Blend Membranes

In this section, investigations of the permeability and diffusion rate of chitosan and chitosan/PEO blends, crosslinked by genipin, were carried out using diffusion cells. vitamin B_{12} was used as the model drug.

9.2.1 Free volume theory of diffusion

In general, solute transport through a polymer membrane is described in terms of two mechanisms: the pore mechanism [281,282] and the partition mechanism [281,282]. In the pore mechanism, the solute diffuses through the water-filled pores or microchannels. The permeability is determined by the average pore size in relation to the molecular volume of the solute and the water solubility of the solute [281,282]. In the partition mechanism, the solute transport is presumed to occur by a process involving the dissolution of the solute within the polymer followed by diffusion through the membrane. Solubility parameters for the system determine the permeability for the most part in such a model based on solution diffusion [281,282].

Molecular transport regulated by free volume was first introduced by Cohen and Turenbull [283]. According to this theory, the solute diffuses by jumping into voids formed in the solvent space by the redistribution of the free volume within the liquid. It is assumed that the free volume can be redistributed without any energy change. The voids are pictured as being formed by a general withdrawal of the surrounding liquid molecules due to random thermal motion. These holes are then filled in by the reverse processes [283].

Solute self-diffusion is dependent on the jumping distance, the thermal velocity of the solute and the probability that there is a hole free volume adjacent to the molecule [283]. At a given temperature, where the rate of diffusion is determined by the probability of a void being formed of sufficient volume to accommodate the solute in the liquid at infinite dilution, the self-diffusion coefficient, D_0, is expressed as

$$D_0 \propto V\lambda \exp\left(-\frac{\gamma v^*}{v_f}\right) \qquad [9.2\text{-}1]$$

in which V is the average thermal velocity, λ is the jumping length roughly equivalent to the solute diameter, v^* is the critical local hole free volume required for a solute molecule to jump into a new void, γ is a numerical factor used to correct for overlap

of free volume available to more than one molecule ($0.5 \leq \gamma \leq 1$), and v_f is the average hole free volume per molecule in the liquid.

Yasuda *et al.* [284,285] were the first to apply this theory to solute diffusion in gels. Within the gel, in addition to the requirement of finding a sufficient free volume within the liquid, the solute molecule also needs to find an opening between the solute chains large enough to allow its passage. Thus, the diffusivity of a solute in the gel is given by the product of the probabilities of finding a proper free volume and a proper opening within the chains. According to this concept, Equation 9.2-1 yields the following expression for diffusion in a gel [284,285].

$$\frac{D_{gel}}{D_0} = p_0 \exp\left(-\frac{Ba^*}{v_{f,w}}\left(\frac{\varphi}{1-\varphi}\right)\right) \qquad [9.2\text{-}2]$$

In Equation 9.2-2, p_0 is the probability of finding an opening between the polymer chains, a^* is the effective cross-section area of the solute molecule, B is an undefined constant of proportionality, φ is the volume fraction of polymer in the gel and $v_{f,w}$ is the free volume per molecule of the water.

Based on the free volume theory, a theory for solute diffusion through hydrated polymer membranes was developed by Yasuda *et al.*, which they indicated explained the experimental results of the dependencies of solute diffusion coefficient on the solute size and degree of swelling. Peppas and Reinhart presented a similar physical model for solute diffusion [286]. According to this theory, the normalized solute diffusion coefficient, that is the ratio of the solute diffusion coefficient in the swollen gel membrane, D_{gel}, to that in pure water, D_{water}, is expressed as follows.

$$\frac{D_{gel}}{D_{water}} = B(v_d)\exp\left(-\frac{\pi r_s^2 l}{V_l(Q_m - 1)}\right) \qquad [9.2\text{-}3]$$

or

$$\frac{D_{gel}}{D_{water}} = B(v_d)\exp\left(-\frac{\pi r_s^2 l(1/H-1)}{V_l}\right) \qquad [9.2\text{-}4]$$

Here, r_s is the Stokes hydrodynamic radius, l is the characteristic length, V_l is the average free volume of water, Q_m is the volume degree of swelling of the network and H is the volume fraction of water in the gel membrane. The term $B(v_d)$ denotes the probability of a diffusion species of volume v_d finding a mesh of a volume of at least v_d, formed by the crosslinked chains of the polymeric network. By assuming that the normalized diffusion coefficient is linearly related to the mesh size, Peppas and Reinhart derived the expression for $B(v_d)$ and presented the following equation [286].

$$\frac{D_{gel}}{D_{water}} = k_1\frac{(M_c - M_c^*)}{(M_n - M_C^*)}\exp\left(-\frac{k_2 r_s^2}{Q_m - 1}\right) \qquad [9.2\text{-}5]$$

Here M_c is the average molecular weight between crosslinks, M^*_c is the threshold value of M_c, below which no diffusion of solute can occur, M_n is the average molecular weight of the polymer before crosslinking, and the constants k_1 and k_2 are structure parameters.

They demonstrated that the experimental data showed reasonable linear dependencies between $\log(D_{gel}/D_{water})$ and r_s^2 and between $\log(D_{gel}/D_{water})$ and $1/(Q_m\text{-}1)$, as expected by Equation 9.2-5.

Reinhart and Peppas [286] have investigated the influence of crosslinking on diffusive properties. They showed that the normalized diffusion coefficient depends on the value of M_c. However, it was concluded that the linear dependence of the diffusion coefficient on the mesh size, which is expressed by Equation 9.2-5, was not correct. Thus, the appropriate expression for the probability $B(v_d)$ has not been presented.

Based on the free volume consideration, the normalized diffusion coefficient in a gel membrane is expressed as Equation 9.2-3. In order to make this theory more quantitative, the term $B(v_d)$ must be determined. The term $B(v_d)$ is a proportionality

factor dependent upon the size and shape of the mesh formed by the crosslinked chains [285]. The characteristics of $B(v_d)$ are as follows. For chains far apart from each other so that there are no entanglements, the solute diffusion is not obstructed by the chains. In such a case, $B(v_d)$ must be unity unless there is no interaction between polymer chain and solute. On the other hand, when the polymer chains are well crosslinked and no solute diffusion occurs, $B(v_d)$ must be zero.

The gel membrane usually has high water content, that is, a large pore portion in the total volume. In such gel membranes, the partition coefficient occasionally may be determined simply by the space volume (mesh size) rather than the interaction between the solute and polymer chains. Furthermore, it is well known that the network of the gel fluctuates in time and space. However, the cooperative diffusion coefficient of the gel is much smaller than that of the small solute [287] and therefore, the gel polymer network behaves as a fixed obstacle for diffusion of small molecules in the gel [288]. It follows that the gel membrane can be treated as a rigid porous material. When the interaction between the solute and the polymer is negligible and the water content in the gel membrane is high, the diffusion coefficient of the solute is determined only by the mesh size of the polymer network and the size of solute [287]. In this case, the probability of a diffusion species of volume v_d finding a mesh formed by the crosslinked chains of the polymer network, $B(v_d)$, depends on the size and shape of the mesh formed by the crosslinked chains. Recently, a new equation based on the free volume theory for crosslinked poly(vinyl alcohol) was presented by Mastuyama [289] as follows.

$$\frac{D_{gel}}{D_0} = K' \exp\left(-\frac{\pi r^2 l(1/H-1)}{V_f}\right) \qquad [9.2\text{-}6]$$

In this equation, the partition coefficient was introduced as the probability of a diffusing species finding a mesh. A linear relationship between $\ln(D_{gel}/D_{water}K')$ and $1/(H-1)$ was obtained for the crosslinked poly(vinyl alcohol).

9.2.2 Vitamin B_{12} release

Vitamin B_{12} was dissolved in phosphate saline (PBS) (pH = 7) solution to prepare solutions with a series of concentrations. Figure 9.2.1 shows UV spectra for the vitamin B_{12} solutions. A strong absorption peak was observed at 361nm, which is indicative of the concentration of vitamin B_{12} solutions. Figure 9.2.2 is the plot of a calibration curve of absorbance (at 361nm) against concentration. In the vitamin B_{12} release study, this standard curve was used to determine an unknown concentration of vitamin B_{12} solution.

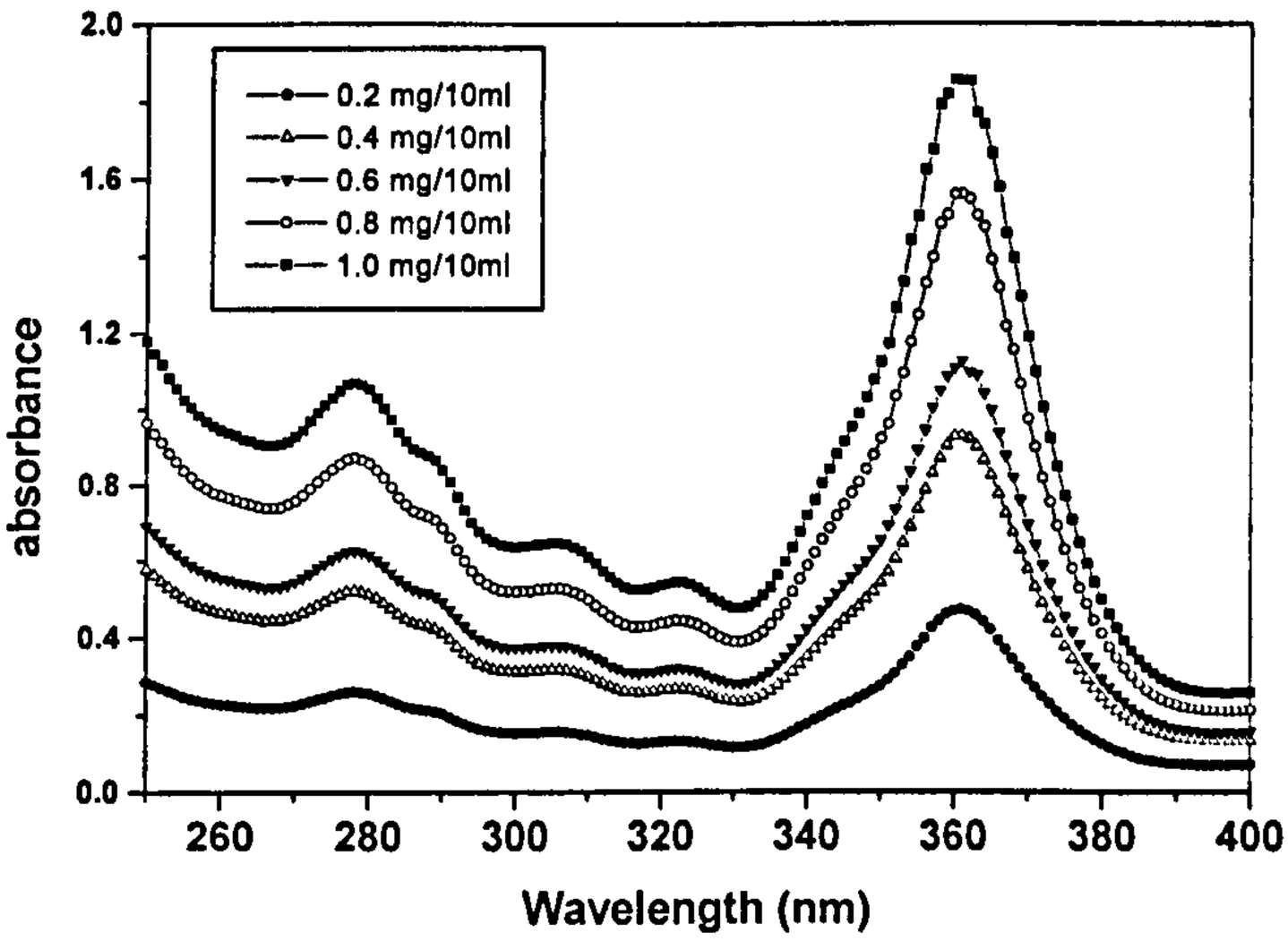

Figure 9.2.1 UV spectra of vitamin B_{12} at different concentrations

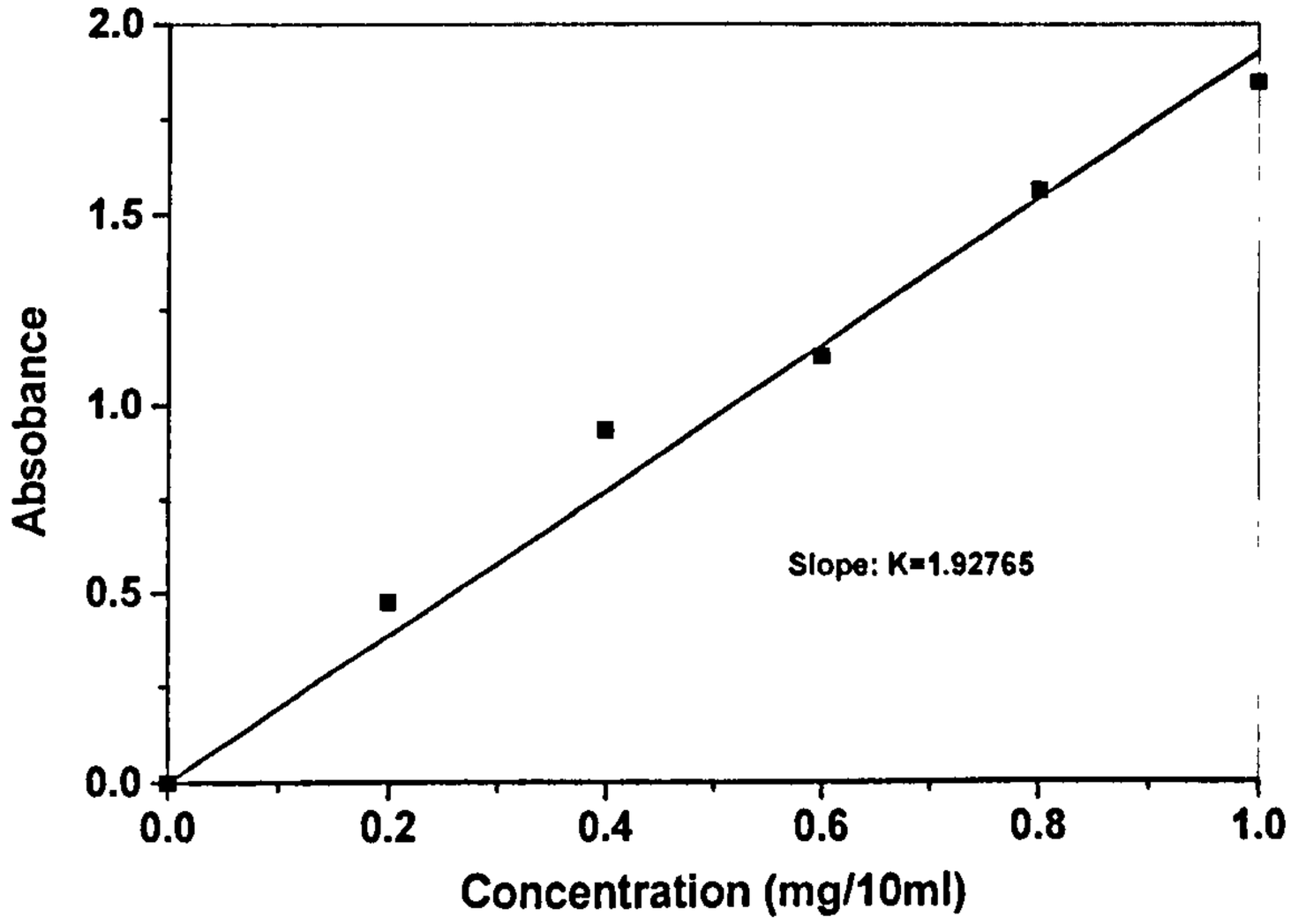

Figure 9.2.2 A standard concentration curve for vitamin B_{12}

From the diffusion cell experiments, the permeability, P, of the membranes for vitamin B_{12} were determined using Equation 3.3.10-3. The vitamin B_{12} diffusion coefficient, D, was calculated from the results of the permeability and partition coefficient, K_d, using Equation 3.3.10-2. The effects of crosslink density, PEO weight content in crosslinked chitosan/PEO blends and pH of vitamin B_{12} solution on the release behaviour were investigated.

9.2.2.1 Effect of crosslinking density on vitamin B_{12} release through chitosan/PEO blend membranes

The permeation of vitamin B_{12} through the crosslinked chitosan membranes with different crosslink densities was studied in phosphate buffer (0.1M) of pH 7.4 at 37°C. Table 9.2.1 lists the calculated values of permeability, diffusion and partition coefficients of the membranes with different crosslink densities. The raw data are shown in Appendix A.

Table 9.2.1 Permeability, diffusion and partition coefficients of vitamin B_{12} through chitosan membranes at pH 7.4 and 37°C

Sample	Crosslinking Density (%)	P (cm^2/s)	D (cm^2/s)	K_d
CSR	0	7.04×10^{-7}	3.44×10^{-7}	2.045
	0.068	5.43×10^{-7}	5.99×10^{-7}	0.906
	0.264	3.12×10^{-7}	2.83×10^{-7}	0.908
	0.985	1.29×10^{-7}	1.26×10^{-7}	1.026
	2.227	1.09×10^{-7}	9.90×10^{-8}	1.101
	4.645	9.57×10^{-8}	8.14×10^{-8}	1.176
	9.220	6.75×10^{-8}	4.63×10^{-8}	1.458
	14.350	4.25×10^{-8}	2.39×10^{-8}	1.779

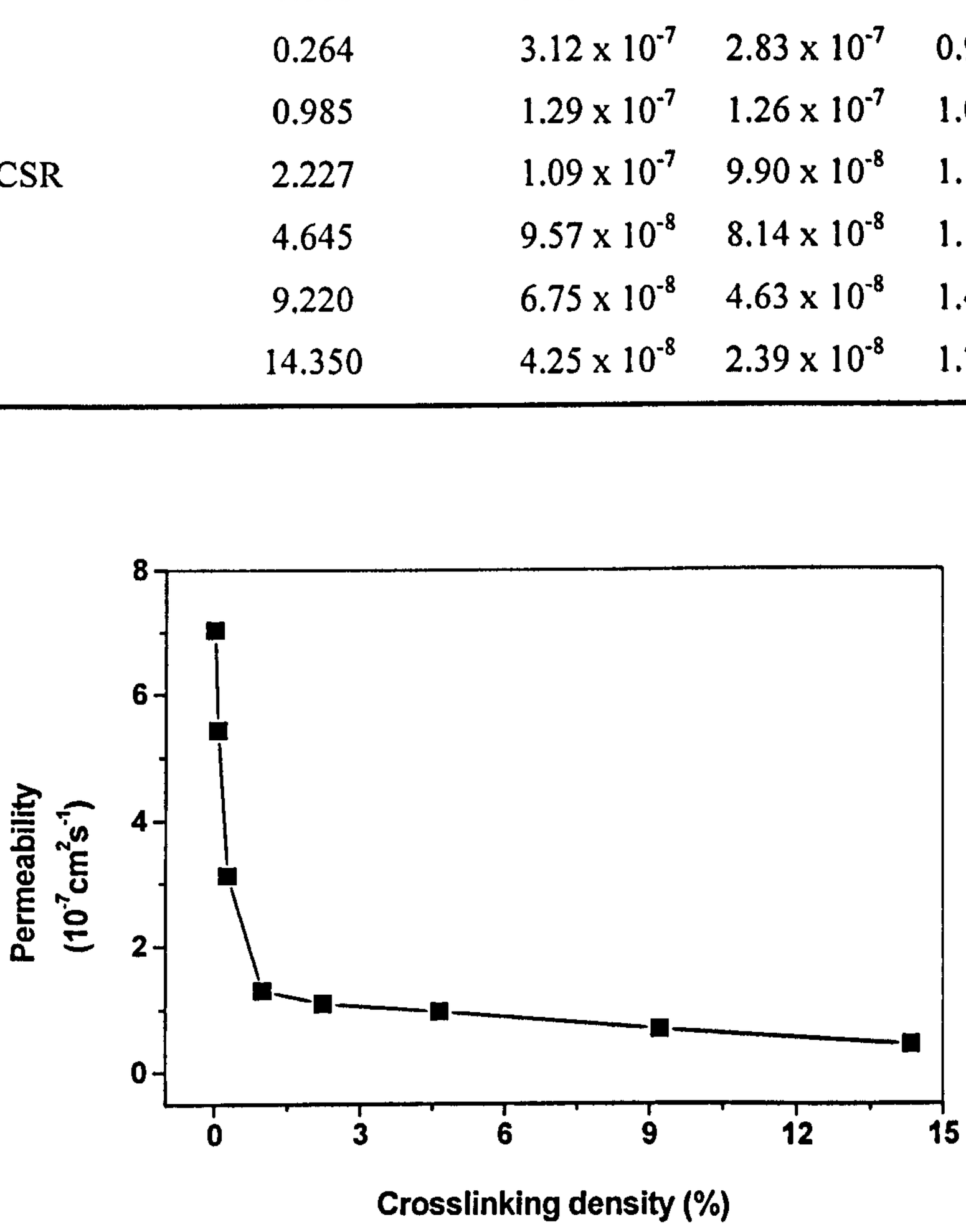

Figure 9.2.3 Effect of crosslink density on permeability of vitamin B_{12} through the chitosan membranes at pH 7.4 and 37°C

Figure 9.2.3 shows the effect of crosslink density on the permeability of vitamin B_{12} through chitosan membranes. The results shown in Table 9.2.1 and Figure 9.2.3 indicate that the drug release rate was found to be dependent on the crosslink density. As expected, the permeability decreased with increasing crosslink density. It can also be clearly observed from Figure 9.2.3 that permeability was particularly sensitive at low degrees of crosslink density, which could provide useful information for controlled drug release.

The permeability and release rate of hydrogels are influenced by the type of solute and the mesh size of the membrane [279]. The mesh size is the space between neighbouring chains in the polymer network, and can be considered as an indication for the available space in the membrane for solute diffusion [290]. Crosslinking a polymer generally leads to a reduction in permeability to solutes [290]. The permeability reduction may be due to a number of causes, such as interactions between the solute and the chains. In the case of hydrogels, the reduction in the mesh size by increasing crosslink density is likely to be a more important factor.

According to the free-volume theory, Equations 9.2-3 and 9.2-4 express a general form of diffusion. When the crosslink points are sufficiently spaced, the jumping rates of the solvent molecules and the interaction between these molecules and their neighbours (which is represented by D_{water}) will not be influenced by the presence of crosslinks. Following this line of reasoning, one is led to conclude that crosslinking a polymer influences only the diffusion coefficient through the thermodynamics of the polymer-solvent interactions and the specific hole volume of the polymer. The addition of chemical crosslinks to a polymer will obviously inhibit the segmental motion of the chains that arise due to thermal fluctuations. Consequently, the free volume of a crosslinked polymer is expected to be less than that of a non-crosslinked polymer. This anticipated behaviour is substantiated by the fact that crosslinking increases polymer density. Furthermore, it can be assumed that loss of free volume associated with the formation of crosslinking reduces the hole free volume, which dictates solvent transport.

According to the free volume theory, the permeability and release rate through membranes made from hydrogels are influenced by the crosslink density, which can

be directly explained by the degree of equilibrium swelling achieved by the network under experimental conditions. The effect of crosslink density on the equilibrium network swelling has been discussed in Chapter 6. A reduction in water up-take by the membrane accompanies increased crosslinked density.

Figure 9.2.4 shows the plot of $\ln(D_{gel}/D_{water}\,K')$ against 1/(H-1) for the crosslinked chitosan membrane. A linear relationship was obtained. Therefore, equation 9.2-6 used for a crosslinked poly(vinyl alcohol) membrane [289], in which the partition coefficient was introduced as the probability of a diffusing species finding a mesh, is suitable for treating our results.

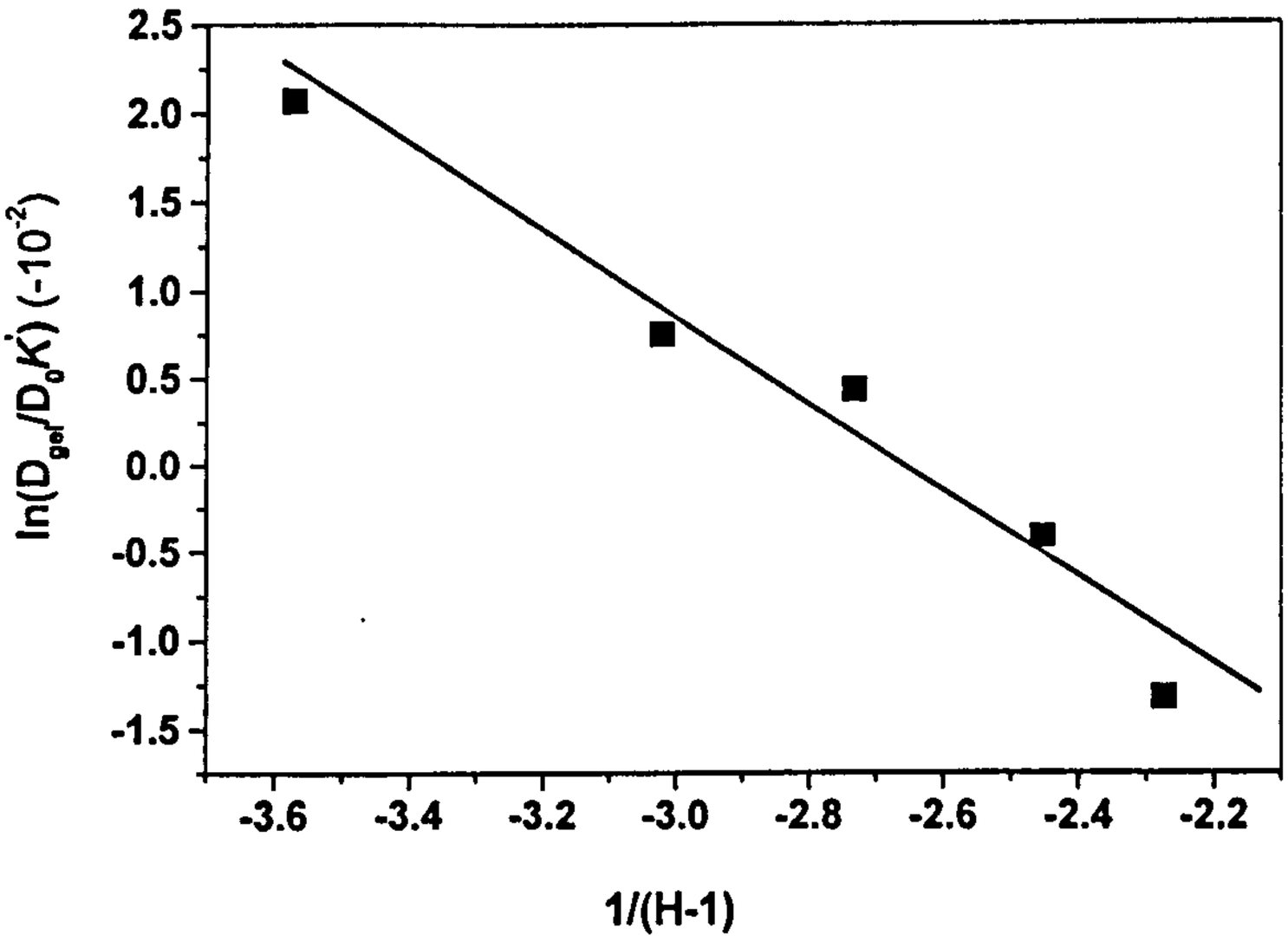

Figure 9.2.4 $\ln(D_{gel}/D_{water}\,K')$ vs.1/(H-1)

9.2.2.2 Effect of PEO on vitamin B_{12} release through crosslinked chitosan/PEO blends

In Chapter 5, the improvements in the mechanical properties of chitosan films after the addition of PEO were discussed, and it was also found that the degree of water wettability increased with increasing PEO content. In this section, the effect of the

PEO content in membranes on the permeation of vitamin B_{12} was examined. Table 9.2.2 shows experimental results (the raw data are shown in Appendix A).

Table 9.2.2 Effect of PEO content on the permeability of vitamin B_{12}

Sample	Genipin content (%)	P (cm^2/s)	D (cm^2/s)	K_d
CS	0	7.04×10^{-7}	3.44×10^{-7}	2.045
CSR/LPEO10	0.5	4.06×10^{-7}	6.33×10^{-7}	0.641
CSR/LPEO20		9.81×10^{-7}	1.56×10^{-6}	0.652
CSR/LPEO30		1.17×10^{-6}	1.20×10^{-6}	0.981
CSR/HPEO10		1.96×10^{-6}	2.89×10^{-6}	0.678
CSR/HPEO20		3.68×10^{-6}	5.07×10^{-6}	0.761
CSR/HPEO30		8.56×10^{-6}	1.06×10^{-5}	0.808

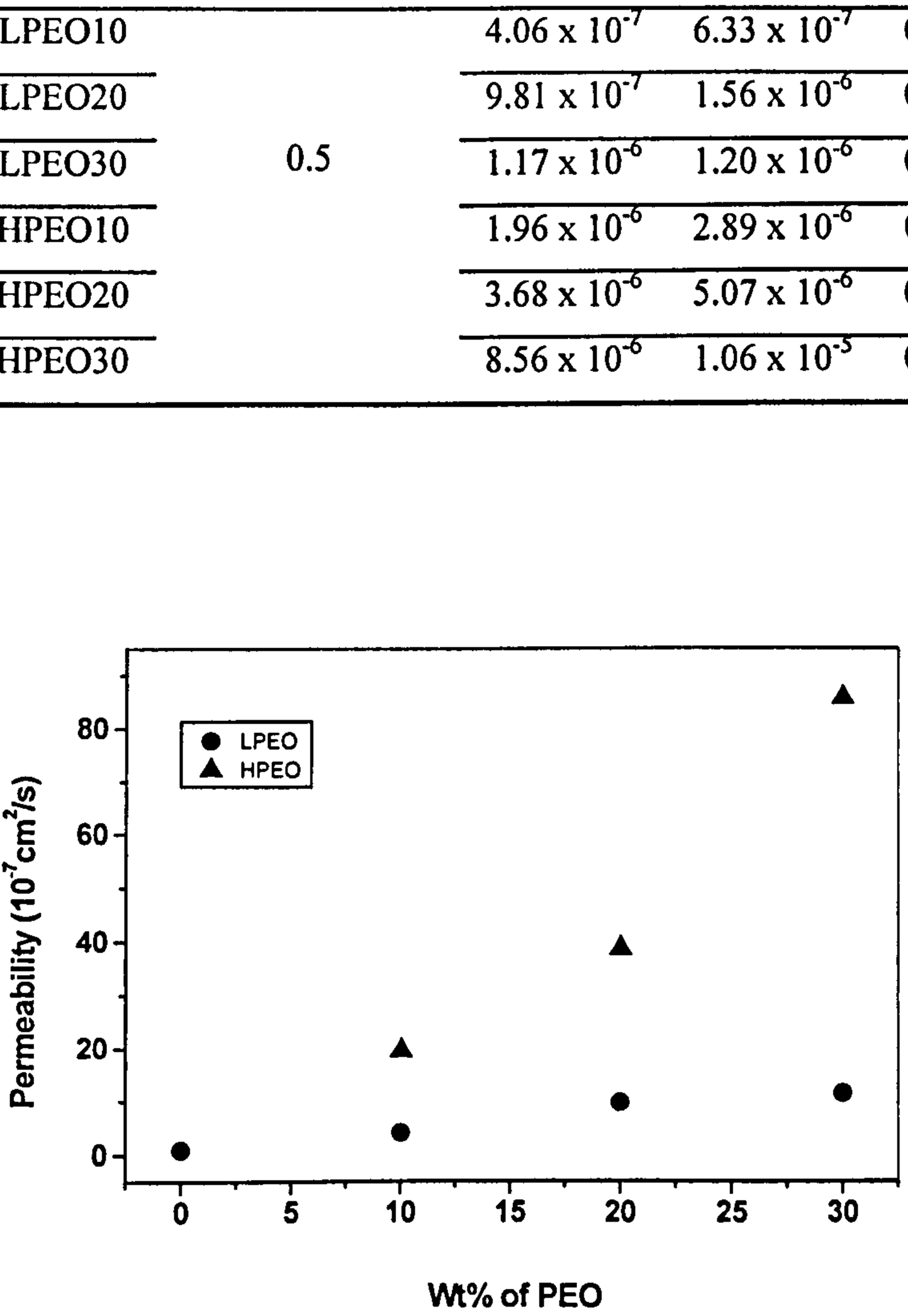

Figure 9.2.5 Effect of PEO content on the permeability of vitamin B_{12} through crosslinked chitosan/PEO membranes

Figure 9.2.5 shows that the permeability of vitamin B_{12} through the membrane prepared by blending chitosan with PEO was much higher than through chitosan alone. The permeability of vitamin B_{12}, for instance, increased with increasing weight ratio of PEO in the chitosan/PEO blend membranes. It can be observed from a comparison between chitosan/LPEO and chitosan/HPEO blend membranes that the rate of drug permeation of crosslinked chitosan/HPEO blend membranes was higher than that of chitosan/LPEO blend membranes.

The permeability through a membrane is controlled by the morphological features of the material, which can alter the mesh size of networks [291]. In Chapter 4, the morphology of chitosan/PEO blends and networks was studied by small angle X-ray scattering. The results indicate that crosslinking resulted in phase separation. With increasing HPEO or LPEO content, the phase separation increased in the crosslinked chitosan/HPEO or LPEO system. Phase separation leads to a reduction of the molecular interaction between the chitosan and PEO in the chitosan/PEO system. This fact has been proven by the previous studies from the stability of crosslinked chitosan/PEO blend film in water. These results indicate that after immersing the film in water some of the PEO dissolved. The lower the HPEO or LPEO content the better was the stability. The stability of the crosslinked chitosan/LPEO film was better than that of the crosslinked chitosan/HPEO film due to the effect of different molecular weight of PEO. Figure 9.2.6 is a schematic diagram of the mesh sizes for crosslinked chitosan, chitosan/LPEO and chitosan/HPEO membranes. The low stability gave rise to larger mesh size for the chitosan/HPEO membrane. From the above discussions, it can be concluded that the PEO content and the different molecular weight of PEO used in the chitosan/PEO blend network can alter the mesh size of the membrane and control drug release rate.

(a) Chitosan

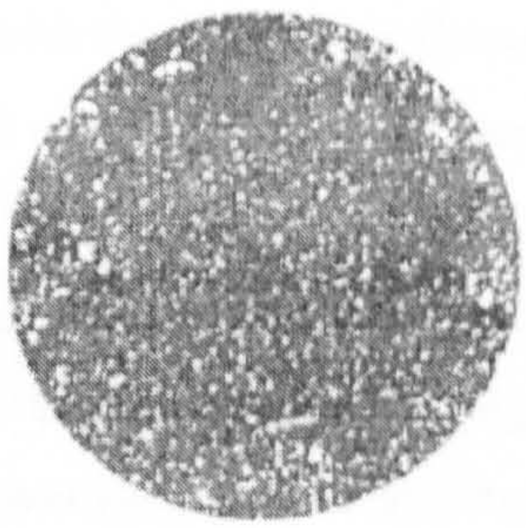

(b) Chitosan/LPEO

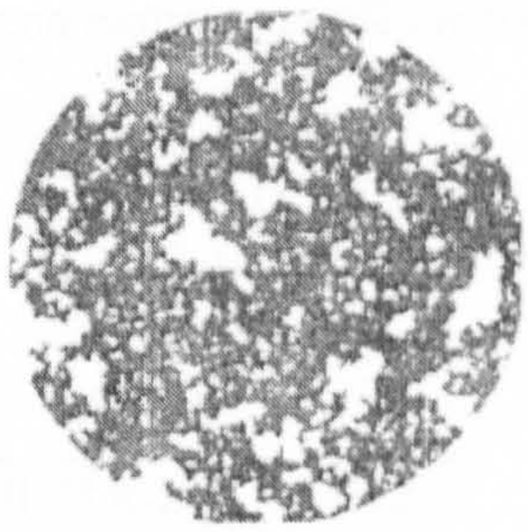

(c) Chitosan/HPEO

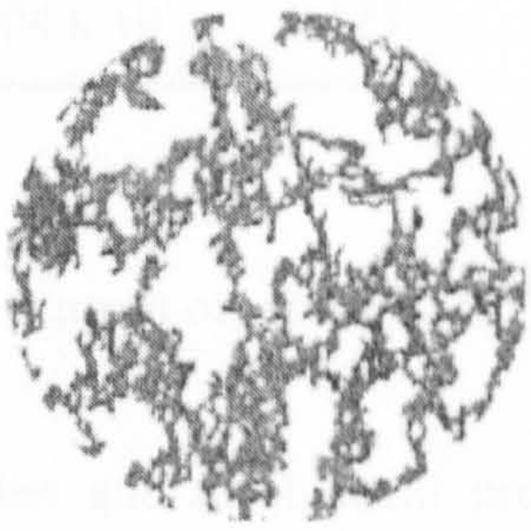

Figure 9.2.6 Schematic diagram of the mesh size for crosslinked chitosan and chitosan/PEO membranes

9.2.2.3 Effect of solution pH on vitamin B_{12} release

The permeation of a drug through crosslinked chitosan membranes (crosslink density: 4.65%) was studied in phosphate buffer solutions at different pHs (3.8, 4.3, 5.5 and 7.4) at 37°C to evaluate of the effect of solution pH on the permeation of vitamin B_{12}.

Table 9.2.3 shows the effect of pH on the permeability and the diffusion coefficient of vitamin B_{12} through the membrane (the raw data are shown in Appendix A). These clearly show an increase in the release rate of vitamin B_{12} when the pH of buffer system becomes acidic. This result agrees with the previously discussed results of the equilibrium swelling nature according to the pH condition. The membrane at low pHs exhibited a high-swelling ratio due to the fact that the repulsive forces between the same charges on the molecules caused greater intermolecular distances and hydrophilicity. The swollen membrane was expected to have a large-sized mesh, and hence higher rates of drug permeation at lower pH could be attributed to the changes in the mesh size.

Table 9.2.3 Permeability, diffusion and partition coefficients of vitamin B_{12} in solutions with different pHs

pH	P (cm^2/s)	D (cm^2/s)	K_d
7.4	0.96×10^{-7}	0.85×10^{-7}	1.123
5.5	1.26×10^{-7}	0.98×10^{-7}	1.284
4.3	1.81×10^{-7}	1.24×10^{-7}	1.456
3.8	2.91×10^{-7}	2.04×10^{-7}	1.425

9.2.2.4 Effect of degree of deacetylation of chitosan on vitamin B_{12} release

Films or membranes with different pore sizes and mechanical properties can be prepared from chitosans with different degrees of deacetylation or molecular weights [43]. The films or membranes thus prepared are important for purification, separation, controlled release etc. In this section, three kinds of crosslinked and uncrosslinked chitosan membranes are used to study the release of vitamin B_{12}. They were formed using three different degrees of deacetylation (72%, 85% and 95%) and some of them crosslinked by a 0.5% genipin content. The results are listed in the Table 9.2.4 (the raw data are shown in Appendix A). The permeability of the uncrosslinked chitosan membrane increased with increases in the degree of deacetylation. The degree of deacetylation affects the physical characteristics of the

membranes. Where the degree of deacetylation is high, chitosan has greater chain flexibility and the flexible molecules result in a larger mesh size in the membrane [292]. Consequently, more drug molecules are released. From the comparison of the data for crosslinked and un-crosslinked chitosan membranes, it can be seen that crosslinking, by causing decreases in the mesh size of the membranes, led to reductions in the permeability and diffusion coefficient.

Table 9.2.4 Permeability, diffusion and partition coefficients of vitamin B_{12} through chitosan membranes with different degrees of deacetylation

Sample	DD (%)	P (cm^2/s)	D (cm^2/s)	K_d
CS	72	4.02×10^{-8}	2.23×10^{-8}	1.797
	85	3.44×10^{-7}	1.67×10^{-7}	2.045
	95	2.68×10^{-6}	1.19×10^{-6}	2.242
CSR	72	1.62×10^{-8}	0.81×10^{-8}	2.011
	85	0.57×10^{-7}	0.49×10^{-7}	1.176
	95	7.26×10^{-7}	6.67×10^{-7}	1.087

9.2.3 Conclusions

The permeability of vitamin B_{12} was investigated through crosslinked and un-crosslinked chitosan and chitosan/PEO blend membranes. The drug release rate was controlled by the mesh size of the membrane, which can be adjusted by a number of factors, such as the crosslink density, the presence of PEO in the membrane, external pH, and the degree of deacetylation of the chitosan. Crosslinking resulted in a decrease of the drug release rate. Furthermore, as the crosslink density increased, the drug release rate decreased. The drug release rate was also very sensitive at low crosslink densities. The introduction of PEO into the membrane changed the mesh size of the membrane, resulting in changes in the drug release rate. These changes depended on the molecular weight and amount of PEO. Increasing the degree of deacetylation led to increases in the drug release rate. The drug release rate was also

sensitive to solution pH, which is in agreement with the swelling nature of these membranes.

These membranes are expected to be very useful in medical applications because solute permeation through them can be controlled.

9.3 Release of Eleutherococcus Senticosus (ES) Drug from Chitosan Film Carriers

In this section, controlled drug release from chitosan and chitosan networks was studied by sorption and desorption experiments under two carrier conditions of fixed and moving boundary. Eleutherococcus senticosus, discussed at greater length in section 9.4, was used as a model drug.

9.3.1 Fixed boundary

9.3.1.1 Fundamental theory of drug release with fixed boundary conditions

The conservation of species in one dimension is given by the following equation [219]

$$\frac{\partial c}{\partial t} = -\frac{\partial}{\partial x} j_x \qquad [9.3\text{-}1]$$

where c is the concentration of the diffusing species, t is the time, and j_x is the flux in the x direction, which is along the thickness of the membrane and is the only direction in which mass transfer is taking place. If A is the area of the face of the membrane, then $A^{1/2} >> l$, where l is the membrane thickness, which makes the dynamics one-dimensional. Equation 9.3-1 assumes that there is no convection. Considering a boundary effect in concentration c, requires that flux be related to the concentration field. According to Fick's law, we have

$$j_x = -D\frac{\partial c}{\partial x} \qquad [9.3\text{-}2]$$

Combining Equations. 9.3-1 and 9.3-2 one has

$$\frac{\partial c}{\partial t} = \frac{\partial}{\partial x}\left(D\frac{\partial c}{\partial x} \right) \qquad [9.3\text{-}3]$$

which is essentially the equation that has to be solved subject to appropriate initial and boundary conditions.

In simple sorption and desorption experiments, the solute dissolves and diffuses into the membrane. The fractional mass uptakes are a function of time. For constant D, Equation 9.3-3 leads to

$$\frac{M_t}{M_\infty} = 1 - \frac{8}{\pi^2}\sum_{m=0}^{\infty}\frac{1}{(2m+1)^2}\exp\left[-\frac{4D(2m+1)^2\pi^2 t}{l^2} \right] \qquad [9.3\text{-}4]$$

where M_t and M_∞ are the mass release at time t and at infinite time, respectively, l is the membrane thickness and m is an integer.

For long times, Equation 9.3-4 may be approximated to the following equation [218]

$$\frac{M_t}{M_\infty} = 1 - \frac{8}{\pi^2}\exp\left[-\frac{4\pi^2 Dt}{l^2} \right] \qquad [9.3\text{-}5]$$

At short times it approximates to

$$\frac{M_t}{M_\infty} \approx 4\left(\frac{Dt}{\pi l^2} \right)^{1/2} \qquad [9.3\text{-}6]$$

A plot of M_t/M_∞ versus $t^{1/2}$ is linear and from the slop, D can be evaluated.

9.3.1.2 Diffusion behaviour of ES from a chitosan carrier with fixed boundary

The release of ES over time was investigated at 37°C. The diffused mass can be calculated on the basis of the measurement of concentration. Figure 9.3.1 shows M_t/M_∞ for released ES versus the time. M_t, the amount of ES sorbate released at time t, was calculated. M_∞, the amount of ES released after infinite time was taken to be the value at which the equilibrium was attained.

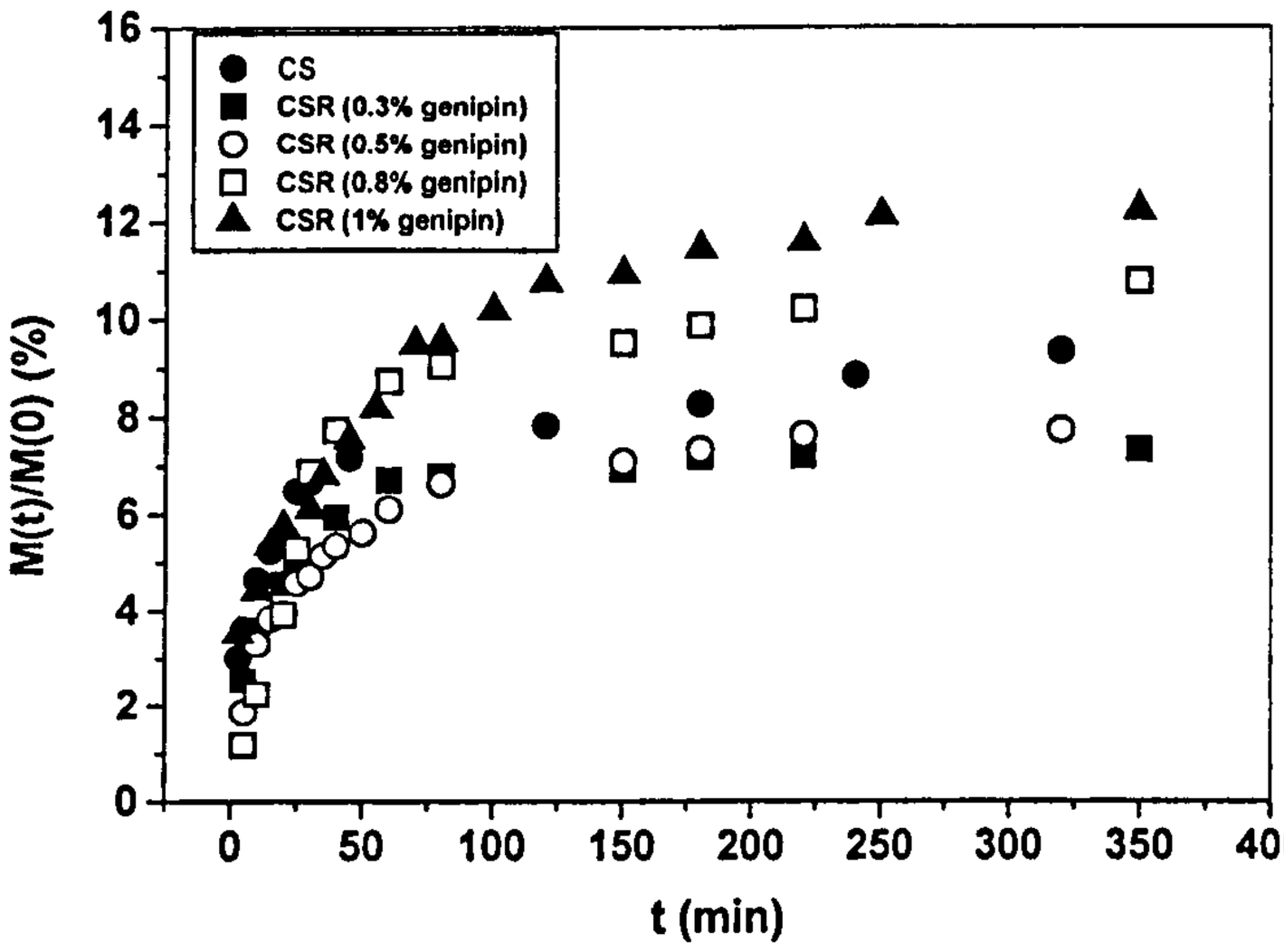

Figure 9.3.1 M_t/M_∞ for released ES versus time

From the linear part of the curves, the diffusion coefficient D was calculated using Equation 9.3-6.

Figure 9.3.2 shows the change of diffusion coefficient with crosslink density. The results indicate that the diffusion coefficient strongly depends on the crosslink density. When the genipin crosslink density was 2.23 % or 4.65%, the diffusion rate was slower than that of the un-crosslinked ones. However, when the crosslinking density was increased to 9.22 % or 14.35 %, the diffusion rate became faster than that of the uncrosslinked ones.

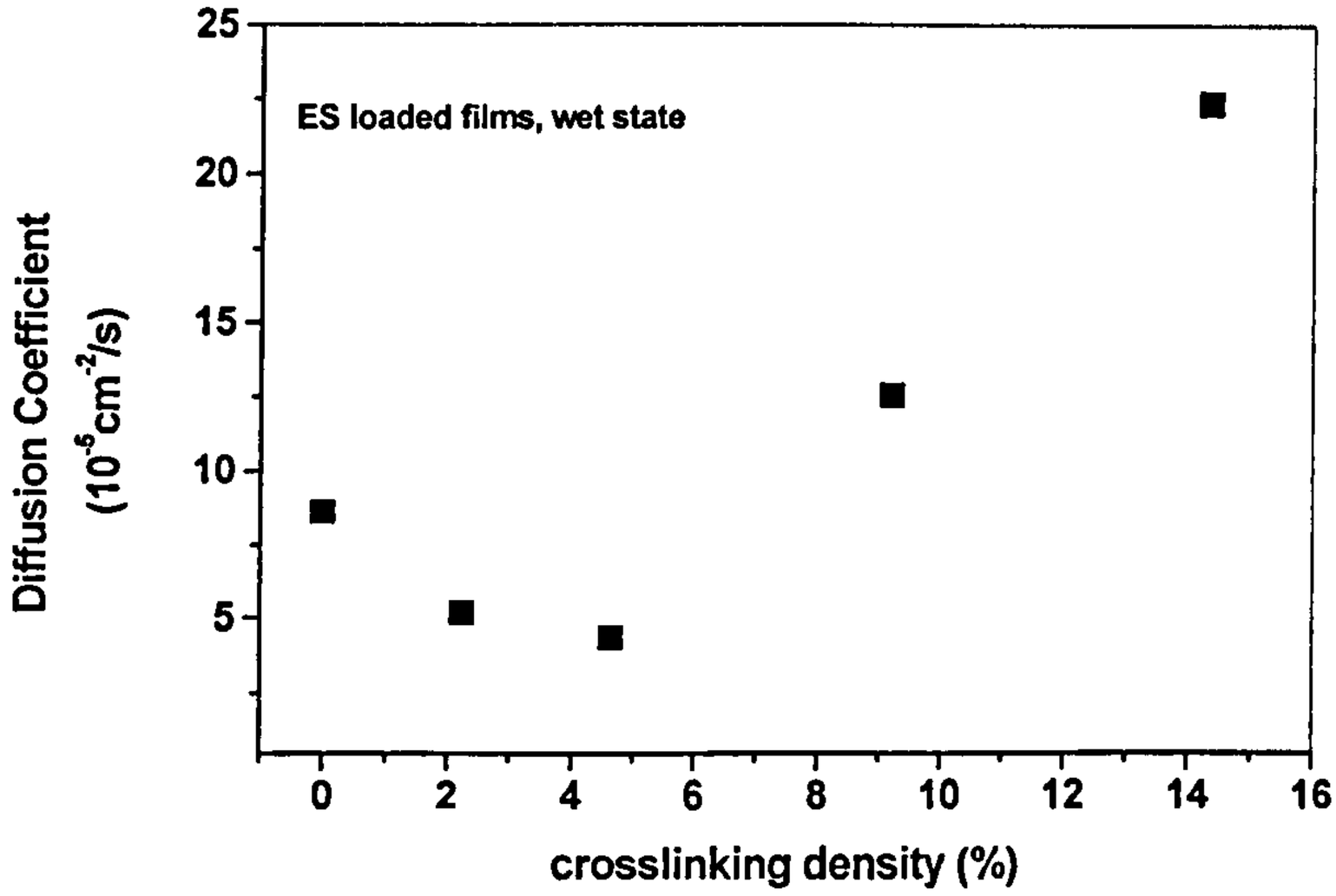

Figure 9.3.2 Diffusion coefficient as a function of crosslink density

It can also been observed from Figure 9.3.1 that the release amount of ES was very small. Even when the release time was 350minutes and the crosslinking density was 14.35%, only about 15% of the loaded drug was released from the carrier. This suggests that for the carrier (chitosan/ES system), the drug release mechanism is not only regulated by the 'pore' mechanism, and that there exist molecular interactions between chitosan and ES. This means that the release rate may be controlled by both the mesh size of the membrane and the interactions between chitosan and ES. In order to understand the above diffusion behaviour, the molecular interactions between chitosan and ES was studied by FT-IR spectra analysis, the results of which are shown in Figure 9.3.3. The frequency of the free amine band of chitosan in chitosan/ES system shifted up from 1558 to 1567cm^{-1}, confirming that ES interacts with chitosan at the position of amino groups.

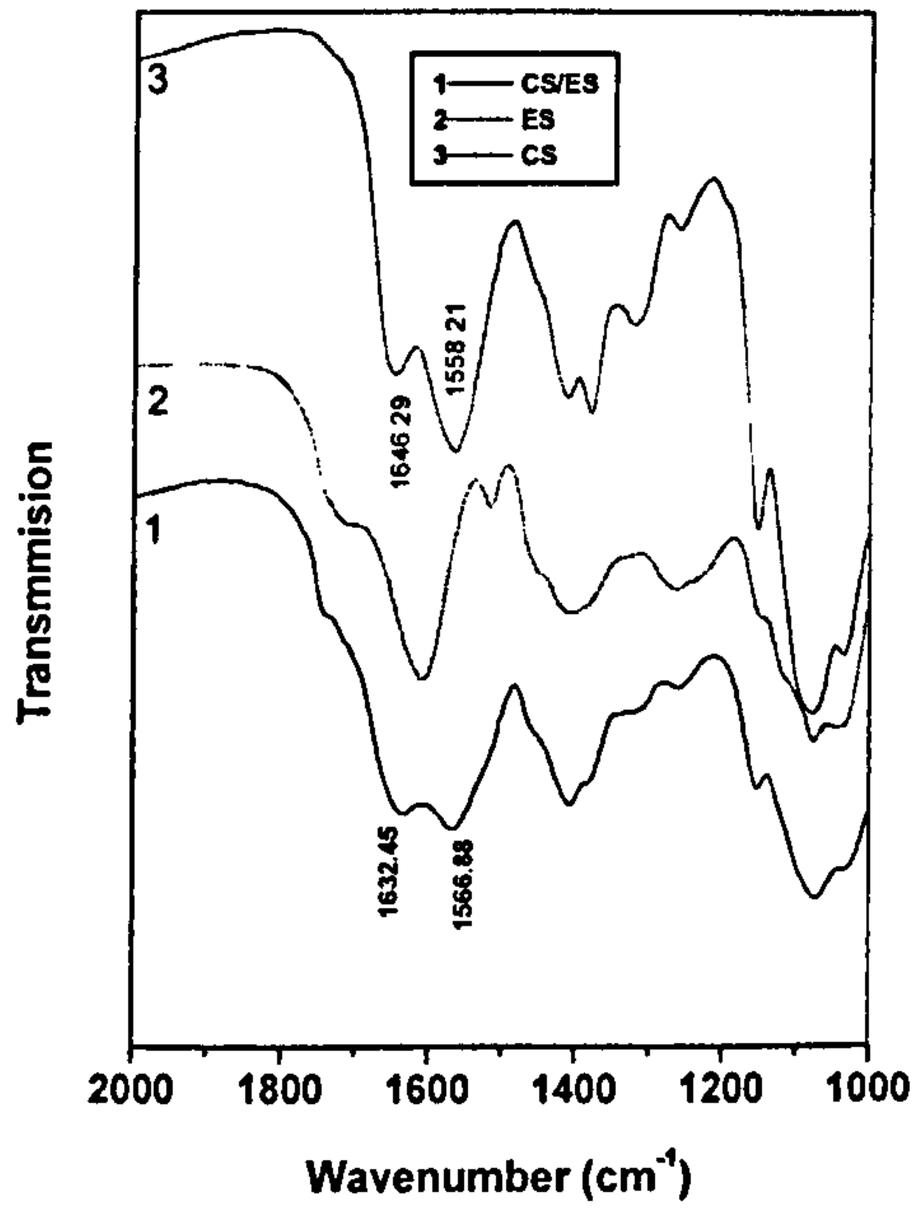

Figure 9.3.3 FT-IR spectra of CS, ES and CS/ES (DD: 85%)

For further understanding of the effect of crosslink density on the interactions between ES and the free amino groups of chitosan, chitosan samples with 72% and 95% degree of deacetylation were employed. Figure 9.3.4, parts A and B, shows FT-IR spectra for chitosan/ES systems with 72% and 95% degree of deacetylation, respectively. Table 9.3.1 gives a comparison of frequency shifts. The results indicate that the molecular interactions were stronger when chitosan with higher degrees of deacetylation was used, which is explained by the greater shifts of the frequency of the free amine band.

The free amino groups of chitosan reacted with genipin, which was confirmed by FT-IR and UV spectra analysis (see Chapter 7). The content of free amino groups of chitosan could be reduced due to crosslinking. According to this, the content of amino group will decrease with increasing crosslink density.

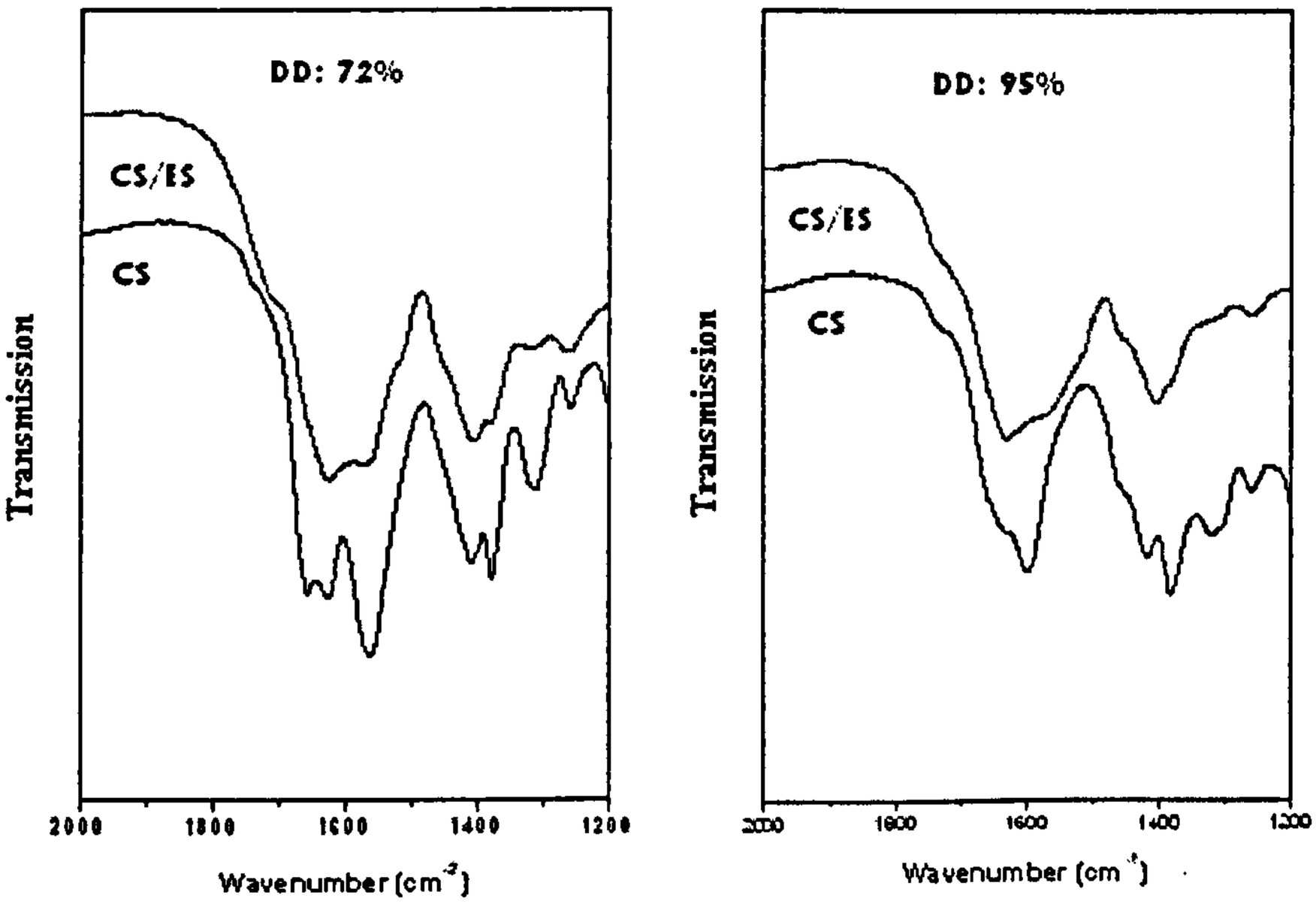

Figure 9.3.4 FT-IR spectra of CS and CS/ES. (A) DD: 72% (B) DD: 95%.

Table 9.3.1 A comparison of frequency shifts using different degree of deacetylation of chitosan

DD	Sample	Wavenumber (cm^{-1})	Shift (cm^{-1})	Wavenumber (cm^{-1})	Shift (cm^{-1})
72	CS	1563	11	1627	1
	CS/ES	1574		1626	
85	CS	1558	9	1647	-15
	CS/ES	1567		1632	
92	CS	-	-	1599	-32
	CS/ES	-		1631	

From the FT-IR results and the above analysis, it can be assumed that the interaction between chitosan and ES in chitosan/ES systems may be reduced when chitosan is crosslinked by genipin. For the crosslink densities of 2.23 % and 4.65%, the diffusion rate deceased because the mesh size decreased, although because of crosslinking the

interaction between chitosan and ES became weaker. In this case, the mesh size is more important than the interaction for controlling the release rate in the chitosan/ES system. However, for the crosslink densities of 9.22 % and 14.35 %, the drug release rate was more dependent on the interactions in the chitosan/ES system.

9.3.1.3 Conclusions

ES drug release behaviour from the chitosan carriers with fixed boundary was affected by the crosslink density of the chitosan films. The drug release rate for the chitosan/ES system was governed by both the mesh size of membrane and specific interactions between chitosan and ES.

9.3.2 Moving boundary

9.3.2.1 Introduction to the moving boundary concept

In the above studies, we investigated the drug release behaviour for fully hydrated monolithic slabs of un-crosslinked and crosslinked chitosan gels. The amount of drug released at any one time could be determined by judicious selection from a number of variables, but invariably the rate of release diminished with time at a $t^{1/2}$ proportionality. Starting off with the drug dispersed in a dehydrated hydrogel offers several practical advantages over the hydrated system. When dried down, the drug substance is essentially immobile, trapped in the matrix, and contact with penetrating water is necessary to unlock the immobilised solute and trigger the release process [4,43,293,294].

For a drug such as prostaglandin E_2 (PGE_2), which degrades in water, a viscous aqueous gel for vaginal application [293] has to be dispensed in the hospital pharmacy prior to administration, whereas a dried hydrogel containing dispersed PGE_2 provides a long-lasting stable formulation, which is immediately available when required. Other advantages in starting with a dried device are the swelling process necessary to activate the release that helps to linearize the decreasing rate normally associated with an initially hydrated device and the extension of the period of effective release.

An initially dried hydrogel containing a dispersed drug with the added safety that it cannot dump the entrapped medication when administered would, in general, be of more interest for pharmaceutical formulations than one swollen with, or containing a solution of the drug [294].

In the context of drug release systems, one important class of problems arises where moving boundary is encountered in the drying of polymer films [4,294]. The boundary can move as a function of time. In particular, the key feature is the jump boundary condition at the interface, where many quantities become discontinuous. A schematic representation of the overall physics of the situation is given as Figure 9.3.5.

In order to solve these problems, a well-defined initial state and the concentration profile to change along with the position of the interface are required. The issue of numerical stability of the algorithm at the moving interface is a complex one. Such swelling and diffusion do not generally follow a Fickian mechanism [219]. Until now, no single model can be used to describe such problems. This section aims at presenting a phenomenological analysis of release results and at contributing to the understanding of the mechanisms of drug release from dried uncrosslinked and crosslinked chitosan membranes.

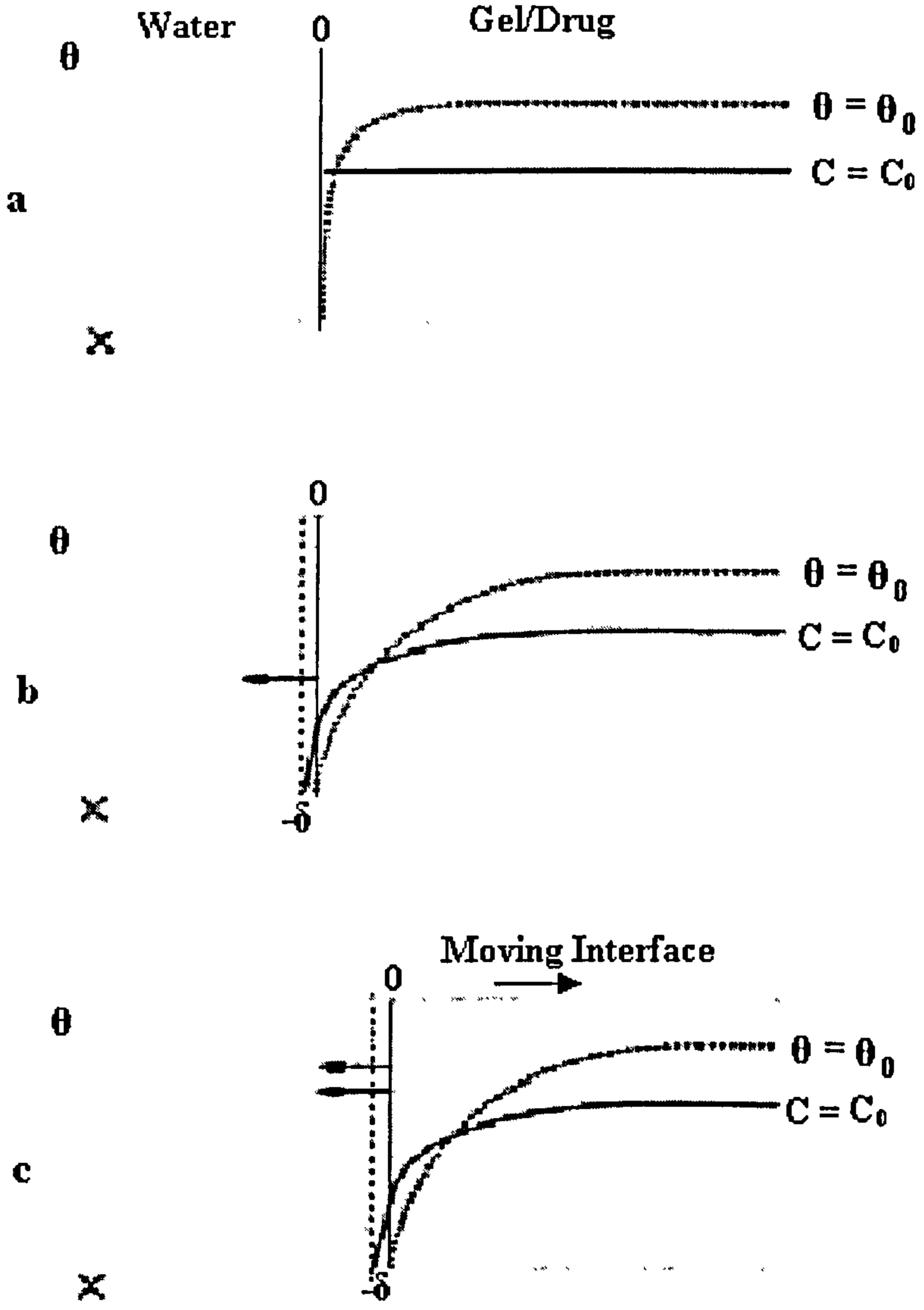

Figure 9.3.5 Schematic diagram depicting the physical situation of drug release from dry polymer films (θ, polymer concentration -----; *C*, Drug concentration —; →, release of drug/polymer into bulk water) [294].

[Figure 9.3.5 (a) shows where water begins to diffuse into a polymer film at initial stage. Since the water continues to diffuse into the film, the drug diffuses out into bulk water as shown in Figure 9.3.5 (b). Then the polymer concentration has achieved steady profile and moves right at constant velocity, drug continues to diffuse out at a rate based on C (x = 0) and dC/dt (x = 0) as shown in Figure 9.3.5 (c). This representation predicts that there will be a period of time (t =0 to t = t_{equ}) where the drug release will be controlled by Fickian diffusion. The diffusion rate of drugs within the film, and the diffusion rate of water into the polymer are all important parameters.]

9.3.2.2 Fundamental theory of drug release mechanism with moving boundary

Release kinetics may employ one of the detailed mathematical models based on the diffusion equations [219]. To describe Fickian and non-Fickian release behaviour of swelling controlled release systems [295], the exponential relation equation shown below can frequently be used.

$$\frac{M_t}{M_\infty} = kt^n \qquad [9.3\text{-}7]$$

where, M_t is the total mass of drug released through time t, M_∞ is the total mount of drug released, k is a constant that characterises the macromolecular network system and n is the diffusional exponent characteristic of the release mechanism. For this analysis, M_∞ was taken as the total initial amount of the drug. An analysis of cumulative release data (M_t/M_∞) versus time for all formulations yields the dependence on time of the drug release, n, as well as the constant, k. This value, *n*, of the exponential dependence on time of the drug release indicates whether degradation, diffusion, anomalous transport or other mechanisms are the predominant factors in the mechanism of drug release. A value of n=0.5 shows that Fickian (Case I) diffusion is observed and the release rate is dependent on $t^{0.5}$. A value of n=1 indicates Case II transport and the release rate is directly proportional to time. For values of $0.5<n<1.0$, anomalous (non-Fickian) transport is the predominating mechanism. For values of $n<0.5$, pseudo-Fickian diffusion occurs. Values of $n>1$ define Super Case II transport [295] in which a pronounced acceleration in solute release by a film occurs toward the latter stages of release experiments, resulting in a more rapid relaxation-controlled transport [291,295]. Such diffusion behaviour can be summarised in Table 9.3.2.

Table 9.3.2 The diffusional exponent characteristic of particular release mechanisms

Diffusional exponent	Diffusion mechanism
n=0.5	Fickian (Case I)
N < 0.5	pseudo-Fickian
n = 1	Case II transport
0.5< n <1	Anomalous
n>1	Super Case II

The general behaviour, known as anomalous transport, is bound by pure Fickian diffusion and Case II transport, which have been observed in several polymer/penetrant systems [292]. Figure 9.3.6 explains the two typical responses of the fractional mass release curves. Transport in all of these physical situations can generally be reduced to three types of driving forces: a penetrant concentration gradient, a polymer stress gradient and osmotic forces [292].

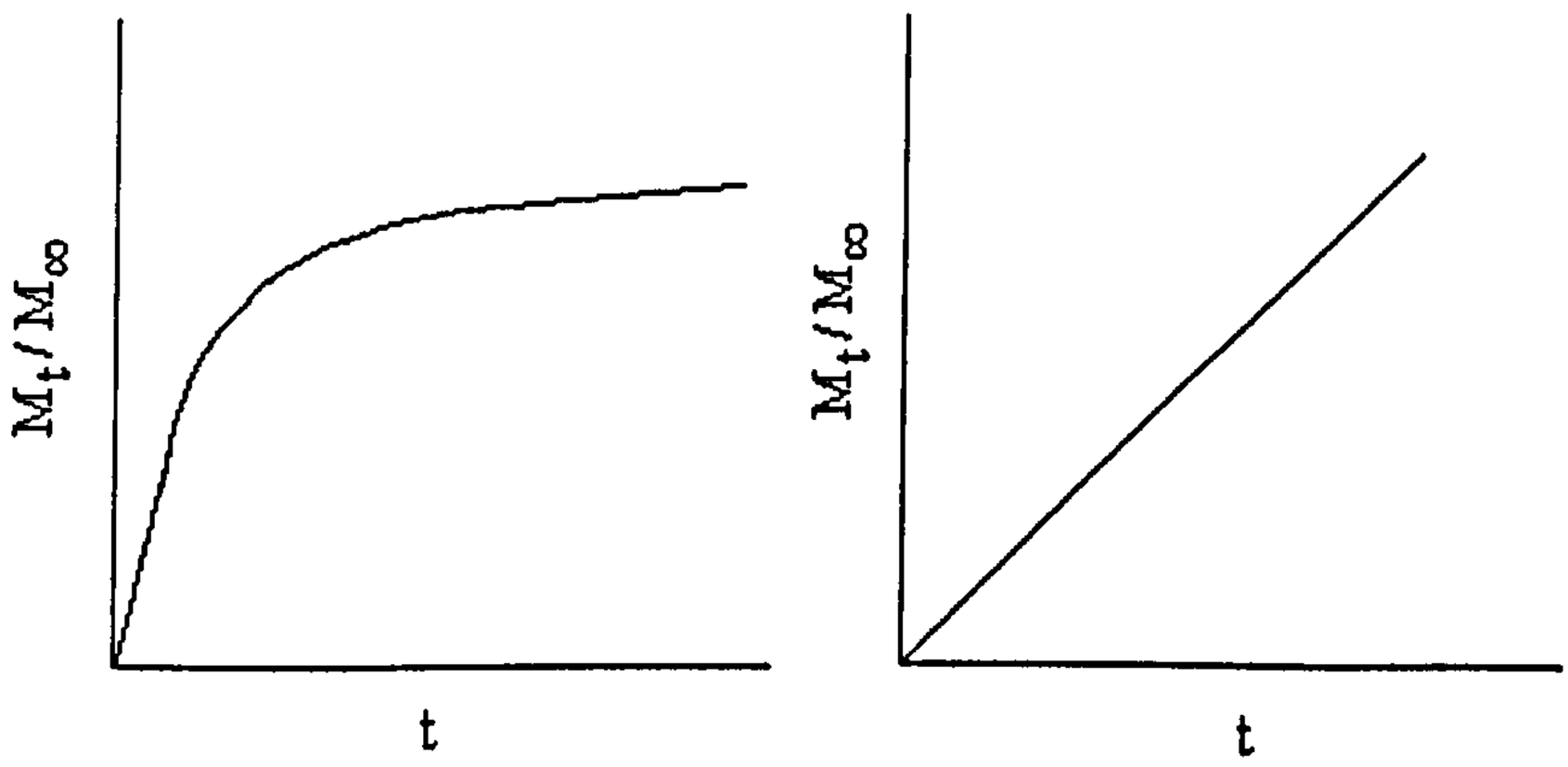

Fickian **Case II**

Figure 9.3.6 The different types of release response curves

Swelling-controlled release systems are based on the above principles, where a polymeric carrier can counterbalance normal Fickian diffusion by hindering the release of an imbedded solute or drug, leading to an extended period of drug delivery under zero-order release conditions [296]. In addition, the presence of a polymer network surrounding a drug molecule has also been shown to act as a stabilizer [296], maintaining biological activity until the solute is released.

9.3.2.3 Effect of dynamic swelling of dried membranes on drug release

Swelling is a common phenomenon for various hydrophilic systems that are widely used as drug delivery devices. Water uptakes with time for un-crosslinked and crosslinked membranes have been plotted as shown in Figure 9.3.7. In order to determine the rate of swelling, the incremental weight difference between each recorded weight was used rather than the gradient of the curve. This method is more sensitive, accurate and less subjective in detecting subtle changes in the swelling pattern [294]. The rates of water uptake at each recorded time were also calculated and are shown in Figure 9.3.8. For a better comparison of the swelling rate of un-crosslinked and crosslinked chitosan membranes, two different scales were used in Figure 9.3.8. As seen there are two distinct peaks in the rate plot for an uncrosslinked chitosan membrane, at 5mins and 15mins and a levelling off period around 80mins. The membrane is still swelling, albeit slowly, after 180 minutes. Similarly, the rates of swelling for crosslinked chitosan membranes were fast in the first twenty minutes and then became slow after 150mins. Swelling was limited by the presence of crosslinking and the uptake rates decreased with increasing crosslink density.

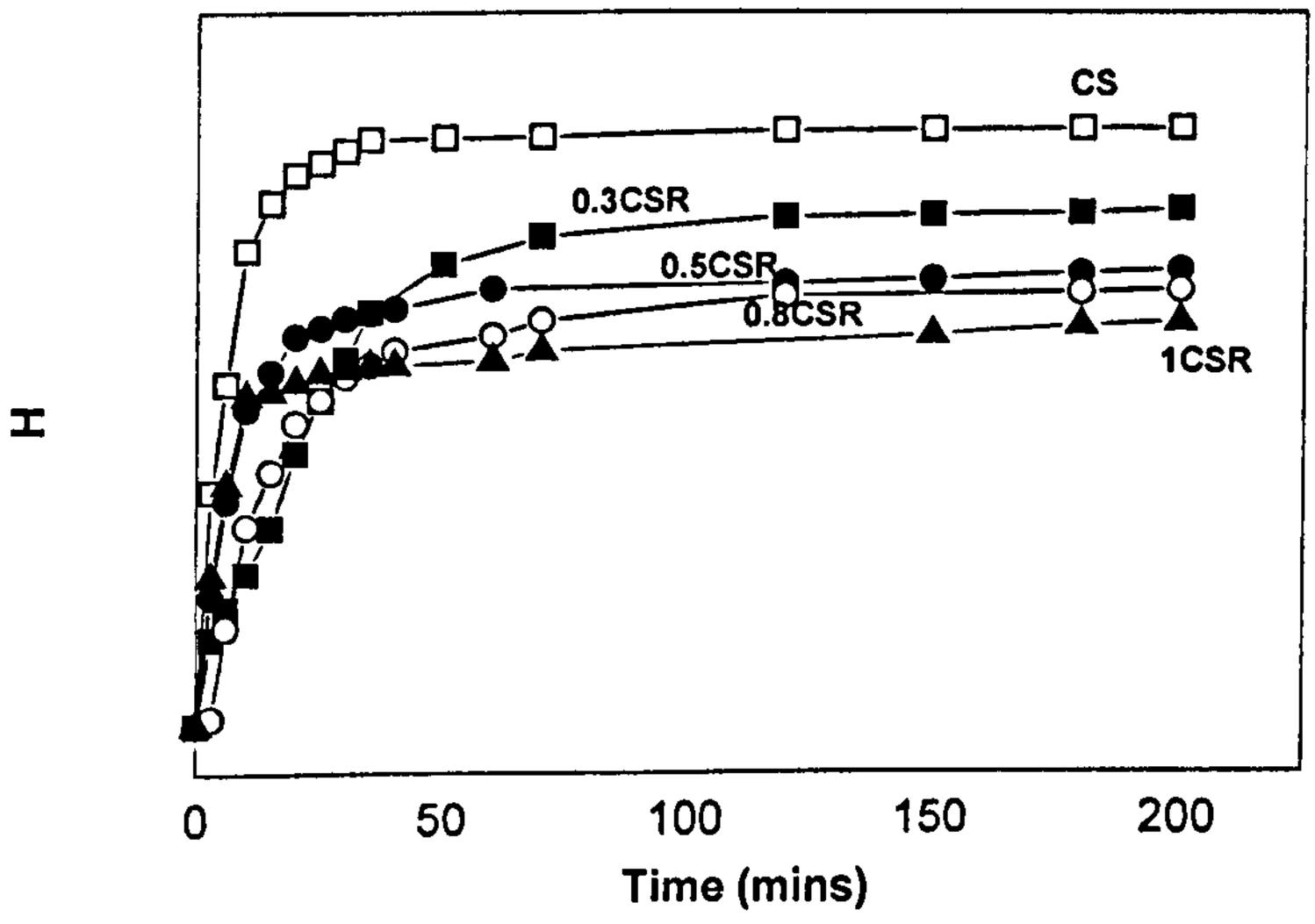

Figure 9.3.7 Water uptake of un-crosslinked and crosslinked chitosan membranes

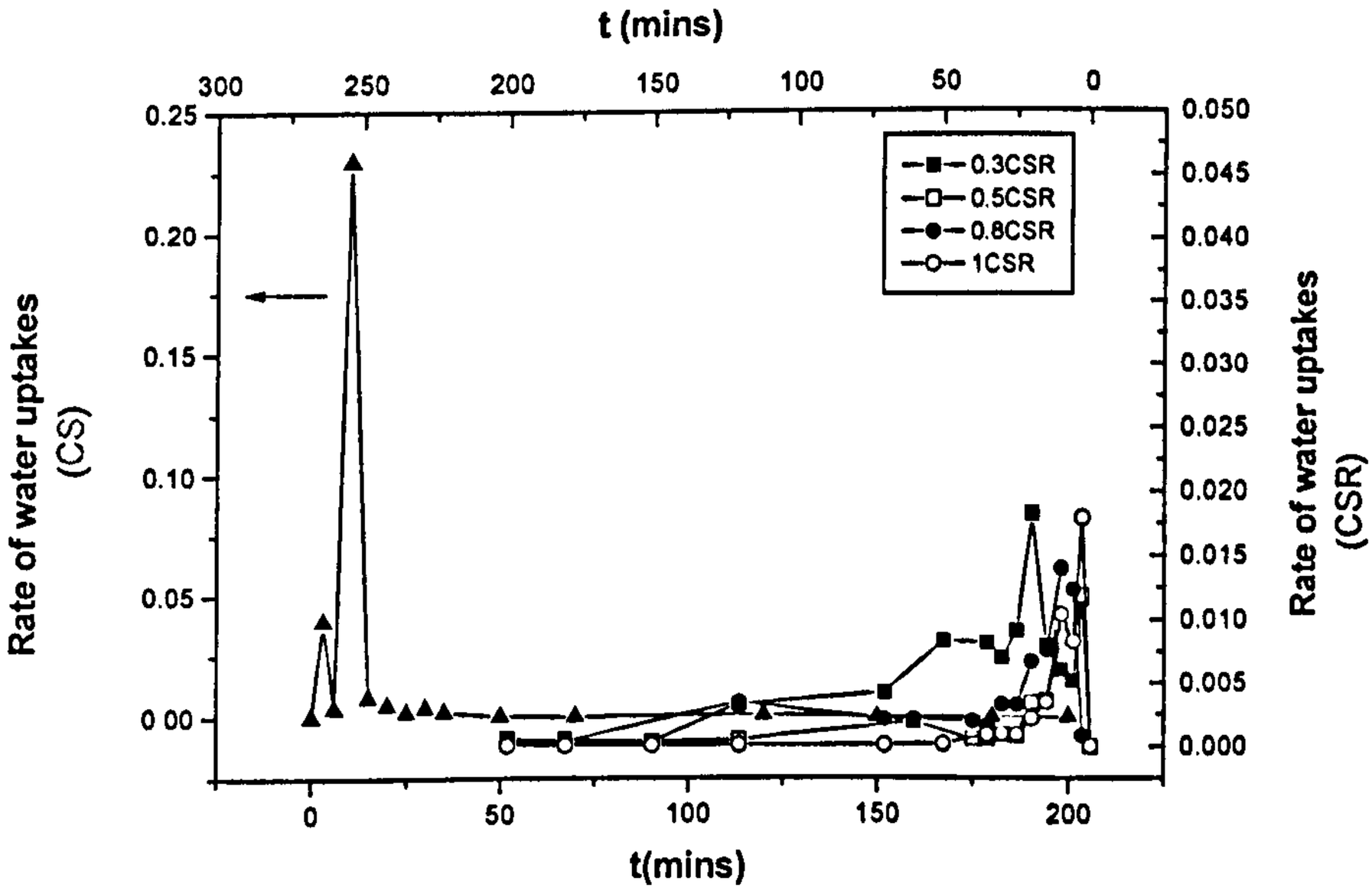

Figure 9.3.8 Rate of water uptake of un-crosslinked and crosslinked chitosan membranes

Swelling of dried thin membranes accompanied by expansion was investigated. CS and 0.3CSR samples were placed in distilled water at 37°C, removed after different periods, measured and returned to the water to continue swelling. The surface area of the membranes was calculated and ratioed to the initial area. The rate of change of surface area for each interval of time was also calculated. The results for both chitosan and crosslinked chitosan membranes are illustrated in Figure 9.3.9. It shows that the peak rate between 5 and 15mins is due to the ease of water absorption at a surface in intimate contact with an aqueous environment. The layer of membrane close to the surface expands rapidly, but is constrained by the adjoining inner dry layer, which can only swell by absorbing water from the outer swollen layer. The rate, therefore, soon falls away as the advancing waterfronts from opposite faces approach to meet in the middle. From all the above dynamic swelling studies, it can be concluded that in early stages of dynamic swelling the rate of swelling was rapid, then became slow and finally reached equilibrium.

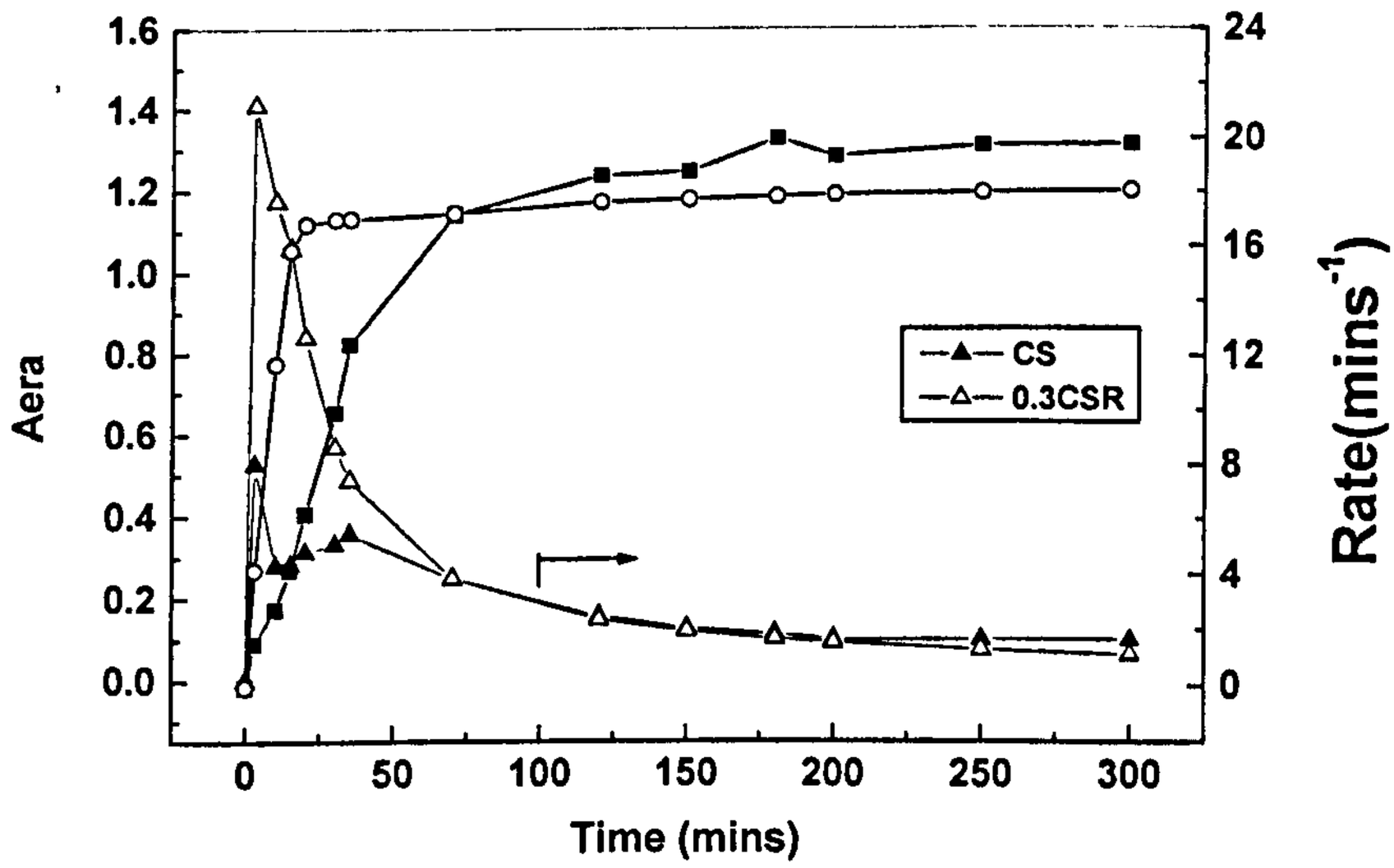

Figure 9.3.9 Surface expansion (red cures), and rate of change of surface area (black cures) for chitosan and crosslinked chitosan membranes

Fractional ES releases from uncrosslinked and crosslinked chitosan films were plotted as a function of time in Figure 9.3.10. The release profiles followed the expected trends, in that the release from the films was most rapid at the initial stages. The highest initial release rate for each film was observed as seen in Figure 9.3.11. For fully hydrated hydrogels containing the dissolved drug, the release into an infinite sink is nearly always Fickian [219,295]. However, starting with a loaded drug in a dried hydrogel, the xerogel has first to absorb water, which act as a solvent for the drug, followed by diffusion of the solute along the aqueous pathways to the surface to be released to the surrounding fluid. From Fick's law of diffusion, the flux is directly proportional to the surface area for fixed values of other dependent variables. Although the diffusion coefficient, D, depends on the water content and has a fixed value for fully hydrated systems, it will not be constant for systems which are swelling while they are releasing active additive. Until the hydrogel is fully swollen, there will be a decreasing gradient of diffusion from surface to the centre. Release across the surface will be partly controlled by the D value in the hydrogel close to the surface [297], which may quickly approach the characteristic D value for the fully hydrated composition.

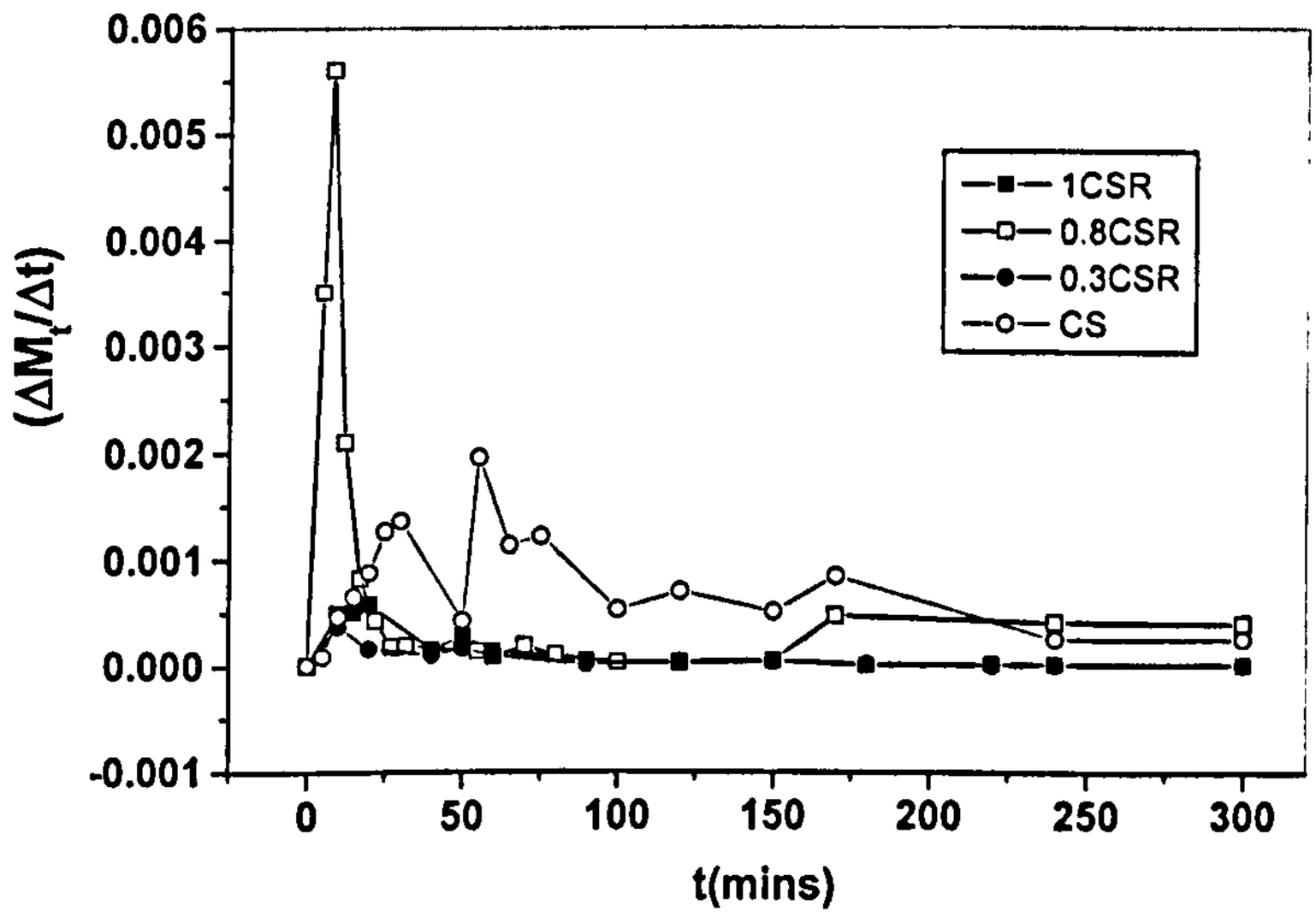

Figure 9.3.10 Fractional ES release from various chitosan films

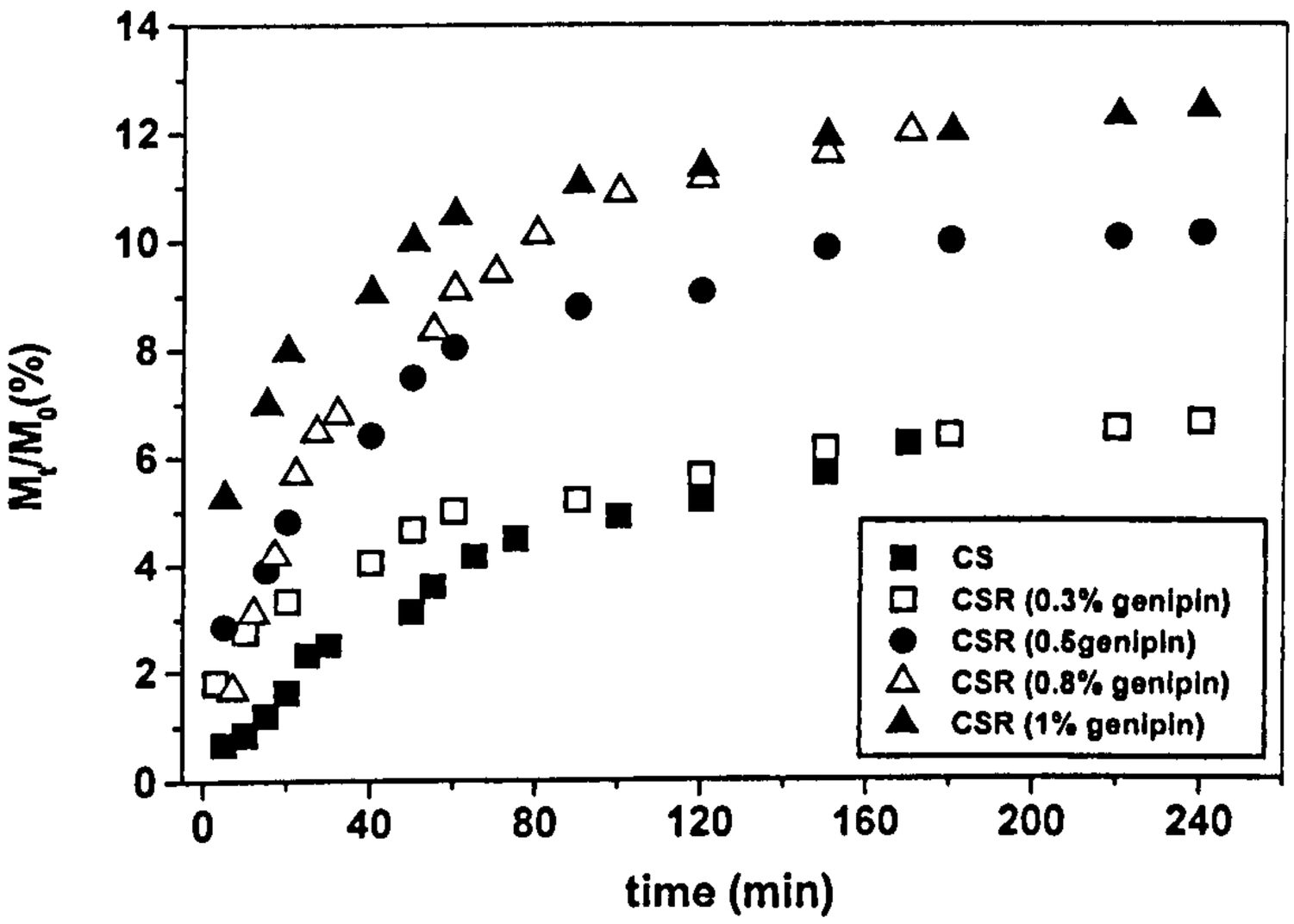

Figure 9.3.11 Rate of drug release as a function of time

Provided the supply of the drug from the interior by diffusion, or dissolution of dispersant in the surface layer can maintain a constant level of concentration of dissolved drug, the flux would be expected to increase along with expansion of the surface in accordance with Fick's Law. Comparing to Figures 9.3.9 and 9.3.11, the mobility of the surface expansion peaks and of the peak rate for ES release is similar. This emphasises the importance of surface expansion with swelling release profiles.

9.3.2.4 Drug release mechanism

According to Equation 9.3-7, the diffusional exponents for ES release were calculated from the release data by plotting log ($M_t/M\infty$) versus log (t) which yielded straight lines. The diffusional exponents were obtained from the slope of these lines, while the diffusional constant (k) was also obtained from the intercept (Table 9.3.3). It can be seen that the exponent *n* for ES release from all crosslinked chitosan membranes, with the exception of the 0.8CSR sample, were smaller than 0.5, such that the release behaviour for ES dispersed in crosslinked chitosan membranes can be categorized as pseudo-Fickian.

Table 9.3.3 Exponential dependence of drug release on time

Sample	Exponent (n)	Constant (k)
CS	0.65	0.24
0.3CSR	0.29	1.37
0.5CSR	0.34	1.74
0.8CSR	0.51	0.93
1CSR	0.22	3.99

However, the exponent for ES release from uncrosslinked chitosan membrane is 0.65, suggesting that the transport process had an anomalous (non-Fickian) character. For 0.8CSR sample (genipin content: 0.8%), the release behaviour is in the nature of Fickian diffusion. From the experimental data, it can be concluded that crosslinking with genipin produced different drug release behaviours.

The mechanism for release would not be expected to be Fickian, but rather more likely to be anomalous and possibly the often desirable zero-order release. The existence of a slow macromolecular relaxational process in the swollen region is believed to be responsible for the observed non-Fickian behaviour [298]. Many parameters may influence the release profile: (1) polymer composition, and hence water uptake; (2) the polymer/drug interactions and the drug load concentration in polymer; (3) association of drug with polymer structure; (4) kinetics of swelling behaviour; etc.

A comparison of the drug release profiles of hydrated and dried crosslinked films, as shown in Figures 9.3.1 and 9.3.11, indicates the differences in drug release behaviour. For hydrated films, when the genipin content was 0.3% or 0.5 % the amount of drug release was smaller than un-crosslinked ones, but when genipin content was 0.8% or 1 % the diffusion rate became faster than uncrossed ones. However, for dried films the higher the genipin content the greater was the amount of drug release. These results could be caused by interactions between ES and chitosan. As a result of intimate contact, there are stronger interactions between ES and the amino group in chitosan in the dried state than in the hydrated state. If crosslink density increased, it could

reduce the number of free amino groups, leading to weaker interactions in the drug release system, and a increase in the amount of ES released from the film. It can be summarised that interactions between dissolution media, polymer and drug are the primary factors in release control.

The controlling mechanisms are essentially quite different to the swelling-controlled systems described above. This can be explained by the fact that after a dry sample was swollen to equilibrium, some macromolecular chains could be disentangled to yield a different structure and different swelling kinetics upon subsequent swelling processes. The release profile derives from a combination of several contributing factors, which may change with time at different rates and various formulation variables influence drug release rate to a greater or lesser extent.

9.3.2.5 Conclusions

The mechanisms that control the release of loaded ES drug from initially dry films are complex. From the above studies, it can be concluded that the drug release behaviour from a dry membrane divides into two stages. In the first stage, the dynamic swelling changes the water content from zero to the equilibrium water uptake over a period. Transport of solute through the network depends on the degree of swelling, ranging from zero in the dry membrane to a maximum which determines the diffusion coefficient, D, for the fully equilibrated hydrogel. In the second stage, the diffusion coefficient is constant. The increase in the surface area with time and the presence of the interaction between the ES drug and chitosan amino groups were shown to be important factors governing the profile and level of the release rate. The diffusional exponent, n, is an important indicator of the release mechanism. When the film was crosslinked by genipin, the value of n decreased and the release behaviour generalised from anomalous diffusion to pseudo-Fickian or near to Fickian diffusion. Furthermore, depending on the crosslink density in the films, a burst or lag effect can be observed at the very early stages of the drug release

9.4 Separation of Protein from Eleutherococcus Senticosus

9.4.1 Introduction

There has been a dramatic revival in recent years in the use of herbal preparations for the treatment of a wide range of ailments [299]. Some products are being recommended for use as 'specific' to treat particular illnesses or conditions much like conventional synthetic medicines are prescribed in North America, Western Europe and the rest of the economically developed world [300]. Eleutherococcus Senticosus (ES) is a typical oriental herb and a herbal medicine that has been widely used in a number of countries, including China, Japan, Korea, Russia and the USA, both as a health supplement and for medical purposes, including enhancing capacity for physical and mental work, increasing the protective functions of an organism against physical, chemical and biological stress, and treating heart disease, diabetes and blood circulatory problems [300]. As a result of its high protein content, ES can only be taken in tablet form and cannot be injected directly into the patient's body [17]. Its use is, therefore, limited. In recent years, research into its use, with a view to widening its application, has been undertaken by a number of countries across the world, including many universities in the USA [301]. There is not yet any report on solutions to this problem.

Proteins are very diverse. They differ by size, shape, charge, hydrophobicity and affinity for other molecules. All these properties can be exploited to separate them from one another. It is well known that this herbal medicine is a very complex compound. Therefore separating protein from ES is also more difficult. Chitosan is capable of absorbing protein due to chitosan molecules containing a larger number of hydroxyl (-OH) and amino groups [30]. In this research, in order to develop novel chitosan films crosslinked by genipin as potential membranes for protein separation from ES, the feasibility study of protein separation will be carried out.

9.4.2 Introduction to Eleutherococcus Senticosus

ES belongs to the family of ginsengs, which is a well-known herbal medicine. It is also named *Acanthopanax senticosus*, *Araliceae* or *Siberian ginseng*. It is a woody

shrub that is usually 1.5-2m tall. Its shoots are 4-6cm in diameter with a very spiny, light grey or brownish bark. The leaves are long-petioled, compound palmate. The flowers are 5-merous, long-pedicelled. Its fruit are black drupes about 0.7cm long. ES is widely distributed in the northern regions of Russia (Siberia) and Northeast Asia, such as China, Korea, Japan *al.* [302], where they have been valued for thousands years. Figure 9.4.1 shows a diagrammatic representation of ES.

ES is a useful medicine plant. The cortical tissues of its roots and shoots contain higher concentrations of biologically-active substances and are used as a tonic in Chinese traditional medicine [303,304]. It became a popular herb plant especially in the last three decades because of the therapeutic properties of its roots. They are considered to have a similar pharmacological action to Chinese ginseng. The biologically-active constituents, showing adaptogenic activity, are heterogeneous compounds known as eleuterosides [303,304].

The chemical composition of ES is very complex [300,302]. In order to verify and confirm the medical use, since the late 1970s a variety of chemical investigation have been undertaken, leading to the isolation of triterpenes, lignans, phenylpropane derivatives and coumarins [300]. ES has been found to contain niacin, amino acids (protein), carbohydrates and other vitamins and minerals [300]. It has been used to promote an overall sense of well-being. Herbalists call this herb an "adaptogen", which means that it helps the body adapt to any situation, which normally would alter its function. The eleutherosides have been shown to be responsible for the adaptogenic properties of the plant. Eleuthosides are a range of glycosides with aromatic alcohol aglycones. The glycosides appear to act on the adrenal glands, helping to prevent adrenal hypertrophy and excess corticosteroid production in response to stress. The eleutherosides additionally help to reduce the exhaustion phase of the stress response, and return the adrenals to normal function at a faster rate than otherwise. As a result, ES has beneficial effects on the heart and blood circulation. It has been shown to increase energy and stamina, and to help the body resist viral infections, environmental toxins, radiation, and other chemotherapy. In Chinese medicine, the roots of ES are used to treat rheumatic diseases and heart ailments. ES is also popular herbal remedy for debility and depression [17,300-304].

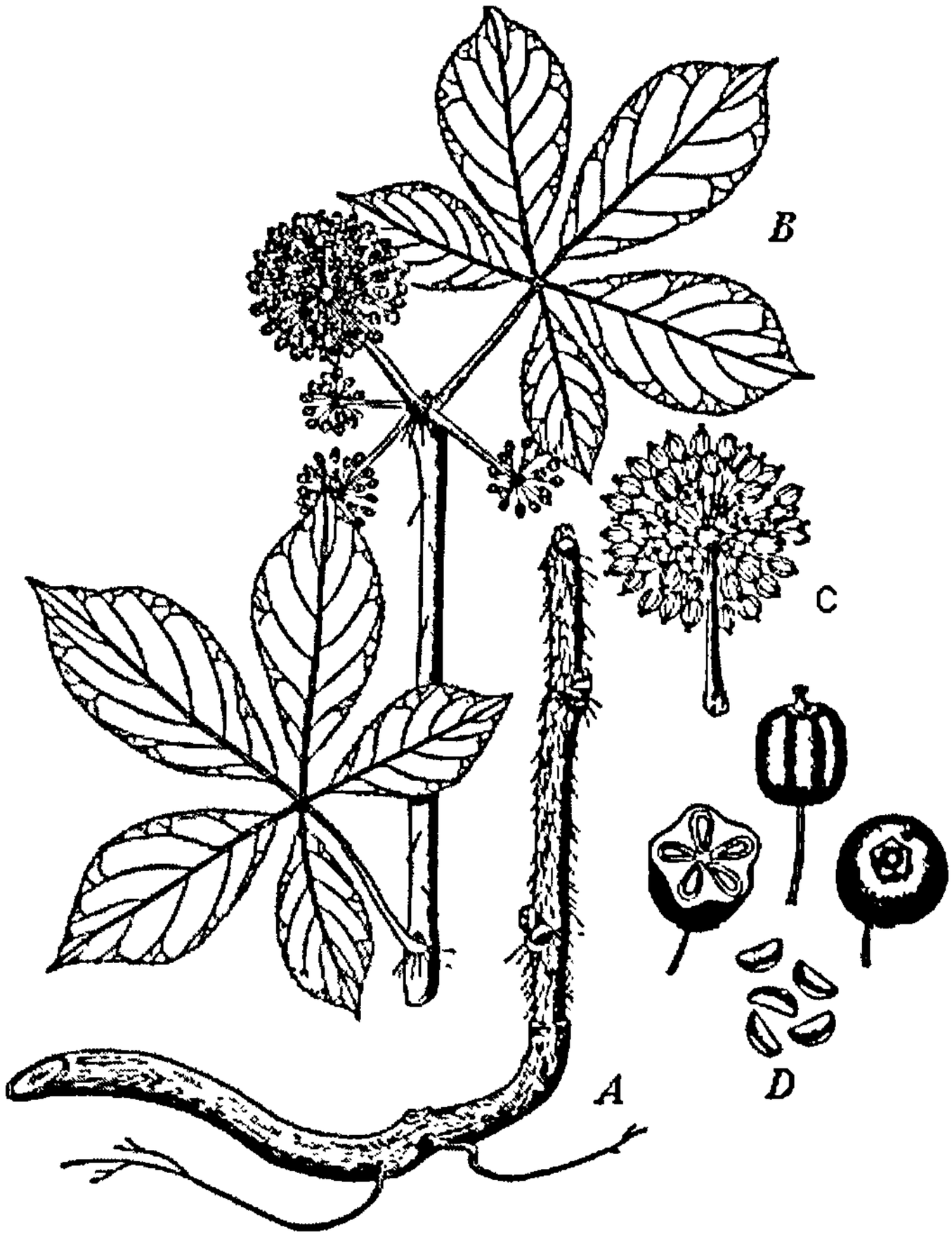

Figure 9.4.1 Diagrammatic representation of eleutherococcus senticosus. (A) portion of root; (B) leaf whorl; (C) inflorescence (D) fruit and seeds [304]

9.4.3 Characterisation of protein content in ES

The methods most commonly used for measuring protein concentration are based on UV absorption of protein solution or visible region spectrophotometry [213]. Most proteins exhibit an absorption maximum at 280nm, which is attributable to the amino acid. The absorbance of the sample can be measured at both 280nm and 260nm with a correction formula applied [305] as follows:

$$\text{Protein (mg ml}^{-1}) = 1.55\, A_{280} - 0.76\, A_{260} \qquad [9.4\text{-}1]$$

In this study, hen egg white was used as a standard protein and its UV spectra for various concentrations of the solutions are shown in Figure 9.4.2. It is clear that the absorption peak at 280 nm increased with increasing the protein content in hen egg white solution. The protein contents in the solutions were calculated by Equation 9.4-1 and shown in the figure. This method was only used for pure protein solution because if a mixture contains protein such as ES, its base line of UV spectrum usually changes. In order to characterise protein content in ES it is necessary to find a new method.

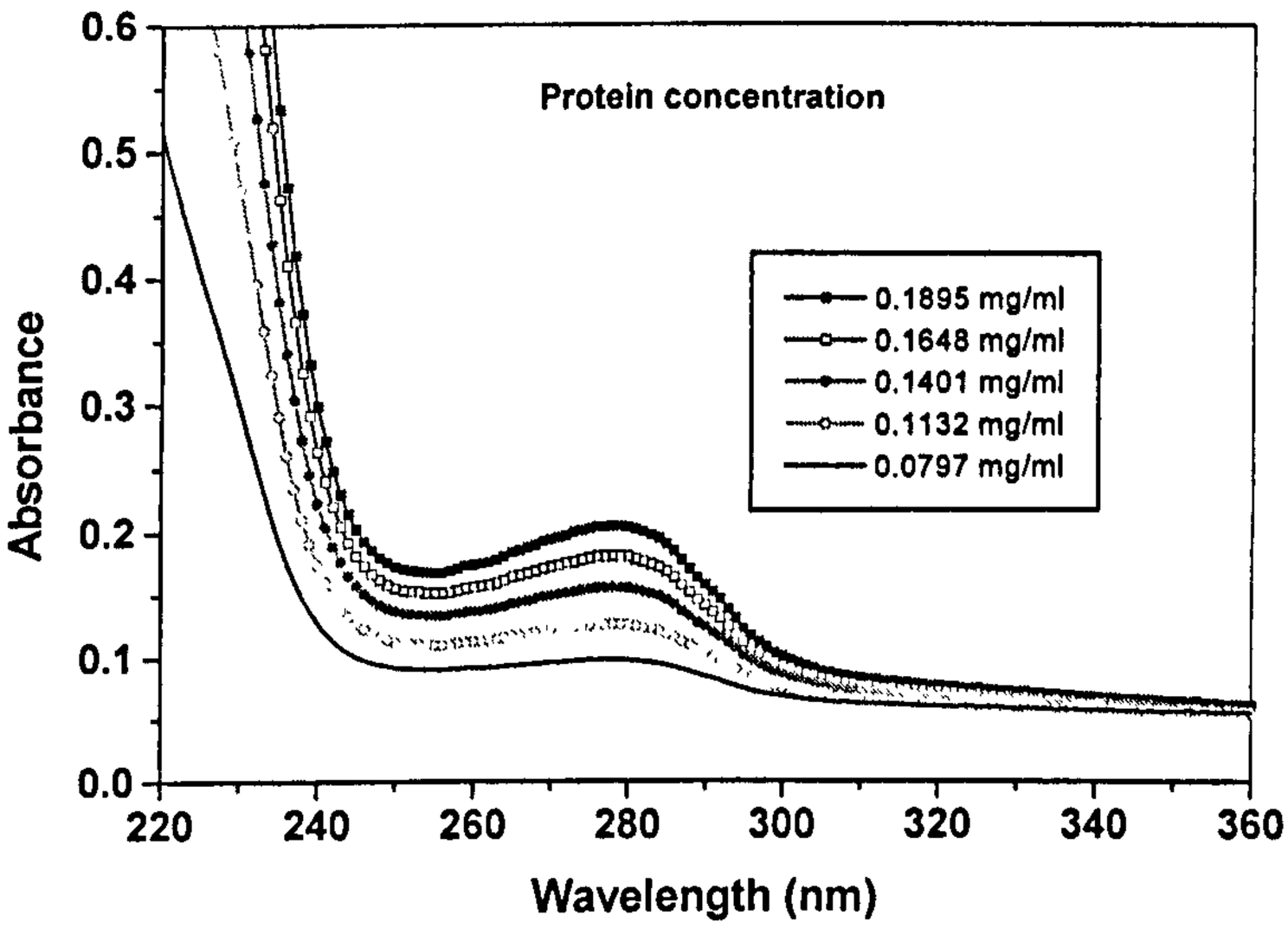

Figure 9.4.2 UV spectra of hen egg white for various solution concentrations

From Figure 9.4.2, the area of each absorption peak at 280nm was calculated and it was found that the linear relationship between the protein concentration and area of absorption peak at 280nm as shown in Figure 9.4.3, is a characteristic that can be introduced as a novel method of quantifying protein content in ES, thus overcoming the problem mentioned above. Figure 9.4.3 introduces a standard curve of protein content and this will be used in the later study.

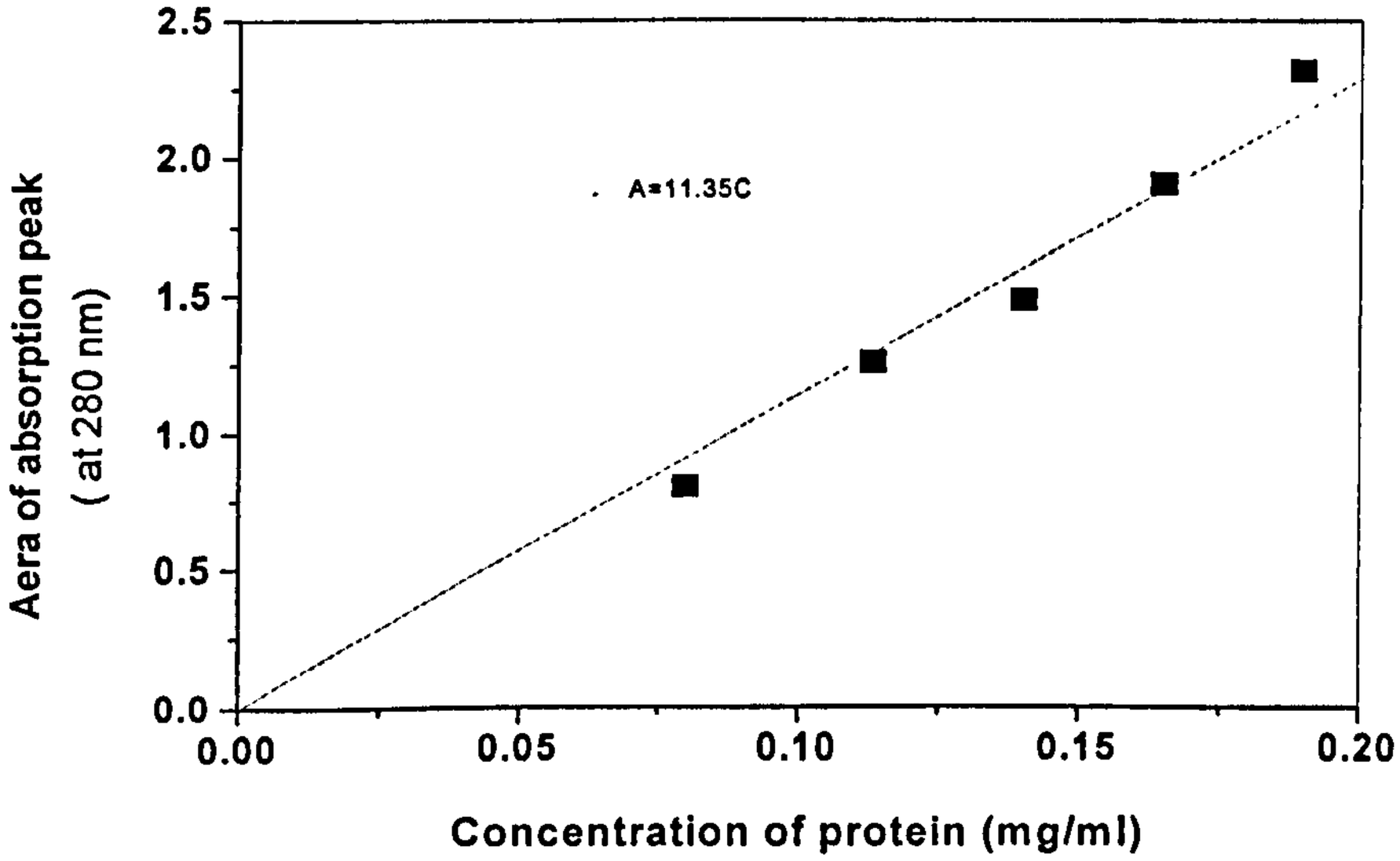

Figure 9.4.3 Relationship between protein concentration and area of absorption peak at 280nm.

Figure 9.4.4 shows a series of UV spectra for various concentrations of ES solution.

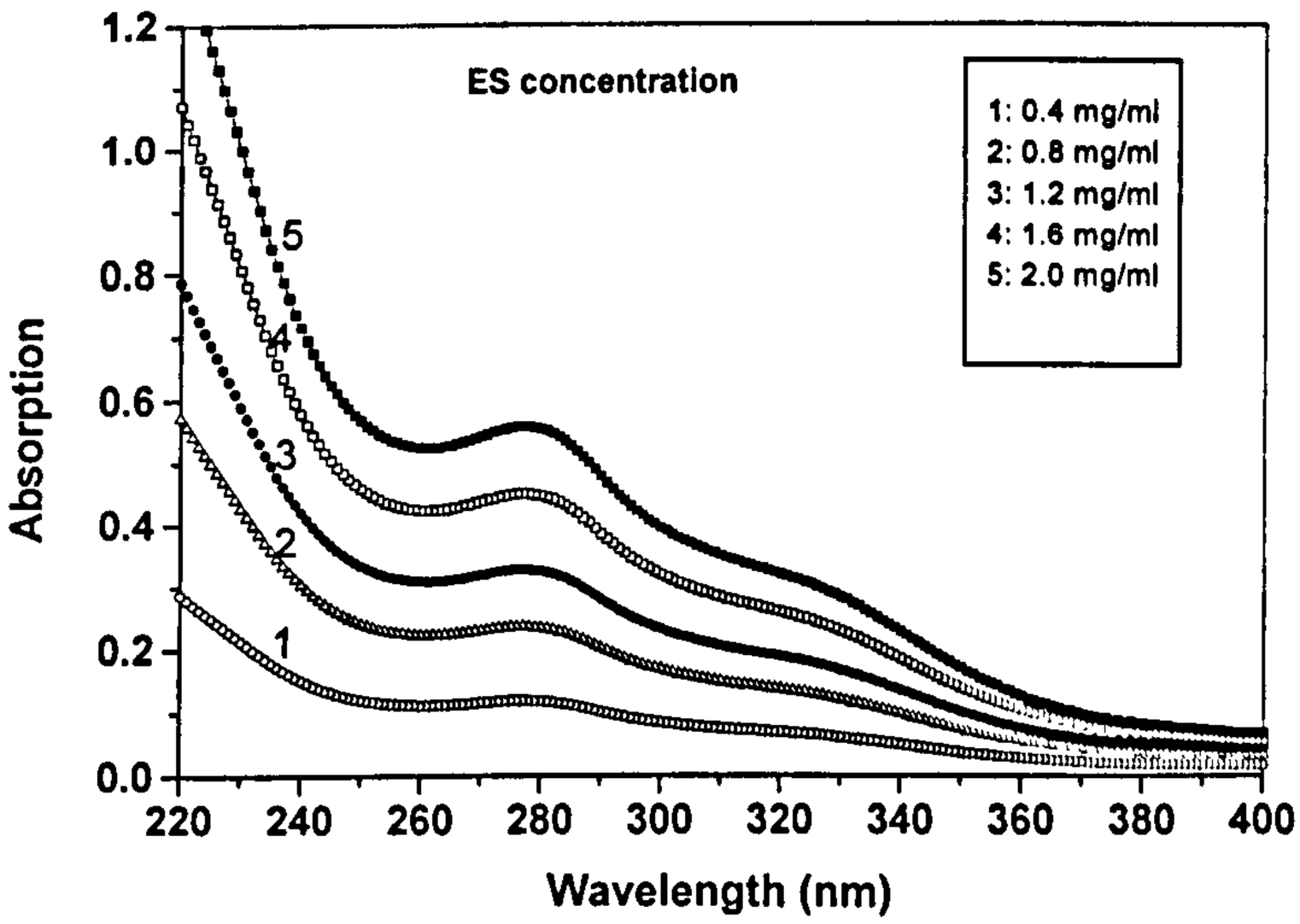

Figure 9.4.4 A series of UV spectra for various concentrations of ES solutions

The area of the absorption peak at 280nm was calculated and using the standard curve as shown in Figure 9.4.3 the protein content in each concentration of ES solutions was estimated. All the data obtained are listed in Table 9.4.1. It was found that the average percentage of protein content in ES solution was about 15%.

Table 9.4.1 Estimate of the protein content in ES solutions

ES concentration (mg/ml)	Protein content (mg/ml)	Protein /ES (%)
0.2	0.0308	15
0.4	0.0559	14
0.6	0.0829	14
0.8	0.1204	15
1.2	0.1709	14
1.6	0.2220	14
2.0	0.2790	15

*Average percentage protein content: 15%, Standard deviation: ± 2%

9.4.4 Absorption method for separation of protein from ES

Chitosan has the ability of absorbing protein from aqueous solutions, which was firstly demonstrated by Hachman [306]. Since chitosan contains chemically reactive groups (-OH and -NH_2 groups), its surface can be easily coupled with various affinity ligands. Hachman's results indicated that maximum absorption occurs at the isoelectric point of the protein and that, at a given pH, the extent of absorption decreases with increases in the ionic strength of the solution. Recently, many researchers have developed novel macroporous chitosan membranes, which possess controlled pore sizes, good mechanical strength and chemical stability, as well as hydrophilicity and biocompatibility [307]. They have been successfully employed for affinity separation or purification of lysozyme and serum albumins [308, 309]. Efficient separation was achieved, and high purity (>99%) lysozyme obtained [308]. In this section, we will examine whether chitosan membranes crosslinked by genipin

are suitable to use for protein separation from ES. The absorption method will be employed.

The equilibrium absorption of protein on uncrosslinked and crosslinked chitosan films was carried out in bath experiments at room temperature. The samples were cut into small pieces (3.0cm^2). The sample membranes were first swollen in phosphate buffer saline (PBS, pH 7.4) solution to reach equilibrium, and then they were introduced into test tubes containing 20ml ES solutions of known initial concentration. These suspensions were gently shaken (at 200rpm) at 25°C during the experiment. It is known that chitosan is insoluble in neutral or alkaline solution, but in this study it was observed that when uncrosslinked chitosan film immersed in the ES solution after two hours, the chitosan film completely dissolved. This suggests that the changes in the solubility of chitosan were brought about by ES due to the interactions between chitosan and ES molecules, which have been studied in Section 9.3.2 (as shown Figures 9.3.3 and 9.3.4). Figure 9.4.5 shows UV spectra for ES solution measured at time of 0, 48 and 72 hours after the sample of crosslinked chitosan film (0.5CSR) had been immersed in the bath. It was clearly observed that the absorption peak at 280nm for the ES solution decreased and the absorption equilibrium was reached within 48 hours.

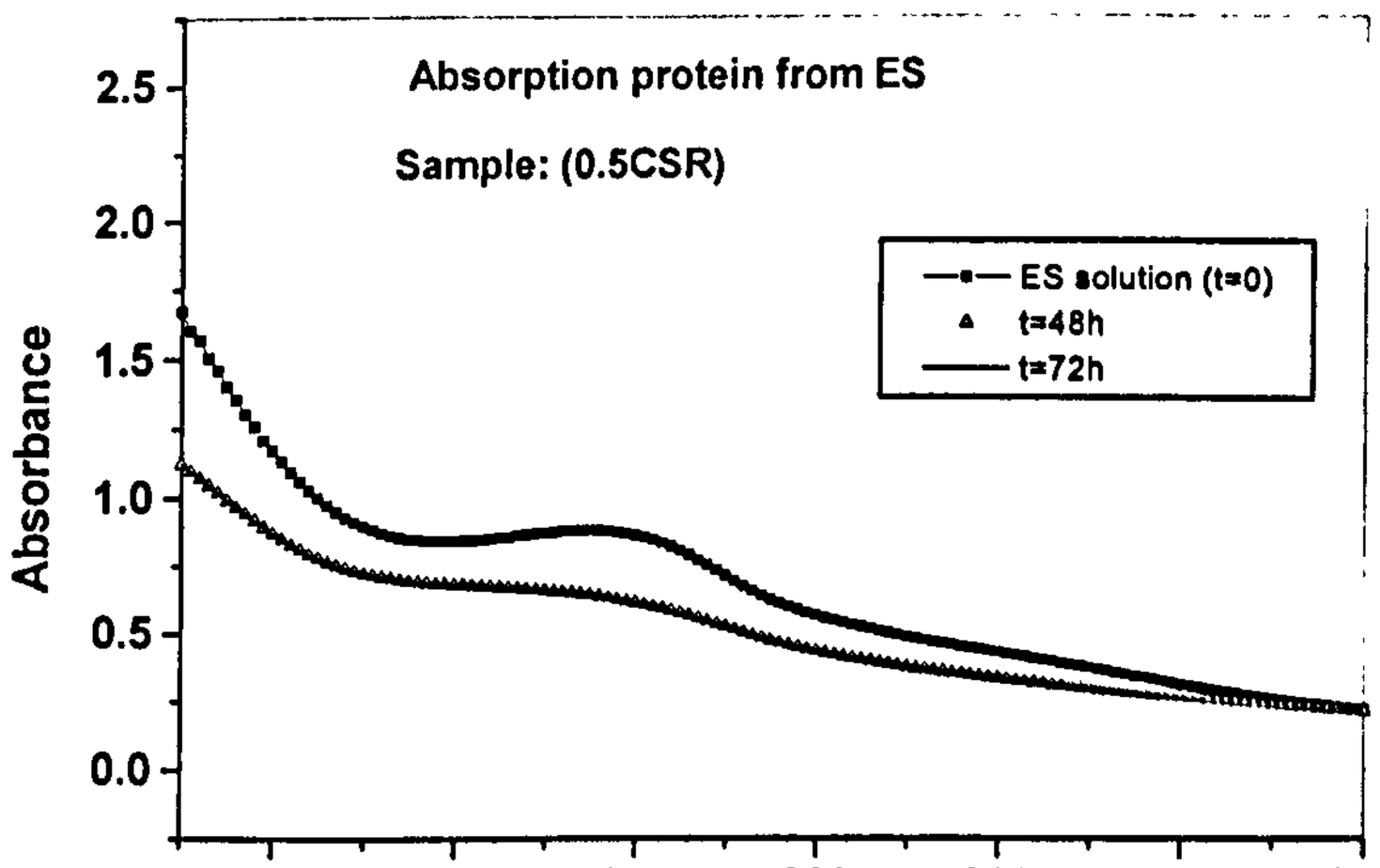

Figure 9.4.5 UV spectra of ES solution before and after absorption of protein by crosslinked chitosan film (0.5CSR)

Figure 9.4.6 shows UV spectra for ES solutions before and 48 hours after samples of 0.1CSR or 0.3CSR were introduced into the solutions. The results again indicate a decrease of the absorption peak of protein at 280nm and these results confirm that the crosslinked chitosan films have the ability to absorb protein from ES solution. However, the results also show that the extent of protein absorption depends on the crosslink density of the chitosan film – the higher the crosslink density the lower the film's ability to absorb protein. In this study, the capacity of protein absorption is defined as the percentage of absorbed protein from the solution onto a unit volume of a film. From the UV spectra results, as indicated in Figures 9.4.5 and 9.4.6, the total protein absorbed on each sample was determined and the capacity for protein absorption for each film was calculated. Each experiment was done 5 times and the average values were taken as shown in Table 9.4.2.

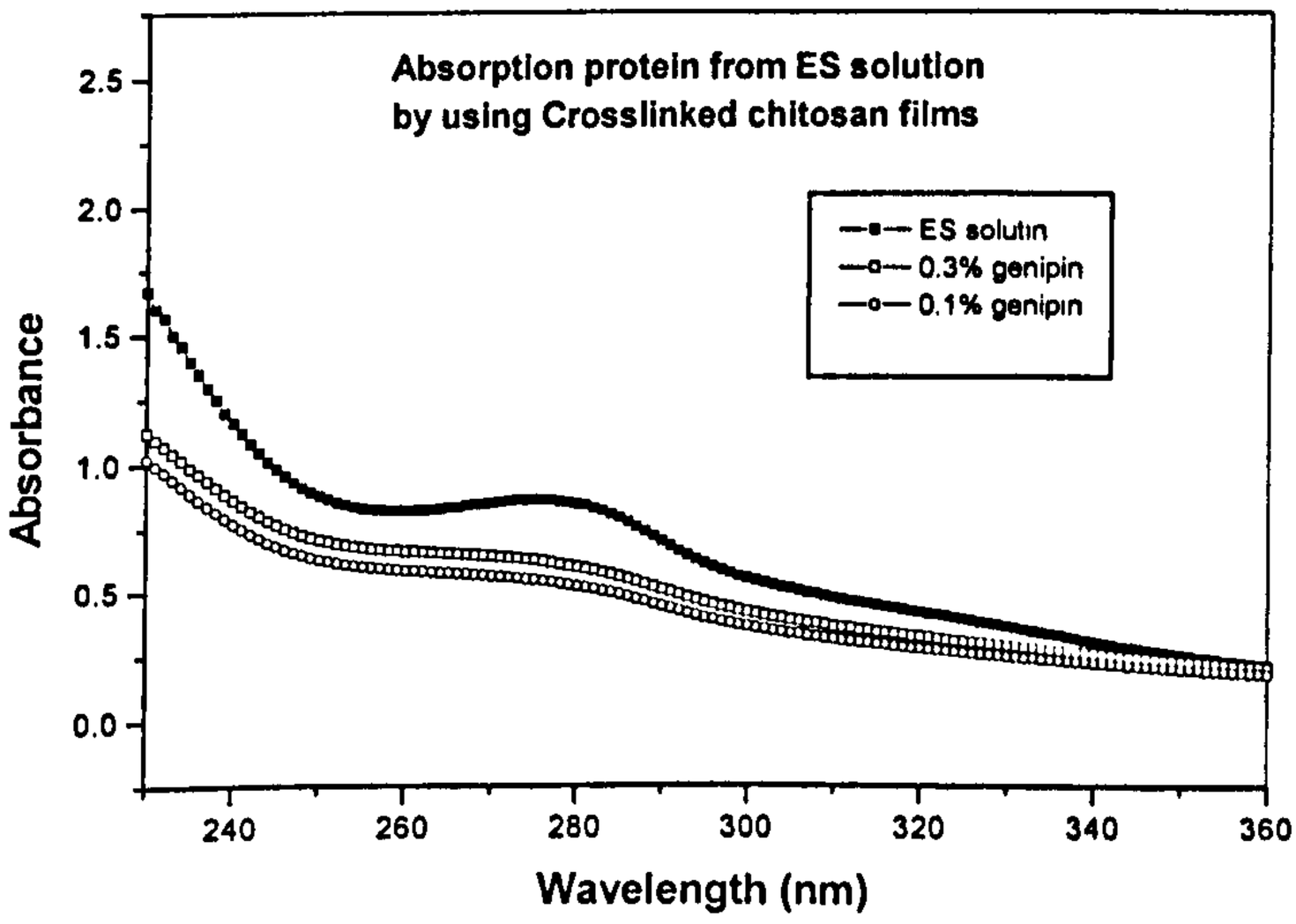

Figure 9.4.6 UV spectra of ES solution before and after protein absorption by crosslinked chitosan films (0.1CSR and 0.3CSR)

Table 9.4.2 Capacity of protein absorption by chitosan films from ES solutions

Sample	Crosslink density (%)	ES concentration (mg/ml)	Capacity (%)
CS	0	0.45	- (Dissolved)
0.1CSR	0.26	0.45	67
0.3CSR	2.23	0.45	60
0.5CSR	4.65	0.45	50

*Standard deviation: ± 5%

The results indicate that over 50% of the protein in ES was removed by the crosslinked chitosan films. The crosslinked chitosan membranes are very stable and maintain their strength in the solution, and the film with lower crosslink density had higher protein absorption capacity than the ones with higher crosslink density. This is because chitosan molecules contain a large number of free amino groups (NH_2), and crosslinking, which reduced the number of free amino groups, probably reduced the number of H^+ bonds in amino groups, causing a decrease in the number of cations and thereby lessening the absorption of proteins which carried negative charge at neutral pH [30].

From the above study, it can be concluded that protein can be separated from ES by means of crosslinked chitosan membranes, although the efficiency is not high. In the practical medicine industry, separation or purification of a mixture by the absorption method is not commonly used due to the appearance of bioactive substances. So, in the following section, protein separation from ES by a membrane separation method was investigated.

9.4.5 Membrane separation of protein from ES

Membrane separation involves separating two phases using a barrier and restricting the transport of various chemicals in a selective manner. A membrane can be

homogenous or heterogeneous and symmetric or asymmetric in structure [310]. Transport through a membrane can be affected by convection or by diffusion of the individual molecules, induced by an electric field or gradients of concentration, pressure or temperature [310]. The membrane thickness may vary from as small as 100 microns to just several nanometres. Membrane separation techniques allow the separation and concentration of solution components without the denaturation of proteins or bioactive substances and without causing any changes. Furthermore, these techniques are energy efficient. As a result, they are considered as particularly useful in the development of raw materials and medicines [310]. ES is a herbal medicine and a functional substance. Membrane separation may be extremely well-suited to ES processing.

Membrane separation of protein from ES solution was investigated using diffusion cells. The details of the method were outlined in Chapter 2. Before carrying out the experiment, the samples of membranes were first swollen in phosphate buffer saline (PBS, pH 7.4) solution to reach equilibrium. From Figure 9.4.7, which shows UV spectra for ES solution before and after passing through chitosan (CS) membrane, two areas of absorption peak at 280nm were calculated.

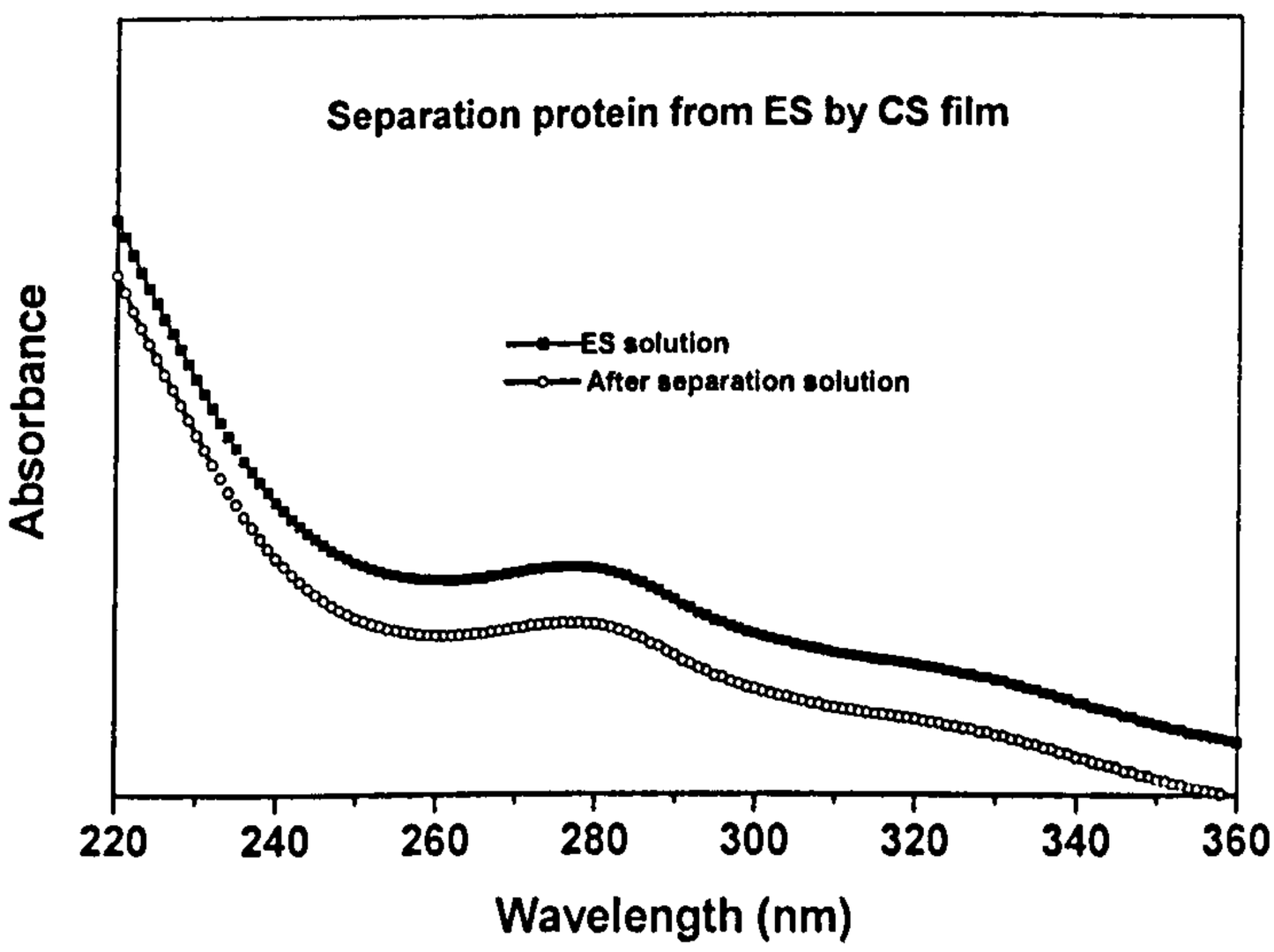

Figure 9.4.7 UV spectra for ES solution before and after separation of protein by the CS membrane

The fact that two values was the same means that there was no change in the protein content after the solution had passed through the membrane. This indicates that the chitosan membrane was unable to separate protein from ES solution.

Figure 9.4.8 shows UV spectra for ES solutions before and after passing through crosslinked chitosan membranes (samples: 0.1CSR, 0.3CSR and 0.5CSR). The area of the absorption peak decreased for the solutions that had passed through a membrane. The decrease was more pronounced where highly crosslinked membrane had been used. For characterisation purposes, in this study, the capacity of protein separation is defined as the decreased area of the absorption peak at 280nm as a percentage of the total area. The capacity of separation protein from ES solution for each membrane was calculated. Each experiment was done a total of 5 times and the average values of the protein separation capacity for each membrane were taken and are summarised in Table 9.4.3.

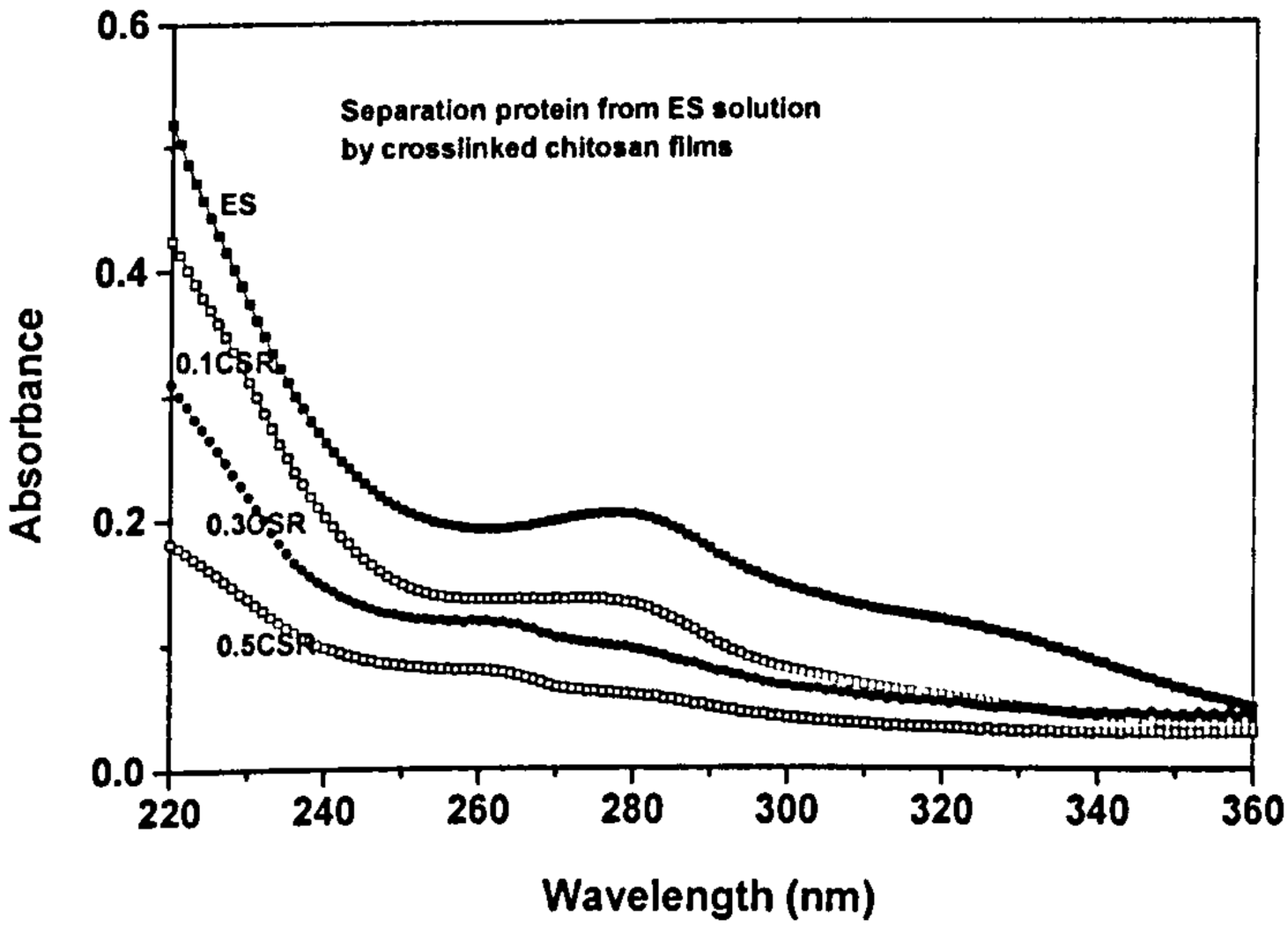

Figure 9.4.8 A comparison of UV spectra for ES solution after protein separation by crosslinked chitosan films

Table 9.4.3 Capacity of protein separation from ES solution

Sample	Crosslink density (%)	ES concentration (mg/ml)	Capacity (%)
CS	0	0.11	0
0.1CSR	0.26	0.11	14.
0.3CSR	2.23	0.11	81
0.5CSR	4.65	0.11	88

*Standard deviation ± 5%

The results of this study suggest that chitosan membrane crosslinked by genipin can be used for the separation of protein from ES. The capacity of protein separation increased with increasing crosslink density. When the film with crosslink density was 2.23%, the capacity reached 81%. However, further increases in the crosslinking density did not give rise to significant improvements in the capacity of the film. Crosslinked chitosan membranes as opposed to uncrosslinked ones are suitable for protein separation from ES, and this method is most optimal when the crosslink density was 2.23%.

The significant differences in the capacity behaviour of a film produced by the two methods of protein separation can be understood by looking to the specifics of the separation mechanisms. There are two main controlling factors of protein separation in the membrane separation method: the molecular interactions between ES and chitosan and the mesh size of a membrane. The effects of crosslink density on the molecular interaction between ES and chitosan and on the mesh size of crosslinked chitosan films were studied in a previous section (9.2 Controlled drug release). The conclusion was that crosslinking of chitosan resulted in decreases in both the mesh size of the film and the interaction between ES and chitosan. For low crosslink densities, the capacity of protein separation is low due to the effect of interactions between ES and chitosan. For high crosslink densities, because of the large size of protein molecules, the capacity is determined mainly by the mesh size of the film.

9.4.6 Conclusions

ES is a useful medical plant and is a well-known herbal medicine. As a result of its high protein content, ES can only be taken in tablet form and cannot be injected directly into the patient's body. It is necessary to separate the protein from ES before injection. From the study in this section, it can be concluded from the protein separation studies that chitosan films crosslinked by genipin offer a potential membrane material for separation of protein from ES.

CHAPTER 10

Conclusions and Future work

10.1 Introduction

Novel crosslinked chitosan and chitosan/PEO blend films were prepared using the solution casting technique. A naturally occurring and non-toxic crosslinking reagent, genipin, was used to form chitosan and chitosan/PEO blend networks. Two types of PEO were used, one with a molecular weight of 20,000g/mol (HPEO) and the other of 600g/mol (LPEO). Genipin is used in traditional Chinese medicine and extracted from the Gardenia fruit. Importantly, it overcomes the problem of physiological toxicity inherent in the use of some common synthetic chemicals as crosslinking agents. The morphology and the physical properties of the films were characterised by a number of techniques, such as differential scanning calorimetry (DSC), infrared spectroscopy (FT-IR), static laser light scattering (SLLS), small angle x-ray scattering (SAXS) etc. The study of the membranes for potential medical application such as drug delivery carriers and for protein separation from eleutherococcus senticosus (ES) was also conducted. Based on the results obtained from this study, the following conclusions can be drawn.

10.2 Conclusions

Morphology and crosslinking

The miscibility of chitosan/HPEO and LPEO blends was investigated by DSC and FT-IR spectroscopy. The spectra of the blends indicated that there are specific intermolecular interactions between the two components. The interaction parameter, χ_{12}, in the chitosan/HPEO blends was found to be -0.16. From a thermodynamic point of view, the more negative the χ_{12} value, the stronger the interactions are in a blend. The degree of crystallinity of HPEO in the samples, which was estimated from DSC data, decreased with increasing chitosan content. A phenomenon was observed for chitosan/LPEO blends: when wt.% of chitosan was smaller than 60%, the melting points increased as wt.% of chitosan increased. From the studies of FT-IR spectra,

DSC and SAXS, it is believed that there were molecular interactions between chitosan molecules and the molecules in crystalline phase in the chitosan/LPEO blends.

The effects of crosslinking on morphology of the films were also investigated. The high scattered intensities from chitosan/HPEO and chitosan/LPEO networks suggest that heterogeneous structures exist in the blends. This indicates that crosslinking the blends, particularly at high HPEO or LPEO contents, leads to phase separation. SAXS and DSC results also demonstrated that using naturally-occurring genipin as a crosslinking agent led to decreases in the crystalline size, meaning that the presence of networks restricts crystallisation.

The temperature-dependence of the crosslinking reaction was studied by means of FT-IR and UV spectra analysis. The results of FT-IR spectra analysis indicated that the crosslinking reaction, where the amino group in chitosan reacted with the ether group in genipin, occurred after the addition of genipin. From the UV spectra study, the results show that the crosslinking reaction rate and the homogeneity of the crosslinking process were influenced by temperature. At 25°C, a homogeneous crosslinking reaction occurred. At higher temperatures, the heterogeneous crosslinking reaction took place due to the restriction of molecular mobility of genipin by the intrinsic viscosity of the chitosan solution and crosslinking reticulation during film-formation.

Conformation of chitosan macromolecules in aqueous solution

For a more comprehensive understanding of the mechanical properties of chitosan films, the examination of the effects of pH on the conformation of chitosan macromolecules in solution were performed by SLLS. The results show that the conformation of chitosan macromolecules in solution was influenced by the pH. The radius of gyration of chitosan macromolecules in solution increased with increasing pH, indicating that chitosan has an extended chain conformation in low pH solutions and a tendency to aggregate in high pH solutions. In the dilute chitosan solutions, a coil to globule transition, the single chain collapse occurred.

Mechanical properties

The mechanical properties of the chitosan/PEO blend films were investigated under various film-forming conditions.

An improvement in the mechanical properties was achieved when chitosan/LPEO was crosslinked with genipin. Tensile tests revealed that the greatest strength (50MPa) occurred at 20wt.% LPEO in the chitosan blend and the greatest extension (30%) at 65wt.% LPEO. The increases in the elongation at break, tensile strength and modulus of the crosslinked films, especially in those with high water content, would prevent them from disintegrating in medical applications. However, for chitosan/HPEO systems, the results clearly show that crosslinking with genipin did not, because of the lower miscibility of chitosan with HPEO, give to rise to improvements in the mechanical properties.

The effects of the solution pH used for film-formation on the mechanical properties of the chitosan films were understood by studying the aggregation behaviour of chitosan macromolecules in aqueous solutions. In low pH solutions, the homogenous gel network was obtained due to intermolecular chain association during gelation, resulting in better mechanical properties (tensile strength and elongation at break) of the chitosan films.

The effects of the crosslinking temperature on the mechanical properties of the chitosan films were also investigated. The results show that crosslinked chitosan films have larger elongation at break when the temperature of 25°C was used. This can be explained by a homogeneous crosslinking reaction. When the crosslinking temperatures were of 40°C and 60°C, the films have greater tensile strength and lower elongation at break. The localised high crosslinked density region, caused by a heterogeneous crosslinking reaction, can be treated as fillers in the film.

Swelling, stability and surface properties

With the use of crosslinking, there were noticeable increases in the stability of chitosan/HPEO or LPEO blends. Genipin crosslinking produced chitosan networks that were insoluble in acidic and alkaline solutions, but were able to swell in these

aqueous media. The swelling behaviour of the films exhibited pH- and temperature-dependent characteristics. The swelling ability can be controlled by the crosslink density.

The surface properties of the films were also examined by contact angle measurements using water and mixtures of water/ethanol. Crosslinked chitosan films increase the wetting properties of the film as shown by contact angle measurement. The results showed that in water the crosslinked chitosan/HPEO and chitosan/LPEO blends were more hydrophobic than the uncrosslinked ones. The addition of PEO and crosslinking by genipin led to the existence of polar forces between the chitosan and water, and therefore, increases in the surface free energy. However, as a result of phase separation in the system, the surface free energy for the crosslinked chitosan/HPEO and chitosan/LPEO films declined. When water/ethanol mixtures (70/30, 50/50) were used as media, the surface free energy of the films was lower than that in water due to lower hydrophilicity of ethanol.

Controlled drug-release

The permeability of vitamin B_{12} through crosslinked and uncrosslinked, chitosan and chitosan/PEO blend membranes was investigated. The effect of crosslink density on the drug-release behaviour was also assessed. The drug-release rate decreased with increasing crosslink density and was particularly sensitive at low crosslink densities. PEO was introduced into the membrane to adjust its mesh size and control the drug-release rate through the molecular weight of PEO and the amount used. The effect of external pH on the drug-release behaviour was also examined. The drug-release rate was sensitive to pH and this was in agreement with the swelling nature. Additionally, the results of the study of the effect of the different degrees of deacetylation of chitosan on the controlled drug-release show that high degrees of deacetylation meant fast rates of drug release.

ES drug-release from chitosan carriers was conducted in two ways: fixed boundary (fully hydrated state) and moving boundary (dry state). For fixed boundary, it was clear that the ES release rate from the carrier was governed by both the mesh size of membrane and the molecular interactions between chitosan and ES. This drug-release

mechanism obeys Fick's diffusion law. For the moving boundary case, the release mechanisms were complex. In the early stages, ES release rate through the carrier depends on the degree of swelling ranging from zero in the dry membrane to a maximum, which determines the diffusion coefficient (D), for the fully equilibrated hydrogel. At the second stage, the diffusion coefficient is constant. When the film was crosslinked by genipin, the value of the diffusional exponent (n), an important indicator of the release mechanism, decreased, and the release behaviour was generalised from anomalous diffusion to pseudo-Fickian diffusion.

Protein separation from ES

The feasibility study of the separation of protein from ES solution by crosslinked chitosan membranes was also carried out. Its results suggest that chitosan membrane crosslinked by genipin can be used to separate protein from ES when the genipin content is higher than 0.3%.

Overall, it is believed that the present study has provided useful information for developing the chitosan/PEO blend films for future medical applications.

10.3 Recommendations for future work

In view of the findings of and the developments in the research, recommendations are proposed for future work leading to the development of chitosan/PEO blend films crosslinked by genipin as potential functional membranes.

Controlled drug-release

It is clearly that crosslinking with genipin produced chitosan networks, which are sensitive to environmental pH and temperature. They showed remarkable characteristics as a drug carrier for control release systems. In this research, drug-release through or from the membranes was conducted using vitamin B_{12} and ES as the only drug models. In order to obtain more useful information for medical applications, other drugs, such as sensitive drugs (anti-cancer drugs), lower molecular weight drugs etc. need to be investigated.

Protein separation from ES

The present feasibility study of protein separation from ES using crosslinked chitosan membranes shall be built upon by collaboration with the medical industry to develop the protein-removed ES for the purpose of direct injection, thereby widening the use of ES.

References

1. J. Jagyu-Grodzinski, *Relative and Functional Polymers*. 39 (1999), 99-138.
2. T. E. Lipatova and Y. S. Lipatov, *Macromol. Symp*. 152 (2000), 139-150.
3. B. L. Seal, T. C. Otero and A. Panitch. *Materials Science and Engineering* R 34 (2001), 147-230.
4. N. V. Majieti and Ravi Kumar, *Reactive and Functional polymers*, 46 (2000), 1-27.
5. J. K. Francis Suh, Howard W. T. Matthew, *Biomaterials* 21 (2000), 2589-2598.
6. T. Chandy and C. P. Sharma, *Biomat Artifi. Organs*. 18 (1990), 1-24.
7. R. Muzzarelli, V. Bladassare, F. Conti, F. Ferrara, G. Biagini, G. Gazzanelli and V. Vasi, *Biomaterials*, 9 (1999), 247-252.
8. J. Knapczyk, L. Kr Wczynski, D. Schenk and Z. Liber, "*Chitin and chitosan: Sources Chemistry, Biochemistry, Physical Properties*", G. Skjak-Break, T. Anthosen and O.Sandford eds, (Elsevier Apllied Science, London, 1989), 665-670.
9. Q. Li , E.T. Dum, E.W. Grandmaison and M. F. A. Goodman. *J Bioact Compat Polym* 7(1992), 370.
10. O. Felt, P. Buri and R. Gurny. *Drug Dev Ind Pharm*, 24(1998), 979.
11. S. Matsuda, H. Iwata, N. Se and Y. Ikada, *J. Biomed. Mater. Res*., 45 (1999), 20-27.
12. G. Goissis, E. M. Junior, R. A. Ch. Marcantonio, R. C. C. Lia, D. C. J. Cancian and W. M. D. Caevallho, *Biomaterials,* 20 (1999), 27-34.
13. K. A. Jonson, G, J. Rogers, S. C. Roe, C. R. Howlett, M. K. Claytone, B. K. Milthorpe and K. Schindhelm, *Biomaterials*, 20 (1999), 1003-1015.
14. H. W. Sung, R. N. Huang, L. L. Huang and C. C. Tsai, *J. Biomater.Sci. Polym.* Ed, 10 (1999), 63-78.
15. C. J. Thomas Lee, C. K. Lin and H. W. Sung, *World Patent* W09819718, 1998.
16. F. E. Bailey and J. V. Koleske, *Poly(ethylene oxide)*. Academic Press. New York, NY 1976.
17. S. Palapura and J. Kohn, *J Biomaterial. Appl*, 6(1992), 216-250.

18. Q. Zhao, M. P. Agger, M. Fitzpatrick, J. M. Anderson, A. Hiltner, K. Stokes and P. Urbanski, *J. Biomed. Mater. Res,* 24(1990), 621-637.

19. R. K. Kullkarni, E. G. Moore, A. F. Hegyei and F. Leonard, *J. Bioned. Mater. Res.*5 (1971) 196.

20. C. C. Chu, *J. Biomed Mater. Res.* 15 (1998).

21. M. Vert, S. M. Li and H. Garreau, *J. Biomater. Sci. Polym. Ed.* 6 (1994) 639.

22. B. D. Ratner, A. S. Hoffman, F. J. Schoen and J. E. Lemons, "*Biomaterials Science*: *An Introduction to materials in medicine,*" (Academic. Press. San Diego, 1996), 64.

23. N. P. Ziats, K. M. Miller and J. M. Anderson, *Biomaterials*, 9 (1988), 5-13.

24. R. Muzzarelli, V. Balassarre, F. Conti, P. Ferrara, G. Biagini and G. Gazzanelli, *Biomaterials*, 9 (1988), 247-252.

25. S. Bartnicki- Garcia and E. Reyers, *Biochim. Biophys. Acta*, 165 (1968), 32-42.

26. L. A. Hadwiger and J. M. Backham, *Plant Physiol.*, 66 (1980), 205-211.

27. D. Knorr, *Food Technology*, (1984), 85-97.

28. C. J. Brine, in: "*Chitin, Chitosan and Related Enzymes,* Chapters 17-23, J. P. Zikakais (ed), *Academic Press, Inc,* 1984.

29. G. A. Roberts, *Chitin chemistry*, G.A.Roberts ed, (Macmillan Press. Houndmills, England, 1992).

30. K. Kurita, *Chitin in nature and Technology*, R.A.A.Muzzarelli, C. Jeuniaux, G.W.Gooday eds, (Plenum Press, New York, 1986), 287-293.

31. T.Sannan, K. Kurita and Y. Iwakura, *Makromol Chem.* 177 (1976), 3589

32. K. Kurit, M. Kamiya and S. I. Nishimura, *Carbohydrate Polumers*, 16 (1991), 83.

33. G. W. Rigby, U.S. *Patent US 204087* (1934).

34. E. I. du Pont de Nemours & Company. *UK patent UK 458839* (1963).

35. A. Domart and M. Rinaudo, *Int. J. Biol. Macromol*, 5 (1983), 49.

36. R. A. A. Muzzarelli, *Chitin, Pergamon,* (New York, 1977).

37. R. A. A. Muzzarelli, C. Jeuniauk, and G. W. Gooday, *Chitin in Nature and Technology*, (Plenum, New York, 1986).

38. R. A. A, Muzzarelli, *Natural Chelating Polymers*, (Tornto: Pergamon of Cananda Ltd., 1973), 83-95.

39. W. Paul and C. P. Sharma, *S. T. P. Pharma Science,* 10 (2000), 5-22.

40. E. Errington, S. E. Harding, K. M. Varum, L. Illum, Int. *J. Biol. Macromol.* 15 (1993),13-117.
41. L. Illum, *Pharm. Res*, 51 (1998), 1142-44.
42. S. Dumitriu, *Polymeric biomaterial,* 2nd Ed, (Marcel Dekker Inc. New York, 2002), 187-212.
43. P. J. Flory, "*Principle of polymer chemistry*", (Cornel University Press, Ithaca, New York, 1967).
44. K. Kurita, T. Sannan and Y. Iwakura, *Makromol, Chem.*, 178 (1977), 3197.
45. J. K. Francis Suh, H. W. T. Matthew, *Biomaterials,* 21 (2000), 2589-259.
46. S. Mima, M. Miya, R. Iwamoto and S. Yoshikawa, *In Chitin and Chitosan,* S. Hirano, S. Tokura (eds), The Japanese Society of Chitin and Chitosan, 1982,.21.
47. K. Kurita, T. Sannan and Y. Iwakura, *J.Appl. Pol. Sci.*, 23 (1979), 511.
48. W. Hillyard, J. Doczi, and P. B. Kiernan., *Proc. Soc. Exp. Bio. Med.*, 115 (1964), 1108-1112.
49. M. Houw, M. Takadam and T. Komait, *Chem. Pharm. Bull*, 33 (1985), 3986-3992.
50. Y. Sawayanagi, N. Nambu, and T. Nagai, *Chem. Pharm. Bull*, 30 (1990), 3297-3301.
51. T. Chandy, C. P. Sharma, , *Biomater, Artif. Cells Artif Organs,* 8 (1990), 1-24.
52. R. A. A. Muzzarelli, *Chitin, Pergamon, New York.* 1997.
53. R. L. Monagham, B. Davis and D. E. Eveleigh,E. T. Reese and R. P. Tewar, *Nature New Biology*, 245 (1972), 78.
54. S. Hirano, H. Tsuchida and N. Nagao, *Biomaterials* 10 (1989), 574-6.
55. R. A. Muzarelli, C. Zucchini, P. Ilari, A. Pugnaloni and G. Biagini, *Biomaterials*, 14 (1993), 925-5.
56. S. Hirano, H. Seino, Y. Akiyama and I. Nonaka, *Polym. Mater. Sci. Eng.* 59 (1988), 389.
57. W. Malette, H. Quigley, R. Gaines, N. Johnson, W. Rainer, *Ann. Thor. Surg.* 36 (1983).
58. S. Hirano, H. Inui, M. Iwata, K. Yamanaka, H. Tanaka, T. Toda, *Progress in clinical biochemistry*, K. Miyai, T. Kanno, E. Ischikawa, eds, (Elsevier Applied Science, London, 1992), 1009.

59. W. Malette, H. Quigley and E. Adickes, *Chitin in nature and technology*, R. Muzzarelli, C. Jeuniaux and G. Gooday G, eds, (Plenum Press, New York, 1986), 435-442.
60. P. Molyneux, *Water-soluble synthetic polymers: Properties and Behaviour*, (CRC Press, Inc. Boca Raton, FL, 1983), 19-27.
61. R. Kjellander and R. Florin, *J Chem SOC, Faraday Trans*, 77 (1981) 2053-77.
62. F. E. Bailey and J. V. Koleske, *Non-ionic Surfactants: Physical and Chemistry*, M. J. Schick ed, (Marcel Dekker, Inc, New York, NY, 1987), 927-969.
63. M. Bjorling, G. Karlstrom and P. Linse, *J Phys, Chem*, 95 (1991) 6706-09
64. S. T. Milner, Science, 251 (1991), 905-914.
65. S. Nagaoka, Y. Mori, T. Tanzawa, Y. Kikuchi, F. Inagaki, Y. Yokota and Y. Nioshiki, *Trans. Am. Soc. Artif Intern. Organs*, 33 (1987), 76-78.
66. T. Kato, K. Nakamura, M. Kawaguchi and A. Takahashi, *Polymer J.* 13 (1981) 1037-43.
67. C. W. Hiatt, A. Shelvkov, J. Rosenthal and J. N. Galimore, *J. Chromatography*, 56 (1972), 362.
68. J.N. George, *Blood*, 40 (1972), 862.
69. W. Wasiewski, M. J. Rasco, M. B. Martin, J. C. Dewiler and J. W. Fenton, *Thromb. Res.*, 8 (1976), 881.
70. J. M. Harris, *Poly(ethylene glucol) Chemistry*, (Plenum, New York, 1992).
71. Z. Zalipsky, *Bioconjug. Chem.*, 6 (1995) 150.
72. N. A. Alcantar, E. S. Aydil, J. N. Israelachvili, *J. Biomed. Mater. Res.*, 51 (2000), 343-51.
73. K. D. Nelson, R. Eisenbaumer, M. Pomerantz and R. C. Eberhart, *ASAIO Journal*, 42 (1996), M884-9.
74. J.D. Andrade, V. Hlady, L. Feng, K. Tingey, *Interfacial behaviour of bioproducts*, Brash JL and Wojciechowski P eds, (Drekker, New York, 1996), 19-55.
75. J.D. Andrade and V. Hlady, *Adv. Ploym, Sci.*, 79 (1986), 1.
76. R. A. A. Muzzarelli, *Chitin*, (Pergamon Press, New York, 1977).
77. J. Berger, M. Reist, J. M. Mayer, O. Felt, N. A. Pepppas and R. Gurny, *Eur. J. Pharm . Biopharmace*, 57 (2004), 19-34.
78. J. P. Zikakis in *Chitin, Chitosan and Related Enzymes*, (Academic Press, Inc., Orlando, 1984).

79. H. Struszczyk, *Medical Applications of Chitosan* (Tampere, Finland, 1990-92).
80. *Proceedings of the International Conferences on Chitin/Chitosan*, Trondheim, Norway (1988) and Princeton, USA (1991).
81. T. Uragami, E. Yoshida and M. Sugihara, *J. Appl. Polym. Sci.* 28(1983), 1361.
82. H. S. Blair, J. Guthrie, T. Law, P. Turkington, *J. Appl Ploym. Sci.* 45 (1992), 1857.
83. Y. Kurauchi, T. Yanai, K. Ohga, *Chem. Lett.* 34 (1991), 1411.
84. D. Y. Kim, J. A. Ratto, R. B. Blumestein, *Polym. Prepr.* 31 (1991), 112.
85. M. M. Amiji, *Biomaterials*, 16 (1995), 593.
86. V. R. Patel, M. M. Amiji, *ACS Symp. Ser.* (1996), 209.
87. W. H. Jiang, S. J. Han, *Journal of Polymer Science*, 36 (1998), 1275-81.
88. M. Mucha, J. Piekielna, A. Wieczorek, *Macromol. Symp.*, 144 (1999), 391-412.
89. W. Wang, G. A. F. Roberts, *Advances in Chitin Science*, A. Domard, G. Roberts and K. Varum eds, (1998).
90. V. L. Alexeev, E. A. Keberg and G. A. Evmenenko, *Polymer Engineering and Science*, 40 (2000), 1211-5.
91. C. G. L. Khooa, S. Frantzicha, A. Rosinskia, M. Hoogstraate, *European Journal of Pharmaceutics and Biopharmaceutics*, 55 (2003), 47–56.
92. M. Zeng, Z. Fang and C. Xu, *J Membrane Science* (2004) in press
93. R. H. Chen and H. C. Chen eds, " *Proceeding of the Third Asia-Pacific Chin and Chitosan Symposium*". Advances in Chitin Science, Vol III, 1998.
94. R. A. A. Muzzarelli, in "*Chitin Enzymology" Eur. Chitin Soc.*, (Lyon and Ancona, 1993).
95. M. S. Masri, F. W. Reuter, M. J. Friedman, *Applied Polymer Science*, 18 (1974), 675-81.
96. S. Hirano, H. Senda, Y. Yamamoto and A. Watamabe in *Chitin, Chitosan and Related Enzymes,* J. P. Zikakis ed, (Academic Press, Inc, 1984), 77-95.
97. K. Kurita, T. Sannan and Y. Iwakura, *J. Appl. Polym. Sci.*, 23 (1979) 511-5.
98. K. Kurita, Y. Koyama and A. Taniguchi. *J. Applied Polymer Sci.*, 31 (1986), 1169-76.
99. Y. Koyana and A. Taniguchi. *J. Applied Polymer Sci.*, 31 (1986), 1951-4.
100. R. A. A. Muzzarelli, *The polysaccharides*, G. O. Aspinall ed, (Academic Press, Inc., 1985), 417-51.

101. M. N. V. Ravi Kumar, T. Rajakala Sridhari, K. Durga Bhavani and P. K. Dutta, *Colorage* (1998), 25.

102. M. Teixeira, W. P. Paterson, E. J. Dunn, Q. Li, B. K. Hunter, M. F. A. Goosen, *Ind. Eng. Chem Res.*, 29 (1990), 1205-9.

103. S. Hirano, H. Senda, Y. Yamamoto, A. Watanabe, in *Chitin, Chitosan, and Related Enzymes*, J. P. Zikakis (ed.), *Academic Press, Inc.*, 1984, 95-125.

104. L. A. Hadwiger, B. Fristensky, R. C. Riggleman, in *Chitin, Chitosan, and Related Enzymes*, J. P. Zikakis ed, (Academic Press, Inc., 1984), 291-302.

105. R. A. A. Muzzarelli, *Carbohydrate Polymers*, 3 (1983), 53-75.

106. G. Lanh, G. Maresch and H. R. Lenz, "*Nail Polishes Containing o-Benzyl-N-Hydroxyalky Chitosan as Films-Forming Component*", Ger. Offen. DE. 3,723,811 (1989).

107. S. Matsumura, T. Karigome and K. Nomoto, "Manufacture of N-Carboxymethoxycrabonyl chitosan for Moistureizers," Jpn Kokai Tokkyo JP 01, 14, 203 [89, 14 203] (1989).

108. G. Lang, and H. Wendel, "*Hair and Skin Fixative Based on Chitosan and on Ampholytic Copolymer*", Ger. DE 3,644, 097 (1988).

109. P. R. Austin, C. J. Brine, J. P. Casle, J. P. Zikakis, *Science*, 212 (1989), 749.

110. M. L. Markey, M. L. Bowman, M. V. W. Bergamini eds, *Chitin and Chitosan,* (Elsevier Applied Science, London, 1989) 731.

111. I. V. Yannas, J. F. Burke, *J. Biomed Mater. Res.*, 14 (1980), 65-81.

112. N. Dagalakis, J. Flink, P. Stasikelis, J. F. Burke, I V. Yannas, *J. Biomed Mater Res.* 14 (1980), 511-28.

113. K. Mastuda, S. Suzuki, N. Isshiki, K. Yoshioka, R. Wada, S. H. Hyon and Y. Ikada, *Biomterials* 14 (1993), 1030-5.

114. L. J. Hinrichs, E. J. Lommen, C. R. H. Wildevuur, J. Feijen, *J Appl Biomater*, 3 (1992), 287-303.

115. C. Collumbel, O. Damour, C. Gagnieu, F. Poinsignon, C. Echinard and J. Marichy, "Biomaterials for Artificial Skin and Implants Containing Acethylated Chitosan, Collagens, and Glycosaminoglycans", *Eur. Pat. Appl. EP* 296, 078 (1988).

116. Y. Le, S. C. An, A. R. Horrocks, *Development of anti-bacterial polysaccharide fibres and their performance*, in the European Conference on Advances in Wound Management, Amsterdam, Netherlands (1996).

117. R. Olsen, D. Schwartzmiller, W. Weppner, R. Winandy, in G. Skjak-Break, T. Anthosen, and P. A. Sandford eds., *Chitin and Chitosan: Sources, Chemistry, Biochemistry, Physical Properties and Applications*, (Elsevier Applied Science, New York, 1989).
118. *ACS Symposium Series*, D. A. Sandford, A. Stinnes eds., 467 (1991), 430.
119. I.V. Yannas, H. F. Burke, D. P. Orgill, E. M. Skrabut, *Science*, 215 (1982), 174.
120. M. N. V. Ravi Kumar, *Bull. Mater. Sci.*, 22 (1999), 905.
121. R. A. A. Muzzarelli, C. Muzzarelli and M. Terbojevich, *Carbohydr. Eur*, 19 (1997), 176.
122. M. Nakajima, K. Kifune, in *Chitin, Chitosan and Related Enzymes*, J. P. Zikakis ed., (Harcourt Brace Janovich, New York, 1984), 407.
123. B. Sparkes, D. G. Murray, *US Patent* 4572906 (1986).
124. K. Y. Kim, D. S. Min, *Trans. Soc. Biomater, XI* (1988), 658.
125. K. Kifune, Y. Yamaguchi, S. Kishimoto, *Trans. Soc. Biomater. XI* (1988), 216.
126. F. W. Mi, S. S. Shyu, Y. B. Wu, S. T. Lee, J. Y. Shyong and R. N. Huang, *Biomaterials*, 22 (2001), 165.
127. G. Biagini, A. Bertani, R. Muzzarelli *et al.*, *Carbohydr. Res.* 12 (1991), 281.
128. W. K. Loke, S. K. Lau, L. Lee, E. Khor, and K. S. Chow, *J. Biomed. Mater. Res.*, 53 (2000), 8.
129. S. Miyazaki, H. Yamaguchi, C. Yokouchi, M. Takada and W. M. Hou, *J. Pharm. Pharmacol.*, 40 (1989), 642-3.
130. B. J. Lee, J. S. Choe, and C. K. Kim, *J. Microencapsul.*, 15 (1998), 775-87.
131. K. E. Uhrich, S. M. Cannizzaro, R. S. Langer and K. M. Shakesheff, *Chem. Rev.* 99 (1999), 3181.
132. C. Alvarez-Lorenzo, R. Duro, J. L. Gomez-Amoza, R. Martin-pacheco, C. Souto and A. Concheiro, *Int. J. Pharm.*, 180 (1999), 105.
133. M. N. N. Ravi Kumar and N. Kumar *Iranian Polym. J.*, 5 (1996), 60.
134. K. C. Gupta, M. N. V. Ravi Kumar, *J. Appl. Polym. Sci.* 76 (2000), 672.
135. D. K. Singh, and A. R. Ray, *J. M. S. Rev. Macromol. Chem. Phys.*, 40 (2000), 69-83.
136. C. J. Brine in *Chitin and Chitosan*, G. Sjak-break, T. Anrhonsen, and P. Sandford eds., (Elsevier, New York, 1989), 679.
137. S. Baba, Y. Uraki, Y. Miura, and S. Tokura in *Chitin and Chitosan*, G. Sjak-Break, T. Anthonsen and P. Sandford eds., (Elsevier, New York, 1989), 703.

138. V. R. Patel and M. M. Amiji, *Pharm. Res.*, 13 (1996), 588.

139. Y. Murata, E. Miyamoto and S. Kawashima, *J Controlled Release*, 38 (1996), 101.

140. S. Alamelu and K. Panduranga Rao, *Carbohydr. Polym.*, 24 (1990), 215.

141. S. R. Jameela and A. Jaya Krishnan, *Biomaterials*. 16 (1995), 769.

142. C. Yomota, T. Komuro and T. K. Kimura, *Yakugaku-Zasshi*, 110 (1990), 442.

143. K. Inouye, Y. Machida and T. Nagai, *Drug Des. Deliv.*, 1 (1987), 297-305.

144. K. Inouye, Y. Machiday, T. Sannan, and T. Nagai, *Drug Des. Deliv*, 2 (1988), 165-75.

145. S. Sabinis, P. Rege and L. H. Block, *Pharm. Dev. Technol.*, 2 (1997), 243-55.

146. Y. Sawayanagi, N. Nambu and T. Nagai, *Chem. Pharm. Bull.* 30 (1982), 2935.

147. G. C. Ritthidej, P. Chomto, S. Pummangura and P. Menasveta, *Drug Dev. Ind. Pharm.*, 20 (1994), 2019.

148. S. I. Pather, I. Russel, J. A. Syee, S. H. Neau, *Int. J. Pharm.*, 164 (1998) 1

149. T. Nagai, Y. Sawayanagi, and N. Nambu in *Chitin, Chitosan and Related Enzymes*, J. P. Zikakis ed., (Academic, New York, 1984), 21.

150. S. R. Jameela and A. Jaya Krishnan, *Biomaterials*, 16 (1995), 769.

151. L. S. Lin, S. Q. Lin, S. Y. Ng, M. Froix and J. Heller, *J. Controlled Release*, 43 (1997), 65.

152. D. Thacharodi, K. Panduranga Rao, *J. Chem. Technol. Biotechnol.* 58 (1993), 177.

153. D. Thacharodi, K. Panduranga Rao, *Int. J. Pharm.*, 96 (1993), 33.

154. D. Thacharodi, K. Panduranga Rao, *Biomaterials* 16 (1995), 145.

155. Y. Kawashima, T. Handa, A. Kasai, H. Takenaka, S. Y. Lin, and Y. Ando, *J. Pharm Sci*, 74 (1985), 264-8.

156. R. Vanholder, *Clin Mater* 10 (1992), 87-133.

157. J. S. Schultz, S. M. Linderauer and J. A. Penner, *AGS Symposium Series, Washington, DC: Am. Chem. Soc*, 199 (1982), 317-50.

158. J. M. Lazarus, *Kidney Int*, 18 (1980), 783-96.

159. N. A. Hoenich, D. Levett, S. Fawcett, C. Woffindin and D. N. S. Kerr, *J Biomed Eng*, 8 (1986), 3-9.

160. S. Akizawa, K. Kino, S. Koshikawa, *Trans Am Soc Artif Intern Organs*, 35 (1989), 333-5.

161. G. H. M. Engbers, W. L. J. Hinrichs and J. Feijei, *Trans Soc Biomater*, 17 (1994), 109.

162. J. R. Frautschi, J. A. Hubbell, B. D. Clark, J. A. Gelfand, W. B. Dolman, R. C. Eberhart, *Trans Soc Biomater*, 13 (1994), 235-239.

163. M. T. Qureshi, H. S. Blair and S. J. Allen, *J Appl Polym Sci* 46 (1992), 263-9.

164. T. Chandy and C. P. Sharma, *J Appl Polym Sci* 44 (1992), 2145-56.

165. S. Hirano, J Noishiki, J. Kinugawa, H. Higashijima and T. Hayashi in *Advances in Biomedical Polymers*, C. G. Gegelein ed., (New York: Plenum Press, 1987), 285-97.

166. M. Miya, S. Yoshikawa, R. Iwamoto and S. Miya, *Kobunshi Ronbunshu*, 40 (1983), 645.

167. M. Miya and R. Iwamoto, *J Polym. Sci., Polym. Phys. Ed.*, 22 (1984), 1149.

168. T. Uragami, F. Yoshida, and M. Sugihara, *J. Appl. Polym. Sci.*, 28 (1983), 1361.

169. C. T. Reinhart and N. A. Peppas, *J. Membrane Sci.*, 18 (1984), 227.

170. J. H. Kim, J. Y. Kim, Y. M. Lee, and K. Y. Kim, *J. Appl. Polym. Sci.*, 44 (1992), 1823.

171. S. Nakatsuka and A. L. Andrady, *J. Appl. Polym, Sci*, 44 (1992), 17.

172. T. Chandy and C. P. Sharma, *Biomater. Artif Org*, 18 (1990), 1.

173. N. Kubota, K. Ohga, and M. Moriguchi, *J. Appl. Polym. Sci.*, 44 (1992), 1823.

174. S. Hirano, *Agric. Bio. Chem.*, 42 (1978), 1938.

175. S. Gabbay, U. Bortolotti, F. Wasserman, N. Tindel, S. M. Factor, R. W. M. Frater, *J Thorac Cardiovasc Surg* 88 (1984), 758–63.

176. J. D. Araujo, D. M. Braile, J. O. Azenha Filho, *J Cardiovasc Surg* 28 (1987), 434–9.

177. L. V. Segesser, N. Jornod, B. Faidutti, *J Thorac Cardiovasc Surg* 93 (1987), 616–9

178. M. E. Nimni, D. Cheung, B. Strates, M. Kodama, K. Sheikh, In: *Collagen, Vol. III*, M. E. Nimni ed, (Boca Raton, FL: CRC Press 1988), 1-38.

179. Y. Noishiki, K. Kodaira, M. Furuse, T. Miyata, "Method of preparing antithrombogenic medical materials", US Patent 4,806,599, (1989).

180. D. P. Speer, M. Chvapil, C. D. Eskelson and J. Ulreich, *J Biomed Mater Res.*, 14 (1980), 735.

181. C. Nishi, N. Nakjima and Y. Ikada, *J Biomed Mater Res* 29 (1995), 829.

182. H. Endo and H. Taguchi, *Chem Pharm Bull*, 21 (1973) 2684.

183. Yang Yifang, *Chinese Herbal Medicines Comparisons and Characteristics*, (Churchill Livingstone, London: **2002**).

184. S. Fujikawa, T. Yokota, K. Koga, J. Kumada, *Biotechnology Lett*, 9 **(1987)**, 697.

185. T. Akao, K. Kobashi, M. Aburada, *Biol Pharm Bull* 17 **(1994)** 1573–6.

186. J. Y. Lee, T. R. Halm, Y. S. Paik, *Agric. Chem. Biotechnol.* 41 **(1998)**, 610.

187. H. W. Sung, R. N. Huang, L. L. Huang and C. C. Tsai, *J. Biomater. Sci. Polym*, 10 **(1999)**, 63-78.

188. H. W. Sung, I. L. Liang, C. N. Chen, R. N. Huang and H. F. Liang, *J. Biomed. Mater. Res.*, 55 **(2001)**, 538-46.

189. H. W. Sung, R. N. Huang, Lynn L. L. Huang, C. C. Tsai and C. T. Chiu, *J. Biomed. Mater. Res.*, 42 **(1998)**, 568-76.

190. Lynn L. L. Huang, H. W. Sung, C. C. Tsai and D. M. Huang, *Biomed. Mater. Res.*, 42 **(1998)**, 568-76.

191. C. C. Tsai, R. N. Huang, H. W. Sung, H. C. Liang, *J Biomed Mater Res*, 52 **(2000)**, 58–65.

192. H. W. Sung, Y. Chang, C. T. Chiu, C. N. Chen and H. C. Liang, *J. Biomed Mater Res*, 47 **(1999)**, 116-26.

193. H. W. Sung, D. M. Huang, W. H. Chang, L. L. Huang, C. C. Tsai and I. L. Liang, *J Biomater Sci-Polym* 10 **(1999)**, 751–71.

194. H. W. Sung, D. M. Huang, W. H. Chang, R. N. Huang, J. C. Hsu, *J Biomed Mater Res* 46 **(1999)** 520–30.

195. S. Mima, M. Miya and R. Iwamoto, *J Appl. Poly. Sci.* 28 **(1983)** 1909.

196. M. Miya, R. Iwamoto, S. Yoshikawa, S. Mima, *Int. J. Macromol.*, 2 **(1980)**, 323.

197. S. Sabnis and L.H. Blok, *Polymer Bulletin,* 39 **(1997)**, 67.

198. M. Miya, R. Iwamoto, K. Ohta and S. Mima, *Kobunshi Ronbunshu*, 42 **(1985)**, 181.

199. T. Sannan, K. Kurita, K. Ogura and Y. Iwakura, *Polymer,* 19 **(1978)**, 458-9.

200. A. Baxter, M. Dillon, K. D. A. Taylor and G. A. F. Roberts, *Int. J. Biol. Macromol*, 2 **(1992)**, 166.

201. L. Bateman ed., *The Chemistry and Physics of Rubber-Like Substances* (McLaren, **1963**), 464.

202. R. Ravindra, R. Kameswara, R. Krovidi, A. A. Khan, *Carbohydrate Polymers* 36 **(1998)** 121-7.

203. O. Glatter and O. Kratky, *Small Angle X-ray Scattering*, (Academic Press: **1982**).

204. F. J. Balta-Calleja, *X-ray Scattering of Synthetic Polymers*, (Elsevier Publishing Co., **1989**).

205. B. Chu, Laser Light Scattering (2nd ed., Academic Press Inc, London, **1991**).

206. J. L. Koenig, *Spectroscopy of Polymers*, (American Chemical Society, Washington DC, **1992**).

207. H. W. Siesler and K. Holland Moritz, *Infra-red and Raman Spectroscopy of Polymers*, (Marcel Dekker, New York and Basel, **1980**).

208. B. J. Hunt and M. I. James, *Polymer Characterisation*, (Blackie Academic & Professional, **1993**).

209. O. Olabisi, L. Robeson and M. T. Shaw, *Polymer-Polymer Miscibility*, (Academic Press, NY, **1979**).

210. B. Wunderlich, *Thermal Analysis*, (Academic Press, Boston, **1990**).

211. B. Ke, *Newer Methods of Polymer Characterisation*, (Wiley, New York **1964**).

212. C. N. R. Rao, *Ultra-Violet and Visible Spectroscopy*, (Butterworths & Co, London, **1961**).

213. G. Odian, *Principles of Polymerisation*, (2nd ed, New York, **1981**).

214. L. M. War, *An Introduction to Mechanical Properties of Solid Polymers*, (John Wiley & Son, Chichester, **1993**).

215. T. Young, *Trans Roy Soc* 95 **(1805)** 65.

216. F. M. Fowks, *J Phys Chem* 67 **(1963)** 2538.

217. D. K. Owens and R. C. Wendt, *J Appl. Polymer Sci*, 13 **(1969)**, 1740.

218. J. Crank, *The Mathematics of Diffusion*, (Clarendon Press, Oxford, **1975**).

219. W. Jost, *Diffusion in Solid, Liquid and Gases*, (Academic Press Inc., New York, **1969**).

220. S. Nakatsuka, and A. I. Andrady, *J. Appl. Polym. Sci.* 44 **(1992)**, 17.

221. C. K. Colton, K. A. Smith, E. W. Merrill, P. C. Farrell, *J. Biomed Mater Res* 5 **(1971)**, 459-88.

222. J. G. Domszy and G. A. F. Roberts, *Macromol Chem* 186 **(1985)**, 1671.

223. A. Wrzyszczynski, X. Qu, L. Szosland and E. Adamszakn, *Polym. Bull*, 34 **(1995)** 493-500.

224. W. Zhao, L. Yu, X. Zhong, Y. Zhang and J. Sun, *J Macromol Sci Phys*, 34 **(1995)**, 231.

225. O. Olabasi, L. M. Robeson and M. Shaw, *Polymer-Polymer Miscibility*, (New York, Academic Press, **1979**).

226. B. Riedl, R. E. Prud'homme, *Polymer Eng. Sci.*, 24 **(1984)**, 1291.

227. T. Nishi, T. T. Wang, *Macromolecules*, 8 **(1975)**, 909.

228. P. J. Flory, *Phys. Chem.*, 10 **(1942)**, 51.

229. M. L. Huggins, *J. Phys. Chem.*, 9 **(1941)**, 440.

230. B. Wunderlich, *Thermal Analysis*, (Academic Press, Inc, San Diego, **1990**), 193.

231. Y. S. Lipatov and A. E. Nesterov, *Thermodynamics of Polymer Blends, Vol.I* (Technomic Publishing Co. Inc, Lancaster U.S.A. **1997**).

232. M. M. Coleman, J. F. Graf and P. C. Painter, *Specific Interactions and the Miscibility of Polymer Blends*, (Technomic Publishing Co. Inc., Lancaster, U.S.A. **1997**).

233. L. Kohovac, G. Porod, H. Ruck and Z. Z. Kolloid, *Polymer*, 133 **(1953)**, 16.

234. R. A. A. Muzzarelli, *Carbohydrate Polymers*, 29 **(1996)**, 309.

235. C. M. Lehr *et al.*, *Int J Pharm*, 78 **(1992)**, 43-8.

236. S. Sabnis, P. Rege, L. H. Block, *Pharm Dev Tech*, 2 **(1997)**, 243-55.

237. P. Wanichpongan and S. Chandrkachang in *Advances in Chitin Science, Vol.II*, A. Domard A and G. A. F. Roberts eds., (Jacques Andre Press, Lyon, **1998**), 449.

238. C. P. D. Moor, L. Doh and R. A. Siegel, *Biomaterials*, 12 **(1991)**, 836.

239. A. S. Hoffman, *J Controlled Release* 6 **(1987)**, 297.

240. Y. H. Bae, T. Okano and S. W. Kim, *J Polym Sci Part B: Polym Phys*, 28 **(1990)**, 923.

241. F. Alhaique, M. Marchetti, F. M. Riccieri and E. Santucci, *J Pharmacol*, 33 **(1981)**, 413.

242. J. Ricka and T. Tanaka, *Macromolecules*, 17 **(1984)**, 2916.

243. I. C. Kwon, Y. H. Bae, T. Okano and S. W. Kim, *J Controlled Release*, 17 **(1991)**, 149

244. A. M. Lowman and N. A. Peppas in *The Encyclopaedia of Controlled Drug Delivery*, E. Mathiowitz, ed., (John Wiley & Sons, **1999**), 397-418.

245. Kost J in *The Encyclopaedia of Controlled Drug Delivery*, E. Mathiowitz, ed., (John Wiley & Sons, **1999**), 445-459.

246. K. D. Yao, T. Peng, H. B. Feng and Y. Y. He, *J Polym Sci, Part A: Polym Chem*, 32 **(1994)**, 1213.

247. T. Sakiyama, C. H. Chu, T. Fuji and T. Yano, *J Appl Polym Sci*, 50 **(1993)**, 2021

248. Y. H. Bae, T. Okano, R. Hsu, S. W. Kim, *Makromol. Chem. Rapid Commun*, 8 **(1987)**, 481.

249. T. Okano, Y. H. Bae, H. Jacobs, S. W. Kim, *J Controlled Release*, 11 **(1990)**, 255.

250. D. K. Yao, T. Peng, J. J. Yu, M. X. Xu and M. F. A. Goosen, *J.M.S. Rev. Macromol. Chem Phys*, 35 **(1995)**, 155.

251. F. L. Mi, H. W. Sung, S. S. Shyu, *Journal of Polymer Science: Part A: Polymer Chemistry,* 38 **(2000)**, 2804-14.

252. T. Baker, H. W. Blanch, J. M. Prausnitz, *J Appl Polym Sci*, 52 **(1994)**, 783.

253. D. Hariharan, N. A. Peppas, *J Controlled Release* 23 **(1993)**, 123.

254. S. Wu, *Polymer Interface and Adhesion*, (Marcel Dekker, Inc., New York and Basel, **1982**).

255. A. K. Rastogi and L. E. Pierre, *J. Colloid Interface Sci.*; 35 **(1971)**, 16.

256. A. W. Adamson, *Physical Chemistry of Surfaces,* (2nd ed., Wiley-Interscience, New York, **1967**).

257. F. D. Petke and B. R. Ray, *J. Colloid Interface Sci.*, 31 **(1969)**, 216.

258. E. G. Shafrin, W. A. Zisman, *J. Phys. Chem.*, 76 **(1972)**, 3259.

259. L. Vachoud, N. Zydowicz and A. Domard; *Carbohydr. Res.*, 302 **(1997)**, 169.

260. P. H. Chen, J. H. Lin and M. H. Yang, *Carbohydr. Polym.*, 24 **(1994)**, 41-6.

261. J. H. Pa, T. L. Yu, *Macromol Chem. Phys*, 202 **(2001)**, 985.

262. C. Wu, S. Zhou and W. Wang, *Biopolymers,* 35 **(1994)**, 385.

263. M. W. Athonsen, K. M. Varum, A. M. Hermansson, O. Smidsrod and D. A. Brant, *Carbohydr. Polym.* 25 **(1994)**, 13.

264. G. S. Manning, *Q Rev Biophys.* 11 **(1978)**, 179.

265. W. H. Stockmayer, *Macromol. Chem.* 35, **(1960)**, 54.

266. H. Yamakawa, *Modern Theory of Polymer Solution*, (Harper & Row, New York, **1971**).

267. A. Y. Grosberg and D. V. Kuznetsov, *Macromolecules* 25 **(1992)**, 256.

268. P. G. de Gennes, *J. Phys. Lett.* 36 **(1975)**, L55.

269. I. C. Sanchez, *Macromolecules* 12 **(1979)**, 276.

270. C. Wu and S. Zhou, *Macromolecules,* 28 **(1995)**, 8381.

271. C. Wu, K. K. Chan and K. Q. Xia, *Macromolecules*, 28 **(1995)**,1032.

272. S. S. Davis, *Pharm Int* 2 **(1981)**, 41.

273. R. S. Langer and N. A. Pappas, *Biomaterials* 2 **(1981)**, 201.

274. J. R. Robinson ed., *Sustained and Controlled Release Drug Delivery Systems*, (Marcel Dekker, New York, **1978**).

275. A. F. Kydoieus ed., *Controlled Release Technologies: Methods, Theory and Applications*, (Boca Raton, FL, **1980**).

276. N. B. Graham, *Chem. Ind.* 15 **(1990)**, 482.

277. J. Kost and R. Langer in *Hydrogels in Medicine and Pharmacy*, N. A. Peppas ed., (CRC Press, Boca Raton, **1987**), 95.

278. K. E. Uhrich, S. M. Cannizaro and R. S. Langer, *Chem. Rev*, 99 **(1999)**, 3181-98..

279. F. L. Mi, H. W. Sung, S. S. Shyu, *J Appl. Polym. Sci.*, 81 **(2001)**, 1700-11.

280. G. M. Zentner, J. R. Cardinal and S. W. Kim, *J. Pharm. Sci.*, 67 **(1978)**, 1347.

281. S. J. Wisniewski, D. E. Gregonis, S. W. Kim and J. D. Andrade, *Hydrogels for Medical and Related Applications*, J. D. Andrade ed., (Symposium Series, 31, ACS, Washington, DC, **1976**), 80.

282. M. H. Cohen and D .J. Turnbull, *Chem. Phys.*, 31 **(1959)**, 1164.

283. H. Yasuda, C.E. Lamaze and L. D. Ikkenbery, *Makromol.Chem.*, 118 **(1968)** 19.

284. H. Yasuda and C.E. Lamaze, *J. Macromol. Sci., Phys.*, B5 **(1971)** 111.

285. C. T. Reinhart and N. A. Peppas, *J. Membrane Sci.*, 18 **(1984)**, 227.

286. T. Tanaka, L. O. Hocker and G. B. Benedek, *J. Chem. Phys.*, 59 **(1973)** 5151.

287. M. Tokita, T. Miyoshi, K. Taegoshi and K. Hikichi, *Phys. Rev.*, E53 **(1996)** 1823.

288. H. Matsuyama, M. Teramoto, H. Urano, *J Membrane Sci.*, 126 **(1997)**, 151-60.

289. T. Canal, N. A. Peppas, *J Biomed Mater Res*, 23 **(1989)**, 1183-93.

290. W. R. Vieth, *Diffusion In and Through Polymers*, (Oxford University Press. **1991**).

291. R. H. Chen, M. L. Tsih, W. C. Lin, **Carbohydro. Polym.** 31 **(1996)**, 141.

292. I. Z. Mackenzie, F. R. Burnet, M. P. Embrey, *Br. J. Obstet Gynaecol* 87 **(1980)**, 292.

293. D. A. Wood, in: *critical Reports on Applied Chemistry*, A. T. Florence ed, (Blackwell Scientific Publications, Oxford, **1980**).

294. P. L. Ritger, N. A. Peppas, *J. Cotrolled Release* 5 **(1987)**, 37.

295. G. Astarita, G. C. Sarti, *Polymer eng Sci* 28 (1978), 1299.

296. M. E. McNeill, N. B. Graham, *J Biomater Sci Polym Edn*, 76(**1993**), 305-22.

297. P. I. Lee, C. J. Kim, *J Control Release* 16 (1991), 229-35.

298. D. M. Eisenberg, R. B. Davis, S. L. Ettner, S. Appel, S. Wilkey, R. C. Kessler, *Journal of the American Medical Association* 280 **(1998)**, 1569-75.

299. P. Richard, M. D. Brown, L. Patricial and M. D. Gerbarg, *J. American Botamical Concil*, 56 **(2002)**, 40-52.

300. M. Davydov and A. D. Krikorian, *J. Ethnopharmacology*, 72 **(2000)**, 345-93.

301. A. I. Baranov, *J. Ethnopharmacology*, 6 **(1982)**, 339-53.

302. W. T. Lee, *J Pharm* 10 **(1979)**, 103-7.

303. X. Cao and C. Li, *Chung Tsao Yao* 11 **(1980)**, 277.

304. I. I. Brekhman, *Biochem. Pharmacol.* 50 **(1963)**,12.

305. O. Warburg, and W. Christian, *Biochem.* 310 **(1991)**, 384.

306. R. H. Hackman, *Aust. J Biol. Sci*, 8 **(1955)**, 530.

307. E. Ruckenstein, X. F. Zeng, *Ind. Eng. Chem. Res*, 35 **(1996)**, 4169.

308. E. Ruckenstein, X. F. Zeng, *Biotechol. Bioeng*, 56 **(1997)**, 610.

309. E. Ruckenstein, X. F. Zeng, *J. Membr. Sci.* 37 **(1998)**, 159.

310. R. Ghosh, *J Chromatography* 952 **(2002)**, 13-27.

Appendix A: Raw data for study of vitamin B_{12} release

Part 1:
Sample: CS Film thickness: 0.42mm **Temp:** 37°C, **pH:** 7

t (h)	1	2	2.5	3	5	7	10	18	36
C (mg/L)	0.56	0.64	1.23	1.45	1.93	2.40	2.89	3.02	3.17

Sample : 0.05CSR (crosslinking density: 0.068%) **Film thickness:** 0.01mm
Temp: 37°C **pH:** 7

t (h)	1	2	3.5	5	6.5	8	10	18	33
C (mg/L)	1.07	3.482	6.785	11.505	17.251	20.723	22.701	25.122	28.973

Sample : 0.2CSR (crosslinking density: 0.26%) **Film thickness:** 0.17mm
Temp: 37°C **pH:** 7

t (h)	1	2	4	5	6.5	8	10	24	48
C (mg/L)	0.39	0.59	1.34	2.55	4.63	6.02	7.70	15.122	-

Sample: 0.3CSR (crosslinking density: 2.23%) **Film thickness:** 0.03mm
Temp: 37°C **pH:** 7

t (h)	1	2	3	4	6	8	10	18	36
C (mg/L)	2.12	2.84	4.17	5.25	6.00	7.02	7.89	8.06	10.02

Sample: 0.5CSR (crosslinking density: 4.65%) **Film thickness:** 0.0085 mm
Temp: 37°C **pH:** 7

t (h)	1	2	3	4	6	8	10	18	36
C (mg/L)	1.07	2.30	3.64	4.37	5.36	6.18	7.01	8.32	9.89

Sample: 0.8CSR (crosslinking density: 9.22%) **Film thickness:** 0.04 mm
Temp: 37°C **pH:** 7

t (h)	1	2	3	4	6	8	10	18	36
C (mg/L)	0.96	1.89	3.04	3.94	5.23	7.41	9.04	10.67	11.89

Sample: 1CSR (crosslinking density: 14.35%) **Film thickness:** 0.036
Temp: 37°C **pH:** 7

t (h)	1	2	3	4	6	8	10	18	36
C (mg/L)	0.89	1.92	3.09	4.94	5.89	7.49	9.09	12.98	12.89

Part 2:

Sample: 0.5CSR (crosslinking density: 4.65%) **Film thickness:** 0.0085 mm
Temp: 37°C **pH:** 7

t (h)	1	2	3	4	6	8	10	18	36
C (mg/L)	1.07	2.30	3.64	4.37	5.36	6.18	7.01	8.32	9.89

Sample : CSR/LPEO10 (crosslinking density: 9.22%) Film thickness: 0.025 mm
Temp: 37°C **pH:** 7

t (h)	1	2	3	5	7	9	10	24
C (mg/L)	0.36	0.50	0.88	1.72	2.61	3.82	4.96	-

Sample : CSR/LPEO20 (crosslinking density: 9.22%) **Film thickness:** 0.04 mm
Temp: 37°C **pH:** 7

t (h)	1	2	3	5	7	9	10	24
C (mg/L)	0.26	0.39	1.03	2.07	3.47	5.07	-	15.58

Sample : CSR/LPEO 30 (crosslinking density: 9.22%) Film thickness: 0.42 mm
Temp: 37°C **pH:** 7

t (h)	0.5	1.5	2.5	4	5.5	8	10	24
C (mg/L)	2.15	3.32	4.18	5.01	5.77	7.49	8.79	14.1

Sample 4: CSR/HPEO10 (crosslinking density: 9.22%) **Film thickness:** 0.32 mm **Temp:** 37°C **pH:** 7

t (h)	1	2	3.5	5	6	7	10	24
C (mg/L)	0.49	1.45	3.56	6.56	7.78	8.93	9.82	-

Sample: CSR/HPEO20 (crosslinking density: 9.22%) **Film thickness:** 0.55 mm **Temp:** 37°C **pH:** 7

t (h)	1	2	3	5	6.5	8	10	24
C (mg/L)	0.60	1.32	1.93	3.29	4.15	5.19	6.02	11.98

Sample : CSR/HPEO30 (crosslinking density: 9.22%) **Film thickness:** 0.48 mm
Temp: 37°C **pH:** 7

t (h)	1	2	3	5	7	8	10	24
C (mg/L)	0.25	0.57	1.40	2.26	2.88	3.91	4.82	-

Part 3

Sample: 0.5CSR (crosslinking density: 4.65%) **Film thickness:** 0.0085 mm
Temp: 37°C **pH:** 7

t (h)	1	2	3	4	6	8	10	18	36
C (mg/L)	1.07	2.30	3.64	4.37	5.36	6.18	7.01	8.32	9.89

Sample: CSR (crosslinking density: 9.22%) pH: 5.5
Film thickness: 0.15 mm

t (h)	1	2	3	5	7	8	10	24
C (mg/L)	0.42	0.71	1.02	1.64	2.02	3.51	5.12	15.12

Sample: CSR (crosslinking density: 9.22%) pH: 4.3
Film thickness: 0.21 mm

t (h)	1	2	4	5	6	8	10	24
C (mg/L)	0.22	0.49	1.55	1.93	2.56	4.91	-	17.12

Sample: CSR (crosslinking density: 9.22%) pH: 3.8
Film thickness: 0.35 mm

t (h)	1	2	4	5	6	8	10	24
C (mg/L)	0.20	0.39	0.78	1.19	1.46	3.91	-	15.20

Part 4:
Sample 1: CS (DD: 75%) pH: 7.0
Film thickness: 0.19 mm

t (h)	1	2	3	4.5	6	8	10	24
C (mg/L)	0.54	0.80	1.24	2.06	2.70	3.71	4.98	-

Sample: CS Film thickness: 0.42mm **Temp:** 37°C, **pH:** 7

t (h)	1	2	2.5	3	5	7	10	18	36
C (mg/L)	0.56	0.64	1.23	1.45	1.93	2.40	2.89	3.02	3.17

Sample 2: CS (95%) pH: 7
Film thickness: 0.45 mm

t (h)	1	2	3.5	4.5	6	8	10	24
C (mg/L)	0.21	0.34	0.75	1.24	1.46	1.61	2.78	-

Sample 1: CSR (DD: 75%) pH: 7.0
Film thickness: 0.32 mm

t (h)	1	2	3	4.5	6	8	10	24
C (mg/L)	0.44	080	1.14	1.86	2.65	3.51	4.78	-

Sample: 0.5CSR (crosslinking density: 4.65%) **Film thickness:** 0.0085 mm
Temp: 37°C **pH:** 7

t (h)	1	2	3	4	6	8	10	18	36
C (mg/L)	1.07	2.30	3.64	4.37	5.36	6.18	7.01	8.32	9.89

Sample 3: CSR (95%) pH: 7.0
Film thickness: 0.41 mm

t (h)	1	2	3.5	5	6	8	10	24
C (mg/L)	0.012	0.34	0.75	1.24	2.46	3.51	4.78	-

Appendix B: *A Publication*

Biomacromolecules, 5 (2004), *162-168*

Novel Chitosan-Based Films Cross-Linked by Genipin with Improved Physical Properties

J. Jin, M. Song,* and D. J. Hourston

Institute of Polymer Technology and Material Engineering, Loughborough University,

Loughborough LE11 3TU, United Kingdom

Received August 7, 2003; Revised Manuscript Received November 6, 2003

Novel cross-linked chitosan-based films were prepared using the solution casting technique. A naturally occurring and nontoxic cross-linking agent, genipin, was used to form the chitosan and chitosan/poly(ethylene oxide) (PEO) blend networks, where two types of PEO were used, one with a molecular weight of 20 000 g/mol (HPEO) and the other of 600 g/mol (LPEO). Genipin is used in traditional Chinese medicine and extracted from gardenia fruit. Importantly, it overcomes the problem of physiological toxicity inherent in the use of some common synthetic chemicals as cross-linking agents. The mechanical properties and the stability in water of cross-linked and un-crosslinked chitosan and chitosan/PEO blend films were investigated. It was shown that, compared to the transparent yellow, un-cross-linked chitosan/PEO blend films, the genipin cross-linked chitosan-based film, blue in color, was more elastic, was more stable, and had better mechanical properties. Genipin-cross-linking produced chitosan networks that were insoluble in acidic and alkaline solutions but were able to swell in these aqueous media. The swelling characteristics of the films exhibit sensitivity to the environmental pH and temperature. The surface properties of the films were also examined by contact angle measurements using water and mixtures of water/ethanol. The results showed that, with the one exception of cross-linked pure chitosan in 100% water, the cross-linked chitosan and chitosan/PEO blends were more hydrophobic than un-crosslinked ones.